Modelling future range shift gaps in a biodiversity hotspot: a case study of critically endangered plants in Madagascar

Gabriel Unugabo YESUF

A thesis submitted in partial fulfilment of the requirements of Kingston University London for the award of the degree of Doctor of Philosophy (Ph.D)

November 2018

Table of Contents

List of figures

List of tables

Glossary

Terms	Definition
Habitat	Refers to the natural environment in which a species inhabits. Could also refer to species range when describing predicted suitable occurrences.
Range/Niche	Refers to predicted suitable geographical area for species under either current or future scenarios.
Niche-breadth	A singular measure of species environmental space. Used to quantify predicted range sizes.

Abstract

The synergy between climate and land use land cover change is expected to influence species distribution at local and regional scales in tropical regions. However, robust quantification of species responses and species-specific dispersal rates is lacking for most of Sub-Saharan Africa. This project aims to model range-shift gaps for 84 endangered or critically endangered plant species due to environmental change in Madagascar.

To achieve this deforestation and forest degradation rates were quantified from Landsat imagery using sub-pixel analysis in two intervals (i.e., 1994 – 2002 and 2002 – 2014). Next, intensity analysis was used to determine processes of LULCC at eco-regional scale, while morphological spatial pattern analysis was applied for the determination of protected areas connectivity. Furthermore, species distribution models were constructed using hierarchical Bayesian modelling approach that included corridor connectivity and uncertainties in the derived predictions of species distribution under current and future scenarios. Finally, six spatial indices that quantified vulnerabilities, species range-shifts and displacements were derived from these predictions.

The results showed differentiation in rates of deforestation and forest degradation across eco-regions. On average plant species' range were predicted to shift by approximately 300 km under future scenarios with and without connectivity. Corridor connectivity will facilitate more species upward displacements under low emission scenarios compared to high emission scenarios. Eastern humid forests were identified as 'range shift hotspots' and will be characterised by substantial species' range contractions in all future scenarios.

Biodiversity in the region will experience novel threats from climate and land use land cover change. Conservationist need to adapt on-going intervention programmes to prepare for the potential risks of species extinctions due to environmental change through the integration of spatial conservation planning concepts in policy formulation.

Acknowledgement

In many ways my experience as a PhD student in Kingston University, London, has been quite impressive as well as challenging. Several people motivated me and by no small means contributed to the successful completion of this project. I therefore wish to acknowledge them.

First, I want to thank my first supervisor, Dr. Kerry. A. Brown for his open-door policy from the onset of this project and giving me the opportunity to specialise as a spatial ecology. The fact that I am able to complete this project is largely due to his invaluable guidance during the never-ending analysis phase and patience while I was writing my thesis. I also want to thank my co-supervisor, Prof. Nigel Walford for making himself available whenever the need arose and his input to my research. I wish to express my profound gratitude to the faculty of science, engineering and computing for the award of studentship which enabled me to commence this research. I would like to say thank you to Colin Bethell and Adam Hobbs of Kingston's high-performance computing unit for ensuring that I had access to the cluster and Kingston's computing facilities.

My gratitude to Dr. Osaretin Oviasu for showing me the advert for this project in 2014. I want to show gratitude to my big brothers here in the UK: Tunde, Nosa, Ekerette and Uncle Eze for their moral support, especially during the period when I took ill. I also want to express gratitude to a rare bunch of friends who have provided delightful company in the last few years and cheered me during difficult phases, a big shout out to: Edwin (Eddy), Malcolm (Malcom X), Tonna (Tocrespo), David (Dave), Okechuckwu (Okey) and Ibrahim (Ibro).

My gratitude to Fabio da Silva, Dr. Andreas Hahn, Dr. Philip Bird, James O'Connor, Patrick Meila and Delano Henry whose company in the laboratory and research office made for some cheerful moments.

I want to specially say thank you to members of my immediate family (Daddy, Mummy, Esther, Adebayo and Patience) for the sacrifice you all have made towards me to ensure that I completed my PhD.

Finally, I thank God for the gift of life.

Chapter One

Introduction

1.1 Environmental change, range-shifts and biodiversity conservation

Climate and land use land cover change are expected to greatly impact future biodiversity patterns in the tropics, particularly the distribution of species (Parmesan and Yohe 2003, Anderson-Teixeira et al. 2013, Segan et al. 2015, Kuhn et al. 2016). However, while climate change is anticipated to be active at broad regional scales (Pressey et al. 2007), land use land cover change (LULCC) may drive and concentrate the impact of climate change at local scales (Asner et al. 2010). Such synergy may result in regional intensification of both these drivers of environmental change. For instance, deforestation modulates changes in evapotranspiration rates and water balance (Lathuilliere et al. 2012), establishing land—climate feedbacks that affect atmospheric circulation and rainfall (Nobre et al. 2009). In the tropics, net emissions of carbon from deforestation and forest degradation averaged 1.4 ± 0.5 PgC $\mathbf{yr^{-1}}$ between 1990 and 2010 (Houghton 2013), this suggests that already LULCC from the regions is actively contributing to global climate change. One potential consequence of the coupled effect of climate and LULCC in tropical habitats is predicted to be widespread range shifts for many species across multiple taxa (Colwell et al. 2008, Feeley and Silman 2010, Rodríguez-Castañeda and Sykes 2013).

The absence of overlap between current and future habitats (i.e., range shift gaps) due to contractions or expansions in response to climate and LULCC is an expected outcome for most species – including plants (Kearney et al. 2010, Warren et al. 2018). In environments affected by climate change, flora and fauna must adapt to new temperature and precipitation extremes to survive, where expectedly species would be pushed to the limits of their environmental tolerances (Rodríguez-Castañeda and Sykes 2013). Therefore, their survival in the absence of adaptation depends on the rate at which they can migrate to different elevations and latitudes with suitable environmental conditions (Urban 2015).

Some species may adapt in response to climate change, others with longer generation times may not have enough time for natural selection to act (Skelly et al. 2007, Hoffmann and Sgrò 2011). As a result, climate change will determine shifts in species distributions (Hong-Wa and Arroyo 2012), where they will have to track suitable climate conditions, for instance, towards higher elevations and latitude when adapting to rising temperature (Raxworthy et al. 2008, Kreyling et al. 2010) or downhill to optimise water balance (Crimmins et al. 2011). Some studies have shown losses of tropical biodiversity under environmental change scenarios (Ferrer-Paris et al. 2013, Mantyka-Pringle et al. 2015, Struebig et al. 2015). This is because tropical species are restricted to a narrower range of climate variables compared to temperate species (Dillon et al. 2010, Colwell 2011, Marta et al. 2016), often poor dispersers (Urban et al. 2012) and the majority are already adapted to the warmest and wettest part of the climate spectrum (Addo-Bediako et al. 2000).

To better understand the range of possible species responses to environmental change, ecologists rely on species distribution model (SDM), which combines species occurrences or abundances with environmental variables (that may include LULCC) to predict distributions (Elith and Leathwick 2009, Elith et al. 2010). High resolution satellite data and geographic information systems (GIS) now permits detailed modelling of several aspects of the environment, doing so at multiple scales (Achard et al. 2010, He et al. 2015). The common approach is to combine GIS-derived products (e.g., LULCC) with climate data from general circulation models (GCMs) to investigate environmental associations (Kearney and Porter 2009). Despite these advances, other challenges exist which relate to techniques for predicting LULCC for regional and heterogeneous habitats (e.g., tropics) (Verburg et al. 2009, Pickard et al. 2017), as well as the practicality of integrating ecologically relevant data (e.g., landscape connectivity) (Foltête et al. 2012). Incorporating factors that estimate the ability of landscapes to facilitate species dispersal is likely to improve SDM output and provide more realistic estimates of species range shifts (Fuller et al. 2006, Porfirio et al.

2014). This is especially true for tropical regions, since high deforestation and forest degradation rates are likely to continue to drive future habitat loss and fragmentation (Hansen et al. 2010, Sloan and Sayer 2015). To mitigate the potential consequences of future range-shift gaps for tropical plants, improvements must be made in our ability to estimate deforestation and forest degradation, model landscape connectivity and habitat fragmentation, and build future scenarios that combine these factors (Feeley et al. 2012, Ryan et al. 2016). This could potentially provide in-depth understanding of the constraints plants are likely to encounter when adapting to environmental change, either through latitudinal or poleward shifts in their distribution (Thuiller 2004, Beaumont et al. 2007).

The climax of this Thesis is the determination of range-shifts for the most vulnerable plant species in Madagascar because of climate and LULCC. As a result, several products will be derived using different analytical approaches presented under separate data chapters (Figure 1.1). For this reason, some chapters are not motivated by a suite of research questions *per se,* but rather are designed to highlight specific approaches. *Chapter one* provides general background information about the research and includes a brief introduction to climate and LULCC. *Chapter two* describes the materials and methods that are common to multiple data chapters, namely: sub-pixel analysis (Asner et al. 2009) and intensity analysis (Aldwaik and Pontius 2012). These analyses were implemented mainly to model LULCC. Sub-pixel analysis enabled the mapping of deforestation and forest degradation at fine spatial scales, while intensity analysis was used to quantify transitions between land cover categories in different eco-regions. *Chapter three* addresses eco-regional differences in deforestation and forest degradation from 1994 – 2014 (Figure 1.1). This chapter presents estimates of deforestation and forest degradation rates at eco-regional scale, likewise, their differences along elevation gradient.

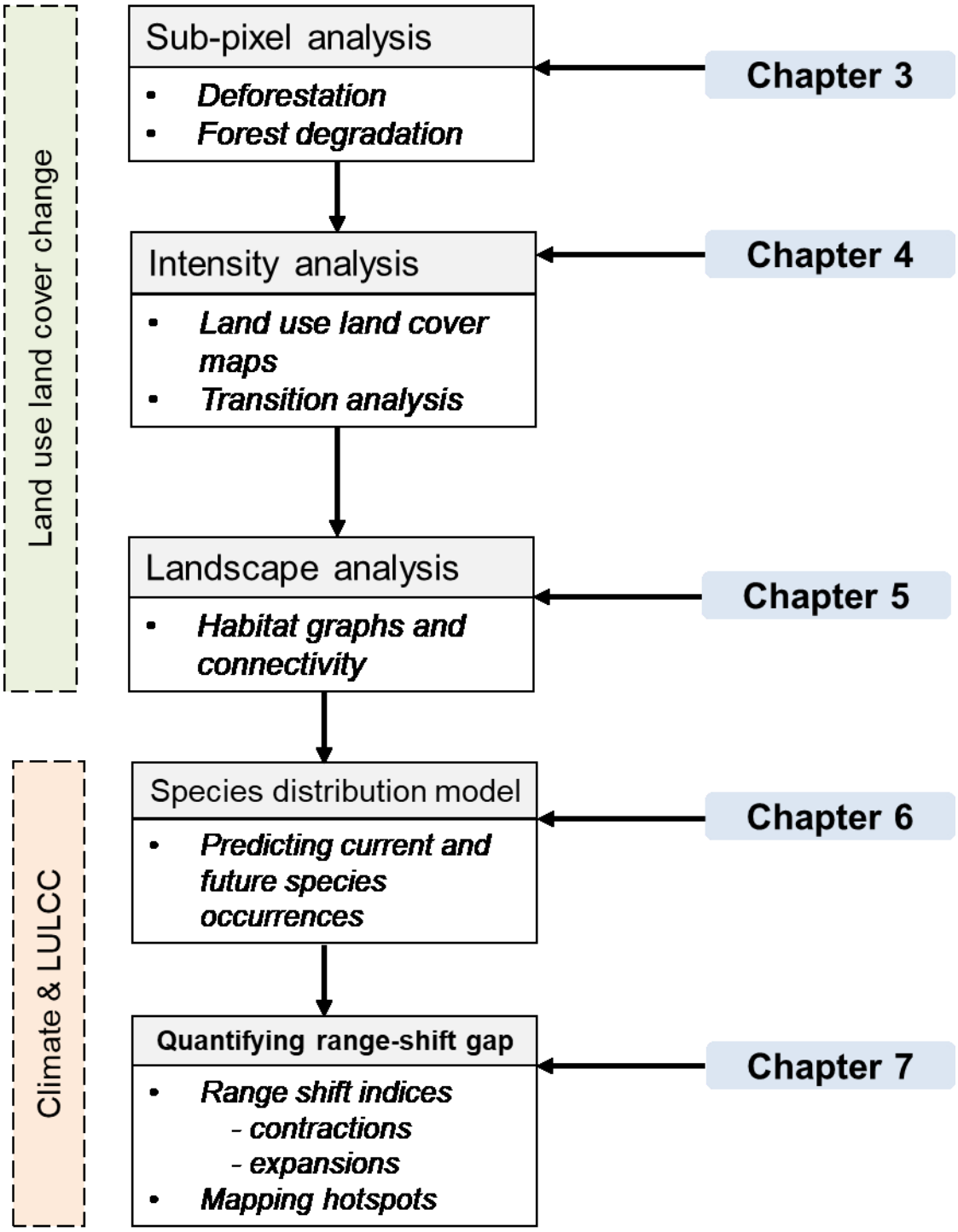

Figure 1.1: A schematic diagram showing the sequence of analytical approach to quantifying range-shift gaps for selected endangered and critically endangered species of Madagascar.

Chapter four focuses on drivers of current LULCC and modelling of future LULCC at eco-regional scales. Intensity analysis in two intervals (i.e., 1994 – 2002 and 2002 – 2014) and land cover category transitions are implemented in Chapter four (Aldwaik and Pontius 2012, Pickard et al. 2017). They are assessed from the perspective of forest gains and losses to determine dominant processes of LULCC in different eco-regions. In addition, predictions of future LULCC (i.e., 2050) for each eco-region was implemented to coincide with the date of future climate models. *Chapter five* applies graph and circuit theoretical concepts to landscape connectivity in selected protected areas (Vogt et al. 2007, McRae et al. 2008, Saura et al. 2011) (Figure 1.1). Similarly, deforestation, forest degradation and habitat fragmentation in protected areas were assessed in this chapter. C*hapter six* addresses species distribution modelling and predictions using a hierarchical Bayesian framework (Latimer et al. 2006, Vieilledent et al. 2014). Under this framework corridor connectivity, current and future LULCC were integrated to climate models of Madagascar and was used to predict the distribution of endangered and critically endangered species. *Chapter seven* addresses several aspects of species-specific range shifts under different future emission scenarios using several spatial indices (Feeley and Silman 2010, Choe et al. 2017, Radinger et al. 2017). *Chapter eight* summarises the main conclusions from each chapter and highlights the main findings of each aspect of this thesis.

Chapter Two

Materials and methods

2.1. Study area: Geographical setting of eco-regions

Madagascar is the fourth largest island in the world and forms the major portion of one of 34 global biodiversity hotspots, characterised by high floral and faunal endemism, as well as threats from deforestation and degradation (Myers et al. 2000). It is located off the southeast coast of Africa and is situated between latitudes 12° 04' 48" to 25° 18' 02" S and longitudes 42° 09' 25" to 51° 05' 36" E. It is approximately 1650 km long and is nearly evenly dissected by a 1200 m mountain ridge with massifs above 2600 m running in a north-south direction. In this chapter, land use land cover assessment is implemented for five of the seven eco-regions on the island (Figure 2.1). These are littoral, lowland, humid, dry and tapia forests. The high plateau grasslands and spiny thickets were excluded because they are not strictly forested regions and mangrove forests because they face different pressures and impacts not present in the previous five eco-regions.

The littoral forest eco-region is situated on the eastern border of the Island close to sea level on sandy sediments, rarely exceeding 800 masl and made mainly of low stature moist forest (20 to 25 m) often interspersed with herbaceous dominated swamps (Insets in Figure 2.1 and 2.2a). Due to low elevation and subsequent easy accessibility, this eco-region has long been under constant pressure from deforestation and is now regarded as the country's most threatened eco-region and have been predicted to go extinct unless drastic and urgent measures are taken (Ganzhorn et al. 2001, Schatz 2002, Crowley 2010). Presently, only a negligible size of littoral forest remains (approx. 275 km^2) occurring in twenty-three patches along the eastern corridor. Some researchers believe that the littoral forest once occupied a major portion of the coast, averaging 3 km wide along the 1500 km stretch from Vohémar to Tolagnaro (Du Puy and Moat 1996). There are prominent occurrences of some endemic species such as: *Uapaca littoralis*, *Labramia bojeri* and *Mimusops coriacea*, *Pandanus* spp., *Asteropeia*, *Cycas thouarsii*, *Dypsis lutescens* and

Brexia madagascariensis (Gautier et al. 2018). The lowland forests constitute the region that mostly borders the Indian Ocean to the east in a northerly and southerly direction, at an elevation range of 0 – 1750 masl (metres above sea level) covering an area of about 60,000 km^2. This ecoregion is made up mostly of closed canopy trees between 20 and 30 m, and emergent trees up to or over 40 m (Figure 2.2b). Epiphytes and lianas are frequent with a sparse undergrowth. Commonly found in the upper tree layer are species of the following families: Annonaceae, Burseraceae, Clusiaceae, Lauraceae and Moraceae. Dominant families in the lower tree and shrub layer include Apocynaceae, Araliaceae, Arecaceae, Ebenaceae, Euphorbiaceae, Rutaceae, Salicaceae, and Violaceae (Gautier et al. 2018).

Following a similar orientation and bordering the lowland forests are the humid forests which range in elevation from 1800 – 2000 masl occupying an area of approximately 72,000 km^2. In Madagascar, the humid forest is characterised by multi-strata closed formation, mainly composed of evergreen trees, often richly branched with a closed canopy between 10 and 20 m and emergent trees up to 30 m (Figure 2.2c). The dominant tree families are similar to the lowland ecoregion, epiphytes and lianas are frequent and trunks and branches are covered with mosses and lichens. Depending on the topographic position, the undergrowth is variable, typically, sparse in low-lying areas, although a significant herbaceous layer can occur on high slopes and ridges, where the canopy is often more open and often sclerophyllous (Gautier et al. 2018).

The western dry forests occur along the western axis and in the extreme north, bordering the Mozambique channel in some parts with an elevation range of 0 – 1350 masl and covers approximately 24,000 km^2 of land area (Moat and Smith 2007). In this ecoregion, largely-intact forest formations are multi-layer, mainly composed of deciduous trees, with a closed canopy between 10 and 20 m, and emergent trees up to 30 m (Figure 2.2d). The undergrowth tends to be sparse, without a continuous herbaceous layer. Dominant families include Malvaceae (*Adansonia*, *Grewia* and *Hildegardia*.), Fabaceae, Burseraceae

(*Commiphora* and *Ambilobeia*), Capparaceae, Bignoniaceae (*Stereospermum*), Oleaceae (*Noronhia* and Anacardiaceae (Gautier et al. 2018). The Tapia forests are located in the central highlands dissecting the grasslands/shrublands in some places, they are also found in relatively large patches along the south-west region (Figure 2.1). Tapia forests occur between an elevation of 300 – 1800 masl and cover an area of approximately 1470 km^2 (Kull 2002, Rakotondrasoa et al. 2012). They are characterised by closed formation, with a canopy between 10 and 15 m (Figure 2.2e). They are mainly composed of evergreen trees, dominated by Sarcolaenaceae, *Asteropeia* (Asteropeiaceae), and *Uapaca bojeri* (Phyllanthaceae), as well as *Weinmannia* (Cunnoniaceae), Anacardiaceae (*Protorhus* and *Rhus*), and Asteraceae (*Brachylaena merana* and *Dicoma incana*). Epiphytes are limited to some Orchidaceae and lianas are rare (Gautier et al. 2018).

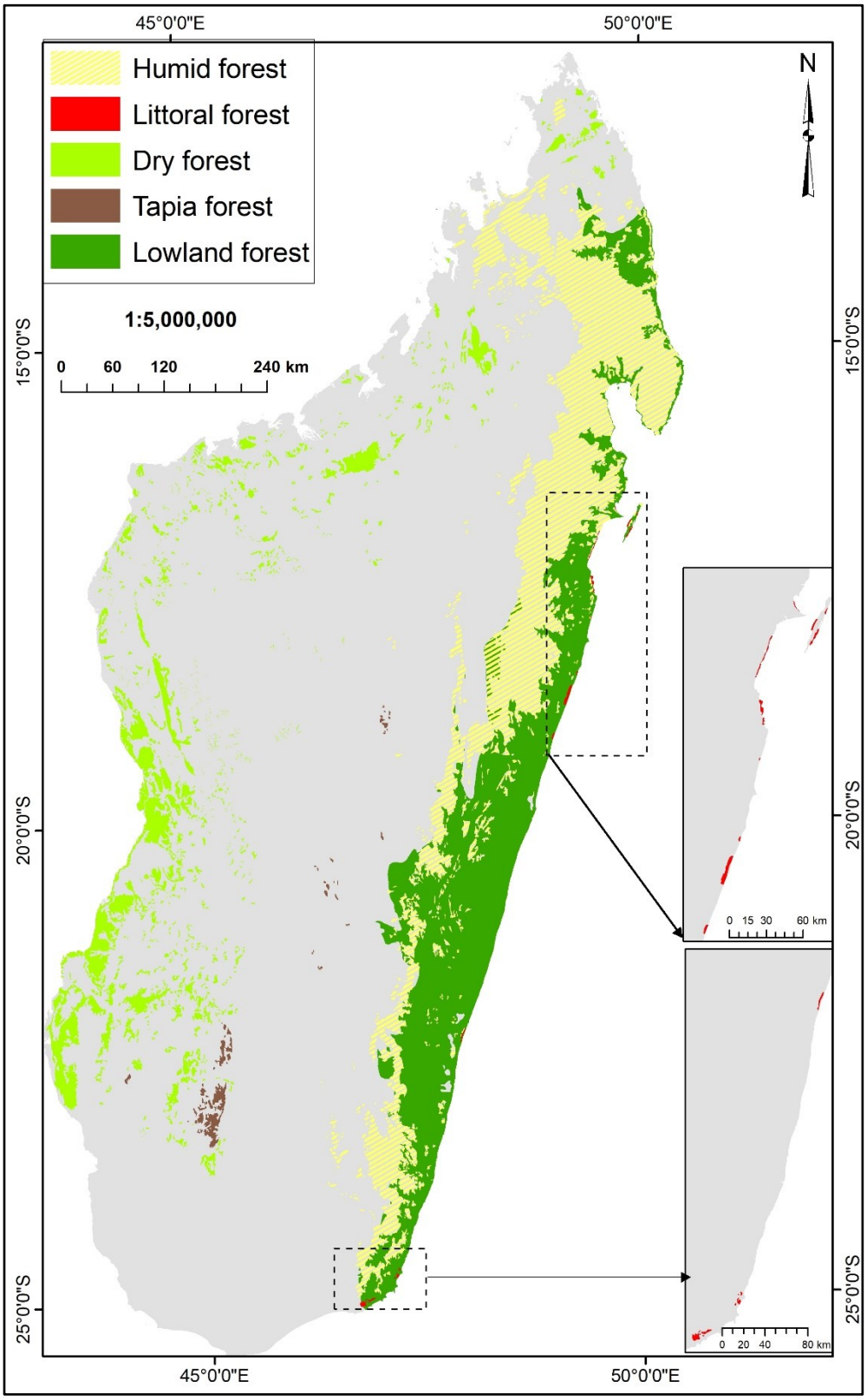

Figure 2.1: Selected eco-regions of Madagascar showing regions of forested areas. Insets are littoral forests on the eastern coast of the Island. Eco-regions shapefiles downloaded from Royal Botanic Gardens, Kew website and cartographic visualisation implemented in GIS. *Map projection: Geographic coordinate system using WGS1984 datum.*

Figure 2.2: Photographs of dominant vegetation types in five ecoregions: *Top row (l-r):* Littoral and humid forests. *Middle row (l-r):* lowland and western dry forests. *Bottom row:* Tapia forest.

The nature of vegetation and prevalent bioclimatic conditions of each eco-region is partly defined by elevational differences, as well as their relative location to the tropical ocean and monsoon wind regimes (Goodman and Benstead 2003, CEPF 2005). These climatic factors also influence the temperature across this region: the mean annual temperatures are highest along the dry west coast and coolest over the central upland plateau. The minimum temperatures are experienced in winter, on average it is less than 5° C during June and July in the highlands, while maximum temperatures (average >36°C) occur in spring between the months of October and November over the west coast (Tadross et al. 2008).

2.2 Selection of satellite imagery

2.2.1 Landsat Image Characteristics

The following imagery were used for LULCC assessment: Landsat Thematic Mapper (TM), Enhanced Thematic Mapper plus (ETM^{+}) and Operational Land Imager (OLI) (consisting of path 157 row 71, paths 158 – 159 rows 68 – 78 and paths 160 & 161, rows 171 -176). All datasets were obtained from the archives of United States Geological Survey via the Global Visualization viewer (GloVis) and had a 30-m spatial resolution (http://glovis.usgs.gov/) (see Appendix 1 for details of temporal resolution). The satellite images collected enabled repetitive measurements of land cover change covering 20 years in three image time stamps. The first-time stamp was composed of Landsat TM images from predominately 1994, but also included 1995 and 1996. The second-time stamp comprised of Landsat ETM^{+} images from 2000, 2001 and predominantly 2002. The third-stamp included Landsat OLI images from 2013 and predominately 2014. In total, 34 image scenes were obtained for each time stamp and were selected based on date of image acquisition (late dry to early rainy season) and absence of cloud cover (<10%). However, in some instances there were significant amount of cloud cover causing data artefacts mainly in the c. 1994 and c. 2002 time-stamps (Table A1 and Appendix 2). Similarly, lack of cloud-free images for some areas resulted in the selection of earlier or later months and years image scenes e.g., path

158 row 77 (TM sensor). There was minimal risk that differences in months could introduce seasonality into the analysis; however, the number of scenes with early or later months were negligible. The analyses were carried out in two intervals: the first interval consisted of images from ca. 1994 to ca. 2002; while the second interval was defined by images from ca. 2002 to ca. 2014. All Landsat imagery was Level 1T, which had been processed for radiometric calibration and geometric correction using digital elevation models of terrestrial surface of Madagascar (Lee et al. 2004).

2.3 Assessing rates of deforestation and forest degradation

The proportion of deforestation and forest degradation in each interval was estimated using CLASlite v3.3 (http://claslite.carnegiescience.edu/en/about/software.html).The analysis required the use of forest cover, deforestation and forest degradation obtained from Landsat imagery to analyse sub-spectral characteristics of pixels across Madagascar (Martínez et al. 2006, Asner et al. 2009). The images were corrected for radiometric errors caused by atmospheric attenuation using rescaled gains and bias (offsets) parameters provided for each band. These steps are standard procedure for radiometric corrections in CLASlite (Figure 2.3). The spectra sub-model is made up approximately 400,000 of field and spaceborne samples collected from tropical forests mainly in Central and South America as well as pacific islands. Such abundance of samples and large geographical coverage in the spectral libraries makes CLASlite suitable for application in assessment of Madagascan forests.

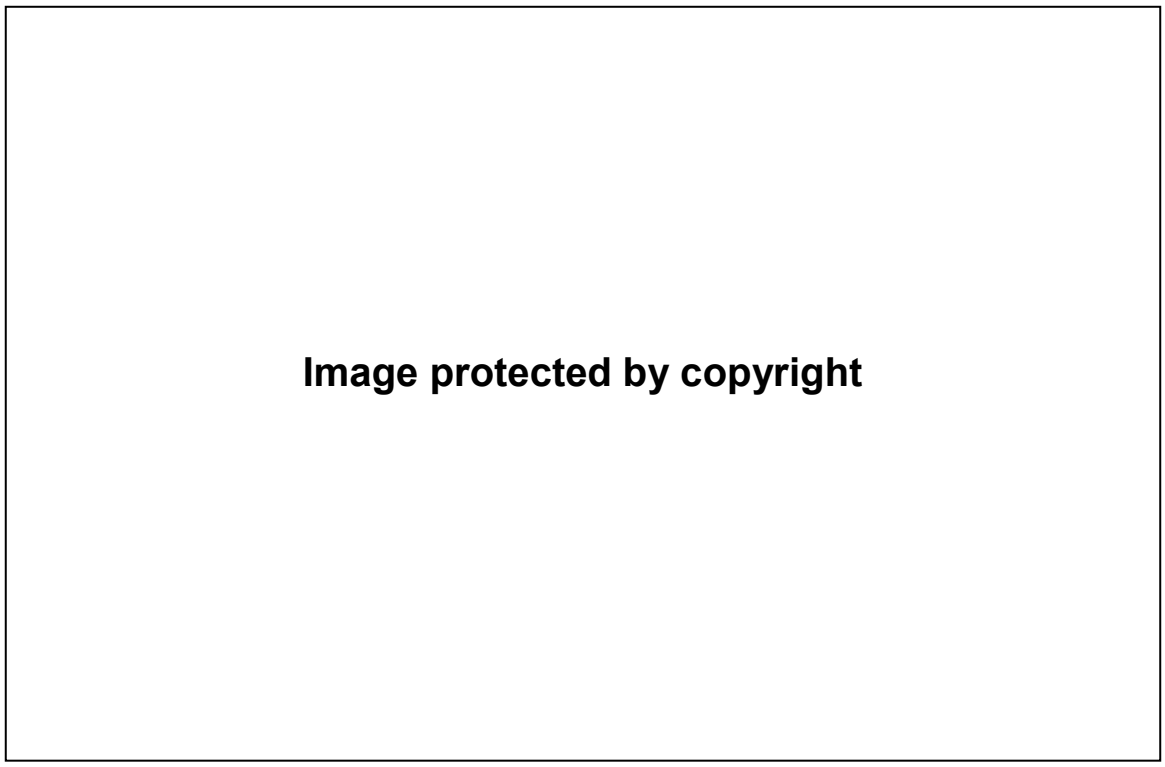

Figure 2.3: Schematic representation of the main processing steps (rhombus shapes) in CLASlite used in detecting deforestation and forest degradation. *Modified from Figure 1, Asner et al. (2009).*

These rescaled values underwent a second simulation (i.e., through 6S transfer model) that resolved errors untreated during the initial rescaling process, before the radiance values were converted to surface reflectance values (Vermote et al. 1997). The simulation model used NASA's MODIS data in the background to modulate the effect of the atmosphere on sun rays as it interacts with the atmosphere and land surface. Afterwards, the raw Landsat imagery input was then corrected by removing the estimated model of the atmosphere, leaving an image of the resultant surface reflectance (0-100%). Thereafter, each image scene was examined to determine the suitable threshold to set the mask for water, clouds and shadow (reduced masking approach); this was done to avoid over-masking, especially in areas of high relief. Next, the composition of each pixel fraction was determined using Auto Monte Carlo pixel-Unmixing (AutoMCU) (Quintano et al. 2012), a probabilistic algorithm that takes each input pixel reflectance value and decomposes it into three component fractions: photosynthetic vegetation (live vegetation), non-photosynthetic vegetation (dead vegetation) and bare substrate using Equation 2.1.

Equation 2.1: $^{p}(\lambda)_{pixel} = \sum [C_e * {}^{p}(\lambda)_e] + \varepsilon$

But, $\sum [C_e * {}^{p}(\lambda)_e] + \varepsilon = [C_{pv} * {}^{p}(\lambda)_{pv} + C_{npv} * {}^{p}(\lambda)_{npv} + C_{substrate} * {}^{p}(\lambda)_{substrate}] + \varepsilon$.

Where: $^{p}(\lambda)e$ *is the reflectance of each land-cover end-member (e)*[1] *at wavelength,* λ. C_e *is the sub-pixel cover fraction and* ε *is an error term explained by the root mean square error.* C_{pv} *is the fraction of photosynthetic vegetation,* C_{npv} *is the fraction of non-photosynthetic vegetation and* $C_{substrate}$ *represents the bare surface, geologic materials, senescent vegetation.*

During the process of pixel decomposition, each fraction component was compared with historical modelled values in CLASlite's spectral libraries. These spectral libraries consisted of large collections of representative samples of individual components (substrate, live and dead vegetation) corresponding to pure spectra for each of the land cover components (i.e., spectral end-members). The end-member libraries in CLASlite are available for tropical regions only and consist of detailed signatures of bare substrate and dead vegetation ground-truthed using field observation. Live vegetation signatures were collected from airborne hyperspectral sensors due to the impediments associated with tropical forest landscapes usually in the form of large crowns and basal areas. Previous studies have demonstrated the effectiveness of AutoMCU in mapping tropical ecosystems, including savanna, woodland, shrubland and broadleaf forests (Asner et al. 2005, Allnutt et al. 2013). Next, the pixel values were analysed using decision trees, where splits were based on analyses of differences between pixel components (i.e., substrate, live and dead vegetation) at the start and end of time intervals (Stage 6, Figure 2.3). The differences in the proportion of these components from 1994 to 2014 were used to determine deforested and degraded pixels. Generally, reductions of live vegetation within pixels that were ≥60% represented deforested pixels, while those ≥40% suggested forest degradation (Asner et al. 2009).

[1] *The land cover end members are representations of the different vegetation states common to tropical forests, namely: photosynthetic vegetation (live), non-photosynthetic vegetation (dead) and bare substrate.*

The process of decomposition required the identification of the optimum threshold for which pixel's component could be quantified into different fractions. In moist eco-regions (i.e., littoral, humid and lowland forests) live vegetation components were predictably higher for most pixels (average 90%), 5% for dead vegetation components and negligible values for bare substrate. Whereas in western dry forests, live vegetation component values were comparably lower than those of humid forests, averaging 80% per pixel, while dead vegetation and bare substrate values were on average around 15% and 5%, respectively. In the tapia forests, there was very wide variation in all three component values measured during pixel un-mixing. Therefore, a 50% threshold was selected for live vegetation decomposition. For each interval, the sizes of deforested and degraded area were determined in GIS and represented the portion of the pixels whose live vegetation fraction was below 60% and 40%. The rates of deforestation and degradation were calculated and a Welch's *t*-test was performed to determine whether there were any significant differences between deforested and degraded area sizes between intervals (i.e., 1994 – 2002 and 2002 – 2014).

2.4 Quantifying errors in sub-pixel analysis

The uncertainties associated with the results of deforestation and forest degradation rates were quantified using a combination of standard deviation and root mean square error (RMSE). Standard deviations were determined for individual pixel solutions (i.e., proportions of substrate, live and dead vegetation) and shows the dispersion from the modelled mean for each pixel (MODIS data) after 30 iterations. The root mean square error compared the difference between predicted end-member values for the region and measured end-member values quantified from the input images. Both the standard deviation and RMSE of the modelled results allowed for assessing the accuracy of the rates of deforestation and forest degradation.

2.5 Modelling land use land cover change

Following the classification scheme of Moat and Smith (2007) for Madagascar, land use land cover categories were identified in each eco-region. Moat and Smith (2007) classification of Madagascar's land cover categories included forest, vegetation matrix, cultivated land and exposed surface (Table 2.1).

Table 2.1: Description of the different land cover classes used in image classification. Land cover classes were modified following the work of Moat and Smith (2007).

Land cover category	Description	Reference in Moat and Smith
Forest	A continuous stand of trees at least 10 m tall, their crowns interlocking	Forest
Vegetation matrix	An open stand of trees between 2-8 m tall with a canopy cover of 40 % or more. The field layer is usually dominated by grasses and other herbs.	Woodland, Shrubland and grassland
Cultivated land	All types of plantation including irrigated and rain-fed farmlands	Cultivated land
Exposed surface	Cleared portions of the landscape made up of expose geological materials or sediments	Rock outcrops, exposed surface

Before classifying the imagery, training sites were identified randomly with the aid of high-resolution Quick Bird images (Google Earth) in ERDAS Imagine (Vieilledent et al. 2013, DeVries et al. 2015), as well as sites selected from multiple land cover categories directly observed by Brown et al. (2013) during their field research in Madagascar. On average 50 training sites were selected eco-region with exemption of the littoral forest. Thereafter, the images (i.e., each time-stamp) were classified into land use land cover maps using the maximum likelihood technique and their accuracy provided **(Sections 2.7 and 4.3.3)**. The derived maps were cross-tabulated to obtain a square contingency table of land cover transitions to determine three-pixel states in each interval: (i) persistence; (ii) gains and (iii) losses. Thereafter, intensity analysis was implemented to determine causes of land cover transitions and to partition the speed and magnitude of these transitions into two-time intervals (e.g., ca. 1994 – 2002 and ca. 2002 – 2014) (Aldwaik and Pontius 2012). This approach of quantifying LULCC follow the method developed by Aldwaik and Pontius (2012) which explicitly measures the annual, category and transition intensity between two images under a unified framework (Figure 2.4.).

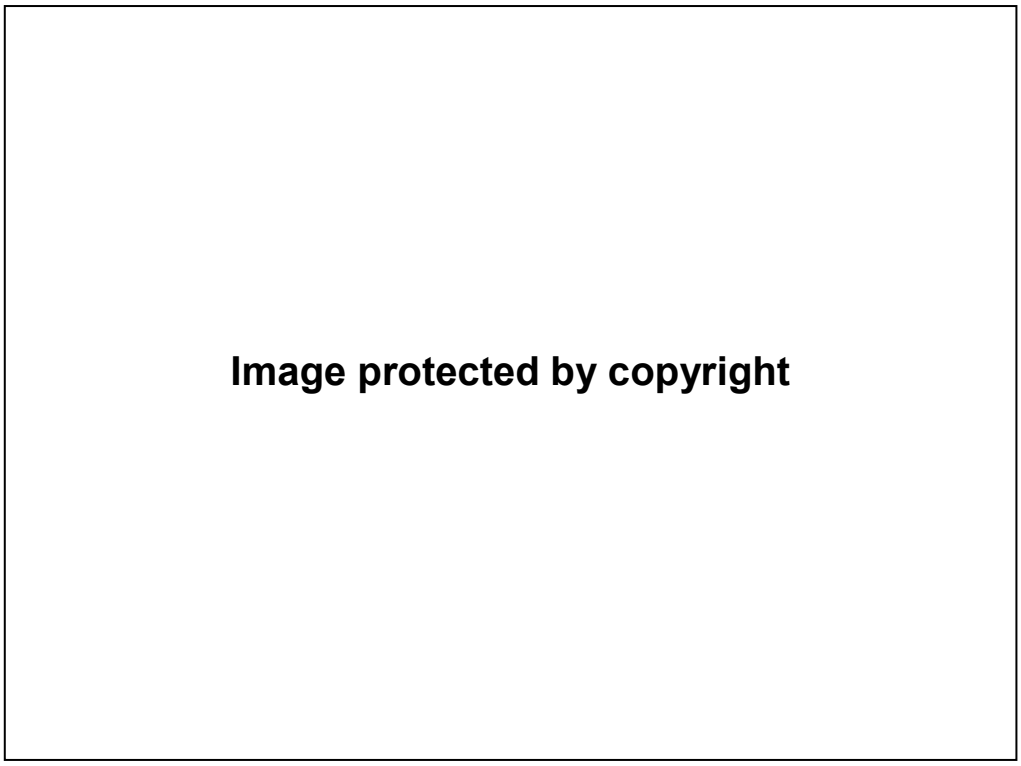

Figure 2.4: Schematic diagram showing the main steps in intensity analysis between two image dates. *Representation from Aldwaik and Pontius (2012), Figure 2.*

Two component parts of transition intensity (i.e., observed and uniform intensities) were quantified. Observed intensity measures annual area of gain or loss from any given land cover category to a new category relative to the size of the new category in subsequent years (i.e., 2002 and 2014). Uniform intensity quantifies the area of gross gain or gross loss of any given category relative to the area of all other categories in subsequent years – i.e., category intensity (Figure 2.4). Thus, in each interval uniform intensity for each observed transition was estimated to explain differences in the rate of change and how these differences affected gross gains or losses. The estimated rates represent measures of speed of category transitions. Furthermore, the annual observed transition intensity for different land cover category swaps relative to the speed of other transitions taking place in each interval was quantified. The observed transition intensities were aggregated to determine the magnitude of land cover category swaps and their intensity of gains and losses in each interval (Table 2.2). Gains were determined relative to magnitudes of LULCC categories in the initial year and losses relative to the magnitudes in the subsequent year for each category

swap in each interval. The differences between observed and uniform intensities indicated whether category swaps were uniform (closer to zero) or systematic (farther from zero); in this instance added differences were a means to determine dominant from random transitions. As a result, transitions were determined from the perspective of gains and losses.

Table 2.2: Description of uniform and observed intensities metrics used in intensity analysis

Metric	Definition	Term used in text
Observed intensity	annual area of gain or loss from any given land cover category to a new category relative to the size of the new category in subsequent year.	Magnitude
Uniform intensity	the estimated rates represent measures of speed of category transitions relative to all non-transiting categories	Speed

Transitions from forest pixels to all non-forest state pixels (i.e., vegetation matrix, cultivated land, exposed surfaces) was used as implicit measure of estimating drivers of deforestation and forest degradation. Likewise, transitions from vegetation matrix to exposed surface and cultivated land, as well as all transitions from cultivated land to exposed surface were considered as drivers both deforestation and forest degradation. Transitions from the perspective of forest and vegetation matrix gains from exposed surface and cultivated land was also quantified, at the same time transitions from vegetation matrix to forest were also determined. The determination was based on the differences in magnitude and speed (fast or slow) across eco-regions. These categorisations allowed assessment of how the magnitude, speed and nature of transitions vary between eco-regions over 20 years.

2.6 Predicting future LULCC

Future LULCC was determined using the land change modeler (LCM), which is a module available in IDRISI TerrSet software package. LCM has shown higher allocation and configuration accuracy when compared with other spatial-based land change models (e.g. GEOMOD), strengths that are particularly suitable for ecological modelling (Pickard et al. 2017). To effectively determine category transitions from the last date (i.e., 2014) to the future 2050, LCM required certain key components to be in place. First, the change analysis described in **section 2.5** was used to determine the number of new pixels to allocate for any given swaps based on change detection (i.e., gain, loss and persistence) during the second interval. Then the transition potential model was developed with elevation, deforestation and forest degradation sizes as drivers. The transition potential (sub-model) estimated the site suitability for allocation of pixels in the future and by using the multi-layer perceptron (MLP) network all possible category transitions were simultaneously produced and based on the main transitions that occurred in the second interval (Atkinson and Tatnall 1997, Maggiori et al. 2017). In addition to handling multiple transitions, it was possible to map the probability of each categories transitioning, given the allocated quantity in the second interval. For each eco-region, 10,000 random samples of pixels encompassing all category state (i.e., gain, loss and persistence) was used and was evenly split to train and test sub-model performance in predicting change. Other default settings were accepted and the model was able to find the optimal training without further intervention. Finally, to determine the expected quantity of pixels that would transition in 2050 in each eco-region, change predictions were implemented using the Markovian module, which takes into consideration the site suitability surfaces and second interval LULC maps. The Markovian process enabled the quantification of the probabilities of pixels transitioning (i.e., soft predictions. Furthermore, Markovian process allowed the allocation of land cover categories in 2050 from a host class in the 2014 maps based on the derived quantity of change (i.e., hard predictions) for each eco-region.

2.7 Accuracy assessment of land cover maps

Accuracy assessment was implemented for two land cover maps (i.e., *ca. 2002 and ca. 2014)* using reference pixels to determine the quality of the maps produced for both time-stamps. Reference pixels were independent of the training samples used during image classifications and were assessed against verification datasets. The verification datasets consisted of 250 locations randomly selected across the landscape. Due to paucity of high-resolution images on Google Earth for the 1990s, there was no verification datasets for the ca. 1994 land cover map. However, the accuracy of the ca.1994 maps should not differ significantly in accuracy from those of subsequent time-stamps, due to similarity in the classification technique and algorithm.

To account for bias in sampling intensity commonly associated with different sized land cover categories, the different measures of accuracy were weighted against the proportion of the categories in each map (Olofsson et al. 2014). The first step was to produce error matrices to express the number of reference (sample) pixels assigned to different land cover categories relative to the verified datasets collected from Google Earth. Afterwards, accuracy of the classifications was calculated and expressed as three metrics: overall accuracy (OA), user's accuracy (UA) and producer's accuracy (PA). The OA for each classification was derived by dividing the number of total correct (diagonal) by the total number of pixels in the error matrix. The PA determines the probability of correctly classifying a reference pixel - also known as error of omission; obtained by dividing the total number of correct pixels of any given category by the total number of pixels of that category in the reference data. The UA provides the probability that a pixel classified on the map corresponds to the same category in the verification data and is known as error of commission. It was calculated from the total number of correct pixels per category divided by the total number of pixels classified in that category.

Chapter Three

Quantifying deforestation and forest degradation at eco-regional scale

3.1 Introduction

Tropical forests make up fifty-two per cent of global forests and are mostly found in Africa, South America and South-East Asia (FAO 2015). They also harbour two-thirds of the world's terrestrial biodiversity (Whitmore 1998) and 96% of the world's estimated tree species (Fine et al. 2009). Despite their global ecological significance, these habitats are under unprecedented pressure from a variety of factors, including large-scale forest clearance, as well as small-scale conversions leading to deforestation and forest degradation (Vieilledent et al. 2013). Deforestation involves rapid clearing of large swaths of forests; while forest degradation mainly occurs from persistent and subtle thinning in forest cover – ultimately resulting in the landscape mosaic comprising of secondary forests, vegetation matrix and fragmented forests (Ghazoul et al. 2015). Both processes are usually accompanied by marked changes to forest structure, species composition, and biodiversity (Achard et al. 2014, Barlow et al. 2016). The recent assessment of global forest conditions showed slight reductions in the rate of forest loss in the last decade, mostly caused by downward trends within temperate and boreal forests (Keenan et al. 2015). Despite these positive signs, elsewhere, tropical forests still showed net losses and accounts for 32% of global forest loss at a rate equivalent to 2010 km^2 per year (Hansen et al. 2013, Sloan and Sayer 2015). Moreover, other global analyses predict an increase in threats to primary forests and increase risks of deforestation in sub-Saharan Africa (Achard et al. 2014). Some of the rising risks are attributed to stricter land use regulations in South America causing translocation/offshoring of export-oriented commodities to sub-Saharan Africa (Elsa et al. 2017).

These recent trends are emerging on the backdrop of concerted efforts towards reducing tropical deforestation and degradation by biodiversity initiatives concentrated in tropical regions (Soares-Filho et al. 2006, Panfil and Harvey 2015). Interestingly, there is evidence suggesting that whilst large-scale forest losses may be stagnant or declining for most regions there are increases in small-scale losses, i.e., forest degradation (Barlow et al. 2016, Aleman et al. 2017). Remote sensing techniques have enabled easy detection and monitoring of deforestation in tropical forests, while degradation is more difficult to quantify even by *in-situ* measurement (Berenguer et al. 2014). Whether natural, anthropogenic, landscape-scale or within-forest disturbances, quantifying tropical forest degradation has been historically challenging (Stibig et al. 2014, Barlow et al. 2016). The restriction has always been that degradation requires identification of subtle changes in canopy cover occurring over small spatial scales, usually not readily available from remotely sensed data. These difficulties notwithstanding, it is becoming increasingly clear that accurate quantification of forest degradation in the tropics is vital, since the proportion of global forest affected by degradation is rising faster than areas impacted by deforestation (Herold et al. 2011, Berenguer et al. 2014, Barlow et al. 2016) and many avoided deforestation schemes rely on estimates of both deforestation and degradation (e.g., Reduced Emissions from Deforestation and Degradation, REDD+). On the other hand, there is evidence that rates of forest loss have not been even historically especially along elevation (Hall et al. 2009, Marshall et al. 2012). For instance, Hall et al. (2009) report that forest loss in the upper montane zones of Eastern Tanzania were lower by 40% than those in sub-montane forests. Furthermore, disparities between high above-ground live carbon at intermediate elevation compared to high elevation suggests more nuanced analysis of deforestation and forest degradation along elevation gradients (Marshall, et al. 2012, Asner et al. 2014). As such in this chapter I characterise deforestation and forest degradation rates along elevation gradients using two approaches namely: equal area and equal interval.

Overall, both deforestation and forest degradation are estimated to account for approximately 18-20% of total carbon emissions from land-use and land-cover change (LULCC) in tropical developing countries (Houghton 2013). Reducing these emissions represents one of the fastest, most cost-effective approaches for mitigating the effects of climate change in the short term (Vieilledent et al. 2013).

3.1.1 Deforestation and forest degradation in Madagascar

Reliable estimates of deforestation and forest degradation rates for Madagascar are affected by a near lack of unified historical baseline data on forest cover (Kull 2012). This has led to different estimates of deforestation and in some cases, contentious assessments of forest cover change (McConnell and Kull 2014, Aleman et al. 2017). Several studies have attempted to characterise changes taking place in Madagascan forests. Hansen et al. (2008) estimated deforestation rates of <0.7% for tropical Africa including Madagascar; others have focused on structural characterisation of lowland forests (Ingram et al. 2005), patterns of forest patches and changes in forest edges in humid and dry forest regions (Zinner et al. 2014) or comparing the accuracy of different approaches in estimating forest cover losses (Grinand et al. 2013). Most of these studies utilise whole pixel image differencing to assess forest cover change and are unable to account for the fine-scale processes caused by forest degradation (Harris et al. 2012). Still, Allnutt et al. (2013) take a sub-pixel approach for investigating deforestation and degradation within Masaola National Park and show significant losses in forest cover within six years, with minimal differences (±0.03%) between deforestation and forest degradation rates.

In this chapter, deforestation and forest degradation rates are mapped for five eco-regions using a sub-pixel analysis, which assessed changes in forest cover at ≤0.1 ha resolution. Secondly, I investigate whether the impact of land-cover driven shifts is already evident in all habitat types, as well as at low, intermediate and high elevations. This is to confirm the severity of lowland attrition in the different eco-regions and whether landscape-

scale changes in forest structure differ with elevation. In addition, I investigate whether available area along elevation gradient influences deforestation and forest degradation rates by assessing the rate of change using equal area and interval methods. Original estimates of deforestation and forest degradation were estimated, rather than rely on a global forest change data set. This eco-regional approach was adopted to highlight regional differences in deforestation and forest degradation across the island as they may be driven by distinct causes locally, or different biomes may respond differently to similar pressures. This assessment includes the following: i) estimates of past rates of deforestation and forest degradation, ii) measures of their associated uncertainty and iii) comparative analysis between intervals (i.e., 1994 – 2002 and 2002 – 2014) of sizes of deforestation and forest degradation. There were no *a priori* predictions about which eco-regions would exhibit the highest or lowest rates of deforestation and forest degradation. Also, a detailed assessment of localized forest changes caused mainly by subtle, small-scale disturbances is provided at an Island-wide scale.

3.2 Methods

The analysis presented here was implemented for estimating deforestation and forest degradation rates from satellite imagery over 20 years by means of sub-pixel analysis to quantify eco-region differences across Madagascar (Figure 3.1) and are described in detail in **Chapter 2, section 2.3**. Likewise, the approach used to determine the uncertainties associated with quantification of deforestation and forest degradation is described in **Chapter 2, section 2.4.** To avoid any confusion in what is considered deforested or degraded areas, regions that possess predominantly grasslands, shrublands and thickets vegetation types were excluded from the analysis. That is to say, only eco-regions with known forest were mapped for deforestation and forest degradation rates (see, Figure 2.1).

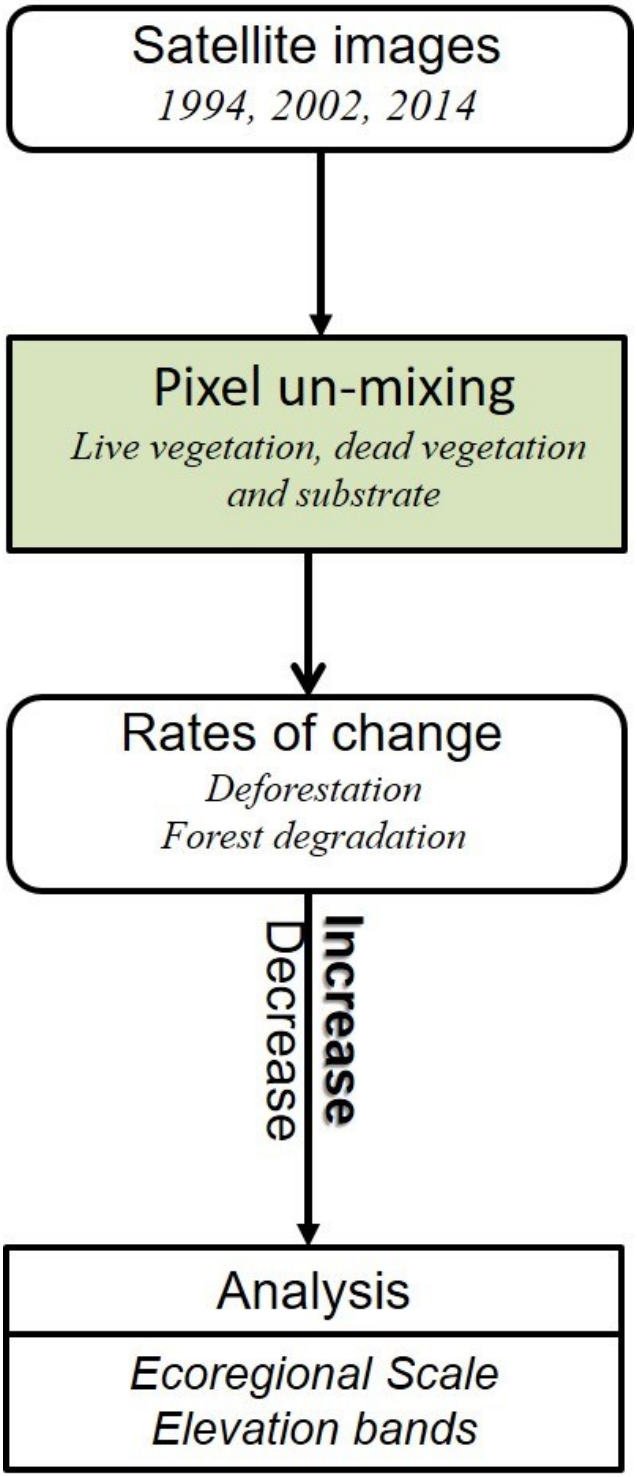

Figure 3.1: Methodological approach showing key steps taken for the implementation of sub-pixel analysis. Steps include interval data (i.e., 1994 – 2002 and 2002 – 2014), decomposition of pixels to three component fractions (i.e., live vegetation, dead vegetation and substrate) and analysis of rate of change by eco-regions and elevation.

3.2.1 Digital Elevation Models

For the discrimination of deforestation and forest degradation rates along elevation gradients at eco-regional scales and across specified elevation bands on an Island-wide scale, I used two sets of digital elevation models of terrestrial surface of Madagascar. These were Shuttle Radar Topography Mission Digital Elevation Model (SRTM-DEM) and the Advanced Space-borne Thermal Emission and Reflection Radiometer Global Digital Elevation Model (ASTER-GDEM). SRTM-DEMs have a spatial resolution of 90 m around the equator, a vertical accuracy of 16 m and utilises synthetic aperture radar to capture the earth terrain using interferometric. They were acquired using Space borne Imaging Radar-C/X-band Synthetic Aperture Radar (SIR-C/X-SAR) mounted on dual antennas (Guth 2010). ASTER-GDEM comprised of high horizontal spatial resolution (30 m), a near-pixel-size vertical accuracy and broad spectral coverage in the visible near, shortwave and thermal infrared regions of the electromagnetic spectrum. SRTM was capable of discriminating between deforestation and forest degradation at different elevation bands in humid, lowland, tapia and western dry forests, however, it was impossible to undertake the same analysis for littoral forests due to their relatively small sizes. As such, for littoral forests, ASTER dataset was utilised for elevation band discrimination of both deforestation and forest degradation.

3.2.2 Elevational analysis of deforestation and forest degradation

Elevation bands were categorised for both ASTER and SRTM DEMs using GIS spatial analyst tools. Five elevation bands were created using two classification methods - equal interval and equal area for each eco-region (Li and Wang 2012). For equal interval classification, the elevation was partitioned into bands such that each band had the same range of values and the difference between the high and low elevation values was similar. In equal area classification, eco-regions elevation gradients were divided into bands of approximately equal total area (Mitchell 1999). Deforestation and forest degradation rates were quantified in each band interval: first in each eco-region and then across the island.

Band interval analysis was performed by clipping the detected areas of deforestation and forest degradation for each band width.

3.3 Results

3.3.1 Eco-regional scale deforestation and degradation rates

Sub-pixel analysis showed that the lowland forest was the only eco-region to show increased deforestation rates (3.72% **yr^{-1}**) on the Island (Table 3.1) and the only eco-region to show increased forest degradation rates was the littoral forest (0.06% **yr^{-1}**). Tapia forest had the lowest deforestation (-0.87% **yr^{-1}**) and forest degradation (-0.61% **yr^{-1}**) rates. Eco-regions with higher deforestation rates did not appear to have equally higher forest degradation rates when compared with other eco-regions (Table 3.1). For instance, although lowland forest showed high deforestation rates, it had one of the lowest degradation rates. As a result, deforestation rates increased in lowland forests and reduced in all other eco-regions, albeit at differing rates of forest loss. Forest degradation rates increased within littoral forests but decreased in the other four eco-regions.

Table 3.1: A summary of deforestation and forest degradation rates as quantified from sub-pixel analysis for selected eco-regions of Madagascar. Rate of change is calculated by taking the difference between first (1994 – 2002) and second (2002 – 2014) intervals divided by first interval area.

Eco-region	Deforestation (ha)		RoC (% yr^{-1})	Degradation (ha)		RoC (% yr^{-1})
	1994 - 2002	2002 - 2014	1994-2014	1994 - 2002	2002- 2014	1994-2014
Lowland forest	204841	966023	**3.72**	91124	53339	**-0.41**
Humid forest	293986	233584	**-0.21**	90159	83965	**-0.07**
Dry forest	222040	135577	**-0.39**	22775	17602	**-0.23**
Littoral forest	859	341	**-0.60**	135	143	**0.06**
Tapia forest	7353	961	**-0.87**	2142	834	**-0.61**

Comparatively, the dry forest had lower deforestation and forest degradation rates (RoC) than the humid forest. On the other hand, while deforestation rates in lowland forest were higher than those in dry forest, forest degradation rates in dry forest higher than those in tapia and lowland forests (Table 3.1).

3.3.2 Comparing sizes of deforestation and forest degradation by intervals

Interval comparisons indicated that deforestation events (measured from individual pixel sizes determined to be deforested) were smaller in the first interval (1994 – 2002) compared to the second interval (2002 – 2014) for humid, lowland and dry forests (Table 3.2). The exceptions were in tapia forests, where first interval sizes of deforestation were on average larger ($\bar{x}$ = 0.52, s = 1.42) than second interval ($\bar{x}$ = 0.48, s = 1.18) and the littoral forests where average numerical sizes of deforested areas were smaller in the second interval ($\bar{x}$ = 0.63, s = 1.93) compared to first interval ($\bar{x}$ = 0.93, s = 5.53). Overall, average sizes of deforested areas in the first interval were statistically larger than in second interval in humid and lowland forests. In littoral, western dry and tapia forests there are no significant differences between the average sizes of deforestation events in the first and second interval.

Table 3.2: Comparative analysis of mean sizes of deforestation (def.) and forest degradation (deg.) categorised by intervals for selected eco-regions of Madagascar. Statistically significant results between intervals are highlighted in bold.

Eco-region	Interval	Mean def. area (Ha)	SD$^{\delta}$	Sig$^{\downarrow}$. (α=0.05)	Mean deg. area (Ha)	SD$^{\delta}$	Sig$^{\downarrow}$. (α=0.05)
Humid forests	1994 - 2002	0.69	3.88	**<0.001**	0.18	0.24	**<0.001**
	2002 - 2014	0.74	3.45		0.19	0.28	
Lowland forests	1994 - 2002	0.50	1.61	**<0.001**	0.18	0.22	**<0.001**
	2002 - 2014	0.58	1.94		0.18	0.26	
Littoral forests	1994 - 2002	0.93	5.53	0.13	0.15	0.17	**<0.001**
	2002 - 2014	0.63	1.91		0.19	0.26	
Dry forests	1994 - 2002	1.45	68.23	0.71	0.17	0.40	**<0.001**
	2002 - 2014	1.52	29.67		0.20	0.54	
Tapia forests	1994 - 2002	0.52	1.42	0.21	0.16	0.19	**0.01**
	2002 - 2014	0.48	1.18		0.15	0.18	

$^{\downarrow}$ denotes the significance of Welch two sample *t*-test analysis and $^{\delta}$, denotes the respective standard deviations

The average sizes of degraded areas were marginally smaller in the first interval than in the second interval in the humid, littoral and western dry forests. In lowland forests, the average degraded area in both intervals were similar (Table 3.2). Only in the tapia forests were first interval ($\bar{x}$ = 0.16, s = 0.19) degraded areas larger than second interval ($\bar{x}$ = 0.15, s = 0.18) sizes. The results indicated that the sizes of forest degradation were larger in first interval compared to second interval in all five eco-regions. Though it is worth mentioning that the sizes of forest degradation did not substantially change between eco-regions (Figure 3.3). When comparing between eco-regions, western dry forests had the largest deforested areas on average, while humid and lowland forests had the largest sizes of degraded areas in the first interval (Table 3.2). Furthermore, the *t*-test analysis revealed that in the second interval, western dry forests had on average the largest deforested and degraded areas compared to all other eco-regions.

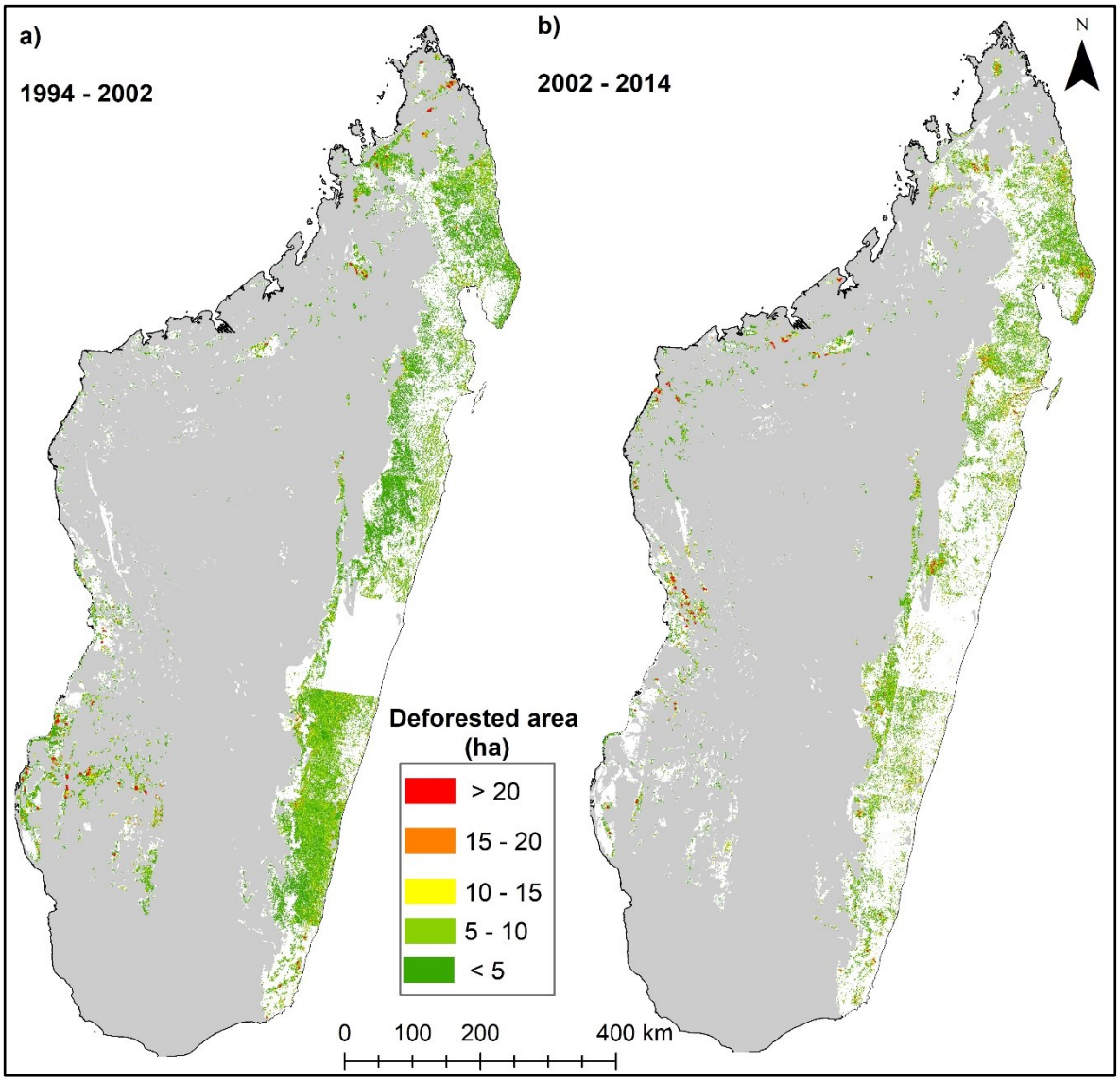

Figure 3.2: Outputs of sub-pixel analysis showing areas impacted by deforestation in a) 1994 – 2002 and in b) 2002 - 2014. Deforested areas were visually enhanced to improve the map representation. Areas affected by data artefacts are clearly visible in the eastern forest corridor and as shown in Appendix 2.

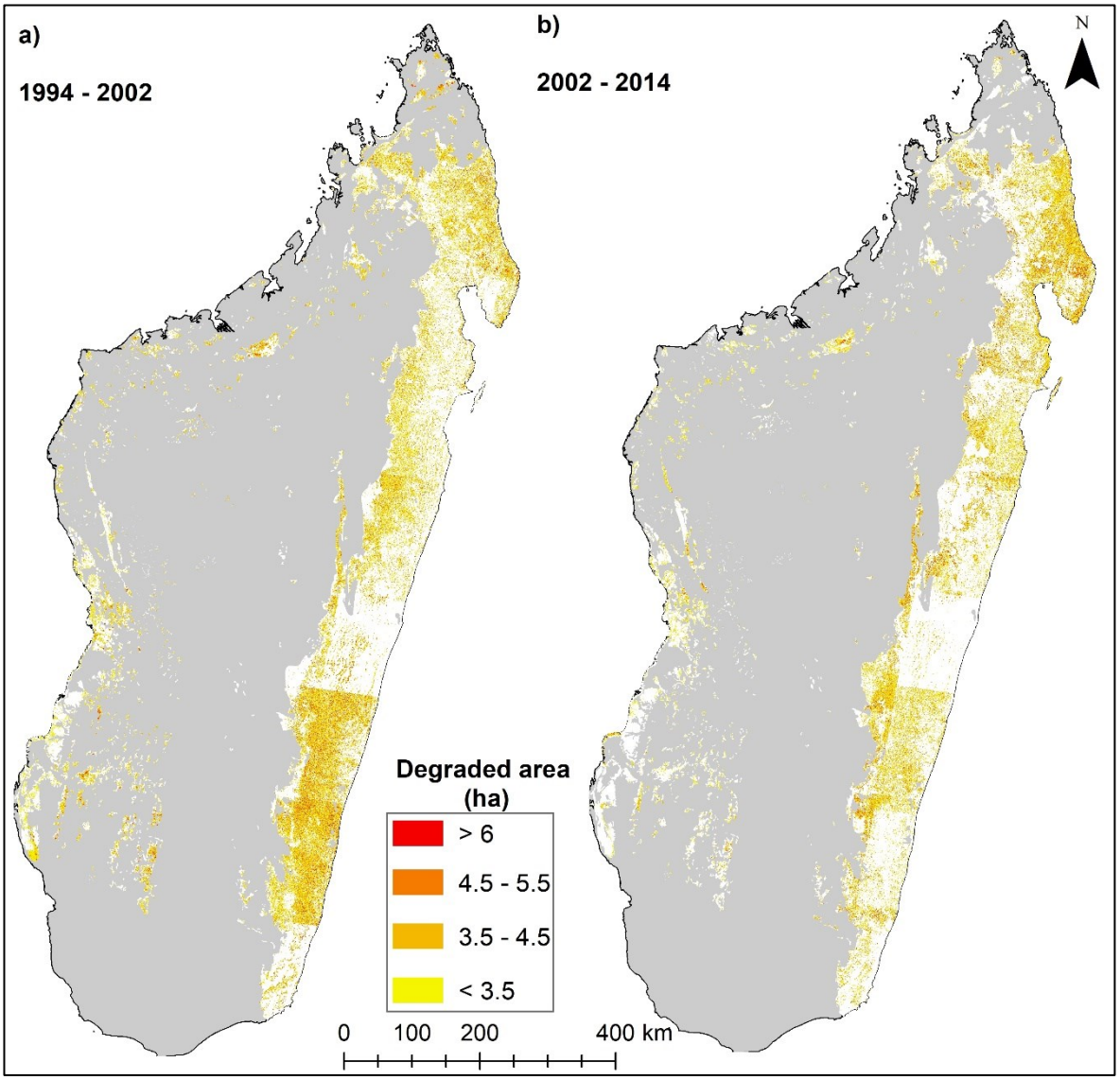

Figure 3.3: Outputs of sub-pixel analysis showing areas impacted by forest degradation in a) 1994 – 2002 and in b) 2002 - 2014. Degraded areas were visually enhanced to improve the map representation. Areas affected by data artefacts are clearly visible in the eastern forest corridor and as shown in Appendix 2.

3.3.3 Accounting for deforestation and forest degradation across different elevation bands

Equal area analysis revealed a mixed pattern in the deforestation rates along the elevation gradients in five eco-regions between ca. 1994 and ca. 2014 (Figure 3.4a-e). For instance, in lowland and tapia forests, the highest deforestation rates were quantified at the highest elevation band. However, deforestation rates did not consistently increase in an upward direction along the elevation gradient in both eco-regions. On the other hand, humid forests showed increases in deforestation rates at intermediate elevations (i.e., *356-632 masl and 633 -889 masl)* but decreased slightly at the highest elevations (Figure 3.4b). In littoral forests, deforestation rates steadily increased between low elevation bands (i.e., *9-10 and 11-15 masl)* and intermediate elevation bands (*16-37 masl)*. However, sharp decreases in deforestation was estimate at the highest elevation (*37-782 masl*).

Equal area analysis of forest degradation showed a mixed pattern within and between eco-regions. In lowland forests, the highest forest degradation rates were in *band 4* (*563-1842 masl*). There were high degradation rates in the low elevation range(s) in humid forests, decreasing at intermediate elevation range (*633-889 masl, 890-1106 masl)* and then increasing sharply at the highest elevation interval (*1107-2744 masl*) (Figure 3.4b). In the littoral forests, degradation rates surpassed the Island-wide mean rate of degradation (thick grey line in Figure 3.4c) at the *9-10 masl* range. Similarly, the fluctuating pattern of forest degradation rates was detected along the elevation gradient in littoral and western dry forests. Equal area elevation analysis of tapia forests showed that rates of forest degradation increased at the highest elevation interval (*1008-1782 masl*) compared to the lowest elevation interval (*319-650 masl*), but as in other eco-regions there was slight decreases at intermediate elevation range(s) (Figure 3.4e).

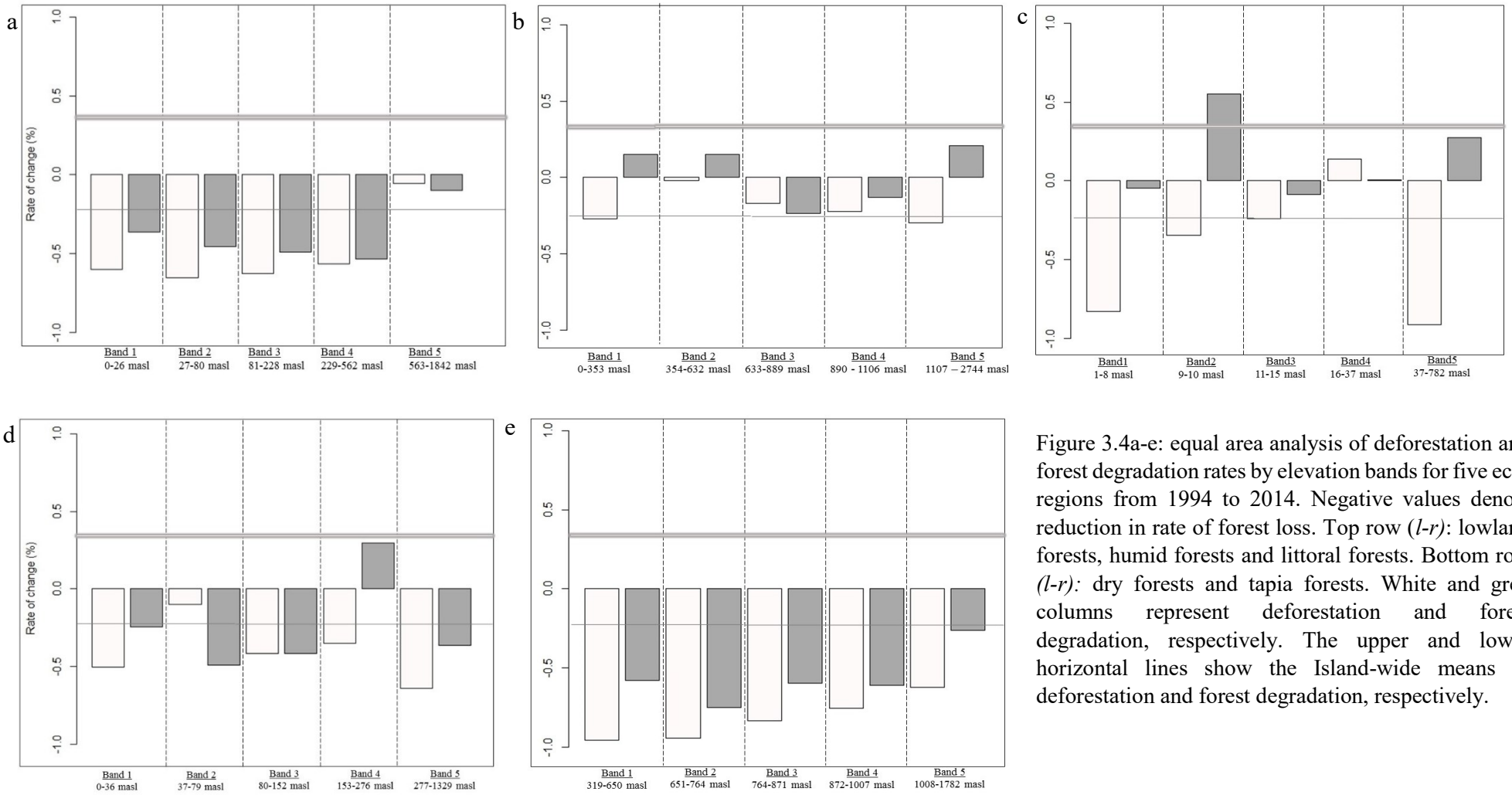

Figure 3.4a-e: equal area analysis of deforestation and forest degradation rates by elevation bands for five eco-regions from 1994 to 2014. Negative values denote reduction in rate of forest loss. Top row (*l-r)*: lowland forests, humid forests and littoral forests. Bottom row *(l-r):* dry forests and tapia forests. White and grey columns represent deforestation and forest degradation, respectively. The upper and lower horizontal lines show the Island-wide means of deforestation and forest degradation, respectively.

Likewise, equal interval analysis showed a mixed pattern in deforestation rates across elevation gradients in most eco-regions (Figure 3.5a-e). Apart from western dry forests, the highest deforestation rates were at topmost elevation band in all eco-regions. In western dry forests, deforestation rates decreased as elevation increased. Comparatively, deforestation rates in lowland forests steadily increased with elevation rising sharply at the highest elevation bands (*1472-1842 masl*) (Figure 3.5a). However, in littoral forests deforestation rates in low elevation bands (*1-157 masl*) were higher than intermediate bands (*157-313 and 313-470 masl*); but no values were recorded at the topmost elevation range(s) (Figure 3.5c). In tapia forests deforestation rates at the topmost-elevation band were considerably higher than those in intermediate to low-elevation bands. Also, forest degradation mimicked deforestation patterns under the equal interval analysis. For example, in the lowland forest, there were similar decreases in degradation rates in low-elevation bands; the exception been the humid (*0-549 masl*) and littoral (*1-157 masl*) forest where modest increases were detected (Figures 3.5b, c). Though for the littoral forest no values were detected in the high elevations. However, across most eco-regions, deforestation and forest degradation rates appear to decline in intermediate elevation range (*band 3*) – only in the lowland forests did this pattern change for both processes.

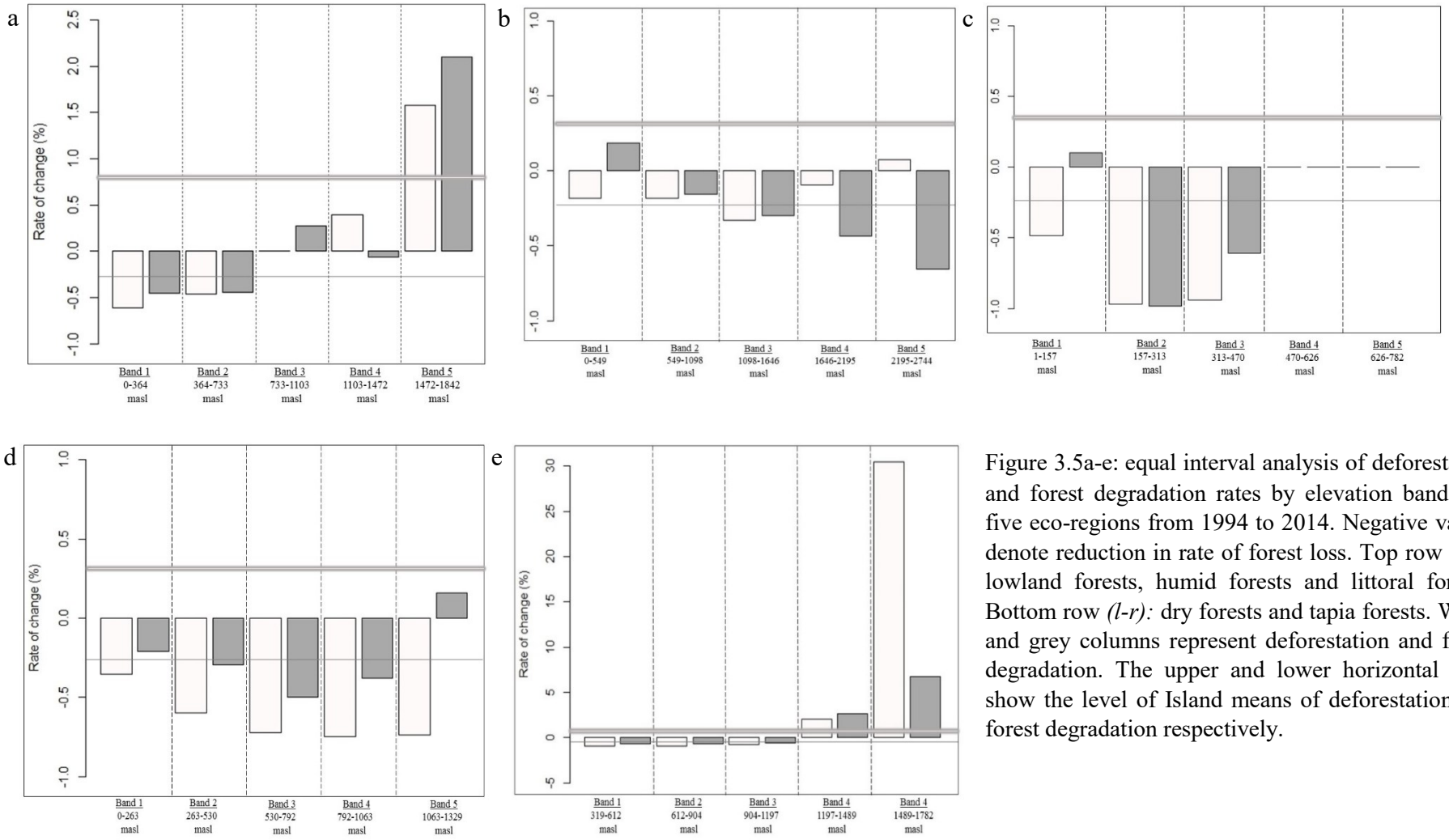

Figure 3.5a-e: equal interval analysis of deforestation and forest degradation rates by elevation bands for five eco-regions from 1994 to 2014. Negative values denote reduction in rate of forest loss. Top row (*l-r)*: lowland forests, humid forests and littoral forests. Bottom row *(l-r):* dry forests and tapia forests. White and grey columns represent deforestation and forest degradation. The upper and lower horizontal lines show the level of Island means of deforestation and forest degradation respectively.

3.3.4 Assessing the accuracy of sub-pixel analysis

The input images showed variations of up to 7% against the modelled end-member values for the six eco-regions (RMSE, Appendix 3). The error values fall within the range of uncertainties (< 20%) reported in other studies (Huang and Asner 2010) and outperformed the application of AutoMCU in Brazilian forests (Asner et al. 2006). Low to intermediate deviation values (1 – 30%) were recorded between the means of iterations. There were slightly higher deviations between iterations for photosynthetic fraction components in the first and second date imagery (Appendix 4). These high deviations in live vegetation fraction were recorded in pixels located in eastern forest corridors compared to western dry forests (south and west). It could be that differences between the spectral libraries for Madagascar and the input satellite imagery used here are large.

3.4 Discussion

3.4.1 Quantified rates of deforestation and forest degradation

These analyses have documented significant eco-regional differences in deforestation and degradation rates in Madagascar, highlighting the importance of partitioning the effects of LULCC at regional scales. Deforestation from lowland forest were the highest, though estimates for this project are higher than the most recent assessments for the region (Allnutt et al. 2013, Hansen et al. 2013). The analysed deforestation and forest degradation rates for humid and dry forests were much lower than Harper et al. (2008), (+0.8% yr^{-1}) possibly because their assessment did not account for degradation within primary forests and perhaps due to an overestimation of deforested areas when using whole-pixel analytical techniques. Overall, the reduction in rates of deforestation in four of the five eco-regions of Madagascar confirms and fits the continent-wide analysis of Aleman et al. (2017), which suggest deforestation rates have slowed down for most regions in Africa due to drastic reduction in available primary forests. Though the magnitude of deforestation in Madagascan forests are likely to be more severe in the future, evident in the large-sized

clearings detected in humid, lowland and dry forests during the second interval. Especially, in western dry forests where natural habitats are relatively smaller, yet the average size of deforestation there were the largest in both intervals compared to all other eco-regions, reinforcing the risks from deforestation to natural habitats for all regions of Madagascar (Brown et al. 2015).

The highest forest degradation rates in littoral forests could be because of the absence of large tract of continuous primary forests (an easy target for deforestation) and the presence of small forest patches that are easily accessible (Consiglio et al. 2006). Moreover, these results also show early evidence that subtle thinning or within-forest disturbances is emerging as an active driver of change, as seen from the results of equal area analysis which showed that forest degradation rates increased at higher elevations in lowland, humid, littoral and tapia forests. Similar patterns were quantified from equal interval analysis of degradation rates in lowland, humid and tapia forests. However, there is no clear explanation for inconsistent forest degradation rates at intermediate elevation range. Such increases in degradation rates support recent studies that have shown that despite some successes in tackling deforestation in tropical regions - forest degradation may have evaded prior regulatory measures and poses a threat to primary forest habitats (Boucher et al. 2014, Barlow et al. 2016, Prestele et al. 2016).

3.4.2 Displacement of deforestation and forest degradation along elevation gradients

Also, presented is evidence of changing deforestation and forest degradation along elevation gradients in all eco-regions. For instance, deforestation rates increased with elevation in lowland and tapia forests under the equal area analysis and decreased in dry forests under the equal interval analysis confirm that landscape - scale changes in forest structure along elevation gradient is happening already (Asner et al. 2014). However, the mixed pattern in forest degradation rates along elevation gradients in most eco-regions could be due to one or a combination of two reasons, which are: i) that forested areas impacted by

subtle changes in their structure are more likely to recover faster than when affected by large-sized clearings and ii) the temporal resolutions of the images used here is insufficient to fully capture the extent or at least serve as proxy for real-time monitoring of forest degradation (Lambin 1999, Kennedy et al. 2010). In any case, the results of elevation gradient categorisation presented here provide a preliminary perspective of shifts in both deforestation and degradation.

Together the results of differences in eco-regional deforestation and forest degradation rates, as well as changes along elevation gradient indicate the complexity of change processes, in Madagascan habitats, which is similar to most tropical regions (DeVries et al. 2015). For example, shifting cultivation, selective logging and cyclones are major agents of forest cover change along the eastern escarpment, which comprises the lowland and humid forests (Brown and Gurevitch 2004, Burivalova et al. 2015); while deforestation and degradation in dry forest are more likely modulated by shifting cultivation, livestock grazing, charcoal production and wildfires, and to a lesser degree, selective logging (Waeber et al. 2015, Feldt and Schlecht 2016). Consequently, although selective logging is often the most common cause of degradation in tropical forests (Asner et al. 2005) local drivers influence at the eco-regional scales may differ or get displaced through a process known as leakages (i.e., spatial displacement of forest loss) (Gasparri et al. 2016). Perhaps, such displacement is the reason for the reported regeneration of primary forests in tapia forests (Kull 2002a). Yet, this analysis detected minimal deforestation and forest degradation rates in tapia forest and critically under equal area and equal interval elevation analysis exceptional increase in deforestation and degradation rates at the highest elevation range. Suggesting that there is still the challenge for sustaining past successes, even where such existed. There are several explanations for possible displacements in forest loss: One could be the consequence of pressures caused by in-migration of re-settlers to high elevation habitats (DeVries et al. 2015). Alternatively, leakage may be driven by shifts in dryland

cropping on slopes (*Tanety*) upland towards montane forests (Vågen 2006), seasonal burning (Kull 2002b) and slow reforestation of dry forests once exposed to disturbances (Zinner et al. 2014). It is therefore possible that leakage may have been one consequence of unbalanced conservation interests in Madagascar: thus, the dominant causes of deforestation and forest degradation have shifted to other eco-regions or are beginning to shift in an upward slope direction. This may have led to upward trends in deforestation and forest degradation in parts of Madagascar (e.g., dry forests) and downward trends in others (e.g., littoral forests).

These results and others (e.g., Waeber *et al*. 2015) suggests adoption of a more balanced approach to future conservation initiatives, since deforestation and forest degradation are often driven by region-specific conditions and therefore require conservation policies tailored for local environments. Additional evidence of forest degradation as one of the dominant process driving LULCC could be seen in the increased rates at the highest elevation gradient in different eco-regions. Perhaps, a sign that previously un-disturbed forest patches are now becoming the target of gradual encroachment. Since these analyses did not explicitly estimate selective logging however, it was not possible to determine to what extent it modulates forest cover change. It should be noted that for the lowland forest there were higher proportion of cloud cover in the ca. 2002 imagery, which resulted in masking of those pixels during sub-pixel analysis and may be a contributing factor to the exceptionally high rate of deforestation and verified with the error quantified for that eco-region. An alternative reason could be fast recovery of forest canopy that help to fill canopy gaps left by low intensity selective logging in a short period of time (Asner et al. 2004).

3.5 Conclusion

This chapter shows that there is considerable heterogeneity in rates of deforestation and degradation in Madagascar, with local and regional distinct patterns of both increasing and decreasing forest loss. Additional evidence of increasing forest degradation rate at higher elevations in lowland and tapia forests suggests that shifts in forest loss along elevation gradient is already happening for some eco-regions. Similar trends could exist for other tropical regions but are often masked by rates of deforestation and degradation averaged across eco-regions and sometimes for entire countries. The differences in rates of forest degradation across Madagascar may be due to bias of conservation projects (e.g., ICDPs, REDD+) in sub-humid and lowland forests, which in turn has resulted in more protected areas in these eco-regions (Ferguson 2009). The important consequence of this finding is that biodiversity conservation in neglected eco-regions continues to be eroded by large, rapid land-use conversions.

Thus, it is imperative that conservation strategies move beyond traditionally threatened habitats to other regions that have historically received less attention when designing future conservation projects, as these areas may be impacted by more extensive losses in natural vegetation. Detection of forest degradation in all eco-regions highlights the value of the additional, often unreported contribution of degradation to forest cover change, the absence of which leads to continued underestimation of LULCC in the tropics. Perhaps this result could inform the on-going debate surrounding the importance of quantifying and monitoring forest degradation in tropical developing countries. In regions where, weak governance and insecure land tenure rights drive shifting cultivation, illegal selective logging and extraction of non-timber forest products — such as many countries in sub-Saharan Africa — estimating forest degradation is equally as valuable as deforestation. Also, it provides an island-wide assessment of forest degradation in a country with heterogeneous habitats, forest types, as well as varying intensity of causes of degradation. However,

assessing degradation in regions with more intense variability in the aforementioned factors, such as Southeast Asia, will require more robust remote sensing approaches (e.g., increased observation frequency) and processing tools (e.g., CLASLite), as well as higher spatial resolution imagery (e.g., SPOT 6 and 7, LIDAR). In coming years, as Madagascar prepares for the REDD+ era, it will become increasingly important to implement robust, reliable and repeatable approaches to assess forest degradation.

Chapter Four

Intensity analysis and land use land cover change

4.1 Introduction

Natural habitats are subject to modifications from land use land cover change (LULCC) with serious implications for species diversity (Rocchini 2014, Keenan et al. 2015, Castello and Macedo 2016). Land-use intensification caused by human-induced processes such as deforestation and forest degradation will increase the vulnerabilities of natural habitats to climate change (Elliott et al. 2014, Dimobe et al. 2015). Yet, the common approach to LULCC is mostly designed to identify forest losses and ignore forest gains and/or changes that are indicative of regeneration (Mukul and Herbohn 2016). For most regions, deforestation is inevitable, and as a result it is highly likely that naturally regenerated forest could provide the required habitats for species preservation and mitigate against carbon emissions (Houghton 2013, Chazdon 2014). Moreover, naturally regenerating forests occupy a substantial portion of tropical landscapes and account for approximately 65% of global natural forests (FAO 2015).

In sub-Saharan Africa, a rapid growth in urban population has placed added pressure on natural habitats for food and other ecological services (DeFries et al. 2010, Sloan and Sayer 2015, Gasparri et al. 2016). Investigating land cover dynamics in the region is often simplified (Lambin et al. 2001), biased towards forest loss (Achard et al. 2007, Hansen et al. 2010, Stibig et al. 2014) and lacks spatially explicit data (Vågen 2006). Therefore, there is an increasing impetus to effectively characterise the dominant patterns responsible for both forest loss and gain in tropical landscapes.

4.1.1 Forest gains and other land cover transitions

Forest gain occurs when tree canopy is established from a non-forest state (Hansen et al. 2013). In the tropics, forest gains are mostly from shifting cultivation fallows, abandoned farms or through natural progression of secondary vegetation (Rudel et al. 2005, Zahawi et al. 2015). Regenerating forests possess faster biomass recovery, higher productivity and carbon uptake compared to old-growth forests in the Neotropics (Zahawi et al. 2015, Poorter et al. 2016, Mora et al. 2018). Also, they can complement existing biodiversity conservation services (Barlow et al. 2007), offer higher resilience to natural disturbances (Bhaskar et al. 2017), as well as ecosystem services, such as regulating nutrient cycles and protecting water catchment (Pete et al. 2016). Moreover, recent studies indicate that forest regeneration may play a significant role in current climate change by mitigating carbon emissions by 25 – 35% (Goodman and Herold 2014, Houghton et al. 2015, Chazdon et al. 2016, Phillips and Brienen 2017), assuming the improbability of slowing or stopping current rates of deforestation (Coe et al. 2013). Equal attention must be given to methods that estimate forest gains and secondary forest regeneration, especially in tropical regions, where rapid LULCC leads to habitat fragmentation for some of the world's most endangered species.

Making forest gains a research priority can complement the core mandates of the UN- Reduced Emissions from Deforestation and Degradation scheme ($REDD^{+}$), especially for Sub-Saharan Africa, where a recent study has estimated a reduction in deforestation rates for eastern and southern parts of the region (Aleman et al. 2017). Regardless, estimates of forest gains are rarely reported for the tropics, despite growing understanding of their role in forest change dynamics in the region (FAO 2015). Specifically, no explicit measures of forest gain were made in previous reports (i.e., GFR 1990, 2000 and 2005) for sub-Sahara African countries, which has negative implications for achieving small-scale conservation targets, the robustness of LULCC assessments and the ability to reliably predict future LULCC for these countries.

The drive to map forest gains in sub-Saharan Africa has many uncertainties, for instance: (i) understanding how to map the distribution of regenerating forests due to spectral similarities with mature forests (Steininger 2000, Neeff et al. 2006); (ii) assessing the potential for regeneration on previously forested areas that are currently in a non-forest state (Chazdon et al. 2009); and (iii) the dynamics of secondary vegetation in forest transitions (Aguiar et al. 2016). Recent efforts to address these problems have been biased towards the Neotropics, specifically Amazonian forests, resulting in relatively fewer studies focused on the state of forest gains in sub-Saharan African forests (Mukul and Herbohn 2016). Despite evidence that some regenerating forests in sub-Saharan Africa also possess high biomass concentration compared to old-growth forests (Cazzolla Gatti et al. 2015).

4.1.2 Land use land cover change in Madagascar

In this chapter the drivers of LULCC and their potential impact on forest losses and gains in Madagascar were determined. Previous assessments that have report minimal forest gains (<1%) in Madagascar, though some of these studies were implemented at global scale and as such it is expected that the dominant signal (i.e., forest loss) of LULCC would be more pronounced than others (*for example,* Hansen et al. 2013, Li et al. 2016). To highlight the subtler differences on the island, intensity analysis was undertaken to quantify the changes taking place within habitats highly vulnerable to LULCC, yet slow to recover due to persistent disturbances. In Madagascar, the expectation is for shifting cultivation to be an active driver in all eco-regions, while increases in exposed surfaces, possibly caused by erosion and/or wildfires to actively degrade arid forests. Similarly, the expectation is for transitions from forest to other land cover categories be less dominant in western dry forests compared to eastern humid forests (Elmqvist et al. 2007, Irwin et al. 2010, McConnell and Kull 2014). Intensity analysis would account for processes likely to increase both deforestation and forest degradation by quantifying significant pixel swaps between subsistence cultivation, exposed surfaces and forests. Likewise transitions that are indicative of forest gains such as vegetation matrix to forest would be analysed in terms of their

observed intensity, magnitude and speed in two intervals (i.e., ca. 1994 – 2002 and 2002 – 2014).

There is no conceptual distinction about the processes leading to forest gain, including forestation, afforestation or reforestation. Rather, intensity analysis is utilised to detect land cover category swaps to and from forest as well as all other transitions taking place in two intervals. In addition to the current trends in LULCC in each eco-region the future land cover states are predicted (i.e., 2050) using land change modeler (LCM). LCM considers the proportion of categories (i.e., quantity disagreement) and their spatial allocation (allocation disagreement) between different dates when projecting to the future (Pontius and Millones 2011, Pickard et al. 2017).

As a result, the objectives here are to:

(i) map the past and current states of land use land cover at eco-regional scale;

(ii) quantity the intensity of LULCC and;

(iii) accurately predict future shifts in land use land cover at eco-regional scales.

4.2 Methods

The data and method describing the steps taken to implement intensity analysis and model LULCC in different eco-regions are described in **chapter 2, section 2.2 and section 2.5** respectively**.** The steps followed to project current trends in LULC to 2050 are explained in **chapter 2, section 2.6**. The products developed in this chapter were used in multiple chapters and to avoid repeating explanations of methodological approaches a separate methods chapter (**chapter 2**) was written.

4.3 Results

4.3.1 Estimating Net LULC changes

Presently, forests occupy the largest proportion of humid and littoral ecoregions; but in the future forested areas were predicted to reduce significantly while large increases in vegetation matrix were predicted to occur in humid forests (Table 4.2). In lowland forests, the proportion of forest was predicted to remain relatively unchanged compared to its present size, but the extent of vegetation matrix was expected to increase (Table 4.1). The portion of the landscape used for cultivation in lowland forests reduced from 29% to 15.1% between the 1994 and 2014. In dry and tapia forests, exposed surface occupied a sizeable portion in both eco-regions (Tables 4.4 and 4.5). However, the proportion of forested areas in dry forest is predicted to increase by 34% without any significant change to the size of exposed surface (Table 4.3).

Table 4.1: Land cover category sizes in **lowland forests** (in Ha and as proportion of eco-region) in first interval (1994 - 2002), second interval (2002 – 2014) and predicted date (2050)

Category	1994		2002		2014		2050	
	Area (Ha)	%	Area (Ha)	%	Area (Ha)	%	Area (Ha)	%
Forest	1499591	26.9	1613450	28.9	1733186	31.1	1725731	30.5
Vegetation matrix	875887	15.7	1260470	22.6	1948458	34.9	2365549	42.4
Exposed surface	1807383	32.4	1644900	29.5	1052446	18.9	620730	11.1
Cultivated land	1394499	25.0	1058540	19.0*	843270	15.1*	865350	15.5*
Total	5577360	100	5577360	100	5577360	100	5577360	100

** Decreases contradict the known trends for cultivated land in lowland forests. This result is likely due to the cumulative effect of cloud cover in several image scenes.*

Table 4.2: Land cover category sizes in **humid forests** (in Ha and as proportion of eco-region) in first interval (1994 - 2002), second interval (2002 – 2014) and future (2050)

Category	1994		2002		2014		2050	
	Area (Ha)	%	Area (Ha)	%	Area (Ha)	%	Area (Ha)	%
Forest	3252547	53.7	2453620	40.5	2832201	46.8	1752348	29.0
Vegetation matrix	739183	12.2	1454900	24.0	2570332	42.5	4214259	69.6
Exposed surface	1327252	12.1	1165050	19.3	399505	6.6	53744	0.9
Cultivated land	6052007	21.9	978437	16.2	249969	4.1	31656	0.5
	6052007	100	6052007	100	6052007	100	6052007	100

Table 4.3: Land cover category sizes in **littoral forests** (in Ha and as proportion of eco-region) in first interval (1994 - 2002), second interval (2002 – 2014). *No future map was produced littoral forests for 2050 due to the inability of the land change modeller to allocate land cover categories to this time.*

Categories	1994		2002		2014	
	Area (Ha)	%	Area (Ha)	%	Area (Ha)	%
Forest	5521	33.8	8308	50.9	11715	71.8
Vegetation matrix	2945	18.0	2074	12.7	4391	26.9
Exposed surface	1451	8.9	1454	8.9	220	1.4
Cultivated land	6409	39.3	4491	27.5	0	0.0
Total	16327	100	16327	100	16327	100

Table 4.4: Land cover category sizes in **dry forests** (in Ha and as proportion of eco-region) in first interval (1994 - 2002), second interval (2002 – 2014) and future (2050)

Category	1994		2002		2014		2050	
	Area (Ha)	%	Area (Ha)	%	Area (Ha)	%	Area (Ha)	%
Forest	877810	38.4	496292	21.7	610035	26.7	769789	33.7
Vegetation matrix	618869	27.1	728096	31.8	648655	28.3	527162	23.1
Exposed surface	703792	30.8	931251	40.7	879761	38.5	851607	37.2
Cultivated land	86240	3.8	131072	5.7	148261	6.5	138153	6.0
	2286711	100	2286711	100	2286711	100	2286711	

Table 4.5: Land cover category sizes **in tapia forests** (in Ha and as proportion of eco-region) in first interval (1994 - 2002), second interval (2002 – 2014) and future (2050)

Category	1994		2002		2014		2050	
	Area (Ha)	%	Area (Ha)	%	Area (Ha)	%	Area (Ha)	%
Forest	48458	34.1	42846	30.1	14437	10.2	2067	1.5
Vegetation matrix	25694	18.1	21126	14.9	47744	33.6	61015	42.9
Expose surface	62532	44.0	58453	41.1	58894	41.4	57499	40.4
Cultivated land	5586	3.9	19845	13.9	21194	14.9	21689	15.3
Category	142270	100	142270	100	142270	100	142270	100

During the first interval, net gains in forest area occurred only in littoral forests (Figure 4.1c). Positive net gains were measured for vegetation matrix in lowland, humid and dry forests (Figures 4.1a, b & d). Cultivated land experienced net increase in area during the first interval in dry and tapia forests. In the second interval, only tapia forests experienced losses in net forest areas (Figure 4.1e). In lowland and dry forests, there were net losses in the proportion of vegetation matrix during the second interval (-2.3%). Similarly, mixed patterns were detected in the net change in exposed surface in most eco-regions.

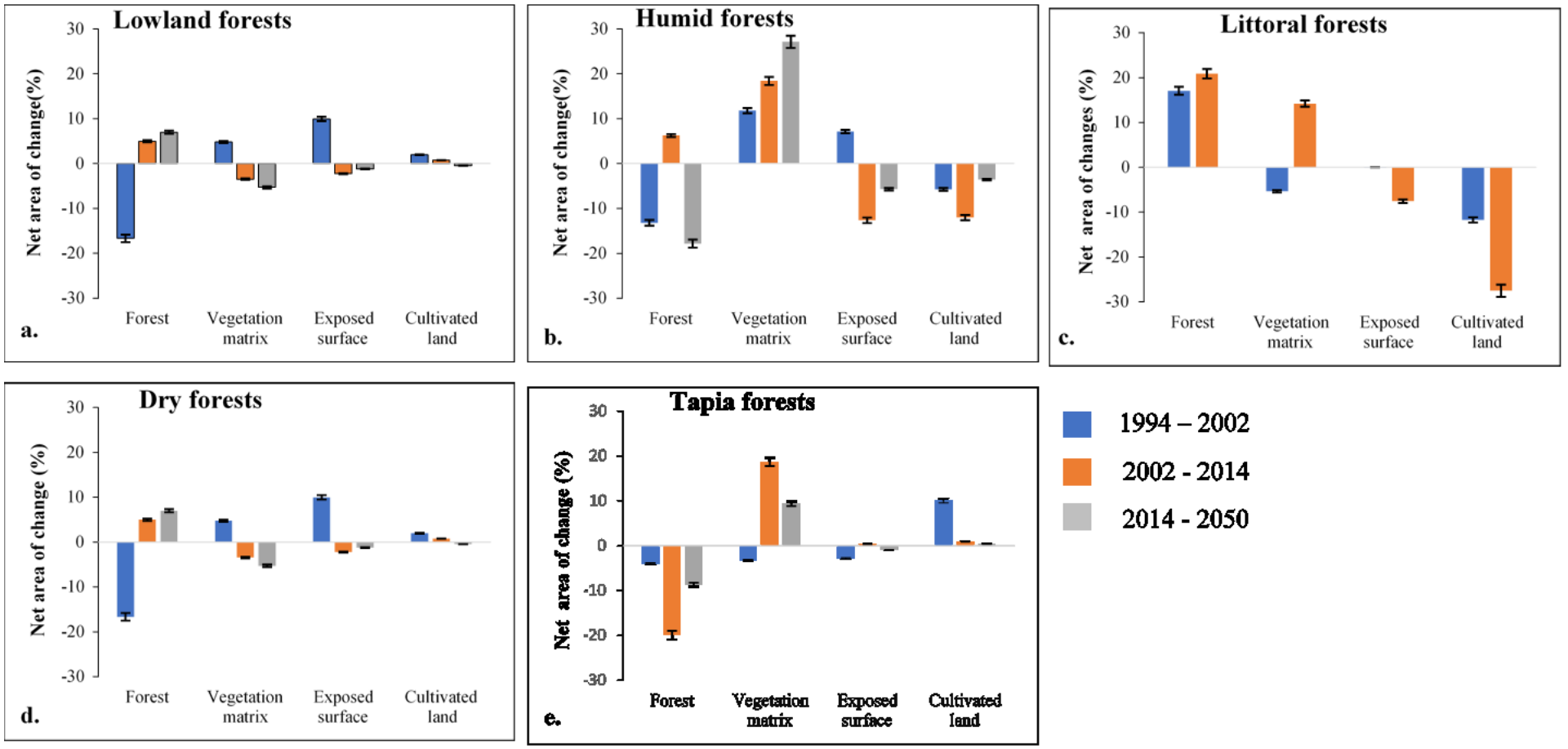

Figure 4.1a-e: Net area of land use land cover categories change in selected eco-regions of Madagascar. Blue, orange and grey bars represent first interval (1994 – 2002), second (2002 - 2014) and third (2014 – 2050) respectively. Error bars indicate 95% confidence interval.

Future LULC models predicted a net loss in forested areas (0.1%) and exposed surface (-7.7%) for lowland forests. Significant loss in forested areas (-17.9%) in humid forests was projected, but the area covered by vegetation matrix was projected to increase (27.1%) in 2050. In all eco-regions, net loss of exposed surfaces was calculated between 2014 and 2050. Although for tapia and dry forests, the net loss of exposed surfaces detected was relatively smaller compared to other eco-regions (Figure 4.1d-e). There was no predicted LULC map for littoral forests, because the Markov chain process sub-model could not allocate future pixels to land cover categories in the landscape. This may be due to the relative small number of pixels that make up the littoral forests. Spatial distribution of land use land cover categories on an island-wide scale for first interval, second interval and future dates (i.e.,2050) are provided in Appendix 5.

4.3.2 Magnitude and nature of land use land cover transitions

4.3.2.1 Quantifying forest loss and other transitions

Largely-intact forest transitions to exposed surface and vegetation matrix, as well as vegetation matrix transitions to exposed surface and cultivated land were on average faster and larger than other transitions and mainly occurred in the first interval (Figure 4.2a – e). Specifically, large and relatively fast transitions from forest and vegetation matrix to cultivated land and/or exposed surfaces dominated transitions in the lowland forests, humid forests and western dry forests (Figure 4.2a, b & e). Tapia forests were dominated by large transitions of cultivated lands to exposed surface in the second interval. However, the fastest transitions were of forest to exposed surfaces, albeit at a lower magnitude (Figure 4.2d). In the second interval, fewer large sized transitions occurred in the humid forests, compared to the lowland forests where more intermediate –to small– sized transitions of forest to

cultivated lands and vegetation matrix to cultivated lands were detected. Again, the transitions taking place within the humid forests occurred at a slower pace than in the lowland forests. On average, second interval transitions in four of the five eco-regions were slower than first interval transitions regardless of the type of transitions. Only within the littoral forests did this pattern differ, with almost identical speeds between large-sized transitions of forest to cultivated lands. Transitions from vegetation matrix to cultivated lands were relatively small-sized and generally slower in littoral and lowland forests in the second interval.

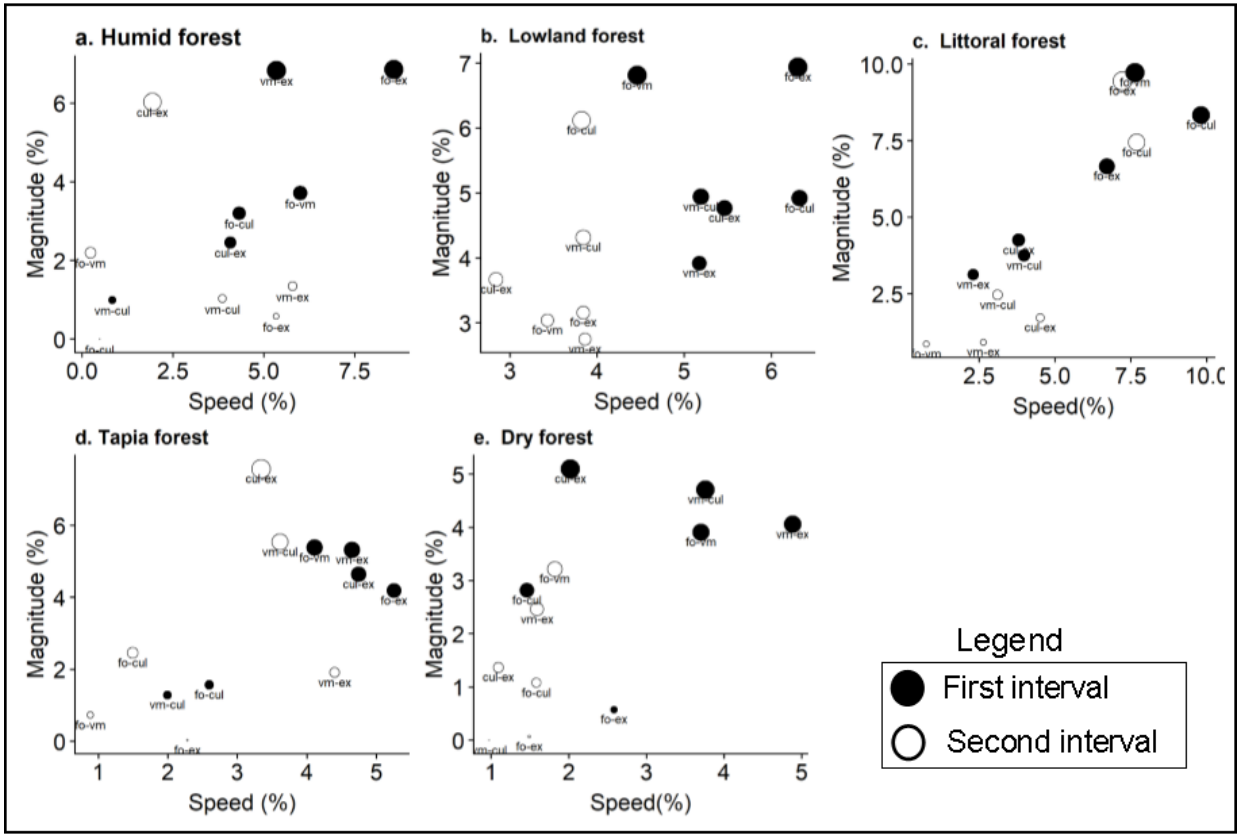

Figure 4.2: Differences between the nature of land cover category transitions from the perspective of loss in two intervals (c.1994 – 2002 and c.2002 - 2014) for five eco-regions: a) humid forest; b) lowland forests; c) littoral forests; d) tapia forests; and e) dry forests. On the x-axis is the aggregation of uniform intensities denoted as speed and y-axis is the aggregation of observed intensities denoted as magnitude. Proportional bubbles depict large and small-sized transitions of land cover categories. Speed indicates the rate of change of land cover category swaps relative to other transitions taking place. First and second intervals transitions are depicted as black and white circles, respectively. **NB:** *cul = cultivated land, ex = exposed surface, fo = forest*, *vm = vegetation matrix*.

In terms of the observed transitions, largely-intact forest transitioned most intensively to cultivated land in humid, lowland and littoral forests in both intervals (Appendix 6, Table A2 – A6). While in the dry forests, exposed surface transitions to vegetation matrix and cultivated lands were the most intensive in first and second intervals, respectively. Though the transitions of largely-intact forest to vegetation matrix and exposed surface were prominent in both intervals in humid and lowland forests, as well as in first interval in dry forests. All observed transitions from the perspective of forest loss during first and second intervals were mapped and presented in Figure 4.3, 4.4 and 4.5 for four eco-regions. Transitions of littoral forests were excluded, due to their relatively small areas and the large map scale making it difficult for the maps to be readable.

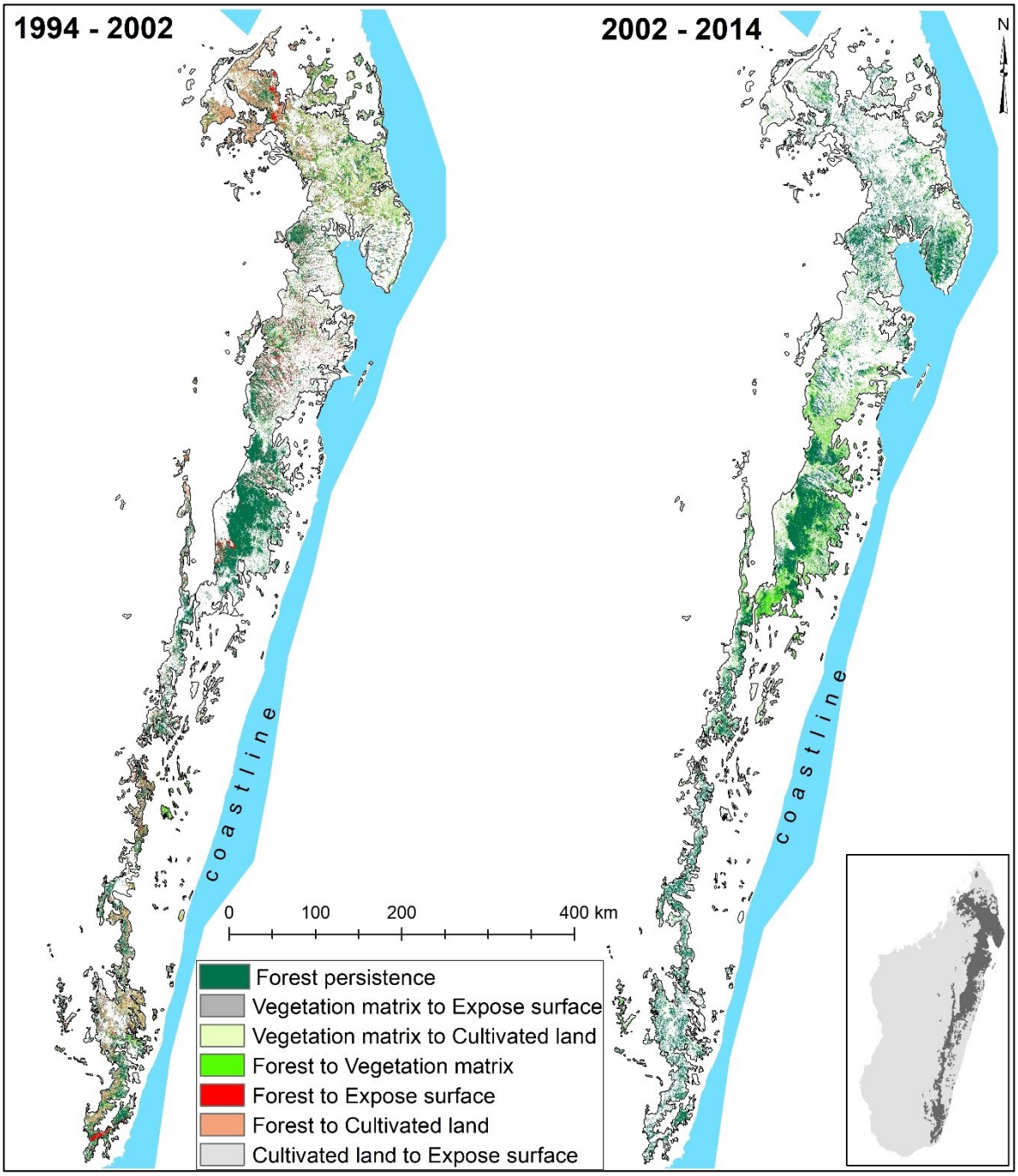

Figure 4.3: Map showing the dominant transitions from the perspective of forest loss during first (*left-side) and* second *(right-side)* intervals in humid forests. Inset figure shows the geographical range of humid forests in Madagascar.

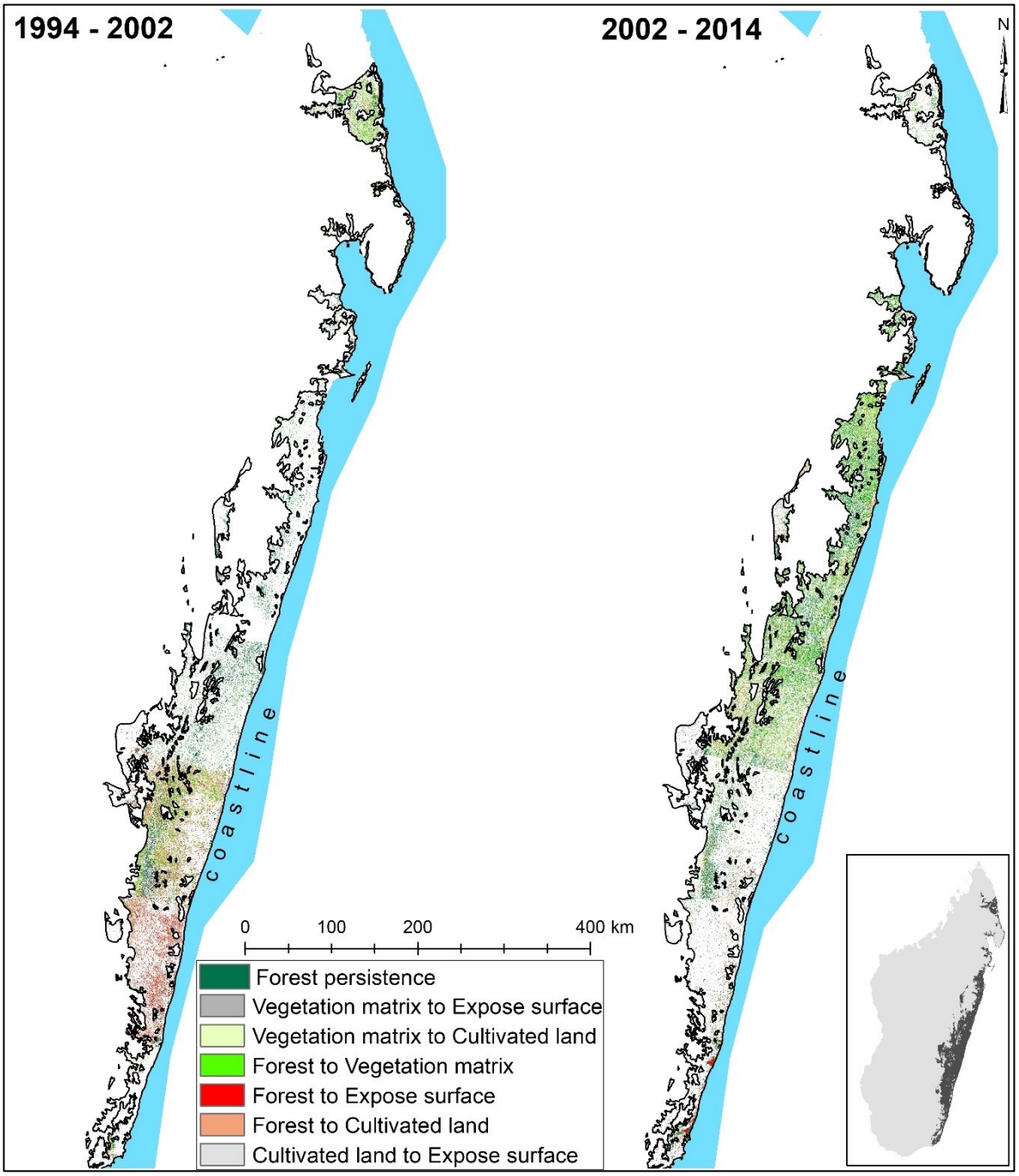

Figure 4.4: Map showing the dominant transitions from the perspective of forest loss during first (*left-side) and* second *(right-side)* intervals in lowland forests. Inset figure shows the geographical range of lowland forests in Madagascar.

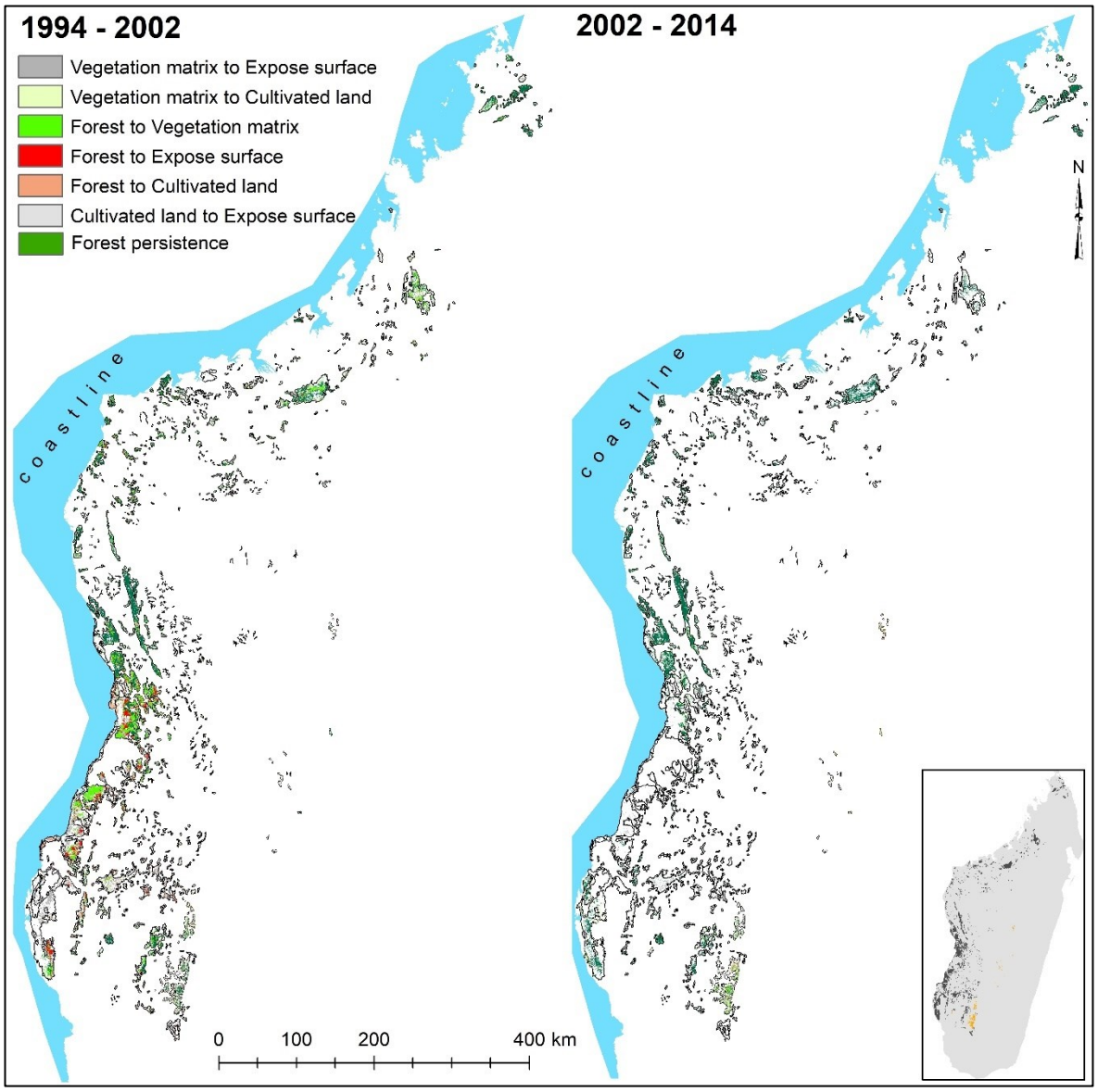

Figure 4.5: Map showing dominant transitions from the perspective of forest gain during first (*left-side) and* second *(right-side)* intervals in dry and tapia forests. Inset figure shows the geographical range of dry and tapia forests in Madagascar.

4.3.2.2 Quantifying forest gain and other transitions

Similarly, intensity analysis revealed fast and large-sized transitions from cultivated land and exposed surface to largely-intact forest occurred in all eco-regions in the first interval (Figure 4.6a - e). Relative to forest swaps, smaller and faster transitions of vegetation matrix to forest were detected in the humid, dry, tapia and lowland forests. Second interval transitions were on average smaller than first interval transitions, particularly in humid forests, where slow and small-sized gains of vegetation matrix to forest were detected (Figure 4.6a). Alternatively, in littoral forests, fast and large-sized transitions from cultivated land to forest occurred; while in tapia forests similarly fast and large transitions of vegetation matrix swaps to forest occurred (Figure 4.6c &d). Mostly, transitions to vegetation matrix from cultivated lands and exposed surfaces were slow and small in the second interval. The observed intensity of each category transitions from the perspective of gains are also presented in the Appendix 7 (Table A7 – A10)

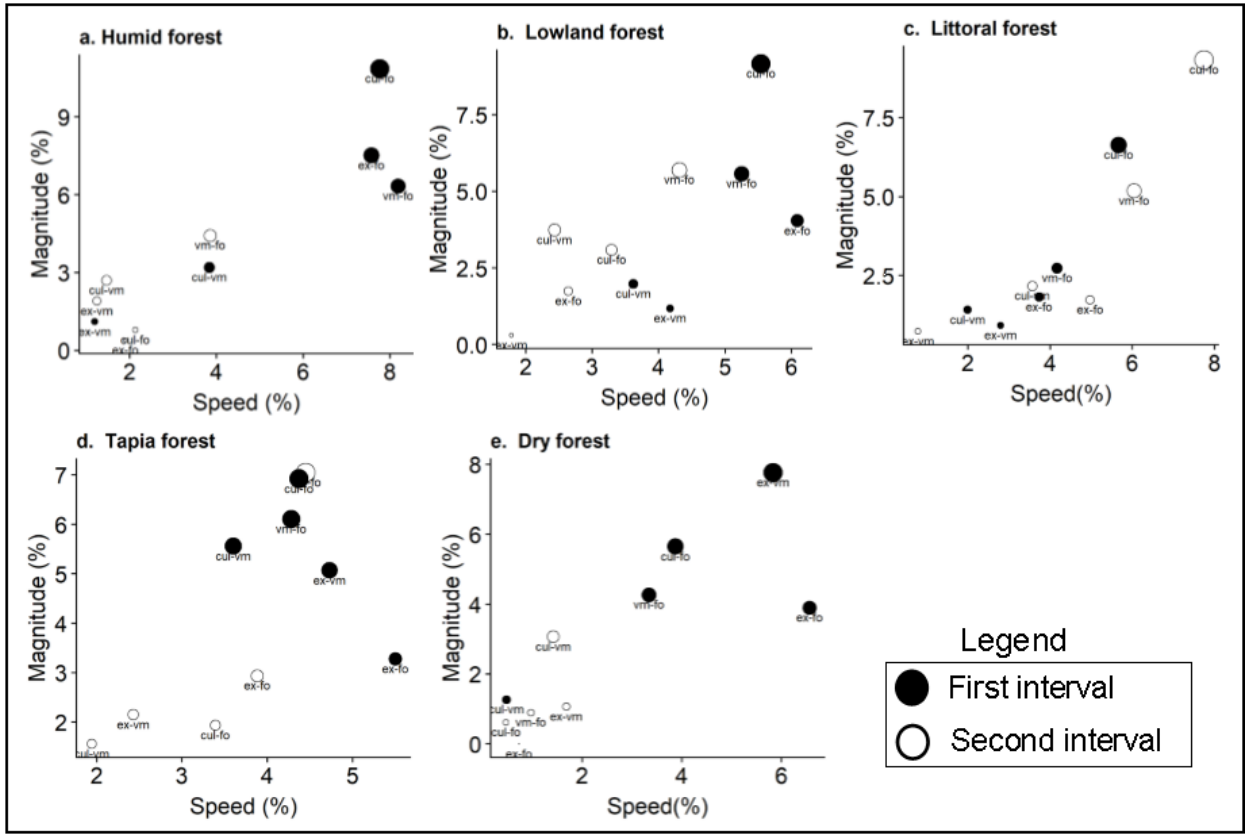

Figure 4.6: Differences between the nature of land cover category transitions from the perspective of gains in two intervals (c.1994 – 2002 and c.2002 - 2014) for five eco-regions: a) humid forest; b) lowland forests; c) littoral forests; d) tapia forests; and e) dry forests. On the x-axis is the aggregation of uniform intensities denoted as speed and y-axis is the aggregation of observed intensities denoted as magnitude. Proportional bubbles depict large and small-sized transitions of land cover categories. Bubbles depict large and small-sized transitions of land cover categories. Speed shows the rate of change of land cover category swaps relative to other transitions taking place. First and second intervals transitions are depicted as black and white circles, respectively. **NB:** *cul = cultivated land, ex = exposed surface, fo = forest*, *vm = vegetation matrix*.

To further illustrate the nature of dominant transitions at eco-regional scales, the spatial distribution of observed land cover category transitions was mapped and provided in Figures 4.7 – 4.9. In humid and lowland forests transitions of cultivated land to forest dominate the northern and southern landscapes in the first interval. In dry forests, the major transitions were from vegetation matrix to forest transitions. During the second interval, the vegetation matrix appeared more dominant transitions in humid forests, as well as dry forests

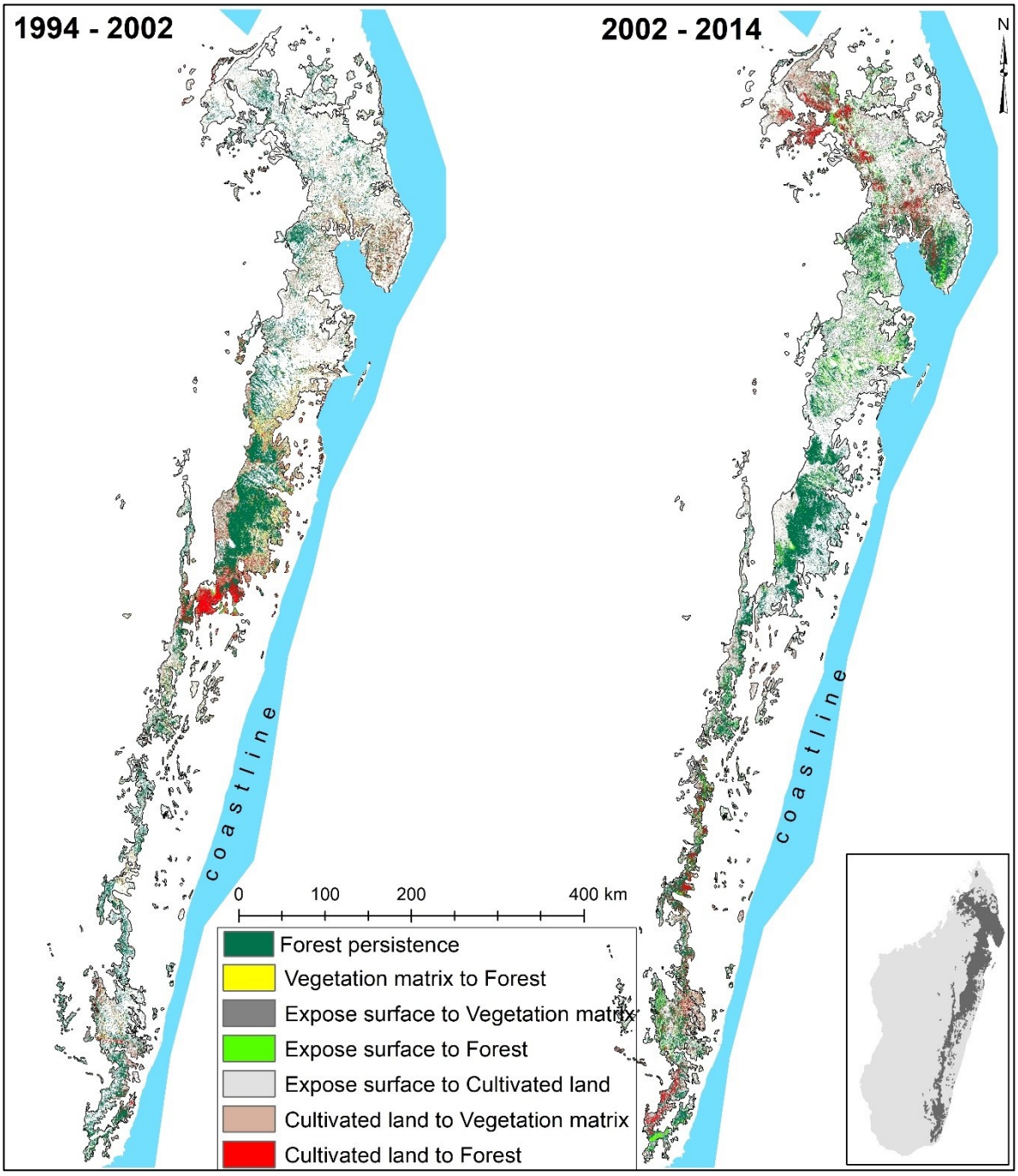

Figure 4.7: Map showing the dominant transitions from the perspective of forest gain during first (*left-side) and* second *(right-side)* intervals in humid forests. Inset figure shows the geographical range of humid forests in Madagascar.

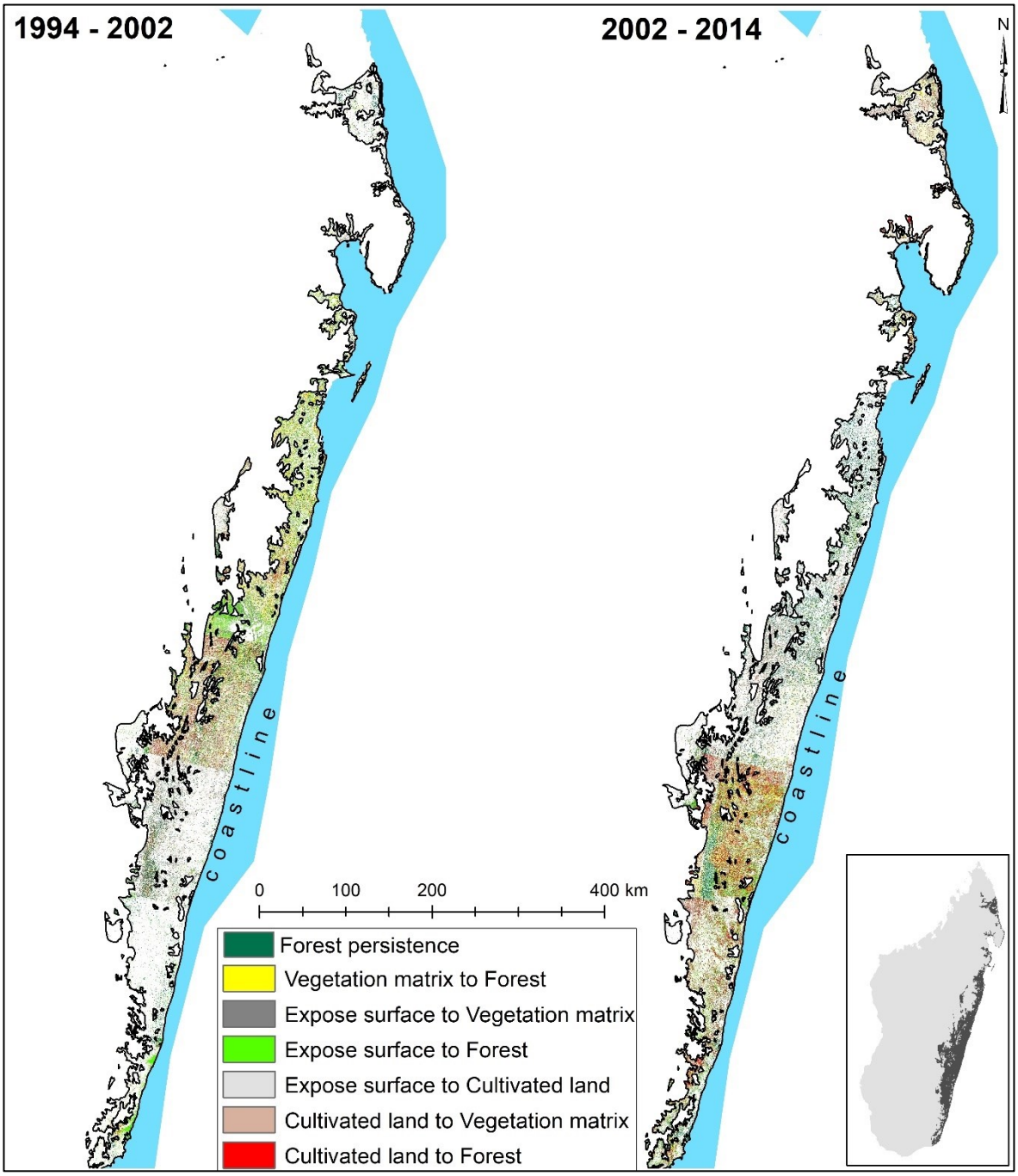

Figure 4.8: Map showing the dominant transitions from the perspective of forest gain during first (*left-side) and* second *(right-side)* intervals in lowland forests. Circled areas show transitions in littoral forests. Inset figure shows the geographical range of humid forests in Madagascar.

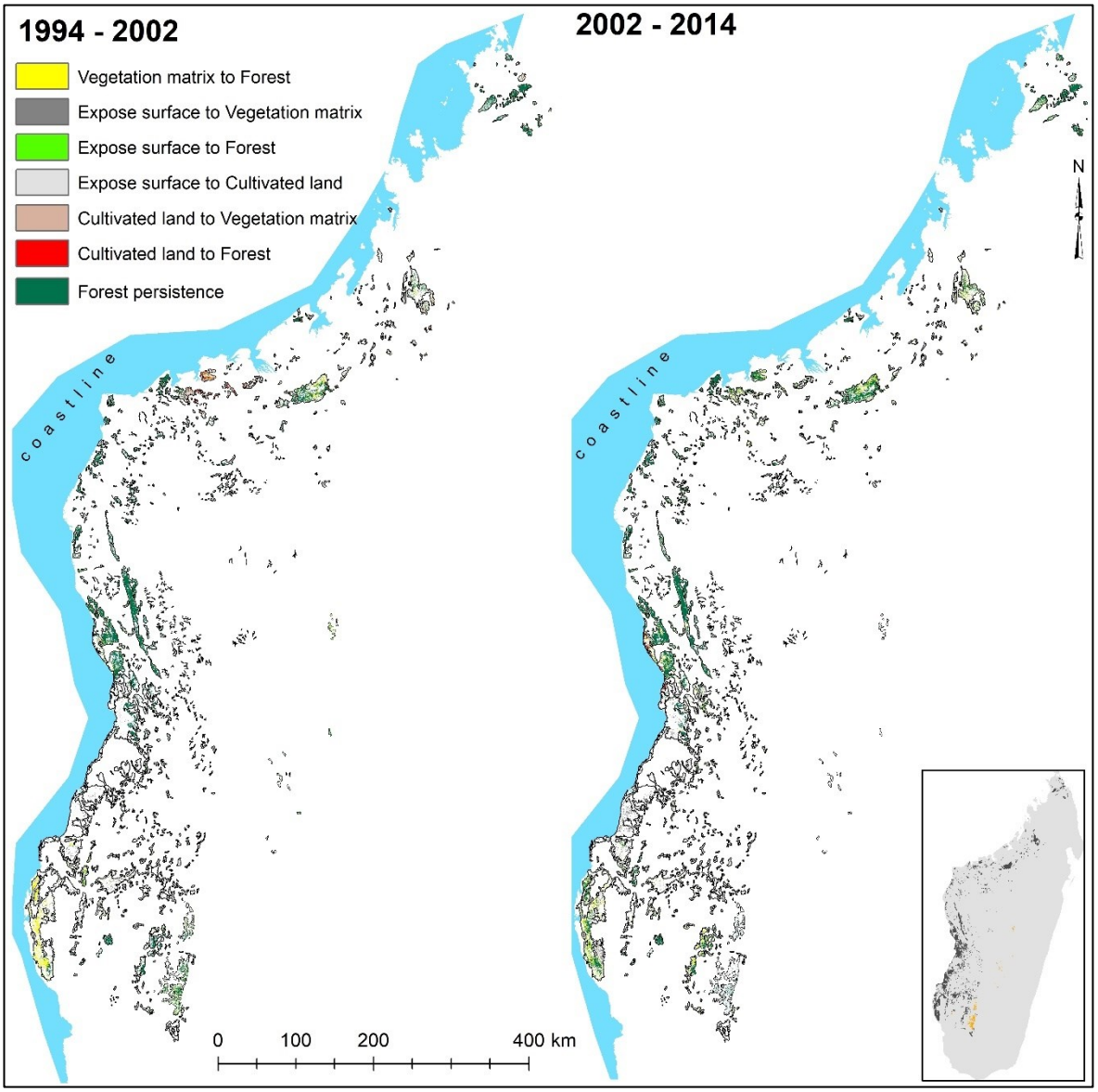

Figure 4.9: Map showing dominant transitions from the perspective of forest gain during first (*left-side) and* second *(right-side)* intervals in dry and tapia forests. Inset figure shows the geographical range of dry and tapia forests in Madagascar.

4.3.3 Accuracy assessment of LULC classification

The lowest user's accuracy (UA) in the 2002 and 2014 maps was recorded for cultivated (0.95) and vegetation matrix (0.92) land categories, respectively; while the highest was recorded for forest (0.99) in the 2002 map and cultivated land (0.99) in the 2014 map (Table 4.6 and 4.7). This means that on average any user of both maps is 90% likely to correctly confirm the land cover categories in the landscape. In the 2002 map, the producer's accuracy (PA) from stratified estimates was highest for vegetation matrix (0.99) and lowest for exposed surface (0.94); while in the 2014 map the highest was recorded for forest category (0.99). The PA from sample counts were generally lower than PA from stratified estimates in both maps (Table 4.6 & 4.7), with the highest PA recorded for forest category in 2000 and 2014 maps, respectively showing, 0.95 and 0.90. Despite these differences in UA and PA the overall accuracy for both stratified estimates and sample counts were similar.

Table 4.6: Error matrix showing the estimated proportion of area for land cover categories (strata) in the ca. 2002 map. The accuracies were determined after verification using Google Earth imagery and Brown et al. (2013). The associated user's, producer's and overall accuracies are given for stratified and sample counts.

		Reference categories					
	Land cover categories	Forest	Vegetation matrix	Exposed surface	Cultivated land	Total	UA
Map categories	Forest	0.28	0.04	0.00	0.01	0.33	0.99
	Vegetation matrix	0.00	0.22	0.00	0.02	0.25	0.96
	Expose surface	0.00	0.02	0.16	0.01	0.19	0.99
	Cultivated land	0.01	0.02	0.00	0.18	0.22	0.95
	Total	0.30	0.30	0.17	0.23		OA = 0.84
	PA (stratified estimate)	0.96	0.99	0.94	0.95		OA* = 0.84
	PA (sample count)	0.95	0.87	0.83	0.83		

OA =overall accuracy (sample), OA = overall accuracy (stratified), UA= User's accuracy, PA = Producer's accuracy*

Table 4.7: Error matrix showing the estimated proportion of area for land cover categories (strata) in the ca. 2014 map. The accuracies were determined after verification using Google Earth imagery and Brown et al. (2013). The associated user's, producer's and overall accuracies are given for stratified and sample counts.

		Reference categories					
	Land cover categories	Forest	Vegetation matrix	Exposed surface	Cultivated land	Total	UA
Map categories	Forest	0.20	0.05	0.00	0.01	0.27	0.96
	Vegetation matrix	0.02	0..22	0.04	0.00	0.29	0.92
	Expose surface	0.00	0.05	0.28	0.03	0.36	0.98
	Cultivated land	0.00	0.01	0.01	0.05	0.07	0.99
	Total	0.22	0.32	0.34	0.11		OA = 0.74
	PA (stratified estimate)	0.99	0.97	0.95	0.81		OA* = 0.74
	PA (sample count)	0.90	0.63	0.83	0.52		

OA =overall accuracy (sample), OA = overall accuracy (stratified), UA= User's accuracy, PA = Producer's accuracy*

4.3.4 Estimating the dominant indicators of change

Adding the intensities from the perspective of loss (Table A1-A5) with those from the perspective of gain (Table A6-A10) reveals the most dominant indicator of change in each eco-region. Observed intensity refers to the annual area of gain or loss from any category relative to the new category in the subsequent year and uniform intensity refers to the rate of gain or loss of any category relative to all non-transiting categories. The farthest values from zero show systematic transitions between categories and took into consideration both positive and negative directions (Tables 4.8 – 4.12).

Table 4.8: Added differences between observed and uniform intensity from perspective of gains and from perspective of losses in **lowland forests**. Category i and n denotes land cover categories in previous dates (i.e., 1994 and 2002). Category j and m denotes land cover categories in recent dates (i.e., 2002 and 2014). *Column headings represent exposed surface (ES), vegetation matrix (VM), FO (forest) and CL (cultivated land)*

	2002	**Category j**					**2014**	**Category m**			
Category i	1994	ES	VM	FO	CL	**Category n**	2002	ES	VM	FO	CL
	ES	0	-2.99	-2.05	3.11		ES	0	-1.47	-0.89	-0.17
	VM	-1.25	0	0.33	-0.25		VM	-1.11	0	1.39	-0.39
	FO	0.64	1.31	0	-2.37		FO	-0.94	-0.96	0	2.3
	CL	-0.69	-1.64	3.63	0		CL	0.83	1.31	-0.2	0

Table 4.9: Added differences between observed and uniform intensity from perspective of gains and from perspective of losses in **humid forests**. Category i and n denotes land cover categories in previous dates (i.e., 1994 and 2002). Category j and m denotes land cover categories in recent dates (i.e., 2002 and 2014). *Column headings represent exposed surface (ES), vegetation matrix (VM), FO (forest) and CL (cultivated land)*

	2002	**Category j**					**2014**	**Category m**			
Category i	1994	ES	VM	FO	CL	**Category n**	2002	ES	VM	FO	CL
	ES		-0.85	-0.05	-0.4		ES		0.67	-1.5	-1
	VM	1.07	0	-1.86	0.11		VM	-1.13	0	0.58	2.07
	FO	-1.34	-1.26	0	2.07		FO	-0.58	-1.13	0	1.78
	CL	-1.61	-0.64	3.09	0		CL	4.1	1.23	-1.34	0

Table 4.10: Added differences between observed and uniform intensity from perspective of gains and from perspective of losses in **littoral forests**. Category i and n denotes land cover categories in previous dates (i.e., 1994 and 2002). Category j and m denotes land cover categories in recent dates (i.e., 2002 and 2014). *Column headings represent exposed surface (ES), vegetation matrix (VM), FO (forest) and CL (cultivated land)*

	2002	**Category j**					**2014**	**Category m**			
Category i	1994	ES	VM	FO	CL	**Category n**	2002	ES	VM	FO	CL
	ES	0	-1.87	-1.91	4.44		ES	0	-0.18	-3.24	0.71
	VM	0.83	0	-1.44	1.16		VM	-0.33	0	-0.85	1.34
	FO	-0.03	2.1	0	-1.47		FO	-0.11	-0.47	0	0.76
	CL	0.45	-1.17	0.97	0		CL	-0.7	-2.07	1.04	0

During the first interval, cultivated land swap with forest was the most dominant change indicator in lowland and humid forests (Tables 4.8 - 4.9), suggesting regrowth of forest in areas that used to be cultivated was prevalent in those eco-regions. Alternatively, in littoral forests exposed surface appeared to systematically transition to cultivated land during the same interval. In the second interval, forest was regularly converted to cultivated land and exposed surface in lowland and littoral forests; while in humid forests transitions from cultivated land to exposed surface was the most dominant category swap.

Table 4.11: Added differences between observed and uniform intensity from perspective of gains and from perspective of losses in **dry forests**. Category i and n denotes land cover categories in previous dates (i.e., 1994 and 2002). Category j and m denotes land cover categories in recent dates (i.e., 2002 and 2014). *Column headings represent exposed surface (ES), vegetation matrix (VM), FO (forest) and CL (cultivated land)*

	2002	**Category j**					**2014**	**Category m**			
Category i	1994	ES	VM	FO	CL	**Category n**	2002	ES	VM	FO	CL
	ES	0	1.94	-2.66	0.82		ES	0	-0.61	-0.73	2.21
	VM	-0.82	0	2.59	0.95		VM	0.87	0	-0.07	-0.97
	FO	-0.36	0.21	0	1.36		FO	-1.42	1.4	0	0.21
	CL	3.08	-1.87	2.05	0		CL	0.28	1.65	0.15	0

Table 4.12: Added differences between observed and uniform intensity from perspective of gains and from perspective of losses in **tapia forests**. Category i and n denotes land cover categories in previous dates (i.e., 1994 and 2002). Category j and m denotes land cover categories in recent dates (i.e., 2002 and 2014). *Column headings represent exposed surface (ES), vegetation matrix (VM), FO (forest) and CL (cultivated land)*

	2002	**Category j**					**2014**	**Category m**			
Category i	1994	ES	VM	FO	CL	**Category n**	2002	ES	VM	FO	CL
	ES	0	0.34	-2.22	5.06		ES	0	-0.28	-0.94	0.28
	VM	0.67	0	1.83	-0.7		VM	-2.49	0	2.6	1.93
	FO	-1.06	1.27	0	-1.02		FO	-2.25	-0.15	0	0.97
	CL	-0.1	1.96	2.55	0		CL	4.23	-0.38	-0.45	0

The most dominant signal of change in dry and tapia forests was the swaps between cultivated land and exposed surface in both intervals. In tapia forests, exposed surface was routinely converted to cultivated land in first interval transitions and reverse swaps was detected in the second interval (Table. 4.12).

4.4 Discussion

4.4.1 Trends of land use land cover change in Madagascar

The intensity analysis detected large-to-intermediate sized conversions of largely-intact forests to exposed surfaces, cultivated lands and vegetation matrix in three eco-regions in the past twenty years. The only exceptions were the littoral and dry forests, which were likely due to the relatively small amounts of remaining largely-intact forests. There are two alternative explanations for these exceptions. First, there may have been fewer forest targets for conversion in these eco-regions due to the relatively smaller proportion of largely-intact forests available for conversion compared to other eco-regions. Alternatively, success in recent efforts towards protecting largely-intact forests in these eco-regions which are mostly demarcated as protected areas (Gasparri et al. 2016). Overall, eco-regional differences in forest area net change in Madagascar confirms the nuance nature of tropical forest transitions (Hansen et al. 2013). For instance, while second interval analysis in some eco-regions revealed net gains in forest (e.g., dry forests) others (e.g., tapia forests) underwent significant net losses. Such mixed patterns provide an additional layer of justification for disaggregated

approach to assessment of tropical forest gains, fragmentation, deforestation and forest degradation (Harris et al. 2012). This is because for some regions, subtle changes in forest disturbances can increase even as large-scale deforestation rates fall (Boucher et al. 2014, Sloan and Sayer 2015, Baker et al. 2016).

On the other hand, the sizes and speed of vegetation matrix conversions to cultivated lands and exposed surfaces were relatively smaller and slower except in the tapia forests and may suggest changes in the way fallow lands are targeted for agricultural activities (Houghton 2013). A critical look at observed transitions to cultivated land from other categories suggest that they are some of the highest during both intervals (i.e., 1994 – 2002 and 2002 – 2014), confirming the initial expectation that shifting cultivation modulates land cover change in Madagascar (Elsa et al. 2017). It is worth noting that smaller-sized, slower transitions in the second interval do not necessarily reflect slowing deforestation and forest degradation. Instead, it may simply indicate that the process of degradation associated with transitions from cultivated / agricultural lands to exposed surfaces is slower than converting largely-intact forests to either of the other categories. Eco-regions exhibiting increased deforestation and/or forest degradation had similarly large transitions to exposed surfaces, which suggests the presence of similar drivers of LULCC in both arid and moist forests (Zaehringer et al. 2015).

4.4.2 Forest gains and future land use land cover states

Intensity analysis provided evidence of secondary vegetation and subsistence agriculture transitions to forest in all five eco-regions, characterised by fast and large swaps from vegetation matrix in both intervals in humid, lowland and littoral forests. Transitions from vegetation matrix to forest states confirms the presence of young second-growth forests in Madagascar, which is not unusual, since similar occurrences have been detected in Brazilian Amazonian forests under the same time-period (Chazdon et al. 2016). Moreover, significant gains in forest category in critical eco-regions such as littoral forests may perhaps

suggest a reduction in deforestation rates for some areas (Aleman et al. 2017). In addition to forest gains, relatively slow and small-sized transitions to vegetation matrix demonstrate the potential for carbon sink in Madagascan forests, considering that secondary regrowth may be a more effective sink of atmospheric CO_2 compared to mature forests (Aguiar et al. 2016). However, such potential must be measured against areas experiencing large-sized transitions from forest and vegetation matrix to cultivated land and/or exposed surfaces. Comparing both sets of transitions will enable the determination of the spatial distribution of areas experiencing forest gains and whether they are sufficiently large enough to offer any or similar ecosystem services.

In humid and lowland forests, transitions from cultivated land to forest was systematic during the first interval, this changed during the second interval in lowland forest to systematic gains of cultivated land from forest and systematic gains of exposed surface from cultivated land in humid forests. This result is perhaps a sign that after the dominance of forest gains in the early 2000s following the creation of more protected areas, there is a return to intensive shifting agricultural practices in the eastern forest corridor (Castella et al. 2013, Mukul and Herbohn 2016, Herrera 2017). The nature of systematic swaps in dry forests notwithstanding, large-size forest gains and transitions to vegetation matrix provides more evidence of the influence of shifting cultivation practices. In dry forests, cultivated land routinely transitioned to exposed surface in first interval and vice-versa in the second interval. In tapia forest the reverse was the case for both intervals. This could be a manifestation of leakages in shifting cultivation practice along land cover gradient common with indigenous people in western Madagascar and considering the proximity between tapia and dry forests (Rakotondrasoa et al. 2012, Burivalova et al. 2015). Though for dry forests, there was a pronounced difference between the sizes of first and second interval transitions to forest and vegetation matrix. Why this is so, is not abundantly clear but there is a suspicion that first interval forest gains are able to offer higher resilience to disturbances and perhaps

a lack of suitable areas for forest to thrive after first interval forest have been established in drier eco-regions (Elmqvist et al. 2007, Poorter et al. 2016).

The method for projecting land-use/ land-cover to future date was done to reflect local-scale change dynamics as detailed by Lambin et al. (2003). Future forest states in lowland and dry forests showed net gains, while humid and tapia forest indicated net losses. However, since there is lack of studies that have utilised spatially explicit prediction techniques of LULCC of Madagascar, it is impossible to compare with the results obtained here. Nevertheless, the LCM tend to identify eco-regions with higher proportion of natural habitats (e.g., humid forests) as the most threatened compared to areas with currently higher rates of deforestation (e.g., lowland forests). Similar discriminatory performance were identified by Pérez-Vega et al. (2012) in their application of LCM in dry deciduous forests in Mexico. Despite this, the projections for the year 2050 are based on the accuracy of current LULC models and offer a possible scenario of the future states of natural habitats at local-scales if current land-use intensifications, deforestation and forest degradation rates are sustained without any meaningful intervention.

4.5 Conclusion

These results suggest that the main drivers of LULCC in tropical forests are active in all eco-regions of Madagascar. Although, for some eco-regions (e.g., humid forests), transitions from forest caused by subsistence farming is more pronounced than others (e.g., dry forests). Transitions from vegetation matrix is an active contributor to forest gains in all eco-regions. Likewise, systematic transitions between cultivated land and exposed surface is a response to LULCC in dry and tapia forests. These results reflect the subtle differences in the drivers of LULCC at eco-regional scales. However, there is need for more studies of tropical forest transitions and the dynamics along environmental gradients (Phillips and Brienen 2017). Especially studies that are designed to combine higher resolution imagery (< 5m) and possibly from multi-sensory platforms to capture longer temporal dimensions of land cover dynamics.

For Madagascar, this is important because quantitative and spatially-explicit analysis of LULCC are rare, at least at eco-regional scales. And considering that one of the expected outcome from climate and LULCC is feedbacks on natural habitats it is paramount that modelling approaches are implemented at meaningful scales for better assimilation with current conservation efforts. Doing so would propagate our understanding of current land cover dynamics, mitigate against species extinctions and realistically prepare all stakeholders for range shifts in this biodiversity hotspot.

Chapter Five

Habitat fragmentation and connectivity in protected areas

5.1 Introduction

5.1.1 Landscape prioritisation assessment

The ability of most protected areas to support species migration in response to the coupled effects of land use and climate change will become increasingly compromised in the near future (Heller and Zavaleta 2009, Thomas et al. 2012). In the tropics, protected areas (PAs) are becoming increasingly isolated due to human encroachment and other environmental pressures (Ruth et al. 2005, Laurance et al. 2012). For instance, fragmentation and associated edge effects due to loss of forest habitats at both local and regional scales dramatically change landscape configuration and threatens biodiversity in the tropics (Laita et al. 2011, Ibáñez et al. 2014). Irrespective of the geographical location however, the erosion of connectivity has become commonplace (Marco et al. 2015) and is often driven by deforestation and forest degradation (Eklund et al. 2016). Although conservation planners have always prioritised identification of remnant forest patches (Wiegand et al. 2005), the current focus is to map network connectivity on a wider landscape scale, as well as understand the consequences of degrading landscape connectivity (Saura et al. 2011, Foltête et al. 2012). One important question associated with connectivity remains unresolved: how does landscape connectivity affects plant dispersal and migration? This is because very few studies explicitly measure landscape connectivity in PAs (e.g., see Eklund et al. (2016) and Laurance et al. (2012) for assessment of PAs without landscape connectivity), therefore there is no clear indication about thresholds above which plant dispersal and migration becomes increasingly difficult.

In tropical developing countries, there is evidence that forest loss occurs in PAs and is mainly because of the prevalence of subsistence and shifting agriculture (Llopis et al. 2015, Bowker et al. 2017). Change detection allows for relatively quick and quantitative analysis of such drivers of LULCC (e.g., shifting cultivation) in PAs and to extend such

quantitative measures to landscape connectivity. Landscape connectivity refers to the degree to which natural environments facilitate or impede dispersal between habitats (Taylor et al. 1993, Taylor 2006). There are two important components of landscape connectivity: (i) structural connectivity which describes the physical linkages between forest areas; and (ii) functional connectivity which focuses on species' responses to landscape structure and addresses the flow of individuals among forest areas (Tischendorf and Fahrig 2000, Aavik et al. 2013, Okin et al. 2015). In spatial ecology, it is widely regarded that the ecological integrity of dispersing species can only be guaranteed by linkages between patches and absence of resistance to movement on the landscape (Hampe 2011, Zeller et al. 2012). Some studies of plant dispersal rates have varied widely from a few meters to several kilometres (Walther et al. 2005, Midgley et al. 2006). But plant dispersals are often influenced by localised environmental conditions, therefore universal rates are likely to be misleading and may have unwanted implications if applied to small-scale conservation projects. The advantages of incorporating landscape connectivity into spatial ecology have been illustrated. For instance, some studies have reported improved predictive power of species distribution models (Foltête et al. 2012), or rapid identification of locations for patch restoration (McRae et al. 2012), or planning for protected areas and the key linkages in them that support functional connectivity (Gurrutxaga et al. 2011, Velázquez et al. 2017) , as well as better understanding of the effect of historical landscape linkages on future species diversity (Lindborg and Eriksson 2004).

One advantage of including LULCC in analysis of landscape connectivity is that historical linkages is explicitly captured and other quantitative measures, such as proportion of land cover categories or their rate of change, can be derived. Regardless of past changes, predictions for most regions indicate more habitat losses and by extension increased fragmentation in PAs with serious implications for biodiversity (Montesino Pouzols et al. 2014). Already, fragmentation of forested areas has led to the isolation of plant communities,

which in turn reduce the chances of re-colonisation (Leimu et al. 2006, Ibáñez et al. 2014) and increases risk of extinction (Vranckx et al. 2012).

In this chapter, landscape connectivity is explicitly quantified for selected protected areas in Madagascar by combining models of habitat spatial patterns (Vogt et al. 2007) with recent indices of habitat network connectivity (Saura and Rubio 2010). By examining the degree of habitat connectivity, an implicit measure of dispersal potential (i.e. functional connectivity) derived for plants that are likely more sensitive to fragmentation (i.e., endangered plants) is achieved for a tropical hotspot. For these reasons, probabilities of habitat connectivity were determined for several dispersal distances (i.e., 250m, 500m, 1000m, 3000m and 5000m) to ascertain whether the structural connectivity within PAs are able to support dispersing plant species at increasingly greater distances. The aim was to incorporate measures of deforestation and forest degradation, as well as LULCC to assess fragmentation and habitat connectivity at the PA-scale. The main objectives were to:

1. model the recent rate of deforestation and degradation for selected protected areas;
2. determine the extent of fragmentation and assess changes in land-use and land-cover between 1994 – 2002 and 2002 – 2014; and
3. calculate the probability of habitat connectivity for different dispersal thresholds for each PA.

When dealing with landscape connectivity, if possible it is important to consider all components of forest habitats (i.e., spatial, environmental and intrinsic components). These spatial components examine forest patch locations, landscape configuration, dispersal distance, dispersal cost and reachability between patches (Vasudev et al. 2015), while the environmental component account for biotic (e.g., competition) and abiotic factors. Intrinsic components of landscape connectivity examine the modes of movement at species-specific scales and how such species traits impact dispersals (Zollner and Lima 2005, Fletcher et al.

2013). However, owing to the lack of data, an all-inclusive component assessment is not feasible and for this reason only the spatial component of landscape connectivity is considered. Therefore, there is no direct link to the physiology of the plant species assessed in later chapters, but rather this chapter seeks to determine whether a suitable environmental matrix exist to support plant dispersal.

5.2 Methods

5.2.1 Protected areas of Madagascar

The polygon shapefiles for 44 PAs in Madagascar were obtained from the World Database on Protected Areas website (https://www.protectedplanet.net/) (Figure 5.1). The focus was on PAs established before 2007 and classified as national parks (16), proposed protected areas (9), special reserve (9), strict nature reserve (2), natural park (1) and no reported classification (7). Other criteria for selecting PAs included:

i) those classified as terrestrial;

ii) those with geographical sizes larger than 500 by 500 pixels (minimum threshold for deriving landscape graphs);

iii) the landscape is not greatly affected by cloud cover ($\leq$10%).

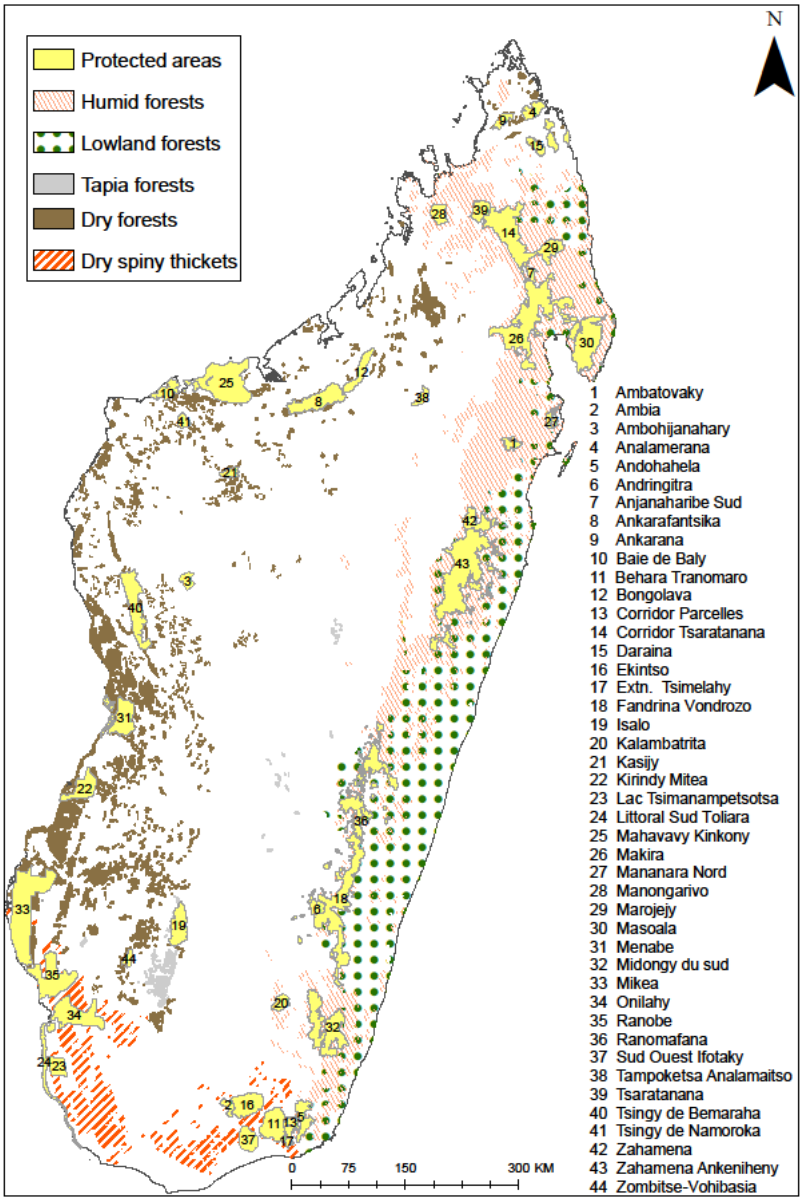

Figure 5.1: Spatial distribution of selected protected areas in Madagascar and eco-regions. 16 PAs are in humid forests, 11 in dry spiny thickets, 14 in dry forests, two in highland plateau grasslands and one each in tapia and lowland forests.

5.2.2 Measuring PA deforestation and forest degradation rates

The rates of deforestation and forest degradation were quantified using sub-pixel analysis and following the method described in **Chapter 2, Section 2.3**. Sub-pixel analysis was implemented for all PAs in two intervals (i.e., 1994 – 2002 and 2002 – 2014). In addition to sub-pixel analysis, the land use land cover maps for each PA were also produced using the method described in **Chapter 2, Section 2.5**. In addition, the rate of change in land cover categories from 1994 to 2014 was calculated for the selected protected areas.

5.2.3 Determining spatial pattern and fragmentation in protected areas

Landscape graphs for each protected area were produced using Morphological Spatial Pattern Analysis (MSPA). MSPA is an automated per pixel classification that allows for description of geometry, pattern and qualitative connectivity of forested landscapes (Vogt et al. 2007) and was done in GUIDOS toolbox (http://forest.jrc.ec.europa.eu/download/software/guidos). First, LULCC maps of each PA was converted to binary raster format of forest and non-forest categories, representing foreground and background area (Figure 5.2). Afterwards, the binary data were then segmented into different and mutually exclusive classes that depicts the spatial pattern (i.e., landscape graph). The edge width was set to three pixels (~ 100 m). This distance was informed by the findings of previous studies conducted in Madagascar (Brown et al. 2009, Brown et al. 2013, Razafindratsima et al. 2018). In their respective studies of Madagascan forests, they established that at approximately 100 m from the edge of densely forested areas, there was a distinct change in forest structure and attributed such differences to edge effects.

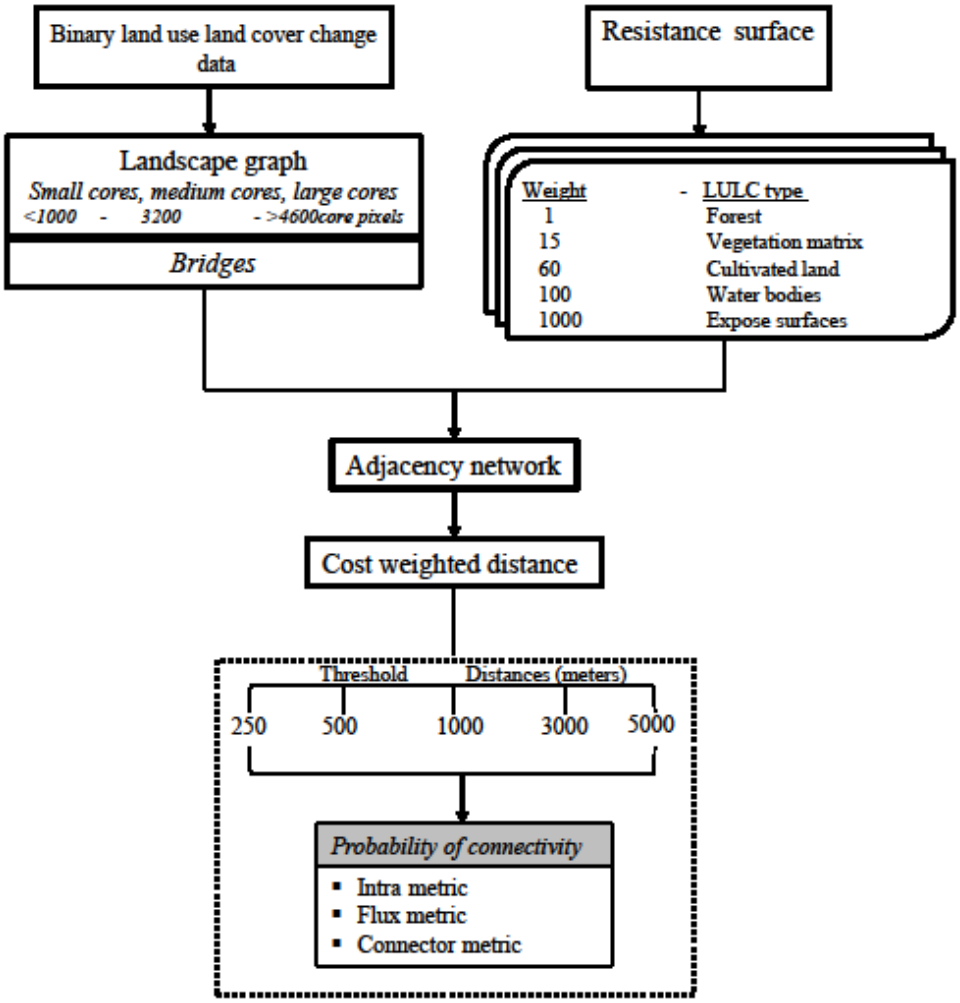

Figure 5.2: Conceptual diagram for the derivation of landscape graphs and development of habitat connectivity using probability of connectivity index for selected protected areas in Madagascar.

Seven landscape classes were derived from the MSPA: cores, islet, bridge, perforation, branch, edge and loop. *Core* was designated to pixels whose distance to non-forested areas (i.e., background) was greater than the edge width. As such, core is the distinct landscape element that is categorised as forest cores and thus represent a proxy for ideal habitats in the PAs. The default setting in GUIDOS for core size classification was used as there was insufficient field data to inform PA-specific determination and by implication no justification to change the setting. Thus, forest cores were classified into three sizes: small-sized cores consisted of less than 1000 connecting pixels; medium cores were between 1000 - 4600 connecting pixels; and > 4600 connecting pixels were designated as large cores

(Figure 5.2). *Bridges* are non-core pixels that connect other core areas at both ends (Vogt et al. 2009, Saura et al. 2011). In this chapter, only *forest cores* and *bridges* were required for the analysis of fragmentation and habitat connectivity in PAs. Other landscape elements were not particularly useful in the determination of habitat connectivity and were not considered.

MSPA was also used to quantify the amount of fragmentation in all PAs. This was done by analysing the proportions of forest cores and bridges in each interval (i.e., ca. 1994 – ca. 2002 and ca. 2002 – ca. 2014) in the different PAs. An increase in the proportion of bridges within landscapes (i.e., PAs) accompanied with decreases in the proportion of forest cores suggest fragmentation may be active during that interval.

5.2.4 Modelling resistance surfaces

To produce landscape resistance maps, the habitat network model approach as described in Gurrutxaga et al. (2011) was implemented within a GIS. This resulted in the recoding and conversion of land-use/land-cover maps (2002 – 2014) into resistance thresholds (Table 5.1 and Figure 5.2). Within the network model, there were three orders of magnitude difference between pixel values classified as very low resistance to movements (assigned a value of 1) and those classified as very high resistance to movement (assigned a value of 1000). The assumption is that forest-patches will facilitate dispersal, while exposed surfaces represent regions of high cost for dispersing plants. The resistance surface was determined using cost weighted distances (CWD), rather than Euclidean distance because it is an ecologically intuitive proxy for species dispersal in heterogenous landscapes (McRae et al. 2008, Zeller et al. 2012). The same thematic scale (i.e., same number of classes) was used for all LULCC products to ensure that resistance values did not change between PAs.

Table 5.1: Pixel resistance values determined from second interval LULCC maps (i.e., 2002 – 2014) using GIS. High and low values correspond to the ease at which pixels can enable or impede dispersals of species.

Categories	Resistance values	Ecological Implication
Forest	1	Very low
Vegetation matrix	15	Low
Cultivated land	60	Medium
Water bodies	100	High
Expose surfaces	1000	Very high

5.2.5 Measuring habitat connectivity in protected areas

In each PA, forest core connectivity was determined using the probability of connectivity (PC) metric and its three indices (see below) (Saura and Rubio 2010). PC was calculated for every core area and bridge in the PAs using Conefor (http://www.conefor.org/coneforsensinode.html). Conefor combines landscape graphs (in this instance, forest cores and bridges) with the derived estimate of CWD to calculate structural connectivity in the landscapes under different hypothetical dispersal distances (Saura et al. 2011). Five threshold dispersal distances were considered for the analysis of connectivity and the determination of forest cores importance (Figure 5.2). The threshold distances range from 250m (probable) to 5000m (improbable).

The importance of forest cores was calculated using the change in probability of connectivity metric (*d*PC). *d*PC determined connectivity between forest cores using a probability connection model that allows for continuous adjustments of the connection strength (Equation 5.1). Saura and Pascual-Hortal (2007) suggest that this metric incorporates all elements of an ideal connectivity measure and is sensitive to habitat loss and fragmentation in an ecologically meaningful way.

Equation 5.1: $PC = \frac{\sum_{i=1}^{n}\sum_{j=1}^{n} a_i a_j \cdot P_{ij}^*}{A_L^2}$

Where n is the total number of patches, a_i and a_j are the sizes of patches i and j, l_{ij} is the number of links in the shortest path between patches i and j, and A_L is the total PA area. P_{ij}^* is defined as the maximum product of all possible paths between patches i and j.

At PA-scales, what is crucial for spatial conservation planning is the importance of forest core area, their role in connectivity and the ability to act as stepping-stones in a network. Therefore, for every given forest core, *x*, its *d*PC metric is the sum of three fractions, namely: dPC_{intra}, dPC_{flux} and *dPCconnector*. dPC_{intra} determines the contribution of core *x* in terms of intra-patch connectivity and does not take into consideration the connectivity of *x* to other core areas in the PA. Similarly, there is no indication of the dispersal capabilities of plant species that inhabit *x*. Therefore, dPC_{intra} remains the same if *x* is isolated and has no bridges connecting it to other forest core area. dPC_{flux} accounts for the area-weighted dispersal flux through the connections to *x* and from all other cores in the PAs when *x* is not the starting and ending node. dPC_{flux} relies on the location of *x* within the forest patch networks and its attribute (e.g. area). Bridges cannot contribute to connectivity through this fraction because they have no habitat area, thus are unable to be origin or destination of fluxes. The last fraction, $dPC_{connector}$ calculates the contribution of core, *x,* or any given bridge to the connectivity between other cores and is how stepping stones were determined in the different PAs. Inter-patch connectivity was measured by dPC_{flux} and $dPC_{connector}$ in the different PAs. Due to the computation intensity required to calculate *d*PC metric only 27 PAs were analysed using this metric as it was generally impossible to implement this analysis for very large PAs.

5.3 Results

5.3.1 Protected areas deforestation and forest degradation rates

Increased deforestation rates were detected in nine (or 26 %) PAs (Figure 5.3), while forest degradation rates increased in sixteen (or 36%) PAs (Figure 5.4). Also, all protected areas with increased deforestation and forest degradation rates were higher than the Island-wide mean rates of deforestation and degradation (red lines in Figure 5.3 & 5.4). Tsingy de Namoroka national park had the highest deforestation rate (90.14%), while Behara Tranonmaro, Ekintso and Extension Tsimelahy proposed protected areas all had the lowest deforestation rates (-0.99%). However, because the deforestation rates measured in Tsingy de Namoroka was significantly higher than the next highest rate (i.e., Kasijy national park) which had deforestation rate of 13.81% it was not plotted in Figure 5.3 for aesthetics. On the other hand, the highest forest degradation rate was estimated for Lac Tsimanampetsotsa[3] PA (5.33%) and the lowest rate in Extension Tsimelahy (-0.99%) proposed protected area.

The mean deforestation rates (n=42, $\bar{x}$=2.86%) in the selected PAs was significantly greater than Island-wide mean rates (0.26%). Similarly, the mean forest degradation rates (n=41, $\bar{x}$=0.05%) in the selected PAs was greater than Island-wide mean rates (-0.19%). A summary of PA-specific deforestation and forest degradation rates is provided in Appendix 8.

[3] MSPA of Lac Tsimanampetsotsa national park was carried out for the dry spiny thickets in this site and not the lake

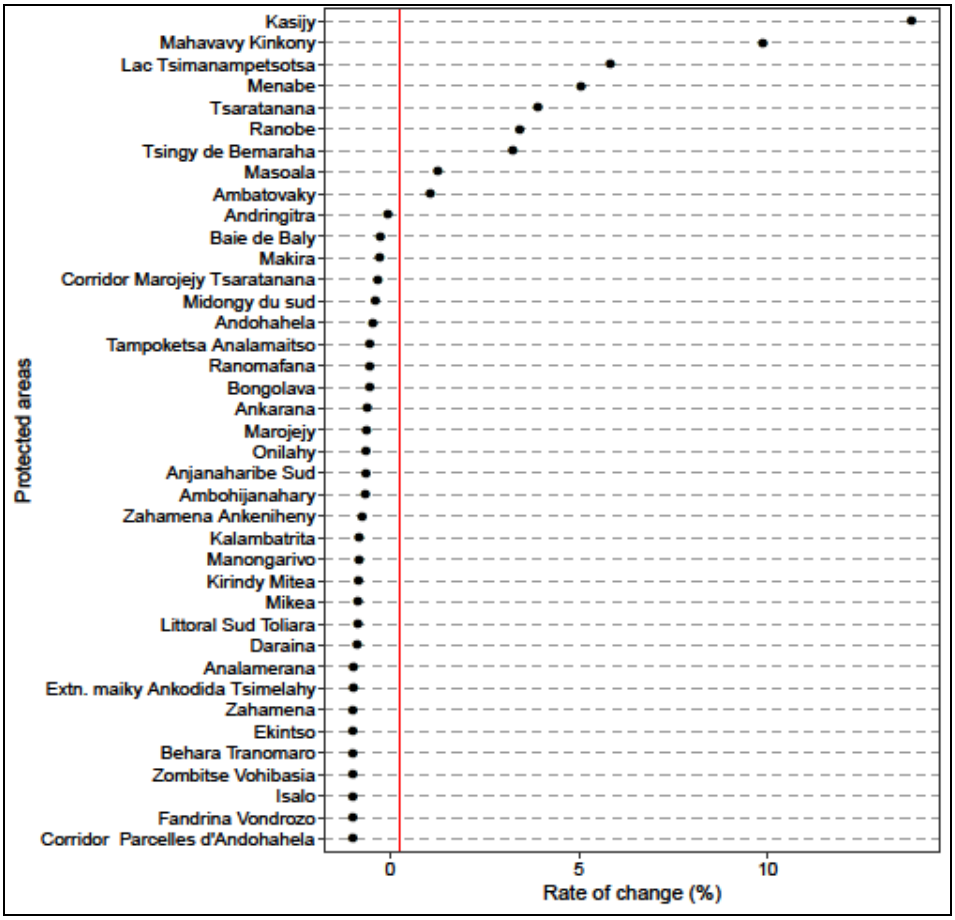

Figure 5.3: Dot plot showing rates of deforestation from 1994 - 2014 as derived from sub-pixel analysis for 39 protected areas of Madagascar. Sub-pixel analysis did not measure deforestation in all PAs. Solid red line shows the mean deforestation rates across Madagascar (0.33%). *Tsingy de Namoroka national park (90.64%) not included here.*

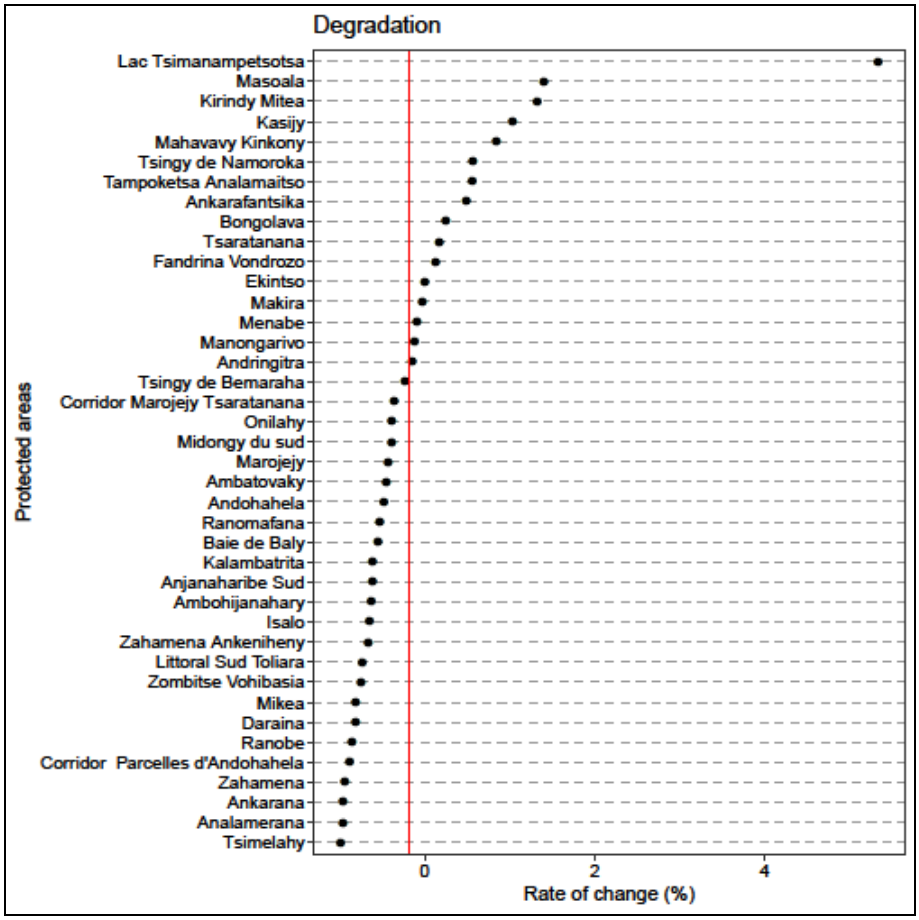

Figure 5.4: Dot plot showing rates of forest degradation from 1994 - 2014 derived from sub-pixel analysis for 40 protected areas of Madagascar. Sub-pixel analysis did not measure forest degradation in all PAs. Solid red line indicates the mean degradation rate across Madagascar (-0.25%)

5.3.2 Analysis of forest fragmentation in protected areas

Morphological spatial pattern analysis revealed that in the second interval small - sized forest cores increased in 25 (57%) PAs. On the other hand, medium-sized forest cores increased in 12 (27%) PAs in the second interval compared to first interval numbers for those PAs (Table 5.2). The number of large-sized forest cores increased in 5 (11%) PAs in the second interval. There was an increase in the number of bridge elements in 15 (34%) PAs in the second interval compared to first interval. In 22 (50%) PAs, forest core area decreased during the second interval (grey bars in Figure 5.5a). During the same interval the area occupied by bridges in 27 PAs increased (grey bars in Figure 5.5b).

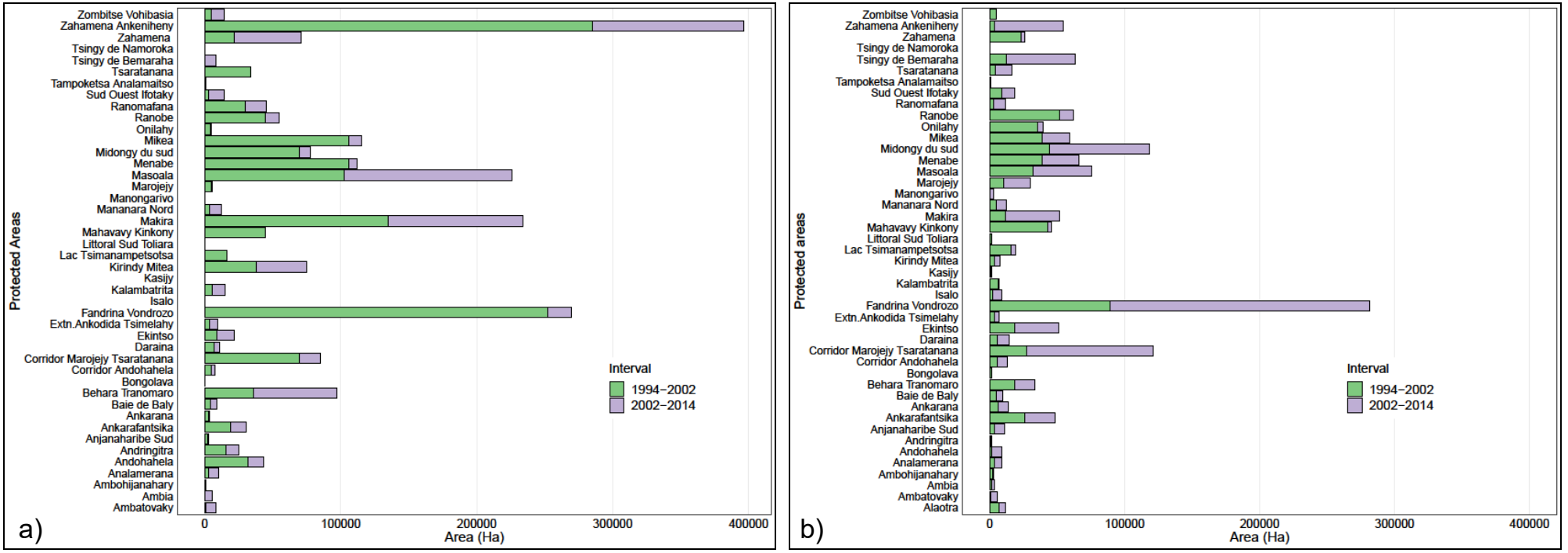

Figure 5.5: a) Interval comparisons of changes in forest core areas and b) changes in bridge areas for 44 protected areas of Madagascar. Average forest core sizes for the first interval *(1994 – 2002)* and second interval *(2002 – 2014)* is *34516 Ha* and *15865 Ha* respectively, while bridge sizes averaged *14305 Ha* and *18635 Ha* in first and second interval respectively.

Table 5.2: Output of morphological spatial pattern analysis showing measures of core and bridge in selected protected areas of Madagascar. Analysis is implemented using first interval (i.e., 1994-2002) and second (i.e., 2002-2014) interval land use land cover change maps. Bold values indicate increase in the number and/or proportions of core and bridge elements in second interval.

			1994-2002									2002-2014								
NAME	Eco-region	PA area (Ha)	Core area (Ha)	Percentage of core (%)‡	Nos. small core	Nos. medium core	Nos. large core	Total nos. of cores	Bridge area (Ha)	Percentage of bridge (%)	Nos. bridges	Core area (Ha)	Percentage of core (%)‡	Nos. small core	Nos. medium core	Nos. large core	Total nos. of cores	Bridge area (Ha)	Percentage of bridge (%)	Nos. bridges
Ambohijanahary	Dry forest	24508	148.87	0.61	94	0	0	94	1843	7.52	19	653.75	2.67	33	0	0	33	734.81	3.00	3
Analamerana	Dry forest	42026	2791.10	6.64	151	2	2	155	3827	9.11	39	7084.30	16.86	**250**	**10**	2	**262**	4830.21	11.49	**90**
Ankarafantsika	Dry forest	135608	18632.15	13.74	880	8	5	893	25983	19.16	103	11701.70	8.63	**933**	**11**	4	**948**	22479.58	16.58	**134**
Ankarana	Dry forest	25334	2698.17	10.65	219	7	0	226	6477	25.57	40	916.68	3.62	**229**	2	0	231	7100.42	28.03	13
Baie de Baly	Dry forest	65856	4257.79	6.47	212	4	1	217	4979	7.56	48	4376.99	6.65	153	2	1	156	4642.36	7.05	35
Bongolava	Dry forest	60819	77.24	0.13	79	0	0	79	1367	2.25	12	5.35	0.01	10	0	0	10	17.23	0.03	1
Daraina	Dry forest	70637	7056.45	9.99	202	4	6	212	5191	7.35	66	3945.05	5.58	**395**	**7**	2	**404**	9357.36	13.25	65
Kasijy	Dry forest	23120	372.48	1.61	41	1	0	42	859	3.72	37	9.49	0.04	9	0	0	9	303.75	1.31	2
Kirindy Mitea	Dry forest	82125	37549.45	45.72	116	0	2	118	3504	4.27	39	37412.45	45.56	**163**	**5**	**3**	**171**	4114.16	5.01	**66**
Mahavavy Kinkony	Dry forest	263231	44558.86	16.93	1791	38	11	1840	42689	16.22	302	284.36	0.11	126	0	0	126	3126.89	1.19	18
Menabe	Dry forest	126205	105815.80	83.84	350	21	8	379	39029	30.93	151	5913.61	4.69	**759**	14	1	**774**	26939.82	21.35	26
Tsingy de Bemaraha	Dry forest	84276	25.86	0.03	13	0	0	13	12600	14.95	5	7825.53	9.29	**1671**	4	**1**	**1676**	50564.61	60.00	**57**
Tsingy de Namoroka	Dry forest	22252	109.73	0.49	15	0	0	15	338	1.52	4	2.30	0.01	4	0	0	4	0.00	0.00	0
Zombitse-Vohibasia	Dry forest	17423	4623.91	26.54	169	2	4	175	4771.38	27.39	23	9434.32	54.15	18	1	1	20	392.61	2.25	16
Mean			*16336.99*						*10961.31*			*6397.56*						*9614.56*		
Ambia	DST	20837	109.67	0.53	54	0	0	54	1613	7.74	9	5520.49	26.49	**1159**	**11**	**1**	**1171**	2199.77	10.56	**1051**
Behara Tranomaro	DST	97018	36102.37	37.21	671	7	6	684	18517	19.09	160	61030.31	62.91	368	4	5	377	14622.16	15.07	65
Corridor Parcelles Andohahela	DST	18308	4583.99	25.04	174	7	2	183	5450	29.77	22	2735.96	14.94	**247**	7	1	**255**	7302.77	39.89	**36**
Ekintso	DST	91580	8840.72	9.65	697	6	4	707	18402	20.09	85	13083.01	14.29	**1050**	**13**	**8**	**1071**	32610.85	35.61	52
Extension Ankodida Tsimelahy	DST	12049	3376.78	28.03	134	0	2	136	3675	30.50	20	6399.59	53.11	108	**2**	2	112	3270.64	27.14	16
Lac Tsimanampetsotsa	DST	46426	16290.59	35.09	493	3	5	501	15594	33.59	35	69.40	0.15	62	0	0	62	3780.82	8.14	2
Littoral Sud Toliara	DST	290172	137.44	0.05	57	0	0	57	1611	0.56	11	42.16	0.01	6	0	0	6	95.28	0.03	2
Mikea	DST	326419	105815.80	32.42	1243	6	4	1253	39029	11.96	192	9231.67	2.83	827	**17**	**8**	852	20186.31	6.18	**229**
Onilahy	DST	160193	4048.07	2.53	1035	5	1	1041	35292	22.03	31	511.45	0.32	180	1	0	181	4107.55	2.56	18
Ranobe PK	DST	170783	44479.15	26.04	1757	14	12	1783	51551	30.19	163	10481.89	6.14	626	10	5	641	10244.77	6.00	**210**
Sud_Ouest Ifotaky	DST	57370	2454.39	4.28	397	1	1	399	8913	15.54	55	11707.43	20.41	**445**	**9**	**5**	**459**	9423.43	16.43	**146**
Mean			*20567.18*						*18150*			*10983.03*						*9804.03*		
Tampoketsa Analamaitso	HPGL	22613	571.00	2.53	48	2	0	50	330	1.46	20	44.32	0.20	21	0	0	21	206.57	0.91	5
Ambatovaky	Humid forest	24865	1056.99	4.25	67	0	1	68	921	3.70	16	7301.34	29.36	**397**	**9**	2	**408**	4736.87	19.05	**74**
Andohahela	Humid forest	75693	31430.00	41.52	398	10	7	415	1701	2.25	915	12052.18	15.92	**4379**	2	2	**4383**	7365.68	9.73	38
Andringitra	Humid forest	31107	15924.18	51.19	459	2	3	464	641	2.06	410	9091.61	29.23	**699**	2	1	**702**	947.04	3.04	**742**
Anjanaharibe Sud	Humid forest	18258	1889.14	10.35	136	0	1	137	3517	19.26	20	843.30	4.62	**257**	2	0	**259**	7455.58	40.83	5
Corridor Marojejy Tsaratanana	Humid forest	229449	69451.00	30.27	1052	13	6	1071	27398	11.94	237	15219.79	6.63	**2948**	**24**	3	**2975**	93843.52	40.90	48
Fandrina Vondrozo	Humid forest	497102	252132.41	50.72	3291	48	33	3372	89028	17.91	780	17683.23	3.56	**5696**	17	4	**5717**	192827.64	38.79	119
Kalambatrita	Humid forest	32159	5235.26	16.28	0	236	0	236		18.58	55	9391.18	29.20	**67**	0	2	69	590.94	1.84	42
Makira	Humid forest	364844	134919.07	36.98	6947	40	21	7008	11450	3.14	6733	99225.90	27.20	**22888**	55	11	**22954**	40117.71	11.00	**22755**
Manongarivo	Humid forest	41648	4552	10.93	345	4	2	351	7672	18.42	66	103.18	0.25	63	0	0	63	3110.14	7.47	6
Marojejy	Humid forest	59744	4621.18	7.73	407	2	1	410	10531	17.63	49	722.93	1.21	**438**	0	0	**438**	19479.88	32.61	3
Masoala	Humid forest	209202	102786.72	49.13	1214	24	13	1251	32185	15.38	346	123135.36	58.86	1333	23	11	**1367**	43423.17	20.76	152
Midongy du sud	Humid forest	206592	69382.59	33.58	1625	21	14	1660	44097	21.34	421	7950.71	3.85	**2344**	11	2	**2357**	74433.24	36.03	81
Ranomafana	Humid forest	40632	29781.15	73.29	103	0	4	107	2547	6.27	44	15746.35	38.75	**343**	**1**	3	**347**	9026.31	22.21	**78**
Tsaratanana	Humid forest	49251	34009.37	69.05	147	0	2	149	4010	8.14	98	116.58	0.24	139	0	0	139	12334.60	25.04	10
Zahamena	Humid forest	63933	21800.88	34.10	1011	5	1	1017	23178	36.25	1515	48951.07	76.57	103	1	2	106	2464.62	3.86	55
Zahamena Ankeniheny	Humid forest	446167	285309.63	63.95	4492	39	21	4552	3729.37	0.84	5268	111236.48	24.93	**30624**	**77**	21	**30722**	50763.12	11.38	**30421**
Mean			*66233.10*						*16995.57*			*29923.20*						*35182.50*		
Mananara_Nord	Lowland forest	23729	3417.76	14.40	237	0	2	239	4765	20.08	48	8687.36	36.61	**328**	**6**	**3**	**337**	7580.27	31.95	**77**
Isalo	Tapia forest	87321	32.71	0.04	42	0	0	42	1994	2.28	7	171.86	0.20	**209**	0	0	**209**	6779.52	7.76	**19**
Total		*4858883*	*1515257.41*						*615128*			*130472.12*						*805574.77*		
Overall Mean			*34516.09*						*14305*			*15864.86*						*18634.88*		

Note: DST and HPGL represents dry spiny thickets and high plateau grasslands

In humid forests, dry forests and dry spiny thickets forest core areas reduced across all PAs in those regions in the second interval compared to first interval (Figure 5.6). At the same time, in humid forests and dry spiny thickets bridge areas increased considerably in the second interval, while in the second interval bridge area PAs located in dry forests experienced slight increases (Figure 5.6). However, the only PA analysed for lowland forests showed an increase in total forest core area from 3418 Ha during the first interval to 8687.36 Ha during the second interval (Table 5.2). Similar pattern was detected in PA located in tapia forests where the total forest core areas increased in the second interval. In high plateau grasslands total forest core and bridge areas decreased in the second interval.

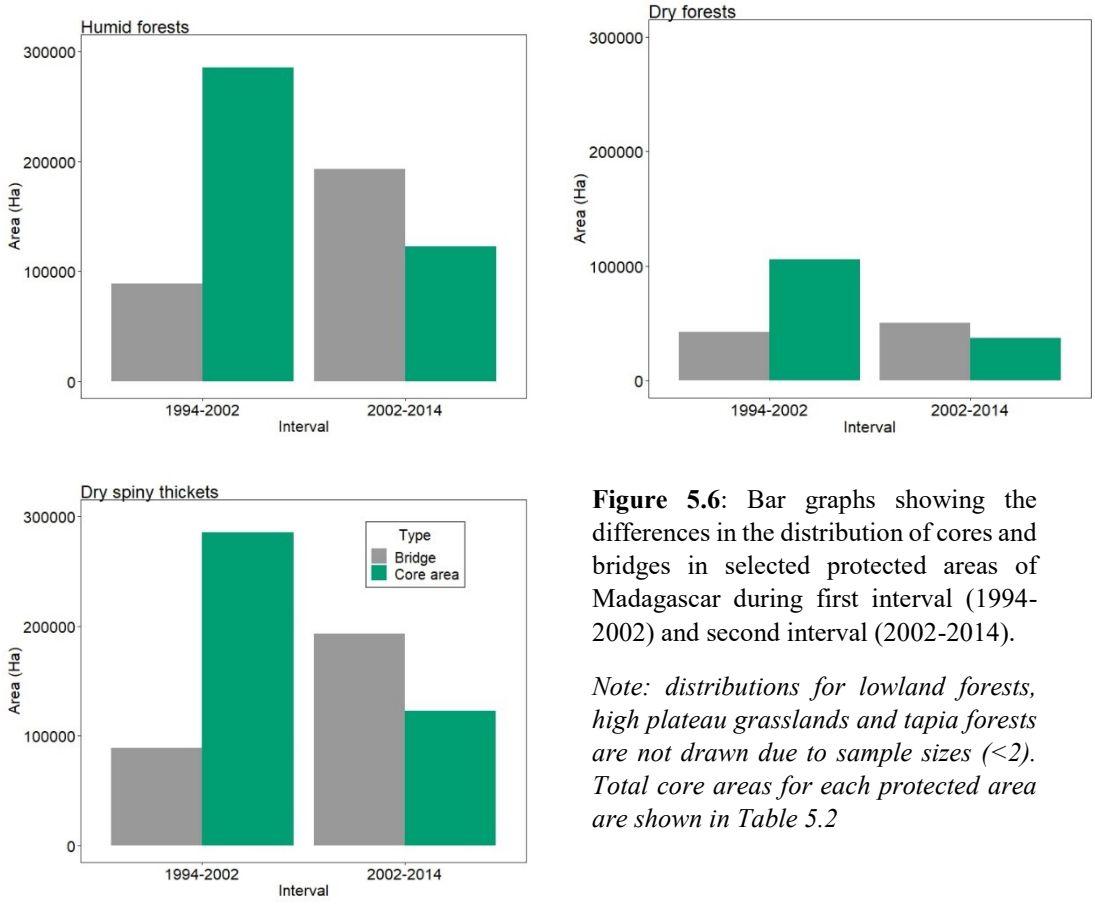

Figure 5.6: Bar graphs showing the differences in the distribution of cores and bridges in selected protected areas of Madagascar during first interval (1994-2002) and second interval (2002-2014).

Note: distributions for lowland forests, high plateau grasslands and tapia forests are not drawn due to sample sizes (<2). Total core areas for each protected area are shown in Table 5.2

5.3.3 Rates of land use land cover change in protected areas

LULCC analysis revealed that exposed surface had the highest increase in area (386%), while cultivated land had the lowest increase in area (12.78%) across all PAs by the second interval (Figure 5.7a-d). However, forest areas in PAs located along the eastern corridor (i.e., humid and lowland forests) and dry spiny thickets generally experienced smaller RoC compared to those in PAs located in western dry forests (Figure 5.7a). Similarly, the RoC in vegetation matrix was generally smaller in humid and lowland forests (Figure 5.7b). Protected areas located in dry spiny thickets, humid and lowland forests experienced increases in cultivated land compared to those in dry forests (Figure 5.7c). Protected areas in dry forests and spiny thickets had more negative changes in exposed surface compared to those located in humid forests.

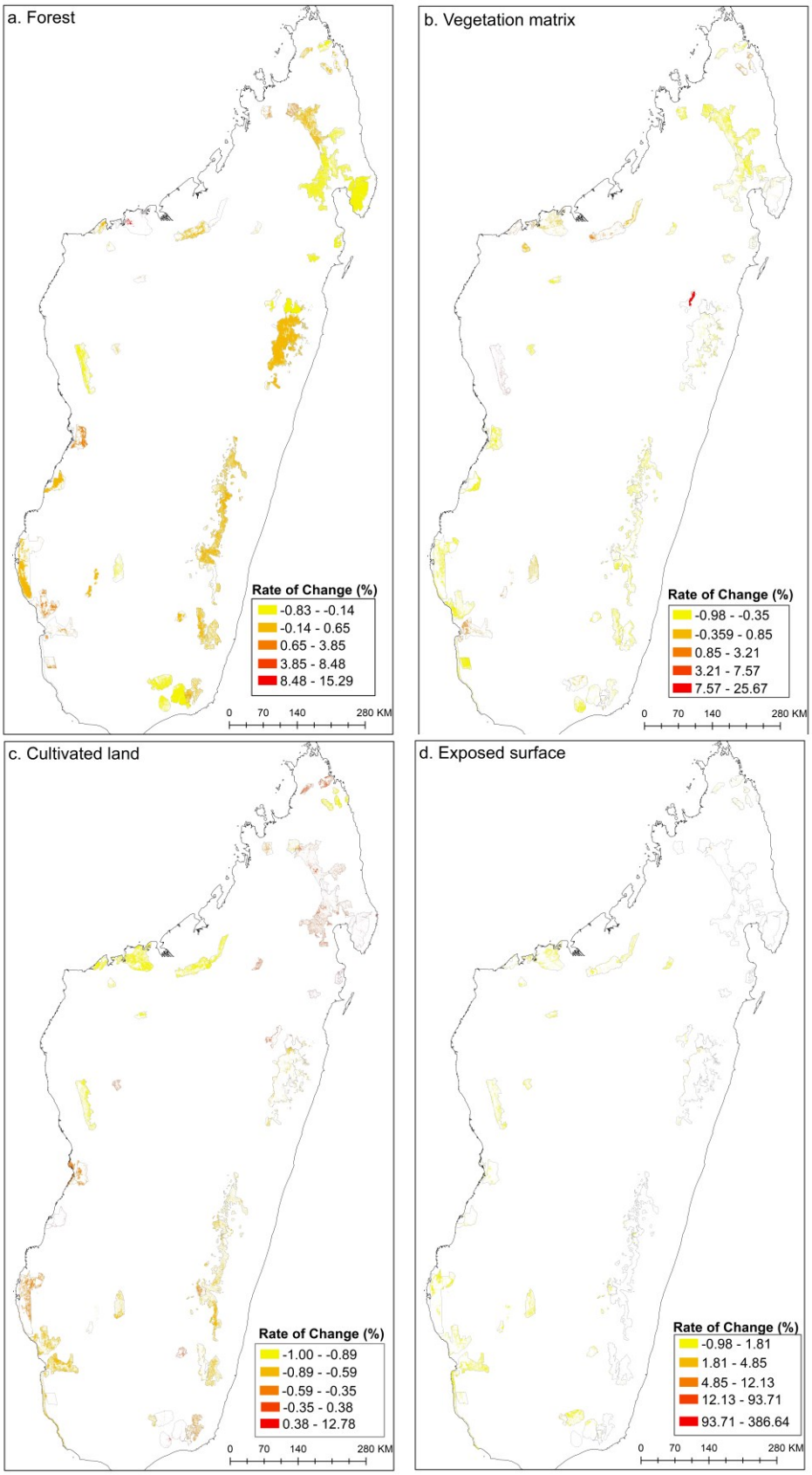

Figure 5.7: Rate of change in selected protected areas in Madagascar. RoCs are derived from the proportion of land cover categories in first and second intervals and show the changes to forested areas (*top left*), vegetation matrix (*top right*), cultivated lands (*bottom left*) and exposed surfaces (*bottom right*).

5.3.4 Probability of forest cores connectivity

The most important forest core and bridge in 27 PAs were identified using the probability of connectivity (PC) metric. Protected areas in dry forests and spiny thickets were predominately characterised by forest cores with low PC values, while forest cores in humid forests had a mixture of high, medium and low PC values (Figure 5.8). On average, the most important forest core had higher PC values and larger sizes than the most important bridge in those PAs (Table 5.3). However, the PC values of the most important habitat resources decreased as dispersal distance increased. For instance, at dispersal distance of 250 m (most probable) the average PC between forest cores was 57.84%, while at dispersal distance of 5000 m (improbably) the average PC value decreased to 56.21%. Similarly, the average PC between bridges across all PAs analysed decreased from 13.5% (most probable) to 12.80% (improbable). In Tsingy de Namoroka bridges were absent, resulting in no PC calculated for bridges in that PA. In seven PAs, there was marginal reduction in the PC values of the most important forest cores at 5000 m, namely: Ambatovaky, Anjanaharibe sud, Ankarana, Daraina, Mahavavy kinkony, Mananara nord, Marojejy (Table 5.3). Likewise, the PC values of the most important bridge decreased in Anjanaharibe sud, Corridor parcelles and Kasijy PAs with increased dispersal distance.

Further analysis of the most important cores and bridges showed connectivity was mostly from their flux and intra attributes or from flux and connector attributes (Figure 5.9 – 5.13). There was no contribution to PC through the combination of the intra and connector fractions at all dispersal distances. Suggesting less influence of stepping stones effects at all dispersal distances in most PAs of Madagascar. Correlation analysis between forest core areas/bridges in the 27 PAs and the derived PC showed similarly positive relationship at all dispersal distances (Appendix 9).

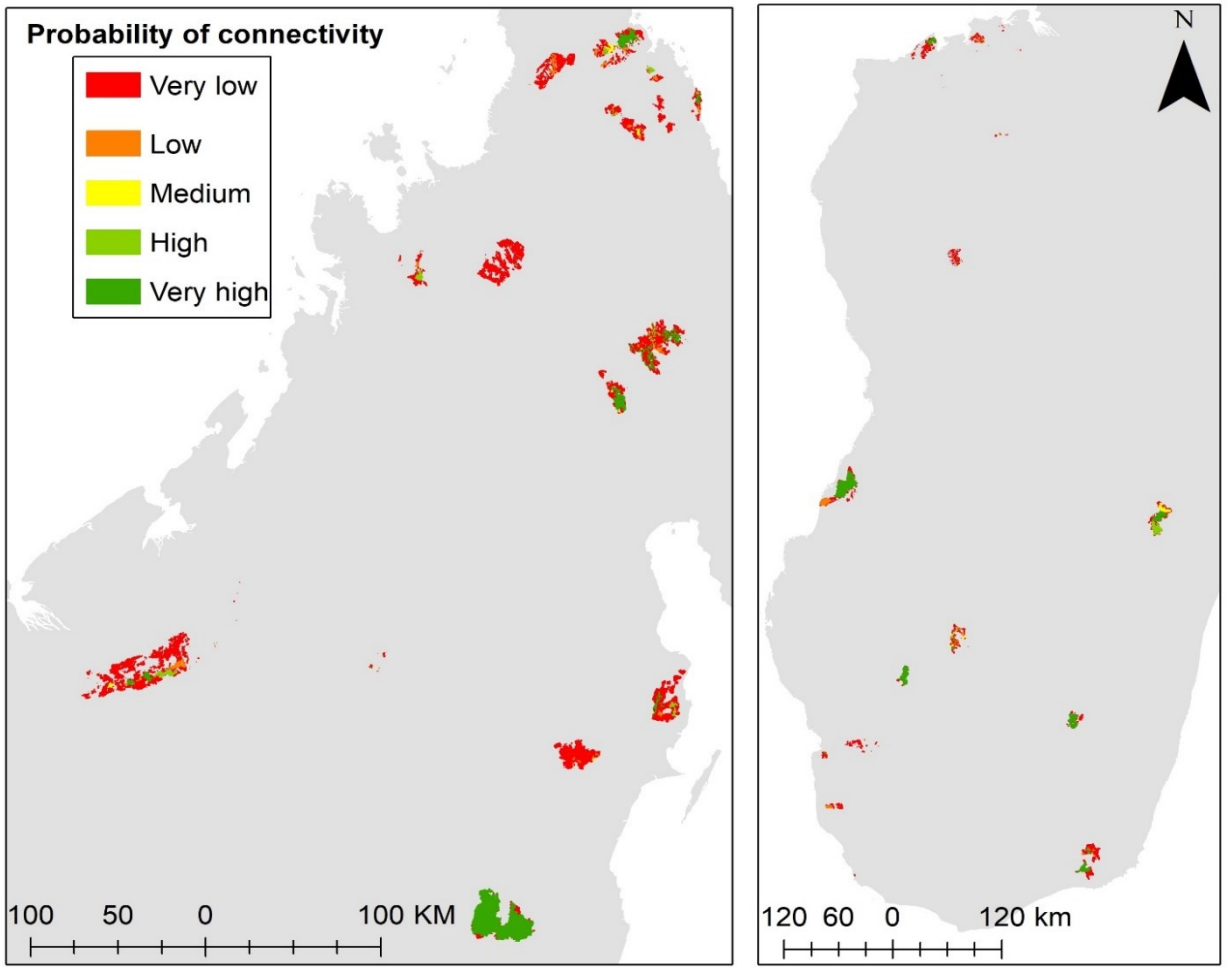

Figure 5.8: Probability of connectivity values of forest cores and bridges in 27 protected areas in northern (*left*) and southern (*right*) Madagascar. PC values are shown for the most likely dispersal distance (250 m).

Table 5.3: Most important habitat resources and bridges determined using probability of connectivity (PC) metric in selected protected areas of Madagascar. Results are shown for dispersal distances of 250 m, 500 m, 1000 m, 3000 m and 5000 m and are the highest PC values in those PAs.

Dispersal distance	250 m						500 m						1000 m						3000 m						5000 m					
Protected area	FCID	PC	Area (ha)	BID	PC	Area (ha)	FCID	PC	Area (ha)	BID	PC	Area (ha)	FCID	PC	Area (ha)	BID	PC	Area (ha)	FCID	PC	Area (ha)	BID	PC	Area (ha)	FCID	PC	Area (ha)	BID	PC	Area (ha)
Ambatovaky	9271	7.29	81.26	8632	2.33	62.33	9271	7.38	81.26	8632	3.06	62.33	9271	6.71	81.26	8632	2.58	62.33	9271	6.44	81.26	8632	2.41	62.33	9271	6.67	81.26	8632	2.55	62.33
Ambohijanahary	15169	26.29	80.25	12502	2.01	4.58	15169	29.61	80.25	12502	2.75	4.58	15169	27.5	80.25	12502	2.29	4.58	15169	26.68	80.25	12502	2.10	4.58	15169	26.68	80.25	12502	2.25	4.58
Analamerana	5289	22.00	3625.54	5549	9.87	57.32	5289	21.86	3625.54	5348	8.21	56.63	5289	22.15	3625.54	5549	9.53	57.32	5289	21.60	3625.54	5549	7.91	57.32	5289	22.09	3625.54	5549	9.63	57.32
Anjanaharibe sud	9181	24.43	106.73	9059	55.28	2729.17	9181	24.89	106.73	9059	56.86	2729.17	9181	24.62	106.73	9059	55.90	2729.17	9181	24.50	106.73	9059	55.48	2729.17	9181	23.90	106.73	9059	53.77	2729.17
Ankarana	3886	53.17	153.11	3920	18.49	489.43	3886	53.87	153.11	3920	22.06	489.43	3886	48.55	153.11	3920	19.77	489.43	3886	46.03	153.11	3920	18.90	489.43	3886	48.11	153.11	3920	19.62	489.43
Baie de baly	3826	96.45	3403.56	4309	0.72	181.17	3826	97.19	3403.56	4309	0.98	181.17	3826	96.76	3403.56	4309	0.84	181.17	3826	96.56	3403.56	4309	0.76	181.17	3826	96.73	3403.56	4309	0.83	181.17
Bongolava	1157	84.50	2.82	564	0.83	5.99	1157	84.71	2.82	564	0.41	5.99	1157	84.64	2.82	564	0.72	5.99	1157	84.56	2.82	564	0.78	5.99	1157	84.63	2.82	564	0.73	5.99
Corridor parcelles	6480	43.72	636.64	6732	25.95	0.88	6480	46.24	636.64	6732	1.74	25.95	6480	44.65	636.64	6732	1.20	25.95	6480	44.02	636.64	6732	0.98	25.95	6480	44.53	636.64	6732	1.16	25.95
Daraina	4358	29.42	598.85	9697	23.02	721.80	4358	29.71	598.85	9697	22.74	721.80	4358	27.41	598.85	9697	23.11	721.80	4358	26.30	598.85	9697	23.11	721.80	4358	27.22	598.85	9697	23.11	721.80
Extn. Tsimelahy	3045	96.18	5109.33	4718	0.78	23.04	3045	96.33	5109.33	4718	0.72	23.04	3045	96.24	5109.33	4718	0.76	23.04	3045	96.20	5109.33	4718	0.77	23.04	3045	96.01	5109.33	4718	0.82	23.04
Isalo	8547	1.00	4.68	21714	12.84	246.061	8547	1.54	4.68	27402	17.86	234.57	8547	1.23	4.68	21714	14.72	246.06	8547	1.08	4.68	21714	13.45	246.06	8547	1.20	4.68	21714	14.50	246.06
Kalamatritra	4602	98.70	8164.55	1883	0.04	6.96	4602	98.73	8164.55	3579	0.04	7.48	4602	98.72	8164.55	1883	0.04	6.96	4602	98.71	8164.55	1883	0.04	6.96	4602	98.72	8164.55	1883	0.04	6.96
Kasijy	655	68.04	3.81	807	62.97	33.90	655	22.40	3.81	807	58.99	33.90	655	68.96	3.81	807	61.30	33.90	655	68.36	3.81	807	62.40	33.90	655	68.86	3.81	807	61.49	33.90
Kirindy mitea	8061	97.03	30217.90	9160	0.98	13.32	8061	96.90	30217.90	9160	1.60	13.32	8061	96.99	30217.90	9160	1.25	13.32	8061	97.02	30217.90	9160	1.07	13.32	8061	96.99	30217.90	9160	1.22	13.32
Lac Tsimanampetsotsa	19725	27.84	11.00	18770	17.75	40.60	19725	26.76	11.00	14834	17.56	22.18	19725	27.40	11.00	14834	17.62	22.18	19725	27.70	11.00	18770	17.67	40.60	19725	27.45	11.00	14834	17.63	22.18
Littoral Sud Toliara	633	92.24	30.40	594	5.97	20.56	633	92.25	30.40	594	6.93	20.56	633	92.24	30.40	594	6.30	20.56	633	92.24	30.40	594	6.08	20.56	633	92.24	30.40	594	6.26	20.56
Mahavavy kinkony	7516	40.53	37.82	9790	16.48	204.53	7516	2.59	37.82	9790	18.98	204.53	7516	2.48	37.82	9790	17.39	204.53	7516	2.45	37.82	9790	16.77	204.53	7516	2.48	37.82	9790	17.28	204.53
Mananara nord	9687	69.08	2645.00	8089	5.37	19.66	9687	12.29	2645.00	449	1.46	208.30	9687	66.54	2645.00	8089	6.92	19.66	9687	64.98	2645.00	8089	5.88	19.66	9687	66.28	2645.00	8089	6.74	19.66
Manongarivo	6235	47.87	27.70	8588	31.87	727.12	6235	49.11	27.70	8588	34.24	727.12	6235	48.32	6235.00	8588	32.77	727.12	6235	48.01	27.70	8588	32.16	727.12	6235	48.26	27.70	8588	32.67	727.12
Marojejy	21747	14.04	30.78	28742	31.56	2254.60	21747	14.09	30.78	24418	32.37	1914.66	21747	13.28	30.78	28742	32.59	2254.60	21747	12.66	30.78	28742	31.93	2254.60	21747	13.18	30.78	28742	32.49	2254.60
Onilahy	15689	45.70	113.15	16954	4.19	29.51	15689	47.79	113.15	16954	4.49	29.51	15689	46.56	113.15	16954	4.31	29.51	15689	45.99	113.15	16954	4.23	29.51	15689	46.46	113.15	16954	4.30	29.51
Ranomafana	9741	74.03	5296.50	2875	9.40	272.71	9741	73.86	5296.50	2875	6.70	272.71	9741	74.67	5296.50	2875	10.52	272.71	9741	74.56	5296.50	2875	9.76	272.71	9741	74.67	5296.50	2875	10.38	272.71
Tampoketsa analamaitso	2791	73.20	19.01	2733	2.87	5.59	2791	76.30	19.01	2633	3.12	5.67	2791	74.56	19.01	2733	2.94	5.59	2791	73.67	19.01	2733	2.90	5.59	2791	74.41	19.01	2733	2.93	5.59
Tsaratanana	12280	66.99	46.70	12870	8.67	160.52	12280	69.86	46.70	12183	11.81	508.61	12280	68.04	46.70	12183	10.34	508.61	12280	70.03	46.70	12183	11.86	508.61	12280	67.91	46.70	12183	10.17	508.61
Tsingy de namoroka	4172	62.03	1.08	NA	NA	NA	4172	63.26	1.08	NA	NA	NA	4172	62.06	1.08	NA	NA	NA	4172	61.94	1.08	NA	NA	NA	4172	62.01	1.08	NA	NA	NA
Zahamena	10089	99.99	48104.30	202	0.00	2.17	10089	99.99	48104.30	3175	0.07	79.99	10089	99.99	48104.30	3175	0.07	79.99	10089	99.99	48104.30	3175	0.07	79.99	10089	99.99	48104.30	3175	0.07	79.99
Zombite vohibasia	2212	99.96	9208.67	1702	0.31	27.98	2212	99.96	9208.67	1702	0.30	27.98	2212	99.96	9208.67	1702	0.30	27.98	2212	99.96	9208.67	1702	0.30	27.98	2212	99.96	9208.67	1702	0.30	27.98
Average		57.84			13.5			53.31			12.93			56.34			12.93			56.01			12.68			56.21			12.80	
Total			117761.14			8341.5			117761.14			8611.16			117761.14			8774.07			117761.14			8792.49			117761.14			8774.07

Note: FCID and BID represents forest core areas and bridges identification numbers

PC stands for probability of connectivity

NA: No available value

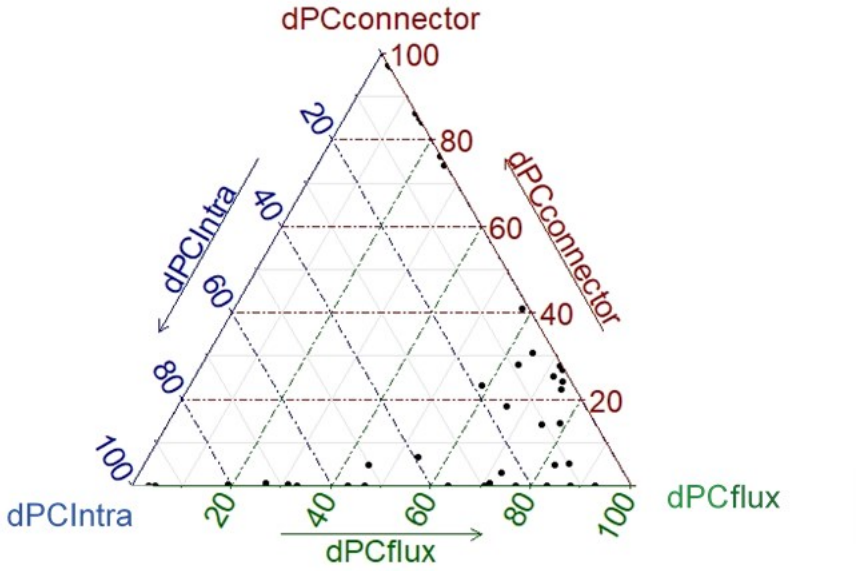

Figure 5.9: Tenary diagrams showing the contribution of three fractions (i.e., dPC_{intra}, dPC_{flux} and $dPC_{connector}$) to PC at 250 m dispersal distances. Dot represents value of probability of connectivity of core areas and bridges in 27 protected areas.

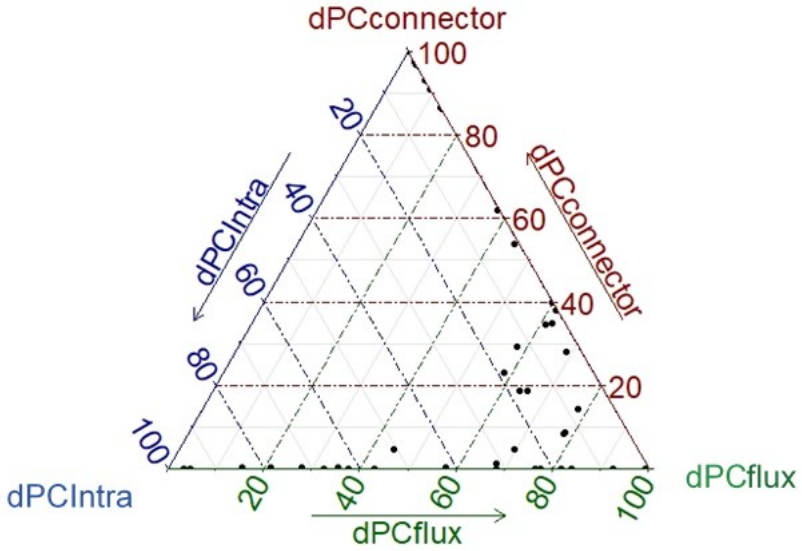

Figure 5.10: Tenary diagrams showing the contribution of three fractions (i.e., dPC_{intra}, dPC_{flux} and $dPC_{connector}$) to PC at 500 m dispersal distances. Dot represents value of probability of connectivity of core areas and bridges in 27 protected areas.

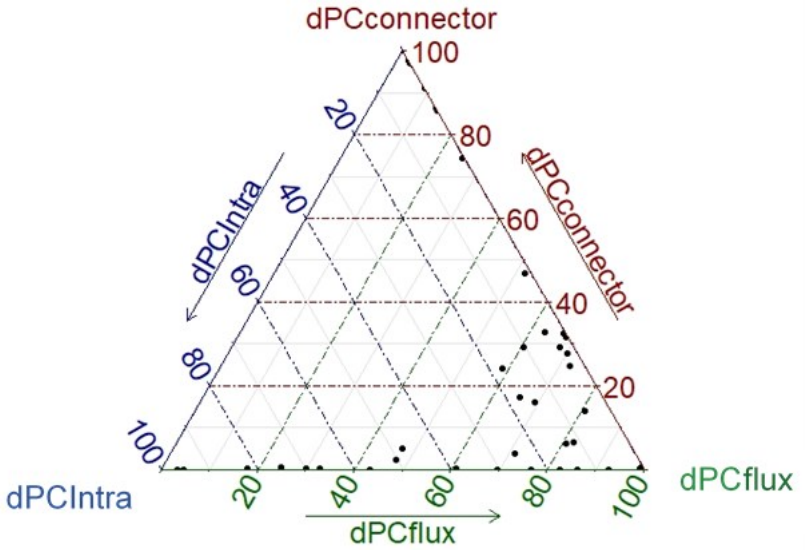

Figure 5.11: Tenary diagrams showing the contribution of three fractions (i.e., dPC_{intra}, dPC_{flux} and $dPC_{connector)}$ to PC at 1000 m dispersal distances. Dot represents value of probability of connectivity of core areas and bridges in 27 protected areas.

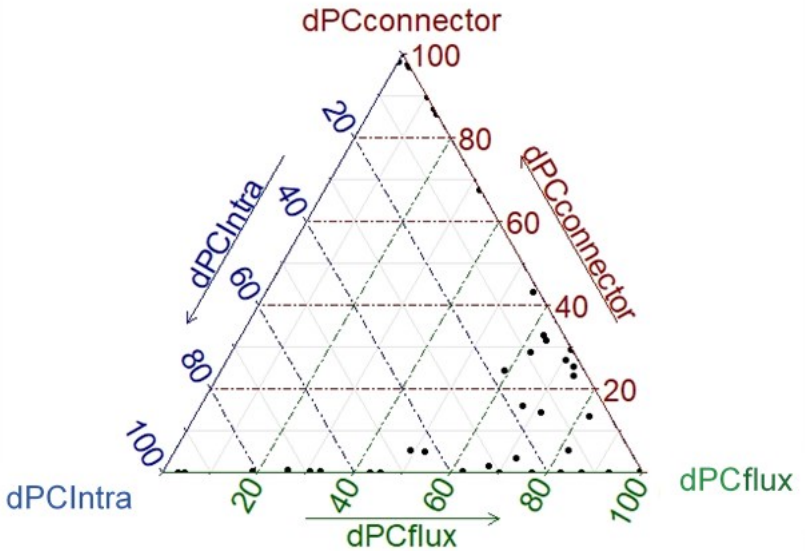

Figure 5.12: Tenary diagrams showing the contribution of three fractions (i.e., dPC_{intra}, dPC_{flux} and $dPC_{connector)}$ to PC at 3000 m dispersal distances. Dot represents value of probability of connectivity of core areas and bridges in 27 protected areas.

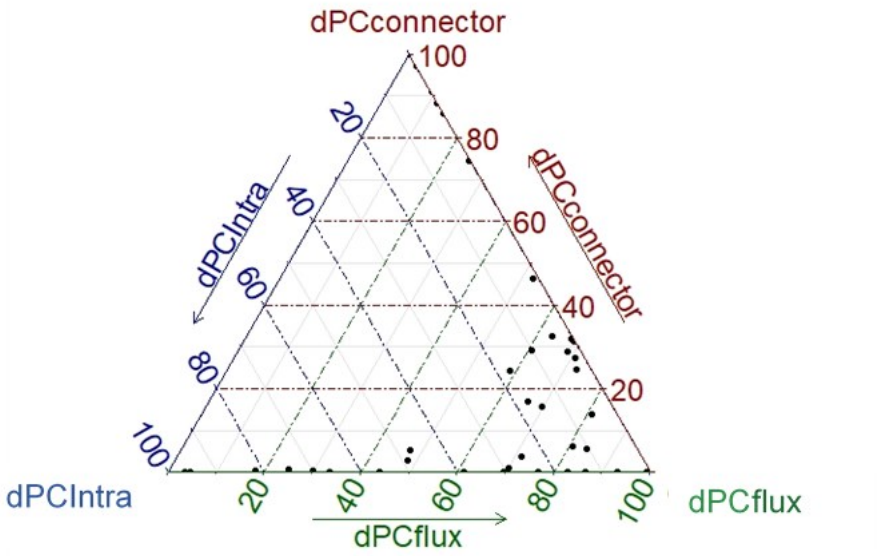

Figure 5.13: Tenary diagrams showing the contribution of three fractions (i.e., dPC_{intra}, dPC_{flux} and $dPC_{connector)}$ to PC at 5000 m dispersal distances. Dot represents value of probability of connectivity of core areas and bridges in 27 protected areas.

5.4 Discussion

5.4.1 Forest loss and fragmentation in protected areas

Deforestation rates in nine PAs were greater than the island mean deforestation rates. In 16 PAs forest degradation rates were also higher than island mean degradation rates. Five of the PAs with increased deforestation rates are in dry forests, suggesting that past attention to humid forests may be disproportionate and may have left other eco-regions exposed to threats from LULCC (Scales 2012, Waeber et al. 2015). It should be noted that the number of PAs (44) used for this analysis is less than half the total number of PAs in Madagascar and may underestimate the processes of forest loss from deforestation and forest degradation across Madagascan PAs. With that said, these results highlight the challenges of maintaining forest habitat in tropical PAs (Eklund et al. 2016, Bowker et al. 2017). For instance, the results show overwhelming decreases in forest cores during the second interval and can be considered as further evidence of fragmentation in PAs, confirming the findings of Bodin et al. (2006). Whether by PA-specific analysis or cumulative analysis by eco-region, there is evidence of increase in the proportion of bridges in these PAs during the second interval. The reasons for such increases vary and include, but are not restricted to, political failure and/or an acceleration of anthropogenic activities in these PAs (Corson 2012). Regardless, interval differences in the proportions of forest cores and bridges could potentially impact forest structure, species composition, species richness and ultimately biodiversity (Lindborg and Eriksson 2004). Though to ascertain the degree to which these aspects of the environment are at risk requires further investigation.

Substantial increases in exposed surface, as well as increases in cultivated land across PAs in humid and dry forests as shown by the derived rates of change is consistent with the pattern for the region (Kull 2012). For most tropical regions, anthropogenic activities are considered as the main drivers of LULCC even in PAs (Gray et al. 2016, Jones et al. 2018).

The evidence of the dominance of these drivers of change in Madagascan PAs could serve as guidance for spatial conservation planning.

5.4.2 Importance of habitat resources and connectivity in protected areas of Madagascar

Structural connectors were identified through the combination of landscape graphs and habitat network analyses under different threshold distances in selected PAs. Similar approaches have been used in the assessment of landscape connectivity of public forests in Europe (see, Velázquez et al. (2017) and Saura et al. (2011)) and none to my knowledge in Madagascar or any other country in Sub-Sahara Africa. The results showed that on average forest core and bridge importance decreased between close and intermediate dispersal distances (250 m – 500 m) and between far and the farthest distances (3000 m – 5000 m). Likewise, the influence of stepping stone effects (measured from dPCconnector fraction) was slightly stronger for the most important forest core area and bridge in some PAs at 250 m dispersal distance. Perhaps a sign that the impact of fragmentation on forest cores limits the ability for linkages at greater distances (e.g., 3000 m). There is also the possibility that comparatively small-sized bridges are facilitating dispersals between long distances (e.g., 1000 m – 3000 m). Overall, these results serve as a proxy for the determination of functional connectivity between different dispersal distances (or dispersal thresholds) and an understanding of what effect habitat fragmentation due to LULCC could have for plant species (Saura et al. 2011, Okin et al. 2015). However, functional connectivity requires a multitude of factors, including landscape structure, species interaction with environment and dispersal vectors (Auffret et al. 2017). In this analysis, there were no variables to measure the latter, neither are there any species-specific parameters. Rather, forest cores and bridges were used as proxies to estimate dispersal mechanism under current LULCC and the responses that plant species may be undertaking to these changes. Locations of forested area with high PC values provides an added layer of information that could aid efforts to preserve local biodiversity by commencing with the most important patches. The results have also

shown that in some PAs there is little opportunity for current species to disperse from one location to the other (e.g., Tsingy de Namoroka).

Climate and LULCC is expected to impact PAs creating new challenges for biodiversity conservation in all regions of the world (Heller and Zavaleta 2009, Struebig et al. 2015). Evidence of fragmentation and reduced connectivity between forest cores at intermediate distances solely from analysis of LULCC suggest that future impacts may be exacerbated in Madagascar, particularly when the coupled effects of climate change are considered. This is especially critically for Madagascan forests which are estimated to be inhabited by approximately 11,000 plant species most of them endemic to the Island; the lack of response mechanism for some of these plants due to environmental change could prove costly. Therefore, shifting conservation resources towards the preservation of the most important forest cores and/or linkages could preserve and/or facilitate stepping stone effects in the landscape and their abilities to support range-shifts.

5.5 Conclusion

Morphological spatial pattern analysis and PC-metric enabled site-level assessment of structural connectivity in PAs of Madagascar. Additionally, the threshold distances at which connectivity is reduced between forest cores and/or bridges is identified, as well as the most important forest cores and bridges. Therefore, revealing the effects of habitat loss and fragmentation in these PAs and the potential for intervention in sites with considerable reductions between forest cores and bridges. These results highlight the importance of forest patches to act as stepping-stones for future plants dispersals in Madagascan PAs. These PAs also face pressures from deforestation and forest degradation albeit at varying rates. An indication that without preserving existing structural connectivity in these PAs, the future landscape is likely to be dominated by isolated patches due to continued fragmentation. Nonetheless, PAs in dry forests tend to have low PC values compared to those in humid and lowland forests and face more pressures from LULCC. More information is needed about species-specific dispersal abilities, given that the threshold dispersal distances adopted here did not explicitly address this. However, spatial conservation planners would benefit from including similar approaches when prioritising protected areas and could potentially get high returns for investment of scarce resources.

Chapter Six

Developing hierarchical Bayesian distribution models

6.1 Introduction

6.1.1 Environmental change and species prediction

Developments in species distribution models (SDM) have enabled ecologists to better understand biodiversity patterns and improve conservation decisions (Guisan and Thuiller 2005, Henderson et al. 2014, Brown et al. 2015, Gonçalves et al. 2016). Due to the anticipated impact of climate change, identifying habitats that may be under threat and prioritizing their management is now of paramount importance (Struebig et al. 2015). For some regions, it is predicted that plant extinctions will be accelerated as natural habitats change faster than species can adapt (Malcolm et al. 2006, Urban 2015). But the severity of extinctions is expected to vary depending on whether global temperatures rise by either 1.5ºC or 2ºC at the end of this century (UN 2016, Betts et al. 2018). Irrespective of which temperature threshold is reached, global warming due to climate change is guaranteed and under such circumstances its effect would determine future species distribution. As a result, quantitative methods capable of accurately defining species habitats affected by novel climate and threats from land use land cover change (LULCC) are equally important to conservation planners (Thuiller et al. 2008, Jantz et al. 2015). Also important are metrics that compare suitable habitat areas from different periods, such as niche breadth (Warren and Seifert 2011) and can be implemented independently without including other ecological indicators like species abundances or proportion of available habitat resources in the landscape (Nunes and Pearson 2017).

Species distribution models can be described as models that quantify the distribution of species using environmental conditions as predictors (Golding and Purse 2016) and allows for the estimation of probability of presence across large geographical space (Guisan and Thuiller 2005). Applications of SDMs in ecology vary widely, from describing species occurrences (Chakraborty et al. 2011) to modelling species geographical patterns under

threats from competition and invasions (Anderson 2002, Blaise et al. 2017). Problems arising from lack of knowledge about whether current occurrence locations would achieve stability with environmental variables in the future hinder the progress of predictive distribution models (Menke et al. 2009). As a result, to gain further insight into the processes driving species distribution, ecologist often use the biotic, abiotic and movement framework (Beale et al. 2014, Soberón and Nakamura 2009) the latter often reflects landscape evolutionary response of species to environmental change. This allows for the incorporation of competition as well as implicit measures of human-driven modifications of the natural environment into the modelling framework (Guisan 2005). Despite this recognition and inclusion of more relevant data predictions of species occurrences vary depending on the modelling approach and the nature of biotic or abiotic factors considered.

Thus, it is commonly accepted that extrapolations to the future will have some inherent uncertainties mostly from data sourced at multiple resolutions (Synes and Osborne 2011). Of course, other sources of bias exist that may affect the output of SDMs including prior biological knowledge of the species, modelling methods and choice of predictors (Austin 2002, Beaumont et al. 2008, Blaise et al. 2017). Typically, modelling approaches fail to account for imperfect detection in occurrence data (Lahoz-Monfort et al. 2014). Since occurrence records may reflect false absences, a situation likely to be encountered with data sourced from online databases and popular herbaria (e.g., GBIF). As a result, when modelling plant species distribution with occurrence records predicted absences may indicate the slow dispersal rates of plants when moving between suitable habitats at a rate that lags survey times (Latimer et al. 2006). Likewise, most plant occurrences tend to exhibit contagious processes (e.g., dispersal, mortality), positive spatial correlation in their patterning, and are influenced by endogenous environmental factors (e.g., climate, soil) (Dormann 2007). Yet, few implementations of SDMs account for these processes in the model when predicting distributions (Higgins et al. 2012). Even without explaining imperfect detections and uncertainties, comparative analytical methods that quantify species

range sizes can determine suitable habitat areas from SDMs and asymmetry between ranges under different scenarios. The latter could provide estimates of species range-shift in habitat area between dates.

6.1.2 Spatial bias in Bayesian models

Spatial Bayesian methods are capable of effectively handling the effect of spatial autocorrelation in the landscape through random effects (Beale et al. 2014, Merow et al. 2014) and quantify the effect of other biotic processes (e.g. dispersal) when predicting distributions (Guisan and Thuiller 2005, Zurell et al. 2016). For these reasons, they are likely to outperform other modelling approaches (e.g., boosted regression trees) when using presence/absence data to determine the potential impact of climate change on future distributions (Golding and Purse 2016, Zurell et al. 2016). In addition to not addressing uncertainties in their output, non-spatial SDM methods predict poorly when predicting with restricted data (Elith et al. 2006, Elith et al. 2011, Redding et al. 2017). Though ensemble methods can effectively account for uncertainties, their output is a summary of several models and variables, thus rendering them inefficient for projecting habitat ranges (Porfirio et al. 2014).

One way of reducing inherent bias when predicting species distribution is to include all relevant environmental variables as predictors. Latimer et al. (2006) and Gelfand et al. (2006) successfully account for spatial autocorrelation and uncertainties using an intrinsic conditional autoregressive model within a spatial hierarchical Bayesian framework when predicting the distribution of plants in Cape Floristic Region of South Africa. Similar applications of spatial hierarchical models for predicting the distribution of freshwater fish species (Domisch et al. 2016) and orchids (Diez and Pulliam 2007) were successfully achieved, demonstrating that hierarchical Bayesian models (HBM) were not constrained by species types or geographical location. In addition to accounting for uncertainties and predicting species distributions, spatial HBMs are able to tackle a wide range of ecological issues, such as: data-pooling from presence-only and survey data (William et al. 2015),

quantifying the strength of covariate associations between different species distributions (Beale et al. 2014) and controlling for overestimates while predicting species richness (Calabrese et al. 2014).

In this chapter, I use an HBM approach to predict current and future distributions for 84 critically endangered or threatened plant species in Madagascar. This modelling approach is robust to small number of occurrence records (e.g., when modelling endangered species) and can mitigate some of the aforementioned biases, as well as quantify errors encountered when forecasting future plant distributions. I used a Bayesian framework fitted with a Markov Chain Monte Carlo (MCMC) and combined occurrence data and eight environmental variables, and two landscape variables (i.e., corridor connectivity and land use land cover change for 2002-2014 and 2014-2050) (Elderd and Miller 2016). The aim was to construct distribution models for endangered plants using an approach that effectively accounts for uncertainties and biases encountered when modelling distributions with limited data (i.e., low occurrence records, clustered presence locations). To achieve this, the following three objectives were implemented:

(i) estimate the current and future distributions for selected endangered and critically endangered plants using an HBM approach;

(ii) map the uncertainties associated with each species' distribution as spatial random effects under different emission scenarios; and

(iii) estimate the niche breadth (i.e., range size) of predicted probabilities of species occurrence.

6.2 Methods

6.2.1 Occurrence data and species selection

The focal plants for this analysis are endemic to Madagascar and categorised under one of the following International Union for the Conservation of Nature (IUCN) red list categories: critically endangered, endangered or vulnerable (IUCN 2017). Their occurrence records were accessed in 2016 and downloaded from the global biodiversity and information facility (GBIF) portal (https://doi.org/10.15468/dl.n9k471). Following the examples of Elith et al. (2010), locally dense sampling was reduced by thinning the occurrences of species to one per pixel (~1 km^2). This also represented the spatial resolution of the bioclimatic variables and only species with a minimum of 10 presence locations were selected. After spatial thinning was implemented a total of 84 species passed the criteria of 10 or more presence locations (Appendix 10, Table A13). In total, the 84-species had 2098 presence locations between them and their associated environmental predictors were extracted using ArcGIS (Mitchell 1999, ESRI 2015).

6.2.2 Environmental variables

Eight bioclimatic variables were selected under current and future climate scenarios (Table 6.1). Together these selected bioclimatic variables have been determined to have strong implication and relevance for the ecological survival of plants and reflect candidate abiotic factors likely to determine the presence or absence of species (Dewar and Richard 2007, Bertrand et al. 2011, Rodríguez-Castañeda and Sykes 2013, Kuhn et al. 2016). Current climate data consisted of WorldClim version 2 model covering the years 1970 – 2000s and corresponds to baseline climate scenario (Fick and Hijmans 2017). The map views of environmental variables under current scenario are present as appendix (Appendix 11)

Table 6.1: List of selected bioclimatic variables under current and future emission scenarios.

S/N	Name
1.	Annual mean temperature
2.	Maximum temperature of the warmest month,
3.	Minimum temperature of the coldest month
4.	Mean temperature of warmest quarter
5.	Mean temperature of coldest quarter
6.	Annual precipitation
7.	Precipitation of wettest month
8.	Precipitation of driest month

The future climate data were derived from the coupled Hadley Global Environment Model 2 – Earth System (HadGEM-ES) models and represent one of several Intergovernmental Panel on Climate Change (IPCC) climate projections of the future (Martin et al. 2011). Two out of four future representative concentration pathways (rcps) were considered: i) **low emissions or rcp 26 scenario** represents a future were radiative forcing reaches 3.1 W/m^2 before it returns to 2.6 W/m^2 by 2100; and ii) **high emissions or rcp 85 scenario** proposes a future climate affected by no changes in policy to guide sustainable practices and development (van Vuuren et al. 2011). In addition to current and future climate data, current and future LULC models (**see Chapter 2, Section 2.5 & 2.6**) and corridor connectivity were also used as predictors for SDMs. As a result, five scenarios were considered and are summarised in Table 6.2.

Table 6.2: Summarised description of current and future scenarios for the implementation of range-shift analysis for 84 selected endangered and critically endangered plant species.

Scenario	Description	Term used in text	References
Current climate and land-use change	describes current environmental variables, as well as current land use land cover	Current scenario	*(Kreyling et al. 2010, van Vuuren et al. 2011, Busch et al. 2012)*
Future climate and land-use change (low emission)	describes future 'best-case' environmental conditions including average global temperatures rising by 0.4ºC-1.6ºC, as well as future land use land cover	Combined scenario (low emission)	*(Martin et al. 2011, van Vuuren et al. 2011, Jantz et al. 2015, Choe et al. 2017)*
Future climate and land-use change + corridor connectivity (low emission)	describes future 'best-case' environmental conditions including average global temperatures rising by 0.4ºC-1.6ºC, future land use land cover and corridor connectivity	Combined with connectivity scenario (low emission)	*(Martin et al. 2011, van Vuuren et al. 2011, Foltête et al. 2012, Jantz et al. 2015, Zurell et al. 2016, Choe et al. 2017)*
Future climate and land-use change (high emission)	describes future 'worst-case' environmental conditions including average global temperatures rising by 1.4ºC-2.6ºC and future land use land cover	Combined scenario (high emission)	*(Martin et al. 2011, van Vuuren et al. 2011, Jantz et al. 2015, Choe et al. 2017, Betts et al. 2018)*
Future climate and land-use change + corridor connectivity (high emission)	describes future 'worst-case' environmental conditions including average global temperatures rising by 1.4ºC-2.6ºC, future land use land cover and corridor connectivity	Combined with connectivity scenario (high emission)	*(Martin et al. 2011, van Vuuren et al. 2011, Foltête et al. 2012, Jantz et al. 2015, Zurell et al. 2016, Choe et al. 2017, Betts et al. 2018)*

6.2.3 Mapping corridor connectivity

An island-wide continuous surface of corridor connectivity was produced from current LULC maps using linkage mapper (McRae and Kavanagh 2014). Linkage mapper is based on the concept of circuit theory and is computationally efficient when working with large datasets, thus making it suitable for estimating country-wide connectivity (McRae et al. 2008). To begin, landscape graphs were mapped (**see Chapter 5, Section 5.2.3)** for each eco-region using GUIDOS toolbox (Vogt 2016) and forest core areas were selected for further analysis (Beier et al. 2011). Also, produced was a resistance surface that required the assignment of values to land use land cover category types across each eco-region (**see Chapter 5, Section 5.2.4** and **Table 5.1**). In the event of species dispersal, it was assumed

that higher resistance values corresponded to higher probability of mortality; while lower values corresponded to areas that can facilitate species dispersals.

Afterwards, adjacent core areas were identified using a cost allocation function in ArcGIS (ESRI 2015). Cost allocation took into consideration forest core area sizes and the surrounding resistant values. In each eco-region, core pairs that were farther apart and had higher resistances between them were not connected in the eco-region network model that was constructed. As a result, core pairs with significantly high cost between them were dropped at this stage to enable the derivation of a more realistic connectivity model. Subsequently, the minimum cost-weighted distances between source and target core areas were determined, while least-cost paths along which the least resistance was accumulated between pairs was mapped (right-side of Equation 6.1). To save time, least-cost paths were mapped to a maximum threshold distance of 5000 m (5 km), thus cost-weighted distance greater than 5 km between habitat pairs were not considered.

Equation 6.1: $NLCC_{AB} = CWD_A + CWD_B - LCD_{AB}$

Where NLCC is the normalised least cost corridor connecting habitat resources A and B, CWD_A is the cost-weighted distance from resource A and CWD_B is the cost-weighted distance from resource B and LCD_{AB} is the cost-weighted distance accumulated moving along least-cost path connecting the habitat pair.

Finally, least-cost corridors were calculated from the sum of cost-weighted distance between core pairs that were connected. Using equation 6.1 as proposed by McRae et al. (2012) the least-cost corridors were normalised by subtracting the least-cost path distance from the sum of cost weighted distance. Thus, producing a normalised least-cost corridors mapped in meters which represents the connectivity between potentially suitable habitats, smaller grid cell values along the corridors (i.e., connected corridors) corresponds to the best or least cost path for connectivity. After normalisation was completed, the corridors were combined using a GIS mosaic function to create linkage maps of the landscape. Kriging interpolation technique was applied to get least-cost paths in other regions outside forested areas. Using spatial interpolation to determine the least-cost path values at other locations

where the graph elements were not available for direct measurements was first proposed by Foltête et al. (2012) as a way to integrate landscape graphs and species distribution models. Kriging interpolation was selected over other interpolation techniques (e.g., inverse distance weighted mean) because the technique accounts for spatial correlation between sample points. The resultant product of interpolation was a country-wide continuous surface of corridor connectivity (Figure 6.1).

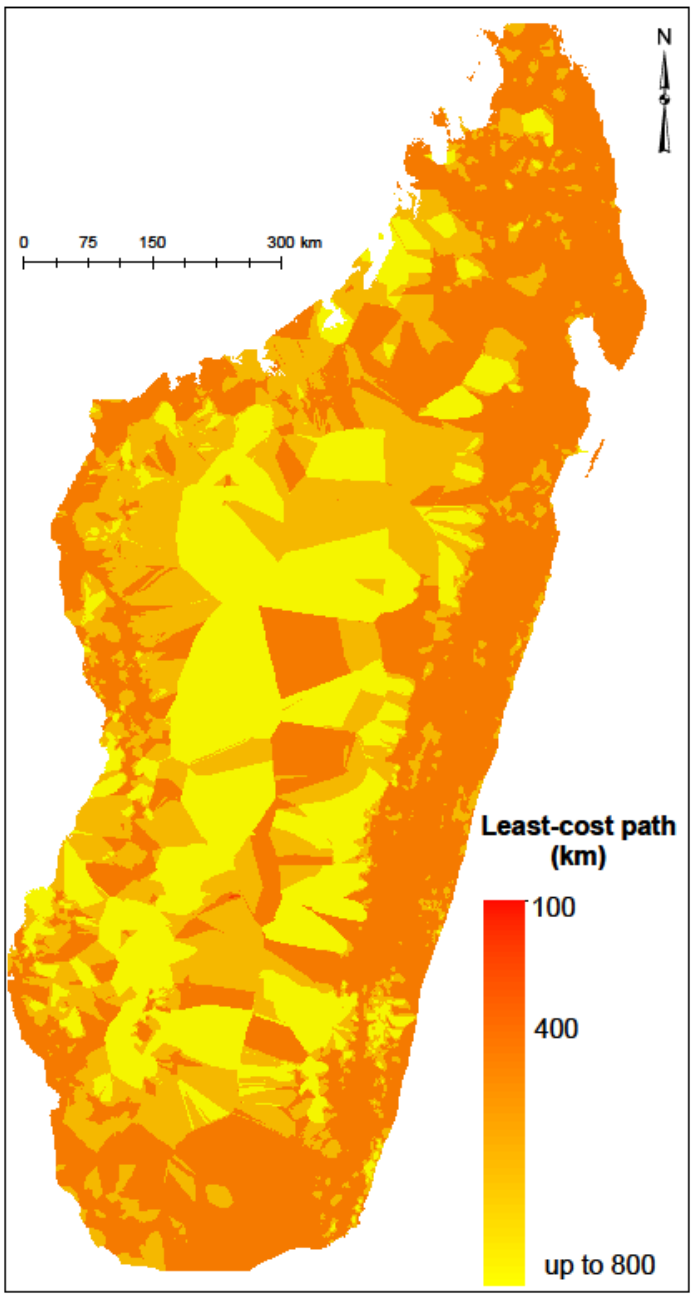

Figure 6.1: Corridor connectivity map of Madagascar derived from spatial interpolation of data points of least-cost paths in forest areas.

6.2.4 Developing hierarchical Bayesian distribution model

Species distribution models were developed using a hierarchical Bayesian framework. HBMs are statistical models that allow data to enter the modelling process at various levels, in this instance the model parameters are themselves a function of other parameters or data (Latimer et al. 2006). This approach allowed for the integration of habitat suitability (i.e., ecological processes) into hierarchical Binomial model (Latimer et al. 2006) (Equation 6.2 – 6.3). To estimate the conditional posterior distribution of model parameters the model utilised a metropolis adaptive algorithm considered for its ability to fit large data sets in a relatively short time (Gelfand and Smith 1990). Habitat suitability follows a Bernoulli distribution of model parameters and describes the suitability at any given pixel for a random variable z_i (Equation 6.2).

Equation 6.2: $z_i \sim Bernoulli(\theta_i)$

Equation 6.3: $y_i \sim Binomial\ (\upsilon_i, \theta_i)$

$$But,\ logit\ (\theta_i) = X_i\beta + \rho_i$$

Equation 6.4: $\rho_i \sim Normal\ \left(\mu_{i,} V_\rho / n_i\right)$

where: y_i represents the total number of presences of a species observed for any given pixel i, which follows a Bernoulli distribution of parameter θ_i (i.e., probability that i is a suitable pixel). υ_i is the index of the spatial entity of observations ranging from 0 to i., Using a logit link function, θ_i can be expressed as a linear model combining the matrix of predictors X_i and β indicates how much each environmental variable contributes to the suitability process ρ_i represents spatial random effect, $\mu_{i,}$ is the mean of ρ_i in the neighbourhood of i, V_ρ is the variance of the spatial random effects, n_i number of neighbours for the spatial entity i.

Prior to modelling the probability of species occurrence, targeted background data locations (3462) were selected and were used to characterise the environmental domain outside known presence locations (Phillips et al. 2009, Brown et al. 2016). These background locations were chosen as absence locations due to lack of survey data for all 84 species under consideration. Targeted background requires fewer assumptions and is regarded as statistically capable of dealing with overlap between presence and pseudo-absence locations (Ward et al. 2009, Phillips and Elith 2013); by carefully selecting pixels without presence

locations care was taken to avoid any overlap between the presence locations and background points when selecting background data.

Modelling the distribution of species occurrences under different emission scenarios began by standardising the predictors. This was done for each variable by subtracting the overall mean and dividing by the standard deviation, which improved the chance of achieving model convergence, normalised error terms and made it easier to interpret coefficient estimates (Diez and Pulliam 2007). Next, the neighbourhood matrix for presence and pseudo-absence locations was determined, assuming that the probability of species occurrence in any pixel depends on the probabilities of occurrence in its surrounding pixels (Lichstein et al. 2002). Thus, neighbourhoods consisted of adjacent pixels (including diagonals) and were used to capture spatial dependences/autocorrelation in the data. Spatial dependence (i.e., spatial random effects) was explained by including an intrinsic conditional autoregressive (iCAR) specification in the modelling process (Besag 1974) (Equation 6.4). Including an iCAR term enabled the model to account for spatial random effects in the variability of probabilities of species presences that could not be explained by the environmental variables.

Thereafter, probability of species occurrence was estimated given pixel suitability as defined in equation 6.3 (i.e., habitat suitability)[5]. Therefore, low suitability pixels surrounded by pixels with higher habitat suitability values will themselves have a higher estimated suitability compared to if their surrounding pixels were also of low suitability. For each simulation, the number of trials (i.e., visits) corresponded to every observation of the focal species (i.e., presences).

The models were fitted using one chain of Markov Chain Monte Carlo (MCMC) simulations in the HBMs for 5000 interactions with a burn-in phase of 1000 iterations and a

[5] Also known as ecological processes and refers to the manner in which presences or absences were explained by suitability in the model.

thinning interval of 5. Due to the low number of presence locations for the selected species, model convergence was difficult to achieve in all instances, making it difficult to determine the variance of spatial dependences. Generally, model convergence represents one of the shortcomings of HBMs (Vieilledent et al. 2014); but can be achieved using multivariate potential scale reduction factor (but see Domish et al. 2016 for MPSRF in HBMs), however this was not possible to achieve using Binomial function in this analysis. Uninformative priors centred at zero were used with a fixed large variance of 100 (Rasmussen and Williams 2006), which allowed the variance of the spatial random effects to follow a normal distribution. Within the HBM framework, coarse-scale species presence locations were integrated with high-resolution predictors (e.g., corridor connectivity) in geographical and environmental space following a suitability process. Additionally, habitat suitability was initialised with assumptions of imperfect detection in cases of absences, conditioned on the suitability of adjacent pixels (i.e., probability of presence). Overall, the characterisation of posterior distributions of the parameters (i.e., probability density functions) and predictions of species occurrences for different scenarios were achieved within the hierarchical framework. All analyses for HBM were carried out using 'hSDM' package in R Studio Version 1.0.136 (R Core Team 2016), by performing a binomial logistic regression in a hierarchical Bayesian framework (Vieilledent et al. 2014).

6.2.5 Estimating model performance

The best performing models across scenarios were determined using the Bayesian Information Criterion (BIC) and identified the accuracy of HBM predictions for each species (Schwarz 1978). BIC is similar to the common performance metric, Akaike Information Criterion (AIC) and was used as a criterion for selecting the best performing scenario. Ideally, designed to work for a finite set of models BIC was adapted to work differently testing one model (i.e., HBM) under several scenarios. This is different to the associated uncertainties which is the measure of accuracy of the predictions explained by spatial dependencies. The advantages of using BIC includes, (i) robust model calibration; (ii) useful

for applications that require occupancy estimates; and (iii) better explanation of relationships underlying species distributions compared to discriminatory metrics, such as Area Under the Curve (AUC) (Warren and Seifert 2011, Lawson et al. 2014). Moreover, the AUC is sometimes biased to the spatial extents of background points, where generally a larger extent gives a higher AUC value (Lobo 2008, Jiménez-Valverde 2012, Jiménez-Valverde et al. 2013). Also, the posterior means of selected predictors were mapped, and the 95% credible interval of habitat suitability projections calculated. The mean detection probability of the species across the landscape was plotted along with the posterior distributions of the parameters using an inverse logit transformation of the mean observability intercept γ_0. An example of the graphical representation of posterior distributions is shown in Figure 6.2, while species-specific beta distribution graphs of environmental variables are provided as Appendix 13.

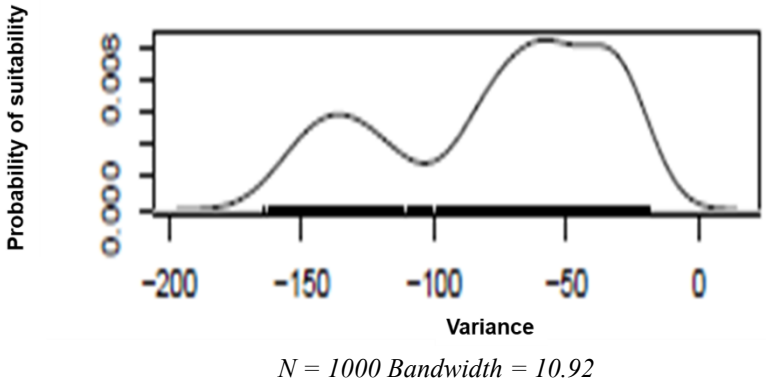

Figure 6.2: Density plot showing estimated conditional posterior distribution parameter for prediction of *Dypsis ceracea*. Bandwidth value refers to local smoothing parameter used to estimate the denseness or sparseness of observations (marks on x-axis).

6.2.6 Measuring observed niche breadth

As a first step and to derive a single measure of range sizes under different scenarios, niche breadth analysis was implemented using the predicted probabilities of species occurrences. Ecological Niche Modelling tools (ENMtools) was used which is designed to specifically measure and analysis changes in range size between different dates (Warren et al. 2010). Range sizes were quantified with Levin's (1968) inverse concentration metric, calculated using the total number of pixels present. From that the minimum and maximum possible suitability scores were derived and scaled such that 0 is minimum and 1 is maximum possible niche breadth over the modelled landscape (Nakazato et al. 2010). Thus, the extent of species habitat specialisation was quantified from predicted probabilities.

6.3 Results

6.3.1 Comparing predicted distributions with IUCN range

Hierarchical Bayesian model predictions for the selected endangered and critically endangered species were consistent with IUCN range data as currently determined for some species (Figure 6.3). This indicates that despite the constraints in the modelling framework and lack of adequate prior information to calibrate conditional parameters, the binomial hierarchical model was still able to predict high probabilities to areas that these species occur as determined by presence locations and IUCN range data. In some cases (e.g., *Adansonia grandidieri and Dypsis rivularis*) there was a close match between predictions from HBM and IUCN range data, while in others HBM appeared to have over-predicted beyond the species known suitable habitats (i.e., *Dypsis ceracea*) (Figure 6.3). Such cases of overpredictions may be due to high uncertainties and/or a lack of other relevant abiotic, biotic and evolutionary history data not accounted for in the HBM. IUCN range data is only available for a selected few species as a result only a few species were selected for comparisons. A select number of species predictions under current and future emission scenarios are Figures 6.4 – 6.11, while the rest are presented in Appendix 12.

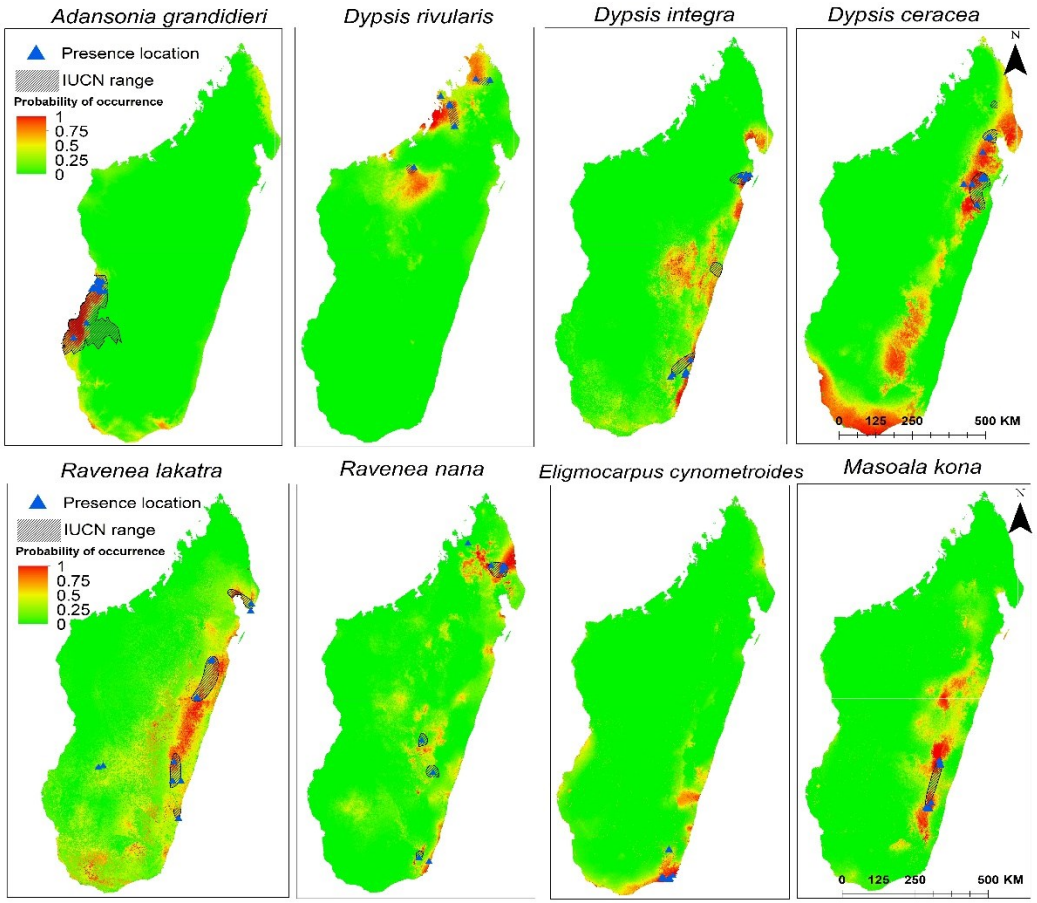

Figure 6.3: Comparing current hierarchical Bayesian model outputs with IUCN range for selected endangered and critically endangered plant species in Madagascar. Maps were produced with overlay operation in GIS and show close matches between prediction and range map. Blue triangles indicate species presence locations.

6.3.2 Predicted distributions and spatial dependences

The probability of species occurrence under current and future emission scenarios shows distinct differences when corridor connectivity is included in the model (Figures 6.4 – 6.11). The influence of spatial effects in HBM under different scenarios showed strong spatial patterning between neighbouring pixels, however, there were no clear associations between spatial dependences and probability of occurrence. For example, high probability of occurrence did not necessarily translate to strong positive spatial dependence across different scenarios. Though, high probability pixels were also not likely to be around regions with strong negative spatial effects. The uncertainties associated with each prediction were summarised as graphs of beta distributions for each environmental variable, as well as the variances of spatial random effect across the landscape (Appendix 13).

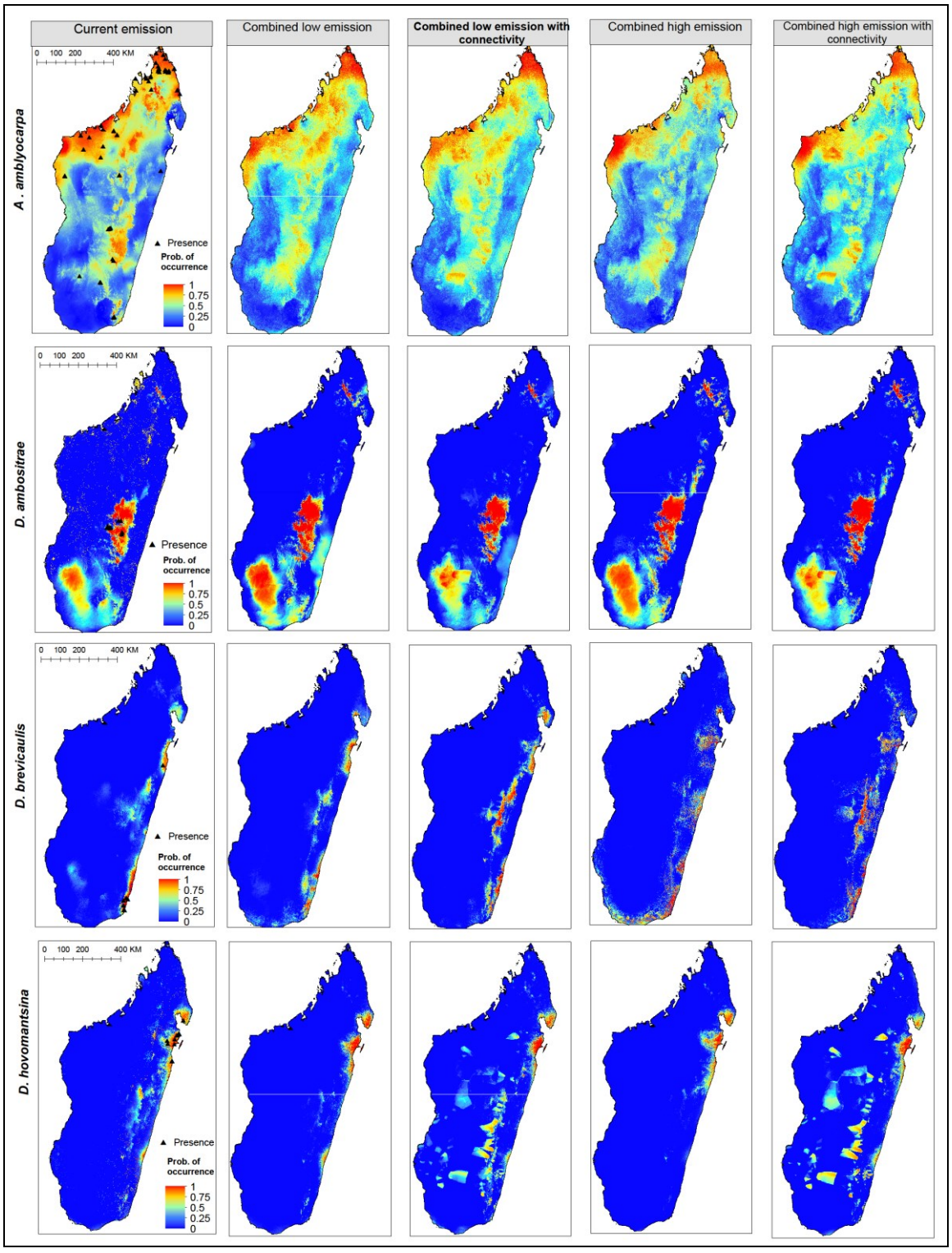

Figure 6.4: Predicted probability of occurrence for selected critically endangered species namely: *A. amblyocarpa, D. ambositrate, D. brevicaulis* and *D. hovomantsina* derived from the mean posterior suitability predictions of hierarchical Bayesian model under current and future scenarios with or without corridor connectivity.

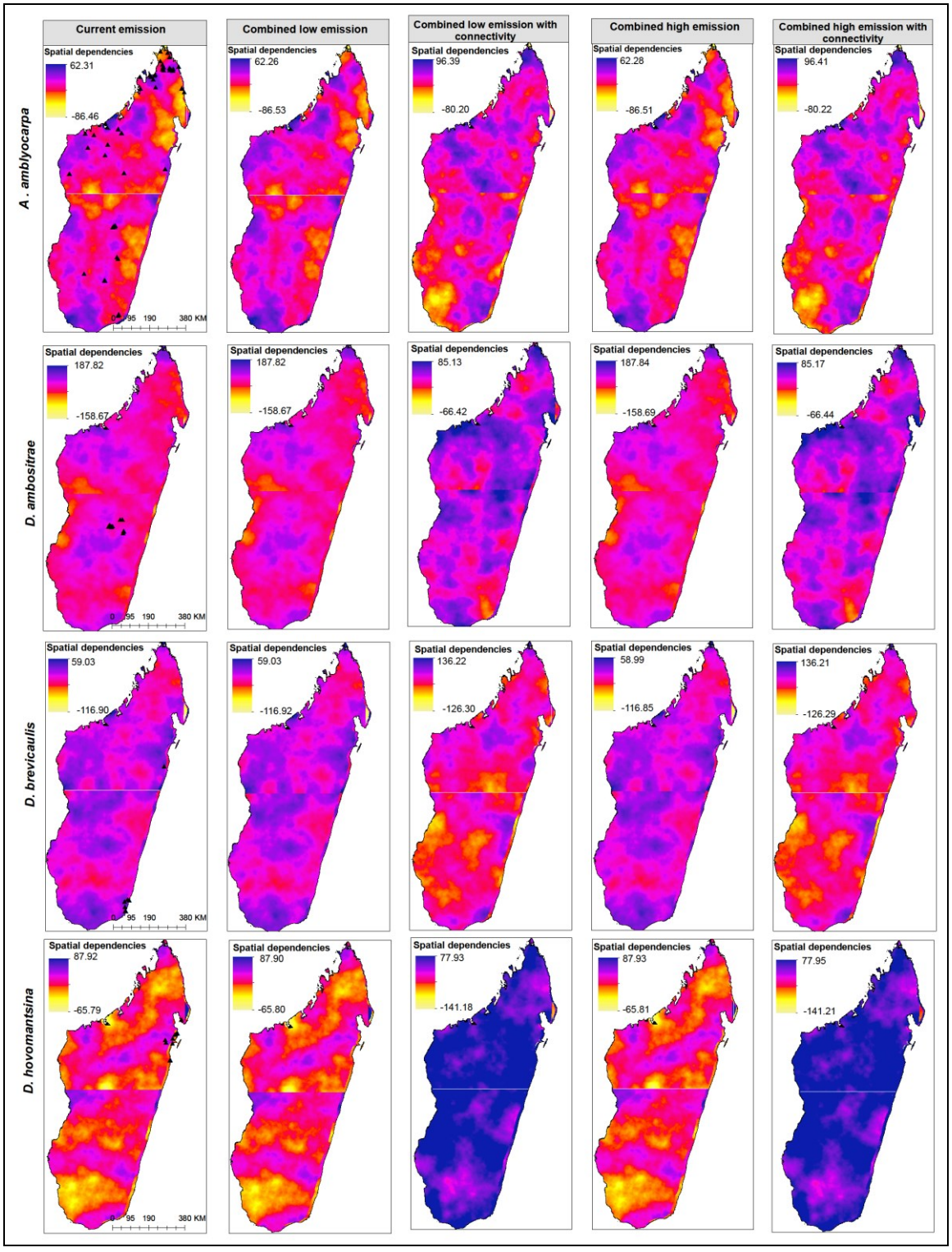

Figure 6.5: Spatial variation in uncertainties associated with predictions of selected critically endangered species (*A. amblyocarpa, D. ambositrate, D. brevicaulis* and *D. hovomantsina*) under current and future scenarios with or without corridor connectivity. Uncertainties estimated from mean of spatial dependencies, ρ.

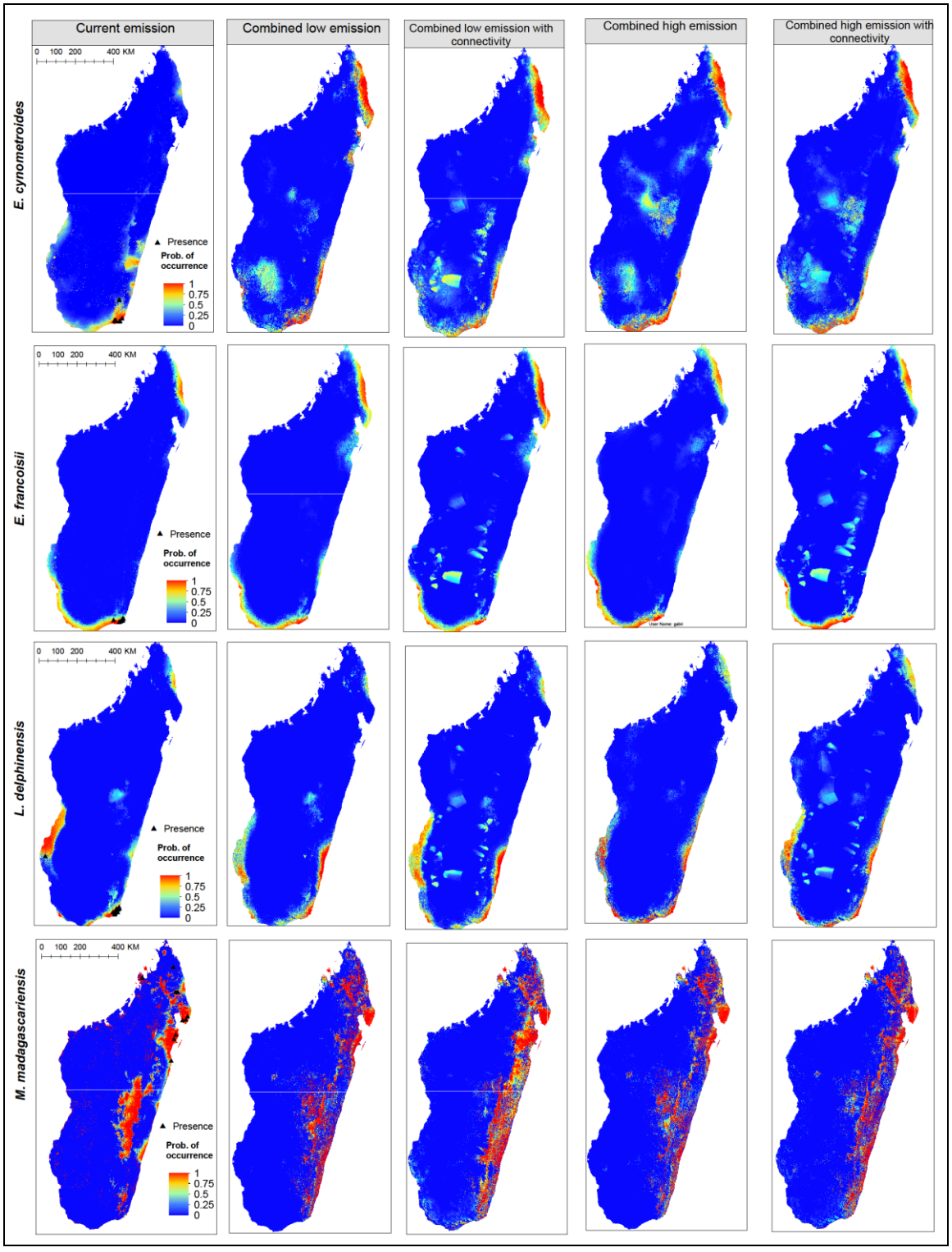

Figure 6.6: Predicted probability of occurrence for critically endangered species namely: *E. cynometroides, E. francoisii, L. delphinensis* and *M. madagascariensis* derived from the mean posterior suitability predictions of hierarchical Bayesian model under current and future scenarios with or without corridor connectivity.

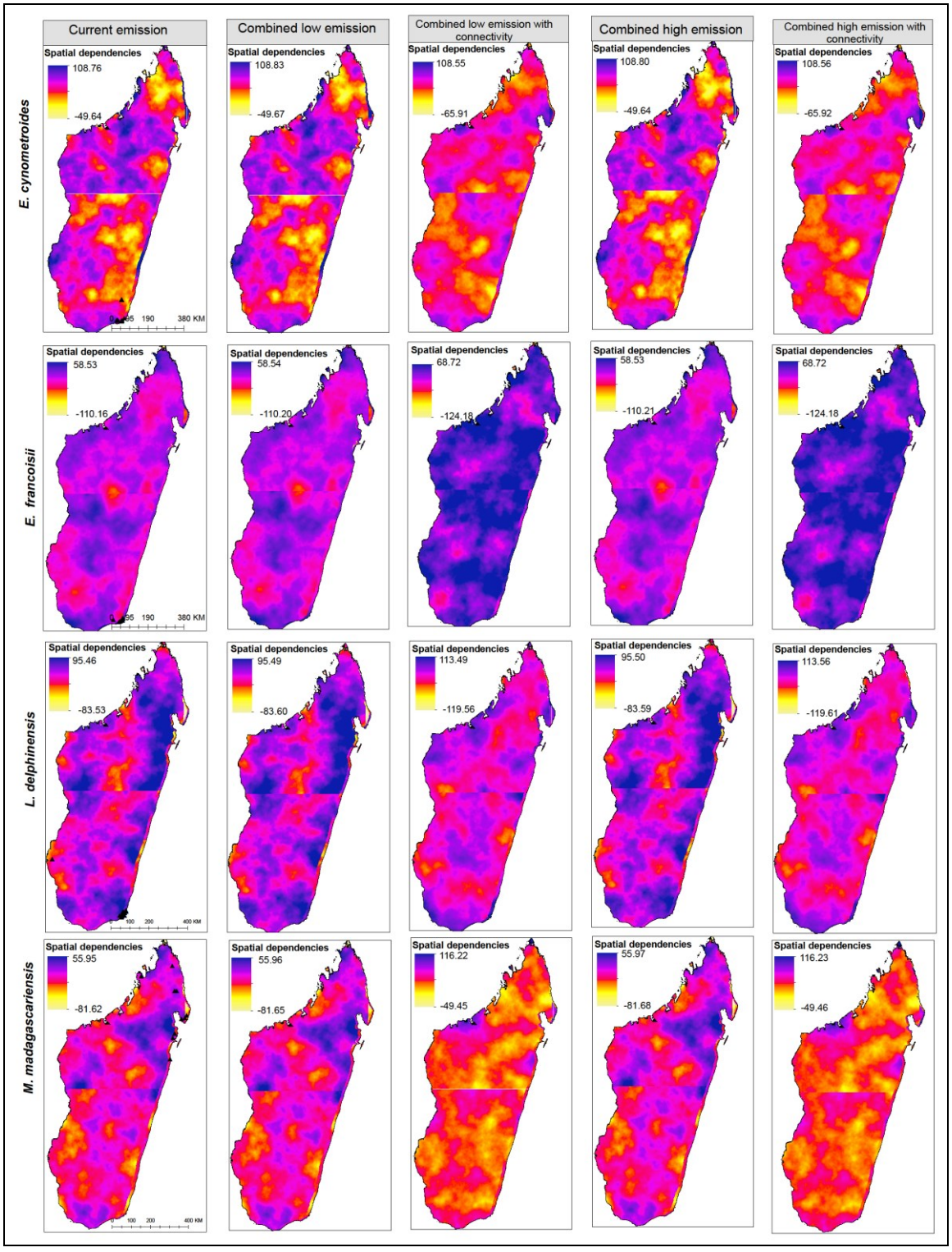

Figure 6.7: Spatial variation in uncertainties associated with predictions of selected critically endangered species (*E. cynometroides, E. francoisii, L. delphinensis and M. madagascariensis*) under current and future scenarios with or without corridor connectivity. Uncertainties estimated from mean of spatial dependencies, ρ.

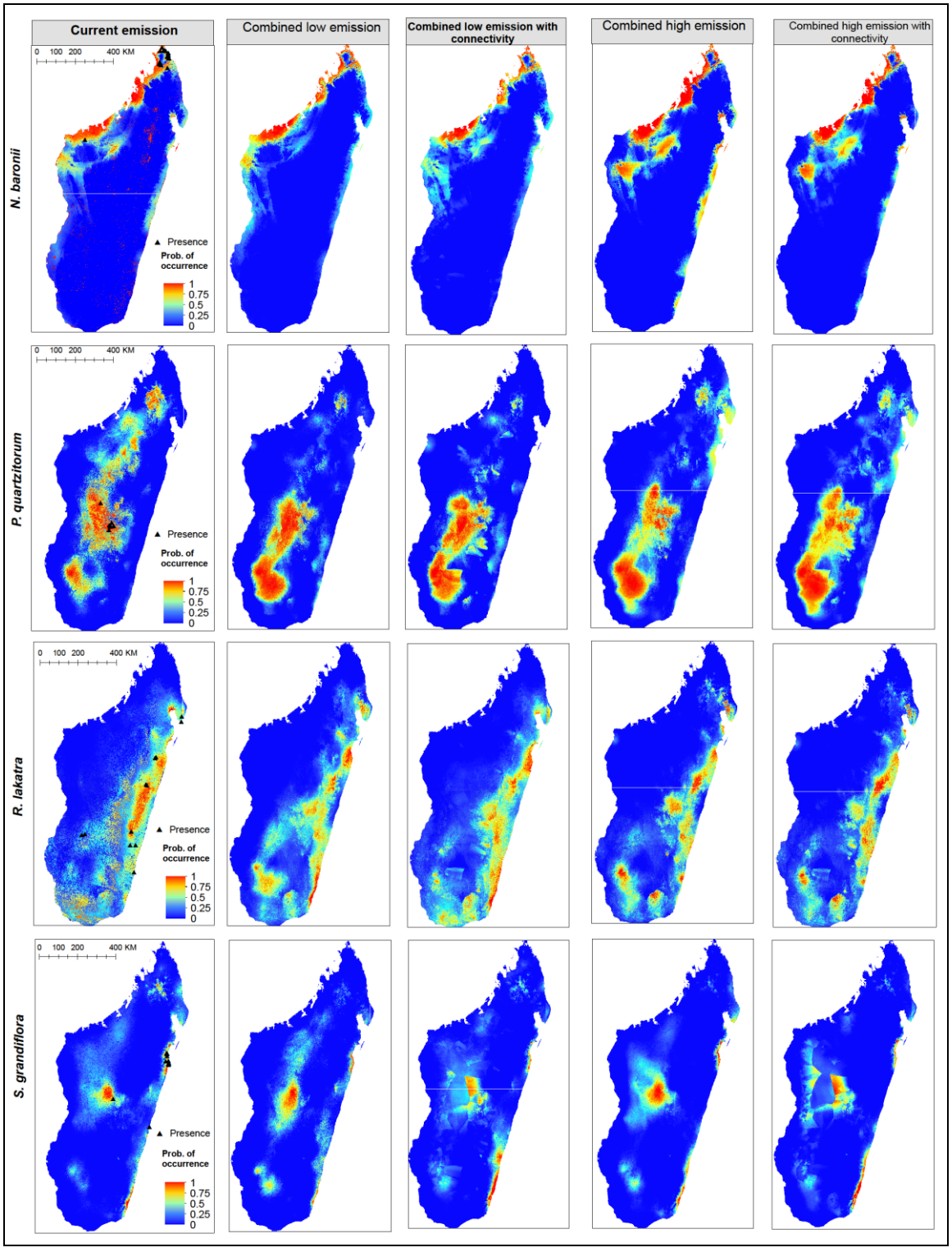

Figure 6.8: Predicted probability of occurrence for critically endangered species namely: *N. baronii, P. quartzitorum, R. lakatra* and *S. grandiflora* derived from the mean posterior suitability predictions of hierarchical Bayesian model under current and future scenarios with or without corridor connectivity.

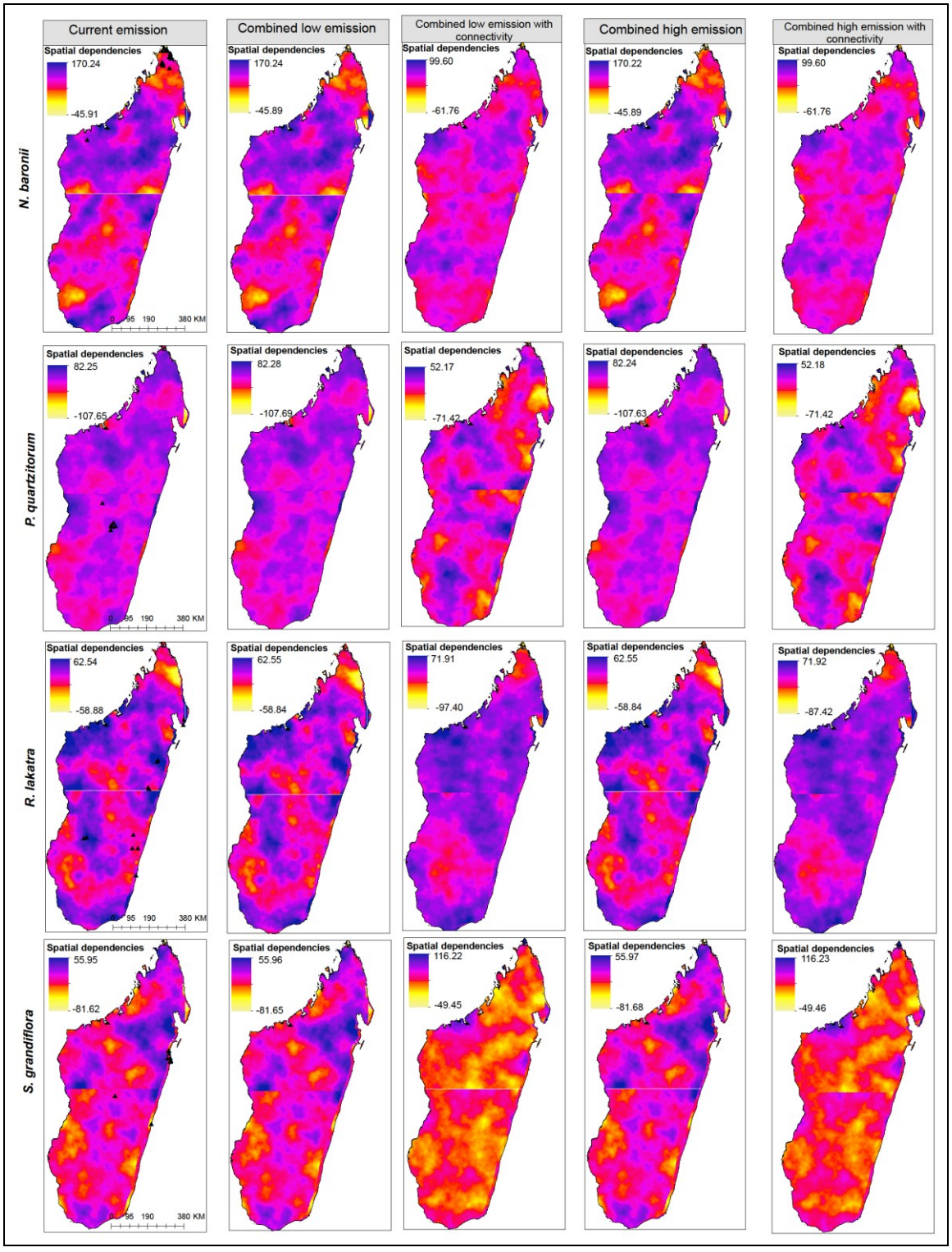

Figure 6.9: Spatial variation in uncertainties associated with predictions of selected critically endangered species (*N. baronii, P. quartzitorum, R. lakatra* and *S. grandiflora*) under current and future scenarios with or without corridor connectivity. Uncertainties estimated from mean of spatial dependencies, ρ.

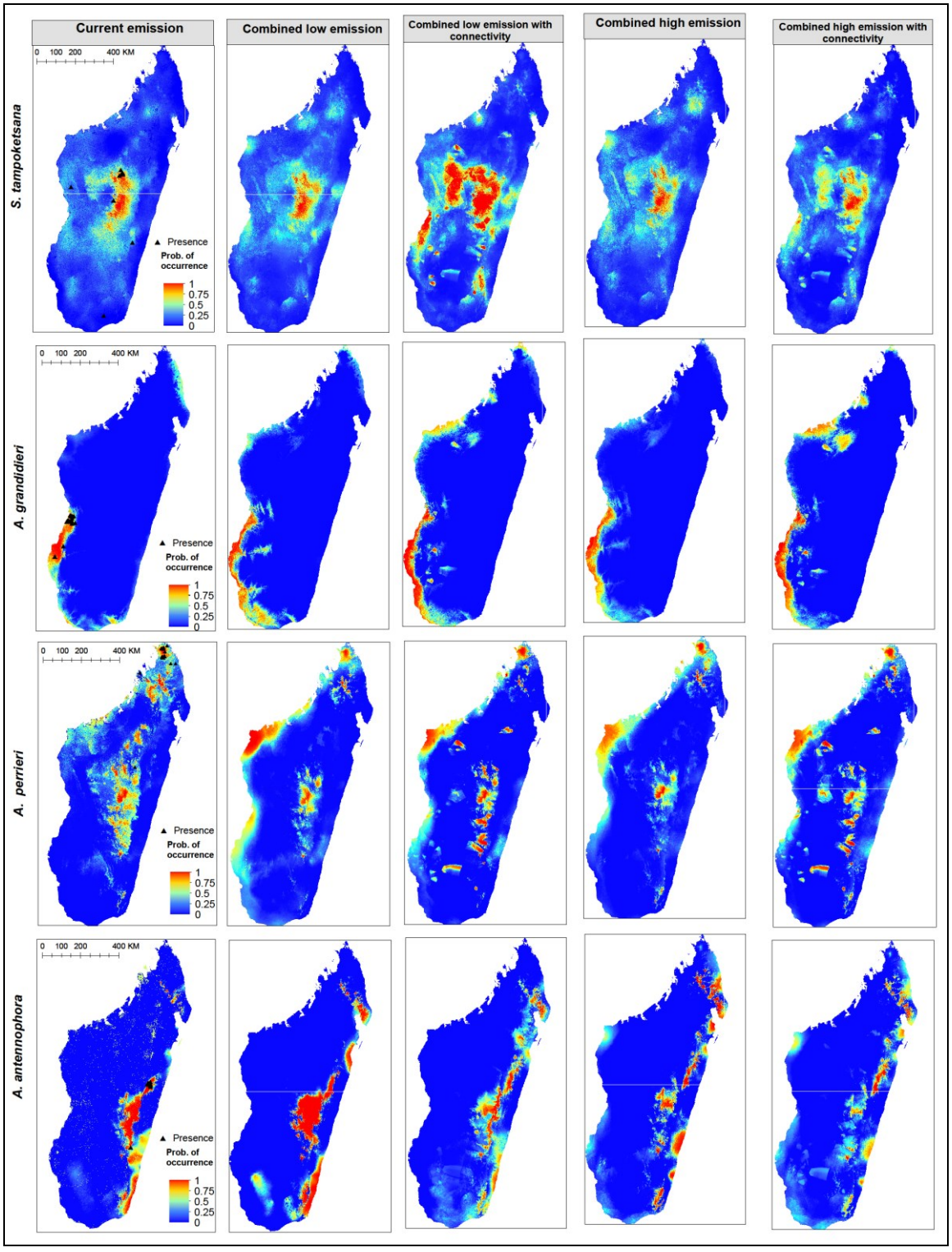

Figure 6.10: Predicted probability of occurrence for endangered and critically endangered species namely: *S. tampoketsana, A. grandidieri, A. perrieri* and *A. antennophora* derived from the mean posterior suitability predictions of hierarchical Bayesian model under current and future scenarios with or without corridor connectivity.

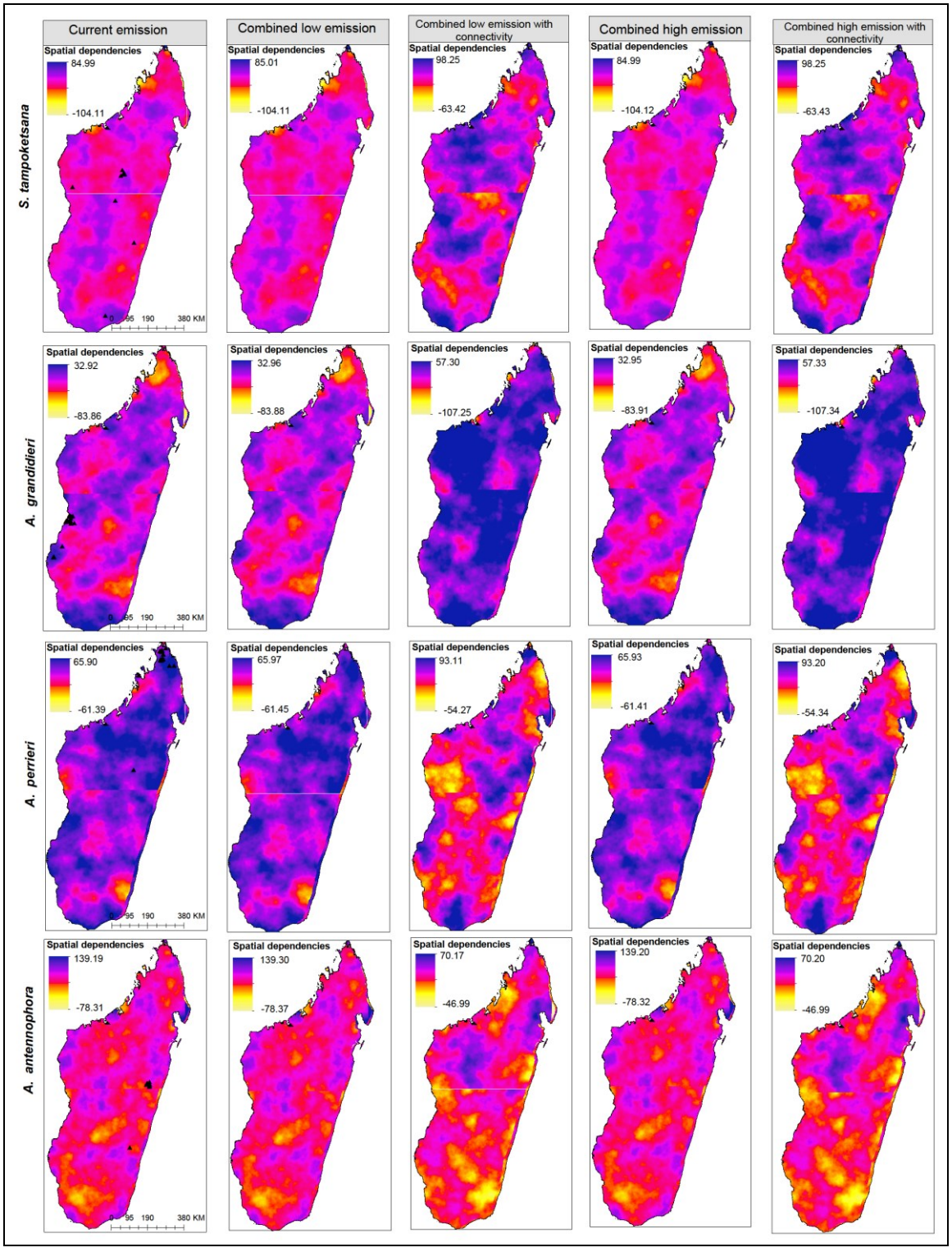

Figure 6.11: Spatial variation in uncertainties associated with predictions of selected endangered and critically endangered species (*S. tampoketsana, A. grandidieri, A. perrieri* and *A. antennophora*) under current and future scenarios with or without corridor connectivity. Uncertainties estimated from mean of spatial dependencies, ρ.

6.3.3 Comparing range sizes between future emission scenarios

Generally, the predicted range sizes of species as determined with niche-breadth analysis were not significantly different for combined scenarios with and without corridor connectivity (low emission) ($t_{0.05,\ 166}$ = 0.02, p = 0.99). Also, there was considerable similarity between range sizes under the high emission scenarios ($t_{0.05,\ 166}$ = 0.03, p = 0.97). Furthermore, species-specific range sizes are graphically presented for future low emission scenarios (Figures 6.12) and high emission scenarios (Figure 6.13).

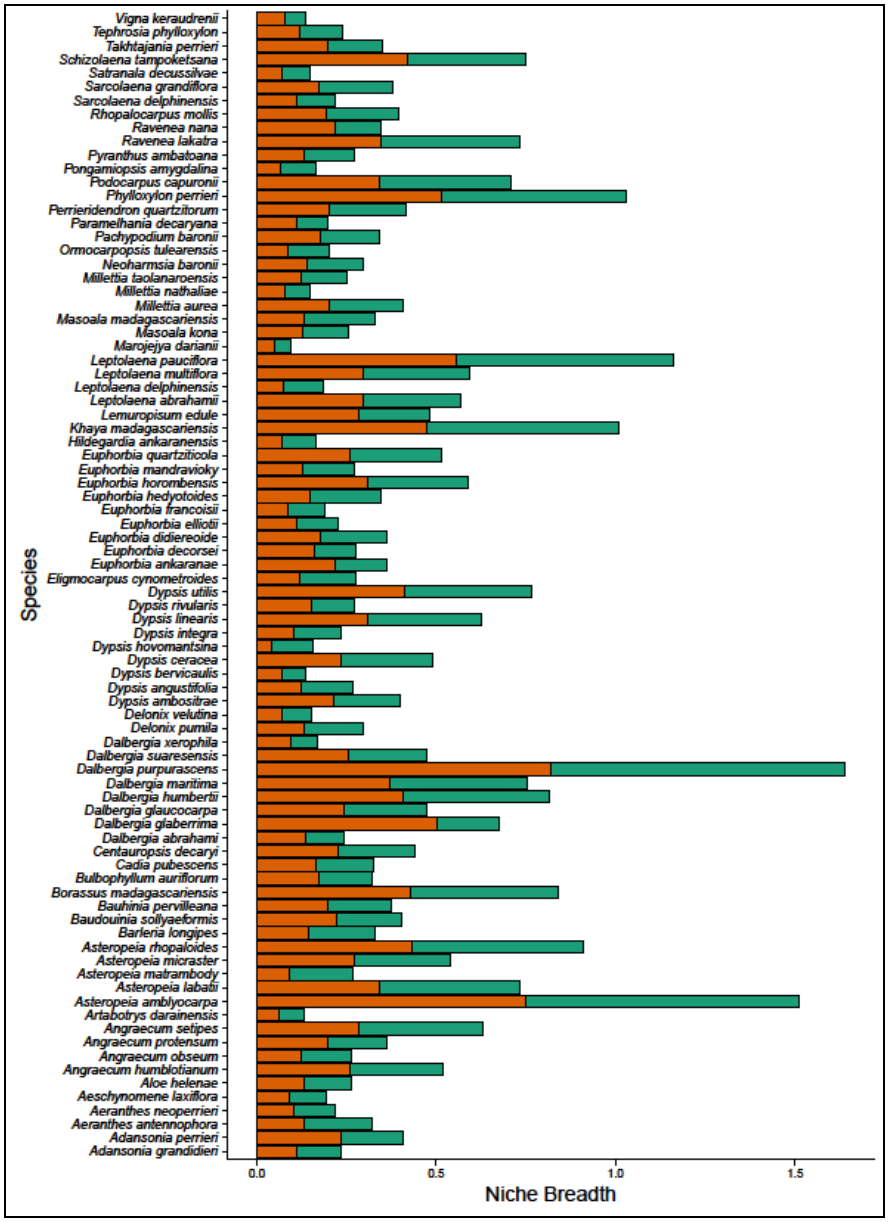

Figure 6.12: Bar graph showing differences in range sizes for selected critically endangered, endangered and vulnerable plant species in Madagascar. Range sizes were derived using ecological niche modelling tools for combined low emission scenario with connectivity (green bars) and combined low emissions scenarios (orange bars). There is no significant difference between niche breadth (or range size) under low emission scenarios ($t_{0.05,\ 166}$ = 0.02, p = 0.99)

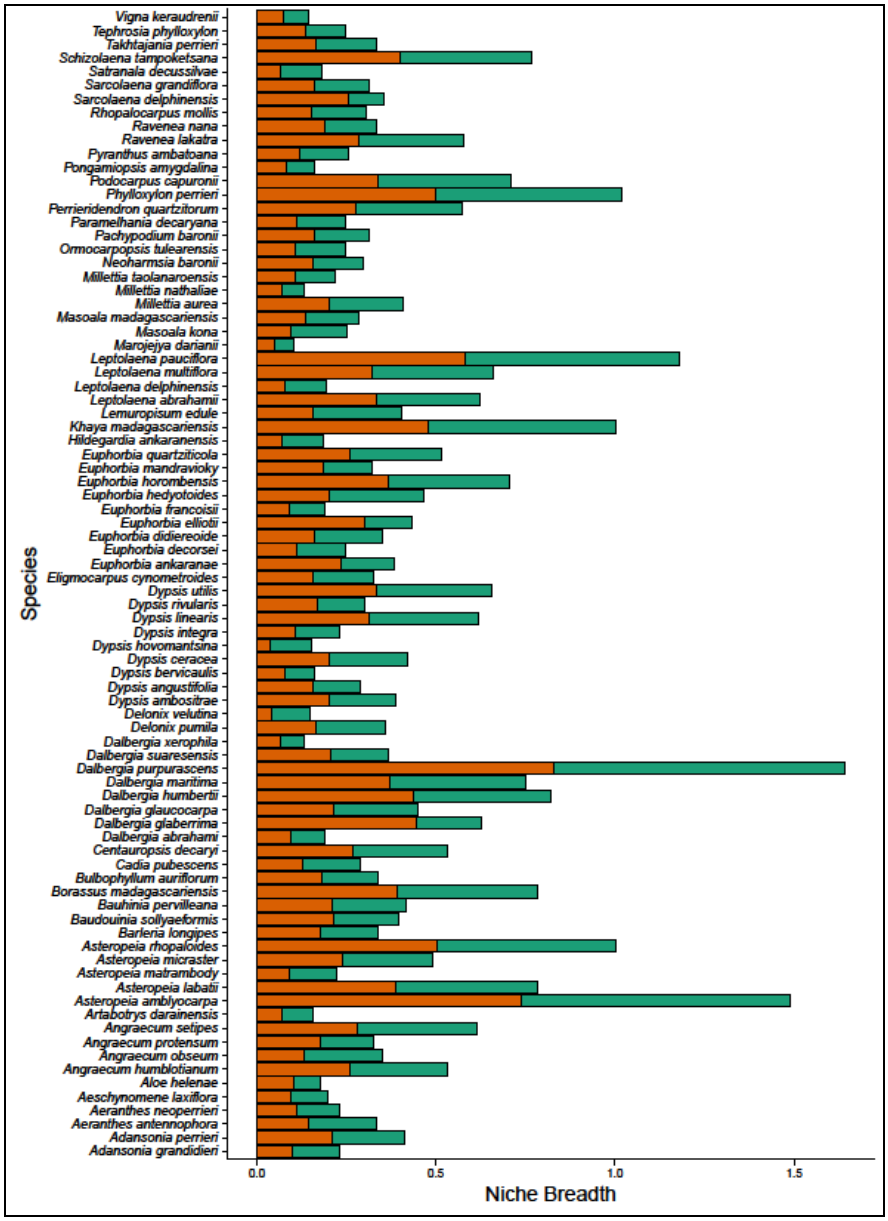

Figure 6.13: Bar graphs showing differences in range sizes for selected critically endangered, endangered and vulnerable plant species of Madagascar. Range sizes were derived using ecological niche modelling tools for combined high emission scenario with connectivity (green bars) and combined high emissions scenarios (orange bars). There is no significant differences between species niche breadth (range sizes) under high emission scenarios ($t_{0.05,\ 166} = 0.03$, $p = 0.97$).

6.3.4 Model performance

BIC values were lower for 21 species in the current emissions scenario excluding ties (Table 6.3). Under the future low emissions scenario with land use and dispersal corridors, BIC values were lowest for predictions of *Angraecum protensum* and *Euphorbia mandroviaky* with the exemptions of ties. In future high emissions with land use and dispersal corridors BIC values were lowest for three species predictions namely: *Angraecum setipes, Leptolaena abrahamii and Phylloxylon perrieri.* Overall, the lowest BIC values were tied for 36 predictions of species occurrence across the five scenarios analysed.

Table 6.3: Model evaluation of five predicted scenarios (HBMs) using BIC for 84 selected species. Bold values indicate the best performing model.

Species	Current scenario	Combined scenario (low)	Combined scenario (high)	Combined low & connectivity	Combined high & connectivity	Species	Current scenario	Combined scenario (low)	Combined scenario (high)	Combined low & connectivity	Combined high & connectivity
A. grandidieri	155.67	157.67	**155.51**	166.16	162.52	*E. cynometroides*	350.75	**134.49**	154.74	147.93	168.01
A. perrieri	**173.42**	174.22	175.86	180.49	182.11	*E. ankaranae*	161.69	161.03	158.56	**147.93**	**147.93**
A. antennophora	**134.49**	**134.49**	**134.49**	147.93	147.93	*E. decorsei*	**134.49**	**134.49**	**134.49**	147.93	147.93
A. neoperrieri	150.42	**134.49**	146.85	147.93	147.93	*E. elliotii*	**134.49**	**134.49**	**134.49**	147.93	147.93
A. laxiflora	**134.49**	**134.49**	**134.49**	147.93	147.93	*E. francoisii*	**134.49**	**134.49**	**134.49**	147.93	147.93
A. helenae	**134.49**	146.56	**134.49**	157.60	147.93	*E. hedyotoides*	**134.49**	**134.49**	**134.49**	147.93	147.93
A. humblotianum	**173.63**	182.72	180.03	196.07	193.44	*E. horombensis*	**147.77**	152.52	152.44	147.93	147.93
A. obesum	**134.49**	**134.49**	**134.49**	147.93	147.93	*E. mandravioky*	169.08	159.07	166.03	**147.93**	169.83
A. protensum	160.73	149.08	155.21	**147.93**	161.25	*E. quartziticola*	**134.49**	**134.49**	**134.49**	147.93	147.93
A. setipes	157.30	156.84	152.94	162.04	**147.93**	*H. ankaranensis*	145.88	**134.49**	**134.49**	147.93	147.93
A. darainensis	**134.49**	**134.49**	**134.49**	147.93	147.93	*K. madagascariensis*	**179.54**	181.98	182.37	194.69	194.97
A. amblyocarpa	268.86	271.47	**268.33**	284.22	280.81	*L. edule*	**134.49**	**134.49**	**134.49**	147.93	147.93
A. labatii	**184.91**	186.95	187.98	199.98	200.97	*L. abrahamii*	191.98	191.36	184.62	193.22	**188.16**
A. matrambody	155.59	**147.19**	150.15	147.93	147.93	*L. delphinensis*	**134.49**	**134.49**	**134.49**	147.93	147.93
A. micraster	**173.55**	178.86	176.74	190.79	188.88	*L. multiflora*	**174.63**	182.13	179.13	194.47	188.10
A. rhopaloides	**207.81**	220.78	215.89	227.90	225.54	*L. pauciflora*	343.51	**340.35**	352.46	351.17	362.98
B. longipes	494.92	**134.49**	**134.49**	147.93	147.93	*M. darianii*	1071.62	**134.49**	**134.49**	147.93	147.93
B. sollyaeformis	**178.11**	179.83	178.32	193.01	191.55	*M. kona*	**134.49**	**134.49**	**134.49**	147.93	147.93
B. pervilleana	**134.49**	147.93	149.93	161.32	163.37	*M. madagascariensis*	**134.49**	**134.49**	**134.49**	147.93	147.93
B. madagascariensis	**185.06**	187.90	185.18	198.01	194.52	*M. aurea*	**158.69**	174.43	174.48	187.29	186.40
B. auriflorum	187.96	**184.98**	187.20	196.53	198.64	*M. nathaliae*	**134.49**	**134.49**	**134.49**	147.93	364.20
C. pubescens	**155.61**	158.89	159.76	171.86	173.11	*M. taolanaroensis*	206.57	**134.49**	**134.49**	147.93	147.93
C. decaryi	149.05	**146.32**	134.49	159.71	147.93	*N. baronii*	157.19	161.71	**156.03**	175.05	168.12
D. abrahamii	148.65	**134.49**	144.83	796.72	158.12	*O. tulearensis*	**134.49**	**134.49**	**134.49**	147.93	147.93
D. glaberrima	164.52	166.28	162.76	**147.93**	**147.93**	*P. baronii*	146.55	**134.49**	**134.49**	147.93	147.93
D. glaucocarpa	**134.49**	**134.49**	**134.49**	147.93	147.93	*P. decaryana*	**134.49**	**134.49**	**134.49**	147.93	147.93
D. humbertii	**155.98**	164.69	162.54	178.14	175.96	*P. quartzitorum*	**134.49**	**134.49**	**134.49**	147.93	241.90
D. maritima	**143.38**	152.60	144.96	164.75	157.39	*P. perrieri*	230.36	226.58	228.57	239.93	**214.36**
D. purpurascens	**259.71**	257.92	255.84	271.01	268.66	*P. capuronii*	**192.36**	196.24	195.22	209.57	208.64
D. suaresensis	**177.25**	181.84	179.42	195.04	192.61	*P. amygdalina*	204.20	202.62	**202.59**	213.94	214.36
D. xerophila	146.11	**134.49**	148.10	147.93	161.41	*P. ambatoana*	154.16	146.49	**134.49**	159.78	147.93
D. pumila	**134.49**	**134.49**	**134.49**	147.93	147.93	*R. lakatra*	180.82	177.56	**176.53**	190.97	189.82
D. velutina	**134.49**	144.27	**134.49**	147.93	147.93	*R. nana*	**160.54**	164.62	168.00	169.49	173.41
D. ambositrae	**134.49**	**134.49**	**134.49**	147.93	147.93	*R. mollis*	156.85	164.39	**148.34**	177.73	160.92
D. angustifolia	146.67	**134.49**	**134.49**	147.93	147.93	*S. delphinensis*	**134.49**	**134.49**	**134.49**	147.93	147.93
D. brevicaulis	143.49	**134.49**	**134.49**	147.93	147.93	*S. grandiflora*	169.46	168.15	**158.02**	181.51	169.53
D. ceracea	149.52	153.95	**134.49**	167.40	147.93	*S. decussilvae*	**134.49**	**134.49**	**134.49**	147.93	147.93
D. hovomantsina	141.15	**134.49**	**134.49**	147.93	147.93	*S. tampoketsana*	175.33	178.01	**172.89**	190.01	185.27
D. integra	159.63	**149.78**	157.88	161.47	170.63	*T. perrieri*	**146.71**	147.01	154.00	147.93	163.75
D. linearis	205.72	**196.93**	202.46	205.73	213.37	*T. phylloxylon*	**134.49**	**134.49**	**134.49**	147.93	147.93
D. rivularis	**160.09**	163.64	165.96	174.84	175.94	*V. keraudrenii*	**134.49**	**134.49**	**134.49**	147.93	147.93
D. utilis	**134.49**	156.13	149.24	167.68	160.35						

6.4 Discussion

6.4.1 Addressing spatial dependencies in predicted distributions

The application of spatially explicit species distribution model (i.e., HBM) accurately predicted current distribution for selected endangered and critically endangered species of Madagascar. As well as successfully prediction species distribution the HBM approach was able to combine factors that represent abiotic and movement component of the environment. Mostly, the HBM performed better when predicting for current emission scenario compared to future scenarios, which may confirm the stability between current species distributions and the environment (Menke et al. 2009, Elith et al. 2010, Blaise et al. 2017). This was confirmed by the match between available IUCN range data and obtained predictions for some species under current emission scenarios. Although in most instances our model predict beyond the IUCN range; perhaps an indication of probable suitable areas in locations that could not be reached during survey times and/or the effect of imperfect detection explained in the HBM. As a result, species distribution extrapolated to future dates (i.e., 2050) may be robust enough under the different emission scenarios that were considered. Besides species-specific prediction also included estimates of their uncertainties which allows for determination of the accuracy for each prediction. But due to lack of adequate species-specific biological data required for such a large-scale assessment it was not possible to include any biotic measure in the modelling process (Guisan, 2005). There is no doubt that including information on species-specific biological interaction could have reduce the uncertainties in the predictions. Implementing hierarchical species distribution models allowed for the inclusion of future LULCC, corridor connectivity and the determination of spatial dependences for the derived predictions under low and high emission scenarios (Gelfand et al. 2006). Specifically, estimates of spatial dependences from HBM was the way autocorrelation was explained in the observed habitat suitability for each species, which was often difficult to interpret from the predictors themselves. In most cases,

HBM allowed for a smoother species-specific prediction with a few exceptions under future emission scenarios where current corridor connectivity appeared to have strongly influenced the parameters used to fit the model and as such resulted in jagged predictions for those species (e.g., *Dypsis rivularis, Dalbergia glaberrima*). Generally, the results of spatial random effects had unrealistically very strong and weak values, which is likely due to the heterogeneous nature of certain environmental surfaces (e.g., land-use/land-cover and corridors) (Domisch et al. 2016). It is possible that using informative priors may have corrected for such effects in the outputs. Higher predicted probabilities often coincided with regions of moderate positive spatial dependences (i.e., spatial random effects). To my knowledge, there are no known studies of species distribution using HBM carried out in Madagascar and at similar scale for comparisons with the results obtained here. The closest was the analysis conducted by Gelfand et al. (2006) in the cape floristic region of South Africa where they measured relatively smaller variation in spatial dependences in their predictions for selected plant species; in terms of size this region is a relatively smaller area compared to Madagascar. This suggests that higher spatial dependences in predictions involving large study sites may reflect the true nature of habitat suitability in such landscapes (such as Madagascar) which in itself is partly explained by spatial autocorrelation.

The HBM did not explicitly evaluate how the Binomial process modelled collinearity between predictors, however the selection of bioclimatic variables with known strong influence on plant species survival may have mitigated this potential bias. Notwithstanding, HBM explicitly modelled the posterior density predictions for each environmental variable which can be used to visually estimate collinearity between predictors (Golding and Purse 2016). It is likely that with priors for the selected environmental variables, each predicted SDM may be different and possibly the model may have better mitigated against bias from the observations. Getting priors from previous studies at species-specific scale remains challenging and a model that quantifies the corridors and/or dispersals are very rare for the region. The spatial framework applied for predicting species distributions and the associated

uncertainties provides additional information to the ongoing discussion on conservation biodiversity.

Measures of range sizes (i.e., niche breadth) enabled the determination of species-specific habitat sizes under each scenario. Incidentally, only minimal differences in range sizes were measured within and between emission scenarios. Perhaps an indication of the short-comings of dealing with measures derived from probability maps as done here with niche breadth analysis in quantifying changes in suitable habitats when extrapolating to the future. This further justifies the argument for threshold transformations from probability maps to binary maps of presence and absences because binary maps are ecologically intuitive (Liu et al. 2016). This is not to say that probability maps are not useful, as several studies have successfully applied niche breadth analysis for species habitat discrimination in different regions (Diego P. Vázquez and Richard D. Stevens 2004, Slatyer et al. 2013). Nonetheless, niche-breadth analysis could only measure subtle differences in species habitat sizes between future emission scenarios. To further interrogate differences between emission scenarios, especially for purposes of current interest (e.g., range shift), transformation of continuous distributions to binary format (i.e., presence/absence) is required. This is likely to better discriminate between emission scenarios, determine the influence of corridor connectivity on species distributions in the future and importantly produce results that are meaningful for conservation planning in Madagascar.

6.5 Conclusion

The probability of species occurrence was aligned with regions of moderate to high spatial dependences, suggesting that ignoring spatial autocorrelations and other possible environmental associations could affect the output of SDMs (Blaise et al. 2017). Also implemented in these analyses are predictions of niche breadth (or range sizes) for critically endangered and vulnerable plant species in a biodiversity hotspot under different emission and environmental scenarios. The results obtained from this modelling approach provides an additional layer of information to the existing body of knowledge of plant species in Madagascar. Specifically, the environmental parameter estimates (i.e., β) can be utilised as prior terms in future research when calibrating either correlative SDMs or spatial models. In anticipation of climate-driven and land-use-driven plant range-shifts, it is important that conservation experts and other relevant stakeholders are made aware of future habitat predictions and the associated uncertainties.

Chapter Seven

Predicting future climate –and– land-use-driven range shifts

7.1 Introduction

7.1.1 Extinction risks, range sizes and range shift

Climate change and land use land cover change (LULCC) are threatening global biodiversity (Watson 2014, Jantz et al. 2015, Mantyka-Pringle et al. 2015). Global warming, deforestation and forest degradation are expected to directly impact and modify future plant habitats (Corlett 2011). As a result, species ranges may contract, expand or experience upslope or downslope displacement, and in some places, species extinctions may occur (McCain and Colwell 2011, Zelazowski et al. 2011, Hong-Wa and Arroyo 2012, Kuhn et al. 2016). For other regions, changes in species ranges will cause lowland attrition and the emergence of upper-zone specialists (Colwell et al. 2008, Laurance et al. 2011a). Plants in the tropics may be the most vulnerable to these emerging environmental pressures mostly because many tropical species are thought to already occupy their extreme ranges (Brown 2014, Marta et al. 2016, Males 2018). Moreover, projections for forests in Amazonia suggest that future climate analogs may be eliminated and lead to increase distances between current and future habitats by approximately 300 – 475 km by 2050 (Feeley and Rehm 2012), thereby causing range-shift gaps between current and future suitable habitats (but see Petitpierre et al. (2012). For plants, it is predicted that if average global temperatures were to rise above 3ºC, then more than one-half of current suitable habitats would be lost (Warren et al. 2018). LULCC and climate change may act synergistically, with deforestation increasing the risk of reduction to future suitable habitats by approximately 30% or 55% under the low or high carbon emission scenarios, respectively (Feeley et al. 2012, Brown et al. 2015, Raúl et al. 2015).

Several studies have investigated plant responses to future climate and LULCC by comparing predictions of range-shift from niche-based and process-based models[7] (Thuiller 2004, Morin and Thuiller 2009), focusing on differences in realised thermal niches in lowland and montane species (Feeley and Silman 2010b) or using spatial metrics for vulnerability assessments (Choe et al. 2017). Recently, emphasis has been placed on building more robust, spatially-explicit or hybrid species distribution models (such as hierarchical Bayesian models; see **chapter 6**) for predictions of range-shift gaps under different environmental scenarios (Zurell et al. 2016). This approach is particularly relevant because it conveniently allows for the incorporation of less commonly used abiotic variables as predictors, whilst accounting for spatial bias in the model. Some examples include the: (i) inclusion of soil data in a Bayesian logistic regression model to predict the distribution of Amazonian plant species (Figueiredo et al. 2018) and (ii) incorporating species-specific physiological data while explaining uncertainties in plant species predictions in the Amazon basin (Feng et al. 2018). For Madagascar, applications of recent analytical techniques lag behind other biodiversity hotspots (e.g., the Amazons), despite evidence that disproportionate changes to plant diversity patterns is expected for the region due to climate and LULCC (Brown et al. 2015), range contraction and expansion of some endemic species (Hong-Wa and Arroyo 2012) and extinctions to more than half the species in one entire genera (i.e., *Coleeae*) (Good et al. 2006). Regardless of geographical location, few studies assess future risks, habitat vulnerabilities and consider the influence of dispersal capabilities when predicting range-shifts (Elith et al. 2010, Choe et al. 2017). This is especially important for sub-Saharan tropical forests where environmental changes will inevitably cause shifts in species ranges (Kreyling et al. 2010, Pienaar et al. 2015, Ryan et al. 2016).

[7] Niche-based models rely on the establishment of statistical or theoretical relationships between environmental predictors and observed species distribution; while process-based models predict the response of an individual or population to environmental conditions by explicitly incorporating biological processes calibrated with observations on individual species

Until recently, the application of species-specific and process-based distribution models at regional scale has been rare, despite the overwhelming evidence of their importance for biodiversity conservation (Zurell et al. 2016). Application of either model to regional assessment of species distribution is important for conservation schemes, especially because studies conducted at global-scales tend to obscure regional and/or local patterns of habitat loss and extinction risks (Boakes et al. 2018). However, environmental scientists still rely to a large extent on abiotic factors as explanatory variables when predicting spatial patterns across large geographical areas. Other explanatory variables that are indicative of biotic interactions (such as competition) at fine scales are often neglected (Staniczenko et al. 2017). However, Schliep et al. (2018) show that dynamic local interactions among species in a community can affect occurrence and/or abundance of any give species when predicting range-shift. Suggesting that including inter and intra-species biotic interactions within the modelling framework could potentially produce realistic predictions of species distribution and likely reduce the uncertainties associated with predictions. Although there remains the challenge of quantifying and collecting data on biotic interactions at regional and global scales. Despite paucity of complete data there is need to use measures that are indicative of environmental change (such as corridor connectivity) while quantifying range-shift gaps.

In this chapter, I model the potential range-shift of 84 endangered and critically endangered plants under future emission scenarios (low and high), predicted estimates of future deforestation and degradation, as well as with and without corridor connectivity. The models were implemented using species distributions constructed using a hierarchical Bayesian framework (See Chapter 6). The aim was to model how future climate and land use land cover change may influence shifts in future distributions of plant species in Madagascar. There were three primary objectives for this chapter. First, I compared the effect of corridor connectivity on future plant range sizes under multiple climate and land-use scenarios. My expectation is that connectivity will facilitate the future expansion of

species ranges provided climate change does not exceed or mitigate the potential for plants to disperse (Feeley and Silman 2010a, Dullinger et al. 2012). Second, I determined whether variation in environmental conditions could lead to upslope displacement of endangered and critically endangered plant species in lowland, humid and dry forests. I expect more upward displacements under future high emission scenarios, as well as lowland attrition to be dominant in all future emission scenarios (Raxworthy et al. 2008, Laurance et al. 2011a). Third, I investigated whether feedbacks between future climate and land cover change would impact range sizes and lead to range shift gaps. Lastly, I mapped range shift hotspots to identify areas where substantial numbers of species range contract under different scenarios. My expectation is that landscape connectivity will drive species range expansions, while climate-only scenarios will lead to range contractions (Feeley 2012, Whitfield et al. 2016).

7.2 Methods

Species distribution maps showing probability of occurrence were produced following the method described in **Chapter 6, section 6.2.3.** Species-specific probability of occurrence maps (showing continuous distribution) were transformed into presence/absence maps using a threshold that maximises the sum of sensitivity (true positive rate) and specificity (true negative rate) (Liu et al. 2005). Among the plethora of threshold transformation metrics available, the maximum sum of sensitivity and specificity was selected because it remains consistent under differing ratios of presence and background points (Liu et al. 2016).

Species' range-shift were assessed under multiple future climate and land use land cover scenarios (Table 6.1). Therefore, range shift analysis was implemented under four future scenarios.

7.2.1 Quantifying changes in predicted species range

Six spatial indices were modified from Radinger et al. (2017), Choe et al. (2017) and Midgley et al. (2006) to determine several aspects of changes in predicted suitable habitats (i.e., species range). The six spatial indices were: (i) *habitat net-change* was derived from the net differences between range gains and losses; negative net change indicate species range contractions in the future, while positive net change indicate species range expansions in the future (Table 7.1) (ii) *habitat direction* was derived from the difference between the mean elevation of predicted species range and their current mean elevation and thus represented an *estimate of upslope displacements in species range* (iii) *rate of change* (RoC) was derived from the product of total number of pixels (692582 pixels) and predicted range area divided by the product of total number of available pixels and current range area. Large RoC values indicate a prediction of range expansion and small RoC values indicate future species range contraction and (iv) *habitat distance* was calculated as the median distance between the centroid of predicted species range and the edges of current range. Thus, the habitat distance index provided an *explicit measure of range shifts* in species distributions in the future. Habitat gain, habitat loss, mean elevation and median distance were modelled using ArcGIS 10.5.1 (ESRI 2015).

Table 7.1: Summary of spatial indices equations used for the determination of range shift for endangered and critically endangered plant species under multiple climate and land-use scenarios

Spatial index	Equation
Habitat net change	$HG_i - HL_i$
Habitat direction	$\overline{x}_p - \overline{x}_c$
Rate of change[+]	$\left(\sum A_j * p_i\right) / \left(\sum A_j * c_i\right)$
Habitat exposure	$\frac{C_i - I_j}{C_i}$
Spatial disruption	$\frac{C_i - p_i}{A_j}$

[+] *The rate of change index used for range shift analysis is different from rate of change metric used to determine deforestation and forest degradation rates (**chapter 3**) and rate of change of land use land cover categories (**chapter 5**)*

Where: i represents suitable pixels for species in current and future emission scenarios, HG_i represents predicted suitable pixels that are currently unsuitable, HL_i represents pixels that were predicted to become unsuitable, $\overline{x}_p$ represents the mean elevation of predicted suitable area, $\overline{x}_p$ represents mean elevation of current suitable area, A_j represents the total number of pixel (692582), c_i represents current suitable area, p_i represents all suitable pixels in future scenario and I_j represents the area of intersection between current and predicted suitable pixels.

(v) *Habitat exposure* was derived from the difference between current range and the area of intersection between current and future range divided by current range (Table 7.1). Habitat exposure index determined how much of a change in climate conditions a species range might experience in the future (Choe et al. 2017). Thus, large exposure values indicate that species are predicted to have higher risk of more exposure and *vice versa*. (vi) *Spatial disruption* was calculated by dividing the differences between current and future species range with the total area of Madagascar and served as a measure of species sensitivity and an estimate of the extent of anticipated future range change (i.e., gain or loss) for a species (Bush et al. 2014). For the spatial disruption index, positive values represented predictions of range contraction and negative values represented predictions of range expansion. Species with large disruption values were considered to be under more risk of further decreases to their range under future emission scenarios and thus were highly sensitive to climate change and LULCC.

Two-sample Wilcoxon signed-rank tests were used to compare habitat gain (i.e., range expansion) versus habitat loss (i.e., range contraction) in combined scenarios (with

and without connectivity). Furthermore, signed-rank tests were also carried out to compare habitat gain, habitat loss, habitat distance and habitat direction between low/high combined scenarios with and without connectivity. Spearman's rank correlation test was used to determine the associations between habitat net change and habitat distance, as well as between habitat net change and habitat direction in low/high combined scenarios with and without corridor connectivity. Correlation tests were carried out to determine whether range shifts and displacements were associated with range contractions or expansions. Predicted changes in species' ranges are described relative to the current state (i.e., all reported results are for future ranges).

Finally, potential range shift hotpots were mapped using the habitat net change index and was determined from measures of species net habitat losses (i.e., range contraction) in the future. These hotspots represented areas where several species' ranges were predicted to contract and were independent of predicted range expansions. To achieve this, the island was partitioned to grids of 2500 km^2 and for each grid species-specific visual inspections were carried out using habitat net change surface to determine species range contractions. Habitat net change surface included spatially-explicit representation of future range expansions (gains) and range contractions (losses). Therefore, for each grid the number of species predicted to experience range contractions (i.e., net losses on the net change surface) were identified and then added up to derive the total number of species per grid. Grids with high numbers of species range contractions were considered as potential range shift hotspots.

7.3 Results

7.3.1 Changes in range size under different multiple scenarios

Habitat net change index showed that the average species range was predicted to contract by approximately 27351 km^2 under the combined scenario (low emission) and by approximately 27910 km^2 under the combined with connectivity scenario (low emission) (Table 7.2). Similarly, the average range contractions under the combined scenario (high emission) was approximately 27810 km^2, while the combined with connectivity scenario (high emission) predicted species' ranges to contract by approximately 30731 km^2. These results indicated that including corridor connectivity in all the models led to contracted ranges under future low and high scenarios.

Overall, habitat net change index showed that identical numbers of species (40) were predicted to experience range contraction under both the combined, as well as combined with connectivity scenario (low emission) (Table 7.2). Species-specific analyses showed that some species under the combined scenario were predicted to experience range expansion, however, under the combined with connectivity scenario (low emission) these same species exhibited range contraction. These species were: *Aloe helenae, Aeschynomene laxiflora, Asteropeia rhopaloides, Cadia pubescens, Dypsis ambositrae, Dalbergia glaberrima, Euphorbia elliotii, Hildegardia ankaranensis, Lemuropisum edule, Millettia nathaliae, Ormocarpopsis tulearensis, and Takhtajania perrieri* (Figure 7.1a & b). Conversely, with connectivity the following species range will expand*: Borassus madagascariensis, Perrierodendron quartzitorum, Asteropeia matrambody, Masoala madagascariensis, Dypsis hovomantsina, Dalbergia glaucocarpa, Millettia taolanaroensis, Asteropeia micraster, Bauhinia pervilleana, Euphorbia mandravioky, Delonix pumila and Euphorbia horombensis.*

Table 7.2: Summary of estimates of spatial indices derived for selected 84-plant species of Madagascar under combined scenarios (low emission) with and without connectivity and combined scenarios (high emission) with and without connectivity.

	Low emission scenarios																**High emission scenarios**															
	Combined scenario								Combined plus connectivity corridors								Combined scenario								Combined plus connectivity corridors							
Species	Habitat gain (km^2)	Habitat loss (km2)	Habitat net change (km^2)	Habitat distance (km)	Habitat direction (m)	RoC	SD	Exp	Habitat gain (km^2)	Habitat loss (km2)	Habitat net change (km^2)	Habitat distance (km)	Habitat direction (m)	RoC	SD	Exp	Habitat gain (km^2)	Habitat loss (km2)	Habitat net change (km^2)	Habitat distance (km)	Habitat direction (m)	RoC	SD	Exp	Habitat gain (km^2)	Habitat loss (km2)	Habitat net change (km^2)	Habitat distance (km)	Habitat direction (m)	RoC	SD	Exp
A. grandidieri	38110	3959	341506	186.58	50	-1.62	-0.06	0.19	65943	3747	62196	342.23	353	-2.95	-0.10	0.18	9633	5735	3897	205.15	47	-0.18	-0.01	0.27	27179	7592	19587	356.59	241	-0.93	-0.03	0.36
A. perrieri	37355	52753	-153978	249.09	7	0.18	0.03	0.61	19051	58382	-39331	244.42	1	0.45	0.07	0.68	10708	72655	-61946	267.49	17	0.71	0.10	0.84	35653	54270	-18617	245.47	1	0.21	0.03	0.63
A. antennophora	26197	27885	-16882	416.77	3	0.03	0.00	0.48	11187	37680	-26493	408.37	-75	0.45	0.04	0.64	15115	39817	-24702	400.96	3	0.42	0.04	0.68	6784	51001	-44217	397.70	-16	0.75	0.07	0.87
A. neoperrieri	19035	1258	177773	136.59	-147	-0.73	-0.03	0.05	22977	1842	21135	136.35	-197	-0.86	-0.04	0.08	19098	1180	17918	149.45	-152	-0.73	-0.03	0.05	17942	1508	16434	140.28	-169	-0.67	-0.03	0.06
A. laxiflora	13468	12356	11115	113.87	6	-0.03	0.00	0.39	15021	16751	-1730	123.77	-41	0.05	0.00	0.53	18343	17979	364	150.04	-220	-0.01	0.00	-0.01	13260	18719	-5458	139.73	-61	0.17	0.01	0.59
A. helenae	31389	11761	196289	230.65	66	-0.47	-0.03	0.28	17841	20310	-2468	227.89	36	0.06	0.00	0.49	3078	33025	-29947	284.05	-192	0.72	0.05	0.79	2041	28263	-26222	320.74	-218	0.63	0.04	0.68
A. humblotianum	32189	17403	147861	326.21	3	-0.16	-0.02	0.19	32039	19773	12266	304.95	3	-0.14	-0.02	0.22	29936	22975	6961	326.74	2	-0.08	-0.01	0.26	33695	19737	13959	308.63	2	-0.16	-0.02	0.22
A. obesum	18428	8496	99321	280.27	-159	-0.17	-0.02	0.15	19670	3766	15903	279.50	-160	-0.27	-0.03	0.07	19162	11262	7900	279.17	-151	-0.13	-0.01	0.20	67684	13410	54274	290.03	-161	-0.92	-0.09	0.23
A. protensum	13260	15809	-25489	179.41	96	0.05	0.00	0.29	21575	27814	-6238	181.94	36	0.12	0.01	0.52	21096	29439	-8343	177.45	205	0.16	0.01	0.55	26859	30144	-3285	179.58	72	0.06	0.01	0.56
A. setipes	5260	99128	-938672	356.15	3	0.56	0.16	0.59	63641	99256	-35615	333.17	-24	0.21	0.06	0.59	21642	74044	-52402	350.45	-51	0.31	0.09	0.44	95063	85974	9088	334.81	-60	-0.05	-0.02	0.51
A. darainensis	5700	20894	-151942	266.28	2	0.43	0.03	0.60	5257	25073	-19816	269.90	6	0.57	0.03	0.72	6348	19231	-12883	262.59	2	0.37	0.02	0.56	9953	19110	-9157	263.44	2	0.26	0.02	0.55
A. amblyocarpa	2875	123166	-1202915	399.59	-15	0.52	0.20	0.53	31687	87560	-55873	366.03	-3	0.24	0.09	0.38	43991	61267	-17276	327.81	0	0.07	0.03	0.26	22434	103658	-81224	363.20	-2	0.35	0.14	0.45
A. labatii	2147	70086	-679392	248.77	46	0.51	0.11	0.53	1927	63096	-61169	231.44	47	0.46	0.10	0.48	2064	69084	-67020	259.20	13	0.51	0.11	0.52	4963	66260	-61298	229.20	39	0.46	0.10	0.50
A. matrambody	3619	22381	-187613	400.02	-554	0.35	0.03	0.42	54520	29055	25464	421.81	-72	-0.48	-0.04	0.55	4553	28147	-23595	430.95	-575	0.44	0.04	0.53	24343	38827	-14484	425.16	-95	0.27	0.02	0.74
A. micraster	4129	13233	-91039	268.73	-223	0.31	0.02	0.46	20420	7731	12689	271.00	166	-0.44	-0.02	0.26	3280	13644	-10363	261.19	-433	0.36	0.02	0.47	54621	1826	52795	260.68	184	-1.83	-0.09	0.07
A. rhopaloides	30447	26635	38118	663.12	1	-0.03	-0.01	0.20	19415	55715	-36300	602.12	3	0.27	0.06	0.42	82455	14033	68422	639.46	1	-0.51	-0.12	0.11	31277	58334	-27057	637.72	2	0.20	0.05	0.44
B. longipes	10744	27866	-171219	752.34	-71	0.24	0.03	0.39	16082	24306	-8223	764.83	-2	0.11	0.01	0.34	7672	24324	-16651	763.57	-33	0.23	0.03	0.34	14521	23937	-9416	756.44	8	0.13	0.02	0.33
B. sollyaeformis	7756	17510	-97541	525.98	127	0.38	0.02	0.68	4104	18869	-14765	559.34	-421	0.57	0.02	0.73	27634	16756	10878	388.74	258	-0.42	-0.02	0.66	73055	14355	58700	407.45	231	-2.29	-0.10	0.58
B. pervilleana	19481	28495	-90140	396.51	37	0.13	0.02	0.41	69870	14102	55769	366.02	542	-0.80	-0.09	0.20	28408	21647	6760	366.24	51	-0.10	-0.01	0.31	30567	24367	6200	352.49	79	-0.09	-0.01	0.35
B. madagascariensis	11748	43090	-313424	453.43	-80	0.26	0.05	0.35	41838	36654	5184	442.28	7	-0.04	-0.01	0.30	40882	28376	12506	418.84	-20	-0.10	-0.02	0.23	77728	25606	52122	420.80	52	-0.43	-0.09	0.21
B. auriflorum	5152	27529	-223772	390.70	-28	0.50	0.04	0.62	14297	30001	-15703	395.86	-77	0.35	0.03	0.67	13682	24230	-10548	397.38	3	0.24	0.02	0.55	11650	30293	-18643	392.35	13	0.42	0.03	0.68
C. pubescens	36004	21002	150017	370.30	17	-0.28	-0.03	0.40	23454	26384	-2930	370.19	-17	0.06	0.00	0.50	21553	19256	2297	364.60	5	-0.04	0.00	0.36	28090	34747	-6657	359.39	-121	0.13	0.01	0.66
C. decaryi	58345	21889	364565	346.20	-22	-0.43	-0.06	0.26	46245	20563	25682	356.11	-23	-0.31	-0.04	0.25	55216	25510	29706	327.21	-24	-0.35	-0.05	0.31	50026	26542	23483	324.76	-24	-0.28	-0.04	0.32
D. abrahamii	20171	45207	-250356	256.53	4	0.26	0.04	0.47	3059	71636	-68577	292.01	23	0.71	0.12	0.74	9278	65052	-55775	270.99	19	0.58	0.09	0.67	9161	67746	-58585	257.92	16	0.61	0.10	0.70
D. glaberrima	39936	27506	124305	243.72	102	-0.13	-0.02	0.27	15556	72151	-56594	289.58	27	0.57	0.10	0.73	77715	15179	62536	198.43	103	-0.63	-0.11	0.15	25504	61566	-36061	282.86	-998	0.36	0.06	0.62
D. glaucocarpa	20522	32120	-115980	297.91	-222	0.15	0.02	0.42	34009	25795	8213	283.76	9	-0.11	-0.01	0.33	47231	24727	22505	235.98	50	-0.29	-0.04	0.32	39950	28666	11284	239.20	-98	-0.15	-0.02	0.37
D. humbertii	23464	214862	-1913982	280.18	2	0.57	0.32	0.64	9945	202043	-192098	295.36	1	0.57	0.32	0.60	23064	152976	-129912	283.36	3	0.39	0.22	0.46	17230	167394	-150164	291.64	3	0.45	0.25	0.50
D. maritima	34917	33156	17609	209.57	86	-0.02	0.00	0.32	66501	12650	53850	211.62	88	-0.54	-0.09	0.12	60114	42355	17759	206.02	15	-0.18	-0.03	0.42	56992	32766	24226	213.62	62	-0.24	-0.04	0.32
D. purpurascens	80592	6315	742777	388.36	144	-0.33	-0.12	0.03	65407	7608	57799	404.92	129	-0.25	-0.10	0.04	89218	11336	77882	396.75	94	-0.28	-0.11	0.05	80858	14253	66605	405.52	84	-0.29	-0.11	0.06
D. suaresensis	18526	49521	-309950	370.52	-105	0.23	0.05	0.37	18164	62387	-44223	364.99	-158	0.33	0.07	0.46	4914	105636	-100722	422.01	-588	0.75	0.17	0.79	24439	79016	-54577	392.83	-200	0.41	0.09	0.59
D. xerophila	27306	732	265740	376.15	151	-2.77	-0.04	0.08	28391	771	27620	386.96	178	-2.88	-0.05	0.08	17371	661	16710	195.93	83	-1.74	-0.03	0.07	18706	1446	17260	274.00	94	-1.80	-0.03	0.15
D. pumila	17695	19218	-15230	177.81	653	0.03	0.00	0.35	34760	14942	19818	199.04	343	-0.36	-0.03	0.27	17186	20409	-3223	156.72	648	0.06	0.01	0.37	43217	9965	33251	213.53	652	-0.61	-0.06	0.17
D. velutina	15042	8922	61194	220.87	365	-0.24	-0.01	0.35	36600	9087	27513	253.69	198	-1.07	-0.05	0.36	4252	19723	-15471	232.36	-91	0.60	0.03	0.77	14866	17059	-2193	232.13	313	0.09	0.00	0.67
D. ambositrae	20568	19658	9095	370.50	4	-0.01	0.00	0.29	10148	25431	-15283	354.58	33	0.22	0.03	0.37	41802	19161	22641	360.07	4	-0.33	-0.04	0.28	15839	23697	-7858	359.72	45	0.11	0.01	0.35
D. angustifolia	41593	370	412223	162.39	311	-2.02	-0.07	0.02	57634	851	56783	162.14	415	-2.79	-0.10	0.04	71520	7768	63752	259.80	634	-3.13	-0.11	0.39	54787	7095	47693	269.91	538	-2.34	-0.08	0.35
D. brevicaulis	7247	2524	47231	343.27	251	-0.77	-0.01	0.40	16898	2112	14786	349.92	566	-2.40	-0.02	0.33	29372	3891	25481	311.50	328	-4.14	-0.04	0.63	21054	3771	17284	355.74	577	-2.81	-0.03	0.62
D. ceracea	39574	8429	311447	414.69	-70	-0.39	-0.05	0.10	88857	2244	86612	415.98	198	-1.08	-0.15	0.03	35736	35323	413	335.77	-202	-0.01	0.00	0.44	67805	38857	28948	311.28	-188	-0.36	-0.05	0.48
D. hovomantsina	1669	16188	-145182	360.70	-319	0.54	0.02	0.60	23880	13287	10593	331.85	136	-0.40	-0.02	0.50	2931	14886	-11956	385.56	-300	0.45	0.02	0.56	32643	14381	18262	341.61	-42	-0.68	-0.03	0.54
D. integra	7980	53056	-450760	378.05	-175	0.60	0.08	0.70	8888	51732	-42844	422.16	-59	0.57	0.07	0.68	22127	41886	-19759	388.14	49	0.26	0.03	0.55	33788	35656	-1868	426.18	53	0.02	0.00	0.46
D. linearis	33102	57791	-246882	418.34	2	0.14	0.04	0.33	38380	61899	-23519	462.85	2	0.13	0.04	0.35	9568	73494	-63925	441.49	1	0.36	0.11	0.41	15319	81999	-66680	438.79	-4	0.37	0.11	0.46
D. rivularis	11308	10433	8745	204.74	22	-0.02	0.00	0.19	33842	29732	4110	208.07	-45	-0.08	-0.01	0.55	23842	14518	9324	169.81	1	-0.17	-0.02	0.27	16678	39501	-22823	202.97	-67	0.42	0.04	0.73
D. utilis	5051	126143	-1210923	315.43	-230	0.63	0.20	0.66	24484	84582	-60098	311.54	-145	0.31	0.10	0.44	39453	86001	-46548	308.64	-80	0.24	0.08	0.45	5337	113822	-108485	306.63	-290	0.57	0.18	0.59
E. cynometroides	57454	4483	529709	401.19	396	-5.60	-0.09	0.48	23246	5516	17730	552.16	216	-1.87	-0.03	0.59	36094	5376	30718	442.21	318	-3.25	-0.05	0.58	31908	5105	26803	475.84	417	-2.83	-0.05	0.55
E. ankaranae	12475	13572	-10969	182.98	-295	0.01	0.00	0.15	15817	49815	-33998	175.17	-227	0.40	0.06	0.58	8657	31405	-22748	170.89	-270	0.27	0.04	0.36	18669	45231	-26562	171.15	-247	0.31	0.04	0.53
E. decorsei	5847	21391	-155433	166.91	-214	0.28	0.03	0.37	3218	30779	-27561	163.11	-261	0.49	0.05	0.54	5349	31482	-26133	252.08	-300	0.47	0.04	0.56	7622	33613	-25991	136.23	-234	0.46	0.04	0.60
E. didiereoides	18239	51988	-337493	232.82	-256	0.35	0.06	0.54	29552	51289	-21736	234.51	-147	0.23	0.04	0.53	18837	55059	-36223	222.89	-281	0.38	0.06	0.57	22611	53350	-30739	226.12	-212	0.32	0.05	0.55
E. elliotii	25018	20667	43517	456.61	-154	-0.16	-0.01	0.79	19910	20469	-559	488.44	-29	0.02	0.00	0.78	20706	22125	-1419	436.95	-32	0.05	0.00	0.85	21581	21306	276	552.98	-255	-0.01	0.00	0.82
E. francoisii	7960	2150	58097	534.09	124	-0.34	-0.01	0.12	12839	2592	10247	569.07	325	-0.59	-0.02	0.15	9112	2442	6670	455.97	361	-0.39	-0.01	0.14	9490	2419	7071	445.27	522	-0.41	-0.01	0.14
E. hedyotoides	11091	16549	-54580	169.35	-31	0.11	0.01	0.34	12155	21236	-9081	151.68	-96	0.19	0.02	0.44	14118	13641	477	169.83	-17	-0.01	0.00	0.28	17457	19108	-1651	161.76	-78	0.04	0.00	0.40
E. horombensis	36646	37274	-6289	261.55	-148	0.01	0.00	0.52	66504	23857	42648	249.15	-9	-0.60	-0.07	0.34	101091	24164	76928	315.58	-135	-1.09	-0.13	0.34	75135	33481	41654	272.62	-112	-0.59	-0.07	0.47
E. mandravioky	17410	24915	-75047	309.45	1	0.14	0.01	0.48	31714	19364	12350	304.35	1	-0.23	-0.02	0.37	19625	28816	-9191	323.08	2	0.17	0.02	0.55	43217	24633	18584	325.42	2	-0.35	-0.03	0.47
E. quartziticola	13610	6832	67783	170.68	-135	-0.17	-0.01	0.17	16140	7954	8186	164.77	-230	-0.21	-0.01	0.20	12022	7057	4964	164.66	-129	-0.13	-0.01	0.18	12318	9432	2886	160.75	-360	-0.07	0.00	0.24
H. ankaranensis	14322	10282	40403	293.73	6	-0.18	-0.01	0.45	12433	12747	-314	307.89	-104	0.01	0.00	0.56	12045	13018	-974	290.60	-22	0.04	0.00	0.57	17530	13107	4423	321.88	-46	-0.19	-0.01	0.57
K. madagascariensis	116262	3281	1129802	259.83	19	-0.64	-0.19	0.02	73633	26053	47580	273.31	-190	-0.27	-0.08	0.14	63407	25831	37576	275.42	-222	-0.21	-0.06	0.14	133851	13980	119871	259.24	22	-0.68	-0.20	0.08
L. edule	9984	7491	24933	653.81	-55	-0.13	0.00	0.39	1306	6211	-4905	549.91	29	-0.26	-0.01	0.07	9431	6865	2566	642.41	-32	-0.13	0.00	0.36	9420	1742	7678	564.51	66	-0.40	-0.01	0.09
L. abrahamii	2561	98759	-961979	329.79	-175	0.62	0.16	0.63	36870	55093	-18223	314.05	-17	0.12	0.03	0.35	15671	46134	-30463	318.66	2	0.20	0.05	0.30	27738	59886	-32148	317.01	-5	0.21	0.05	0.38
L. delphinensis	12887	11819	10687	249.49	293	-0.05	0.00	0.59	15796	5568	10227	281.11	187	-0.50	-0.02	0.27	15278	10917	4361	282.72	-177	-0.21	-0.01	0.54	15382	6326	9055	331.43	-48	-0.44	-0.02	0.31
L. multiflora	17043	28962	-119189	397.76	174	0.11	0.02	0.27	21446	29433	-7986	396.54	200	0.07	0.01	0.27	30499	24306	6193	396.07	203	-0.06	-0.01	0.22	47156	28134	19022	378.09	204	-0.18	-0.03	0.26
L. pauciflora	54465	5286	491788	349.95	-1	-0.60	-0.08	0.07	39207	6555	32652	347.08	-1	-0.40	-0.05	0.08	74681	7049	67631	348.81	0	-0.82	-0.11	0.09	65691	9055	56636	360.64	0	-0.69	-0.10	0.11
M. darianii	8748	25925	-171767	602.89	-214	0.51	0.03	0.77	9097	26331	-17234	623.70	-253	0.51	0.03	0.77	13948	25253	-11305	571.57	15	0.33	0.02	0.75	11280	26476	-15196	488.38	-52	0.45	0.03	0.78
M. kona	24518	21627	28912	241.57	-80	-0.05	0.00	0.40	23367	21860	1507	252.03	-91	-0.03	0.00	0.40	9264	31660	-22396	240.51	-113	0.41	0.04	0.57	34682	27706	6976	318.11	228	-0.13	-0.01	0.50
M. madagascariensis	29488	44223	-147347	393.33	0	0.18	0.02	0.54	57110	39568	17542	401.06	-37	-0.21	-0.03	0.48	35261	40580	-5319	392.63	1	0.06	0.01	0.50	38217	44243	-6025	397.43	-15	0.07	0.01	0.06
M. aurea	33111	20887	122243	265.92	-57	-0.20	-0.02	0.34	29644	22290	7354	239.17	-52	-0.12	-0.01	0.36	39173	24565	14608	304.18	-65	-0.24	-0.02	0.40	40428	26077	14351	306.93	-62	-0.24	-0.02	0.43
M. nathaliae	7837	6627	12099	137.32	192	-0.08	0.00	0.43	4880	8614	-3734	144.28	190	0.24	0.01	0.55	8104	6443	1662	129.90	195	-0.11	0.00	0.41	7253	6504	750	114.95	404	-0.05	0.00	0.41
M. taolanaroensis	7903	17591	-96874	303.57	-116	0.20	0.02	0.37	28354	13482	14872	235.58	36	-0.31	-0.03	0.29	5826	25687	-19861	334.83	-502	0.41	0.03	0.53	7988	25900	-17912	307.34	-81	0.37	0.03	0.54
N. baronii	34	62961	-629269	476.08	-703	0.69	0.11	0.69	18061	28296	-10235	406.10	-567	0.11	0.02	0.31	6267	41769	-35502	406.72	-584	0.39	0.06	0.46	3751	50143	-46392	428.04	-592	0.51	0.08	0.55
O. tulearensis	6000	5445	5544	166.40	54	-0.02	0.00	0.21	9907	11431	-1524	152.82	510	0.06	0.00	0.44	11730	6329	5401	155.04	126	-0.21	-0.01	0.24	17850	10773	7077	157.21	394	-0.28	-0.01	0.42
P. baronii	18823	10735	80882	172.22	-49	-0.16	-0.01	0.21	28290	9636	18653	166.25	-44	-0.36	-0.03	0.19	28887	6359	22528	167.45	28	-0.43	-0.04	0.12	21786	10743	11043	167.24	13	-0.21	-0.02	0.21
P. decaryana	26162	758	254044	183.17	48	-0.68	-0.04	0.02	17253	7108	10145	165.56	38	-0.27	-0.02	0.19	12640	9711	2929	165.14	-141	-0.08	0.00	0.26	12670	11132	1538	164.42	15	-0.04	0.00	0.30
P. quartzitorum	20844	45491	-246471	263.39	-65	0.31	0.04	0.56	57494	27969	29525	255.26	-72	-0.37	-0.05	0.34	40774	39642	1132	257.09	-73	-0.01	0.00	0.49	46625	33366	13259	254.61	-101	-0.17	-0.02	0.41
P. perrieri	64461	2122	623391	282.12	127	-0.62	-0.10	0.02	32312	15486	16826	287.98	-21	-0.17	-0.03	0.16	26233	14096	12137	287.32	-14	-0.12	-0.02	0.14	136056	359	135696	240.34	347	-1.35	-0.23	0.01
P. capuronii	88375	12938	754370	328.37	3	-1.34	-0.13	0.24	59331	15954	43377	331.53	3	-0.77	-0.07	0.29	95919	13525	82394	352.53	2	-1.46	-0.14	0.26	56762	16166	40596	346.97	2	-0.72	-0.07	0.30
P. amygdalina	11641	17339	-56985	537.20	-264	0.18	0.01	0.53	9426	18503	-9077	582.29	-297	0.28	0.02	0.57	3543	17607	-14064	655.54	-370	0.43	0.02	0.54	1744	21948	-20204	685.59	-435	0.62	0.03	0.68
P. ambatoana	10804	7271	35329	286.34	-5	-0.09	-0.01	0.18	15612	10000	5612	295.23	21	-0.14	-0.01	0.25	34133	12685	21448	297.71	-76	-0.53	-0.04	0.32	40978	10919	30060	286.73	-96	-0.74	-0.05	0.27
R. lakatra	52547	61869	-93220	334.02	31	0.06	0.02	0.39	48784	54184	-5400	328.35	42	0.03	0.01	0.34	40112	74107	-33996	332.52	125	0.21	0.06	0.47	37898	71872	-33973	331.08	118	0.21	0.06	0.45
R. nana	92699	8821	838786	280.36	1	-1.76	-0.14	0.19	53816	16634	37182	279.46	0	-0.78	-0.06	0.35	47245	14216	33029	319.76	1	-0.69	-0.06	0.30	26103	23000	3102	328.25	-25	-0.07	-0.01	0.48
R. mollis	18422	16455	19671	202.02	-17	-0.04	0.00	0.30	20705	18123	2582	206.50	-8	-0.05	0.00	0.33	47829	32787	15043	222.13	125	-0.28	-0.03	0.62	50762	31840	18921	297.06	120	-0.36	-0.03	0.60
S. delphinensis	14941	8709	62315	492.36	-75	-0.17	-0.01	0.24	12940	12248	691	527.82	-133	-0.02	0.00	0.34	13069	11747	1322	532.94	-183	-0.04	0.00	0.33	12723	13211	-488	527.46	-247	0.01	0.00	0.37
S. grandiflora	37405	2863	345416	152.07	-224	-2.88	-0.06	0.24	26383	3178	23205	204.46	-43	-1.93	-0.04	0.27	59131	1154	57977	112.43	-55	-4.83	-0.10	0.11	29394	4418	24977	143.02	-71	-2.08	-0.04	0.38
S. decussilvae	18140	20598	-24582	446.67	-296	0.07	0.00	0.59	4551	21528	-16977	436.21	-262	0.48	0.03	0.61	1125	25137	-24012	460.26	-448	0.67	0.04	0.71	8855	24603	-15748	442.58	305	0.44	0.03	0.69
S. tampoketsana	28615	439	281757	88.20	-438	-2.08	-0.05	0.03	41127	2383	38744	111.36	-428	-2.86	-0.07	0.17	27776	1310	26466	95.96	-389	-1.96	-0.04	0.09	64778	778	64000	114.84	-376	-4.73	-0.11	0.06
T. perrieri	28945	13578	153670	265.00	2	-0.28	-0.03	0.25	24526	33780	-9254	285.25	-68	0.17	0.02	0.62	31784	22513	9271	276.56	3	-0.17	-0.02	0.42	8670	41660	-32989	316.19	-66	0.60	0.06	0.77
T. phylloxylon	28088	16485	116023	162.08	-104	-0.25	-0.02	0.35	22989	14529	8460	175.27	-104	-0.18	-0.01	0.31	9806	16686	-6880	144.02	-90	0.15	0.01	0.35	12549	13500	-951	160.22	-76	0.02	0.00	0.29
V. keraudrenii	12645	33250	-206052	262.36	451	0.40	0.03	0.66	2402	37406	-35004	252.03	502	0.69	0.06	0.74	10423	36211	-25788	249.41	442	0.51	0.04	0.71	11658	37050	-25392	248.29	431	0.50	0.04	0.73
Mean	**24090**	**27351**	**-32604**	**315**	**-25.10**	**-0.21**	**0.01**	**0.37**	**27900**	**27910**	**-10**	**320**	**6.40**	**-0.24**	**0.00**	**0.39**	**26891**	**27810**	**-919**	**313.46**	**-38.64**	**-0.21**	**0.00**	**0.40**	**31807**	**30731**	**1076**	**318.53**	**3.14**	**-0.27**	**0.00**	**0.44**
Median	**18425**	**17552**	**8920**	**290**	**0.78**	**-0.02**	**0.00**	**0.37**	**22983**	**20516**	**2045**	**295**	**-1.06**	**-0.05**	**-0.01**	**0.35**	**19393**	**22319**	**1227**	**300.94**	**0.25**	**-0.03**	**0.00**	**0.41**	**24391**	**24618**	**2212**	**313.73**	**-1.09**	**-0.05**	**0.00**	**0.46**

Abbreviations in headings represents: RoC (rate of change), spatial disruption (SD) & exposure (Exp).

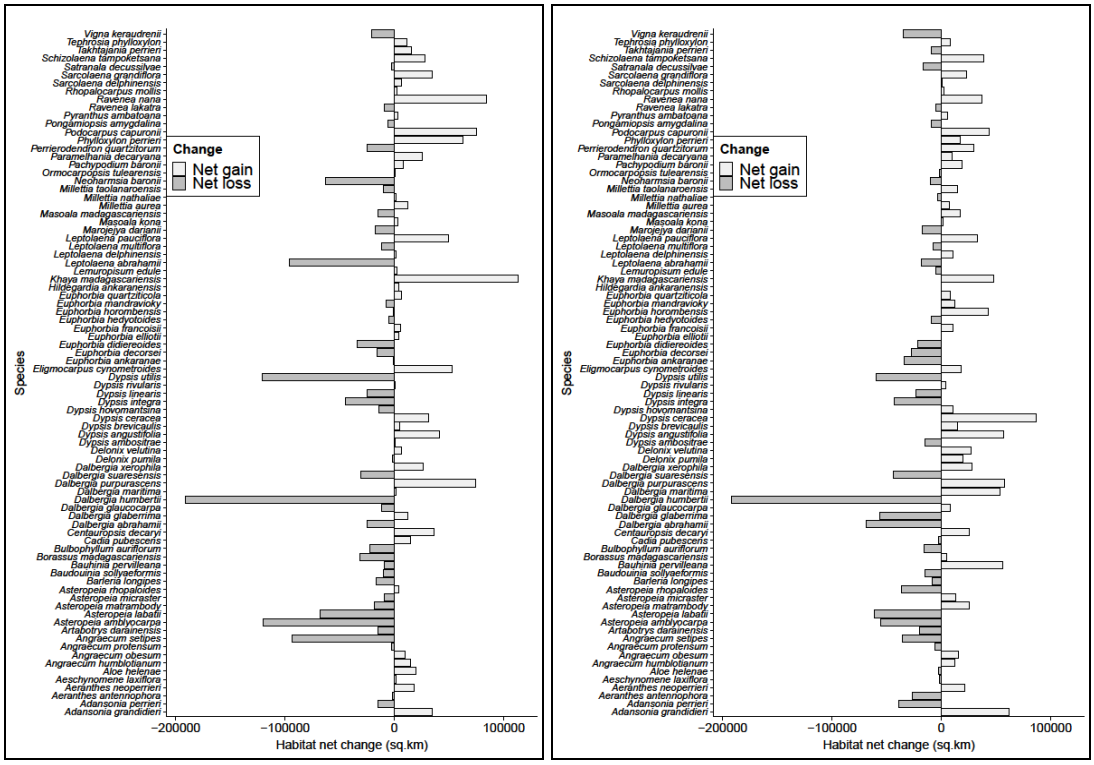

Figure 7.1 a-b: Bar graphs showing differences in habitat net change size between combined scenario (low emission) (*left*) and combined scenario with connectivity (low emission) (*right*). Grey and white bars represent net gains and net losses, respectively. *There is no significant difference between species habitat losses and gains under both low emission scenarios (two-sided Wilcoxon signed-rank tests, p = 0.15, 0.23).*

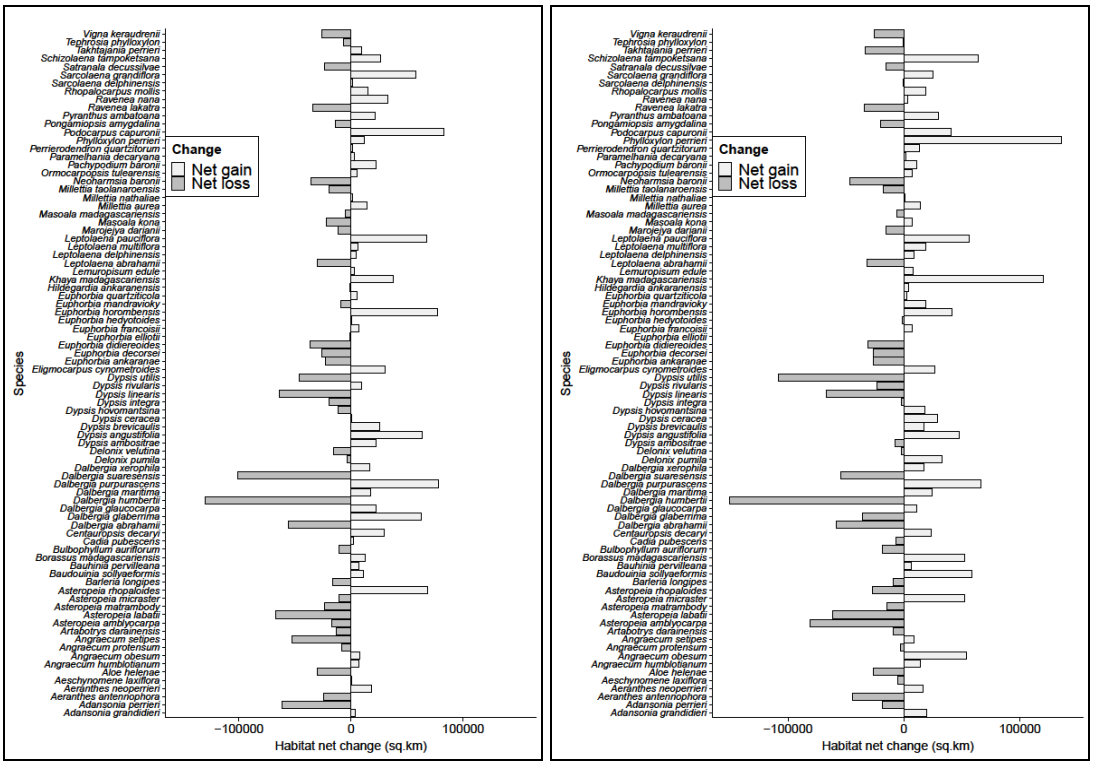

Figure 7.2 a-b: Bar graphs showing differences in habitat net change size between combined scenario (high emission) (*left*) and combined scenario with connectivity (high emission) (*right*). Grey and white bars represent net gains and net losses respectively. *Net loss was significantly different between combined scenario (high emission) and combined scenario with connectivity (high emission) (two-sided Wilcoxon signed-rank tests, p = 0.03).*

In terms of high emissions, 38 species were predicted to experience range contractions (i.e., net losses) under the combined scenario, while 39 species were predicted to experience range contractions under the combined with connectivity scenario (Figure 7.2a-b). Specifically, the following species' range will expand under the combined (high emission) scenario, but contract under the combined plus connectivity (high emission) scenario: *Dalbergia glaberrima, Takhtajania perrieri, Asteropeia rhopaloides, Dypsis rivularis, Dypsis ambositrae, Cadia pubescens, Aeschynomene laxiflora, Euphorbia hedyotoides* and *Sarcolaena delphinensis*. On the other hand, 8 species were predicted to experience range expansions under combined with connectivity scenario (high emission), but under the combined scenarios (high emission) they were expected to experience range contractions. These were: *Angraecum setipes, Masoala kona, Dypsis hovomantsina, Asteropeia micraster, Euphorbia mandravioky, Delonix pumila, Euphorbia elliotii and Hildegardia ankaranensis* (Table 7.2 and Figure 7.2a-b).

There were significant differences between species range contractions under the combined scenario (high emissions) and the combined with connectivity scenario (high emissions) (two-sided Wilcoxon signed-rank test, V = 1298, p = 0.03; Figure 7.2). However, range expansion (i.e. habitat net gain) was not significantly different from range contraction (i.e., habitat net loss) in combined with and without connectivity scenarios (low emission) (Appendix 14 & 15).

7.3.2 Comparing range displacement under multiple scenarios

The mean range displacement for all species was predicted to increase from -25.10 m under the combined scenario (low emission) to 6.40 m under the combined with connectivity scenario (low emission). Similarly, the mean range displacement across all species was predicted to be less in the combined scenario (high emission) than under combined with connectivity scenario (high emission) (Table 7.2). These results suggest species' ranges were more likely to displace upwards with corridor connectivity (i.e., leading

to lowland attritions) and downwards without corridor connectivity. Further analysis revealed that more species' ranges were predicted to displace upwardly under the combined plus connectivity scenario (low emission) compared to the combined scenario (low emission) (Figure 7.3). However, under combined scenario (low emission) the elevational range for some species were predicted to increase compared to the combined with connectivity scenario (low emission). Similarly, there were more species whose elevational range were predicted to displace downwards under the combined with connectivity scenario (low emission), although considering the scenario without connectivity, fewer species' elevational range were predicted to shift downslope or lower elevation.

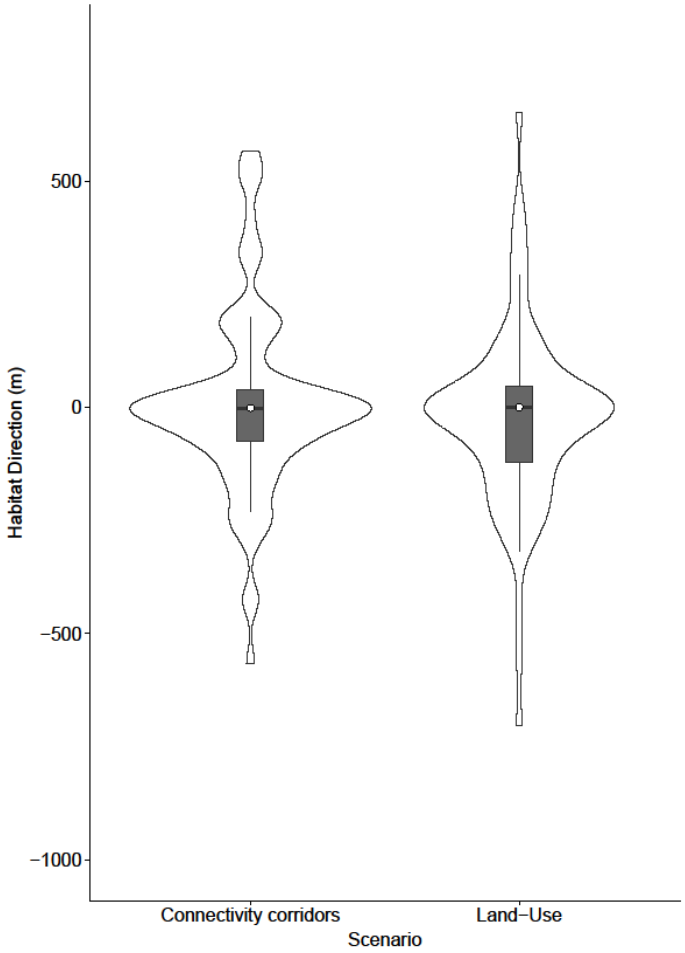

Figure 7.3: Violin plots showing variation in habitat direction under combined scenario (low emission) and combined with connectivity (low emission) for 84 species. Habitat directions represent differences between the means of elevation in current and future suitable areas. Box plots show the range of habitat displacements for all species. Values above zero indicate upward displacement in predicted range compared to current range, while those below zero indicate downward displacement in predicted range.

Under the combined scenario (high emissions), fewer species were predicted to experience upward displacement compared to combined with corridor connectivity (high emissions) (Figure 7.4). The predictions showed that the most upwardly displaced species will reach similarly high elevation under both future high emission scenarios (Figure 7.4). In terms of downward displacement, more species' range were predicted to shift downslope in the combined with connectivity scenario (high emission) than under the combined scenario (high emissions).

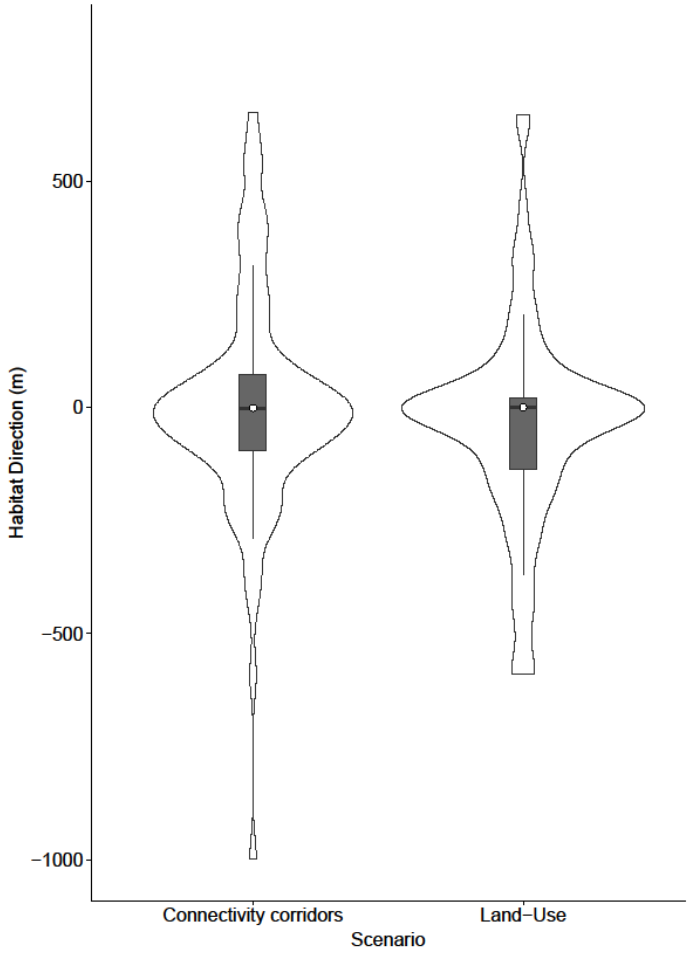

Figure 7.4: Violin plots showing variation in habitat direction under combined scenario (high emission) and combined with connectivity (high emission) for 84 species. Habitat directions represent differences between the means of elevation in current and future suitable areas. Box plots show the range of habitat displacements for all species. Values above zero indicate upward displacement in predicted range compared to current range, while those below zero indicate downward displacement in predicted range.

Correlation analysis showed that under the combined scenario (low emission), habitat net change would be significantly positively associated with range displacement (r_s = 0.30, p = 0.007; Figure 7.5). Similar results were obtained for the combined with connectivity scenario (low emission) (r_s = 0.26, p = 0.02), as well as the combined scenarios (high emission) (r_s = 0.25, p = 0.02). However, for the combined with connectivity scenarios (high emission), habitat net change was not significantly associated with range displacement (r_s = 0.13, p = 0.23; Figure 7.5). This suggests that under combined scenarios (low emission), corridor connectivity will likely determine whether species are able to disperse to areas with favourable climate and land-use/land-cover conditions. Also, under the high emission scenario, corridor connectivity is less likely to facilitate species dispersals to areas with suitable climate and land-use/land-cover.

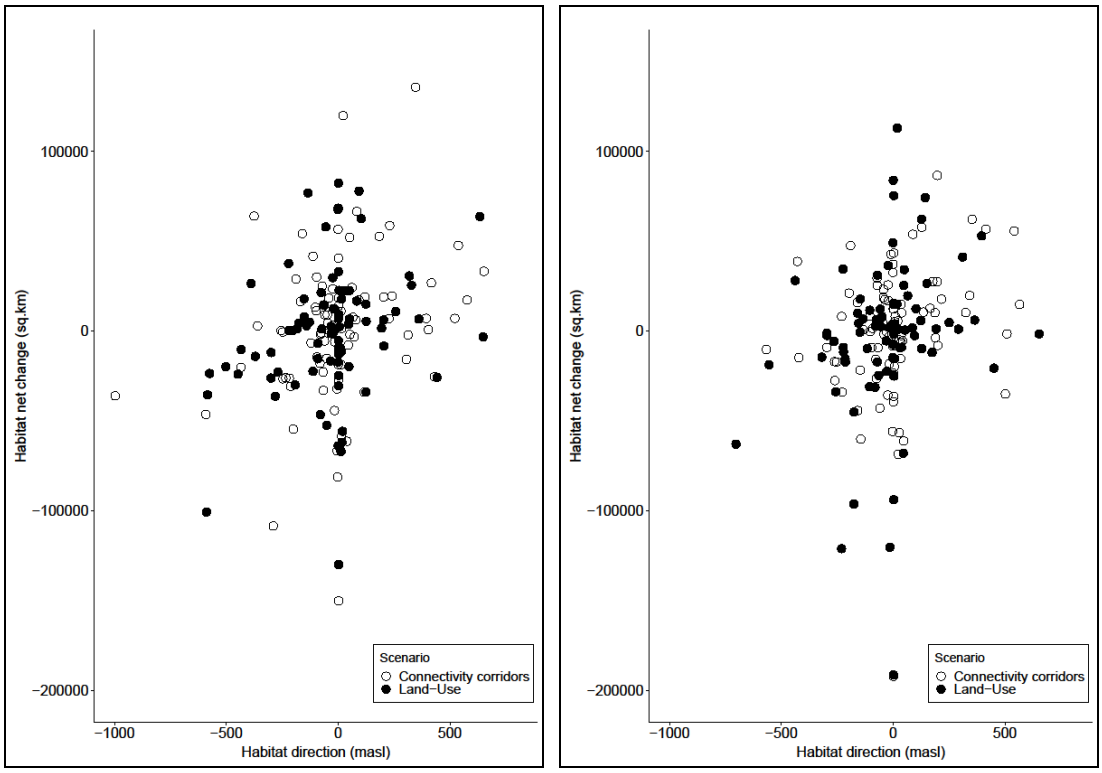

Figure 7.5: Comparing species-specific associations between habitat net change and habitat direction under low emission scenarios (*left-side*) and high emission scenarios (*right-side*) with and without corridor connectivity. *Significant association was determined between habitat net change and habitat direction under combined low emission scenario, combined low emission scenario with connectivity and combined high emission scenario.*

7.3.3 Determining range shift gaps between current and future scenarios

Regardless of the future scenario, all species were predicted to experience some range shift to varying extents (Figures 7.6 & 7.7). Furthermore, corridor connectivity was predicted to increase the mean range shift distance across all species by 5 km under future low and high emission scenarios (Table 7.2). *Barleria longipes* (endangered) and *Schizolaena tampoketsana* (critically endangered) had the largest and smallest predicted range shifts between current and combined scenarios (low and high emissions). Some species showed considerable gaps between current and future ranges in the low emission scenarios. For instance, *Eligmocarpus cynometroides* (critically endangered) range was predicted to shift by approximately 400 km under combined scenario (low emission) and by approximately 550 km under combined with connectivity (low emission). Similarly, *Dypsis integra* (endangered) was predicted to shift by approximately 420 km under combined with connectivity scenario (low emission).

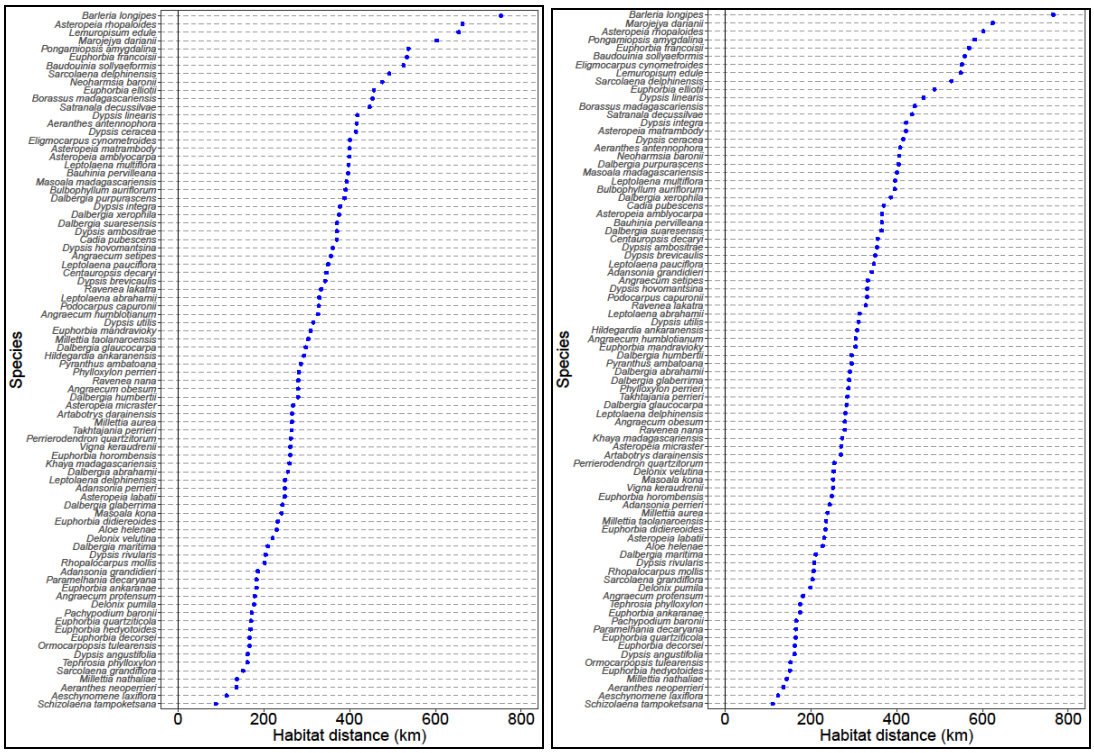

Figure 7.6: Dot plots showing species-specific habitat distances under combined scenario (low emission) (*left*) and combined with connectivity scenario (low emission) (*right*). Habitat distances represent median distances between predicted range and edges of current range. Values closer to zero indicate shorter gaps between predicted and current species range and *vice versa*.

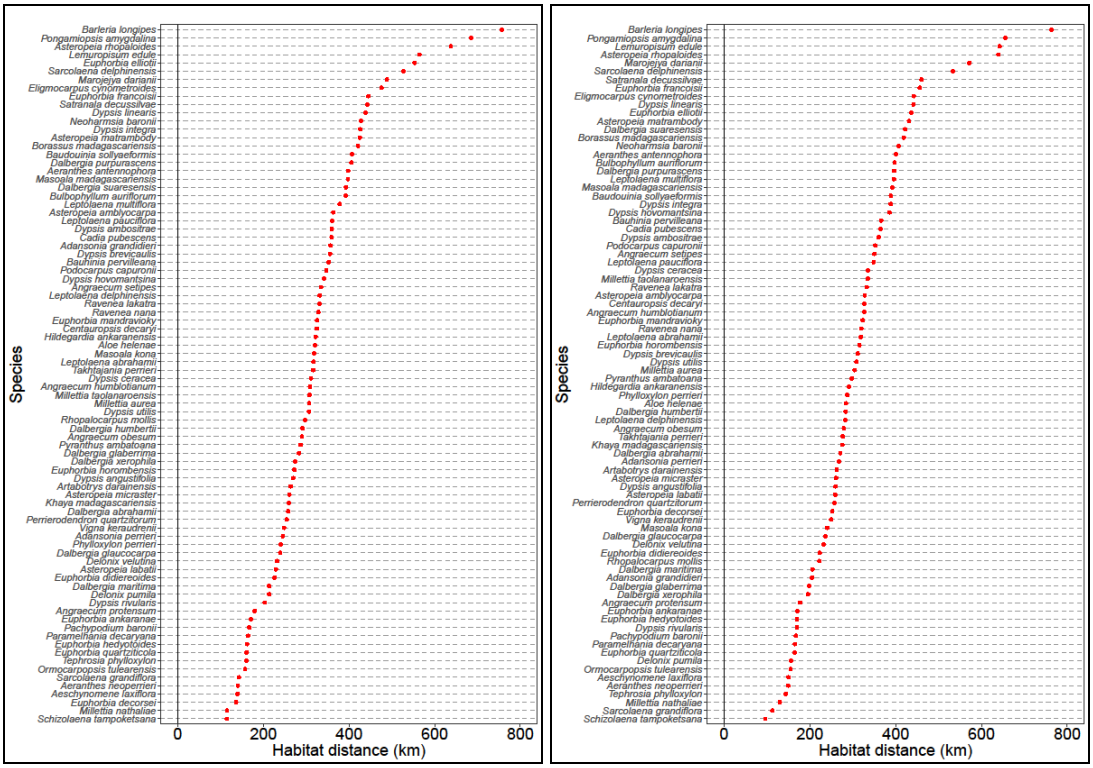

Figure 7.7: Dot plots showing species-specific habitat distances under combined high emission scenario (*left*) and combined high emission with connectivity scenario (*right*). Habitat distances represent median distances between predicted range and edges of current range. Values closer to zero indicate shorter gaps between predicted and current species range and *vice versa*.

Euphorbia elliotii (endangered) range was predicted to shift by approximately 430 km under combined scenario (high emission) and by approximately 550 km under combined scenario with connectivity (high emission). Similarly, *Dypsis integra* (endangered) and *Baudouinia sollyaeformis* (endangered) were predicted to experience large gaps between current and future ranges, with range shift distances increasing under combined high emission scenario with connectivity by more than 25 km.

Range-shift predictions under combined scenario (low emission) were significantly negatively correlated with habitat net change sizes (r_s = -0.24, p = 0.03; Figure 7.8); however, under combined with connectivity scenario (low emission) there was no significant relationship between range shift and range area (r_s = -0.14, p = 0.19). A similarly weak association between species range area and range shifts was detected under combined scenario (high emission) (r_s = -0.13, p =0.23) and combined scenario with connectivity (high emission) (r_s = -0.11, p = 0.33).

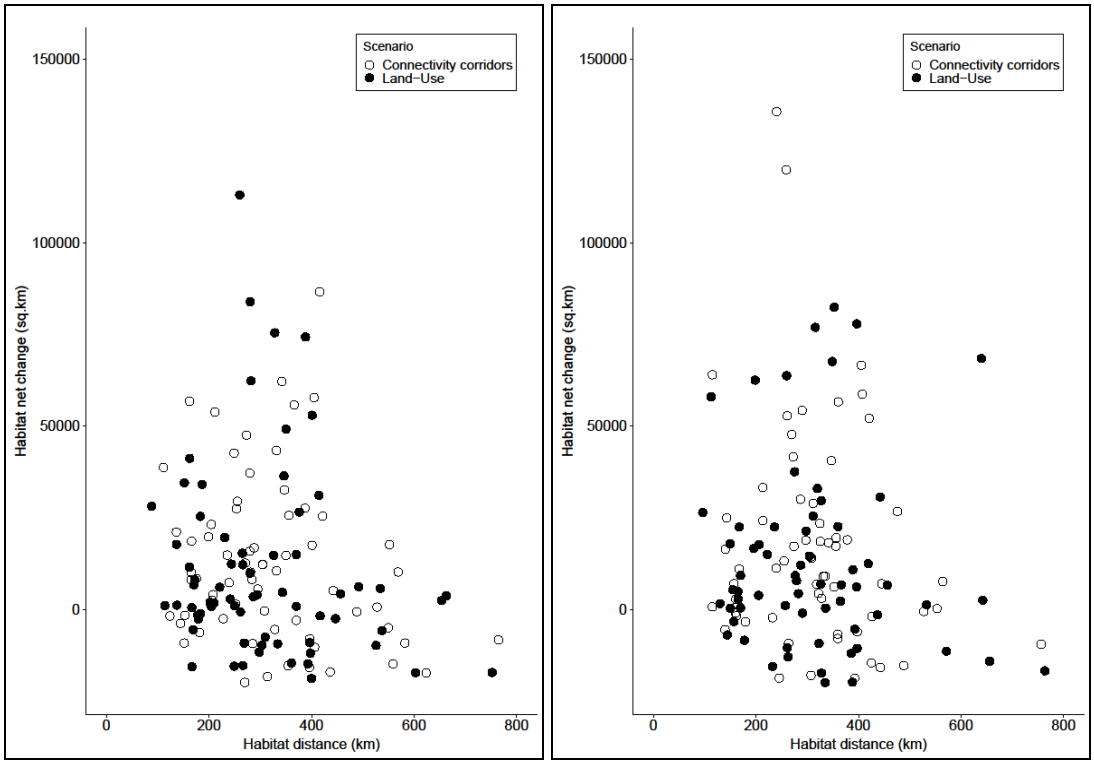

Figure 7.8: Comparing species-specific associations between habitat net changes and habitat distance under combined scenarios with and without connectivity (low emission) (*left*) and combined scenarios with and without connectivity (high emission) (*right*). *Significant association was determined for habitat net change under combined scenario (low emission) scenario (p=0.03).*

7.3.4 Detecting rate of change in suitable habitat areas under multiple scenarios

Analysis of species ranges using the RoC index showed minimal difference between combined scenarios with or without connectivity. For instance, under combined scenario (low emission) the range of 41 species were predicted to increase, while the range of 43 species decreased under combined with connectivity scenario (low emission). Therefore, only the results of combined scenarios with and without connectivity (high emission) are presented and those of combined scenarios with and without connectivity (low emission) are included as appendix (Appendix 16, Table 7.2).

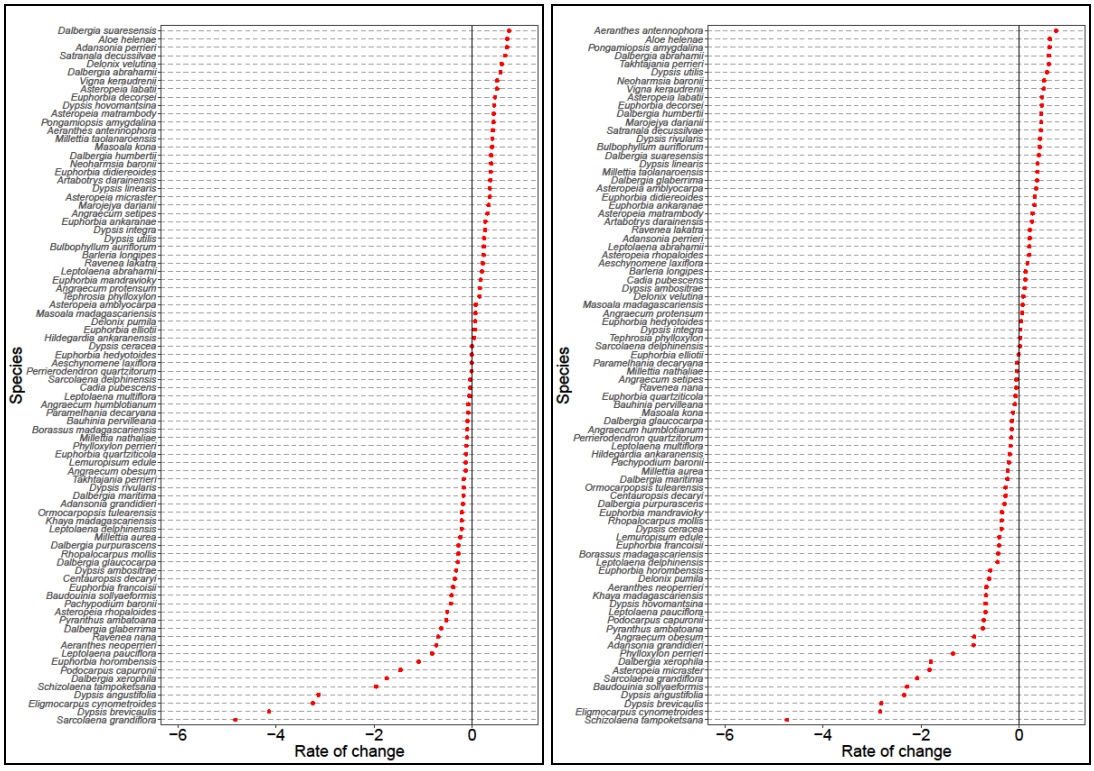

Figure 7.9: Dot plots showing differences between rate of change in suitable habitat area under combined scenario (high emission) (*left*) and combined high with connectivity scenario (emission) (*right*) for 84 selected species in Madagascar. RoC values less than zero indicate decreasing suitable habitat area relative to current habitat area and *vice versa*.

Dalbergia suaresensis (endangered) had the largest range increase under combined scenario and *Sarcolaena grandiflora* (critically endangered) the largest range contraction (Figure 7.8). However, under combined with connectivity scenario. *Aeranthes antennophora* (endangered) range was predicted to undergo the largest range expansion and *Schizolaena tampoketsana* (critically endangered) the largest range contraction. Compared to other species range changes *Aloe helenae* (endangered) was consistently predicted to experience the second highest rate of range expansion under both combined scenarios (Figure 7.9).

7.3.5 Assessing spatial vulnerabilities and risks to species habitats

Analysis of the spatial disruption metric revealed slight variation in the number of species predicted to experience range contraction in all scenarios. For instance, 40 species will contract their ranges under combined scenario (low emission) and the range of 39 species will contract under combined with connectivity scenario (low emission). Also, very similar numbers were predicted to contract under future high emission scenarios (Figure 7.10 & Table 7.2). As a result, only the results of high emission scenarios are presented while those of future low emission scenarios are included as appendix (Appendix 17).

Dalbergia humbertii (endangered) exhibited the highest sensitivity and thus was predicted to experience the largest range contraction under combined with connectivity scenario (high emission) (Figure 7.10). However, *Phylloxyllon perrieri* (endangered) had the least sensitivity under combined with connectivity scenario (high emission) and therefore was predicted to have the largest range expansion.

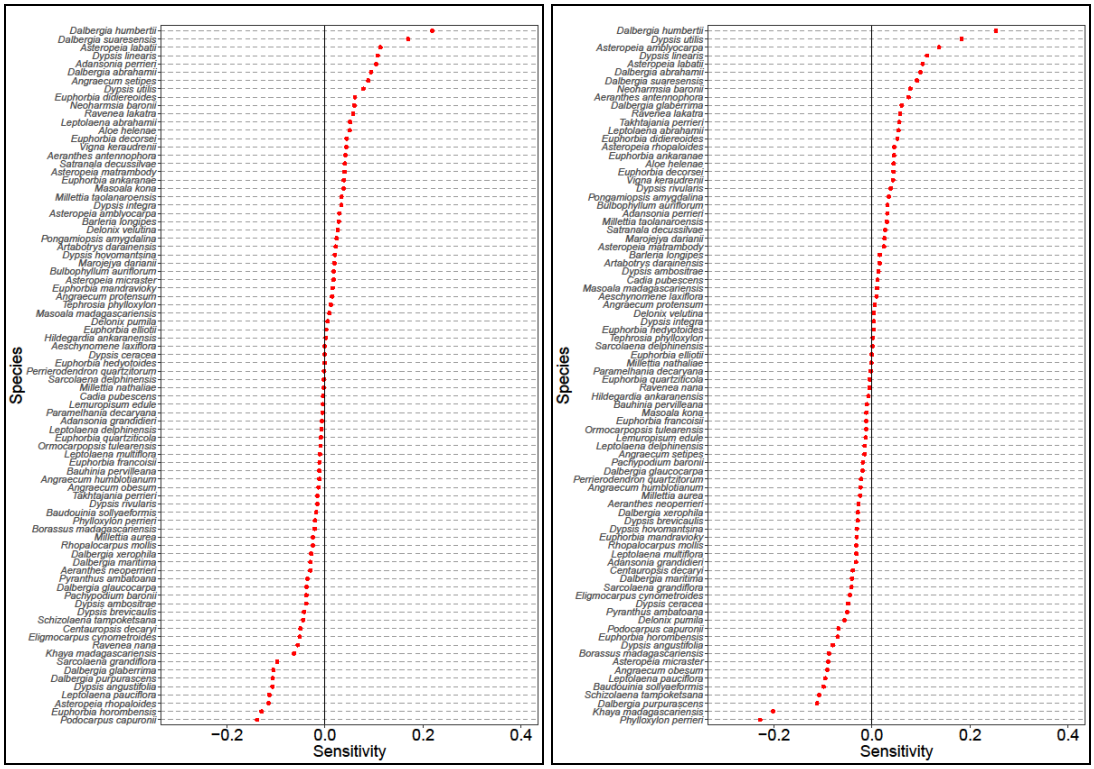

Figure 7.10: Differences in species-specific vulnerabilities as determined from spatial disruption metric under combined scenario (high emission) (*left*) and combined with connectivity scenario (high emission) (*right*). Values greater than zero indicate increasing sensitivity to environmental change and thus likely species range contraction in 2050.

In terms of exposure, all species' ranges were predicted to be at risk of contraction even with corridor connectivity and thus will be threatened by climate and LULCC. For some species, these risks will be higher, while for others they will be considerably less. The low emission scenarios are included as appendix (Appendix 18). *Euphorbia elliotii* (endangered) was predicted as the species to be most at risk to climate and LULCC under combined scenario (high emission). Alternatively, *Aeranthes antennophora* (endangered) is projected to be the most at risk under combined with connectivity scenario (high emission) (Figure 7.11). Conversely, *Aeschynomene laxiflora* (endangered) and *Phylloxylon perrieri* (endangered) were predicted to have the least risks under combined scenario (high emission) and combined with connectivity (high emission), respectively.

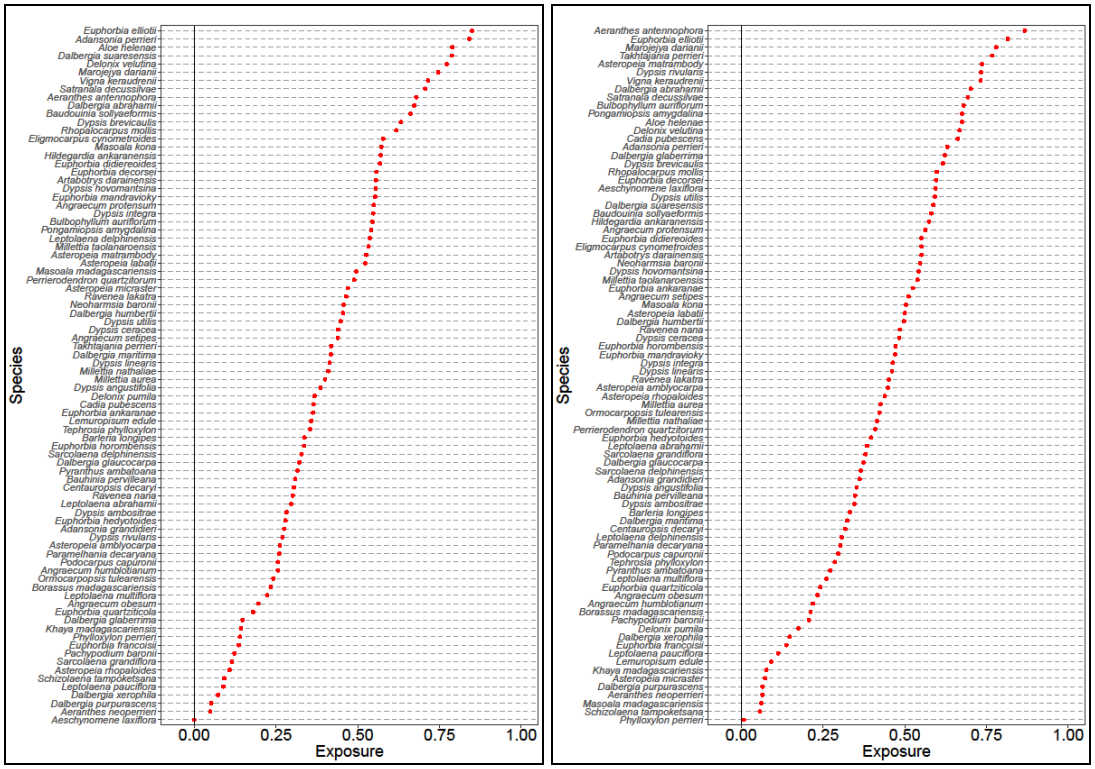

Figure 7.11: Differences in species -specific exposures under combined scenario (high emission) (*left*) and combined with connectivity scenario (high emission) (*right*). Species with exposure values closer to zero are at less risk of range contraction, while those with exposure values farthest from zero are at greater risk.

7.3.6 Mapping range-shift hotspots under multiple scenarios

Coincidence of multiple species experiencing range contractions represent future range-shift hotspots. The predicted pattern suggests that under all future scenarios, connectivity corridors will lead to multiple range contraction in some localities. For instance, the number of species expected to experience range contraction under combined high emission scenario increased from a maximum of eleven to a maximum of thirteen per 2500 km^2 under combined with connectivity scenario (high emission) (Figure 7.12). There is also geographical-bias in the projected distribution of range-shift hotspots, with more pockets of hotspots predicted to be present in the east and north of the country (e.g., combined low emission scenario) (Figure 7.12). However, under combined with connectivity scenario, pockets of hotspot were predicted to concentrate along the eastern part of Madagascar. Overall, predictions show that under future scenarios, range-shift hotspots will be predominantly absent in the west and where corridors are included in the model the distribution of range-shift hotspots will be constrained to the eastern part of Madagascar.

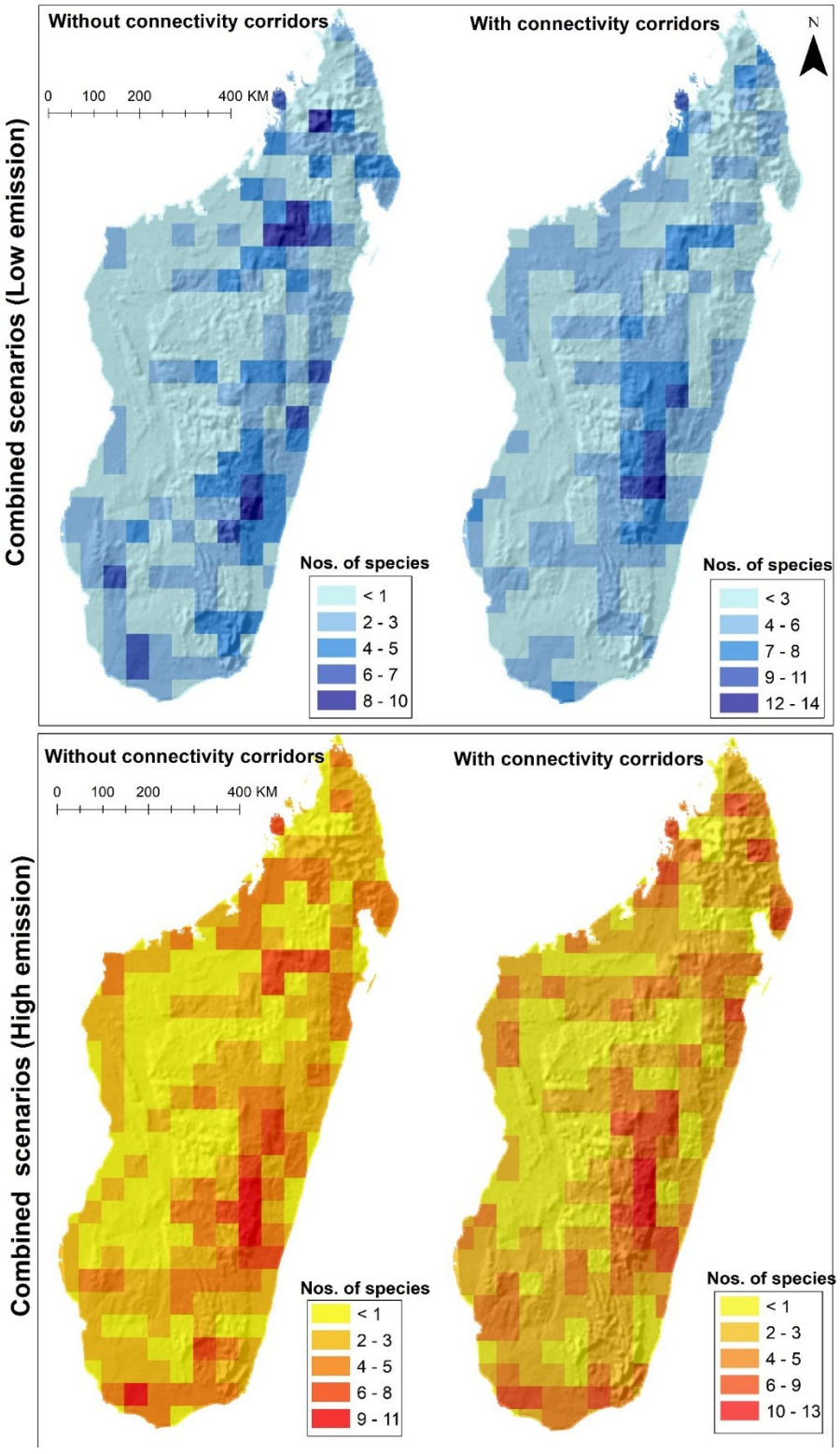

Figure 7.12: Range-shift hotspots under combined scenarios (with and without connectivity). Hotspots were determined from predicted net losses in suitable habitat areas. Top and bottom rows show range-shifts under combined low and high emissions scenarios respectively.

7.4 Discussion

The results indicated that the future response of endangered and critically endangered plants to climate –and– land-use-driven environmental change may be strongly dependent on corridor connectivity. On average, species range contracted with corridor connectivity under combined scenarios (low and high emissions), though species-specific analysis revealed some will experience range expansions. All species responses were detected using several spatial and range-shift metrics, including: habitat net change and rate of change (RoC). The prediction of species range contractions in Madagascar were consistent with previous assessments (Hong-Wa and Arroyo 2012, Vieilledent et al. 2016) and confirms the vulnerabilities of endemic species under climate and land-use change (Malcolm et al. 2006). The inclusion of corridor connectivity in range prediction for some species contradicted the initial expectation (i.e., corridor connectivity did not always mean range expansions). These results suggest that modelling connectivity provides additional level of realism and illustrates that corridors and/or dispersal pathways may be absent in future habitats in Madagascar. That is to say, a climate –and– land-use only model does not adequately represent species' dispersal potential to reach future 'safe sites'. Constraining to only these two scenarios, simply show future habitats that become climatically suitable (Zelazowski et al. 2011), assuming the availability of suitable land-cover (Mantyka-Pringle et al. 2015). Including a layer of habitat connectivity, led to more robust predictions of range-shift, since it not only models climatically suitable habitats, but species' potential to disperse to these locations, highlighting the importance of representing landscape connectivity in future range-shift models. Furthermore, for those species (e.g. *Dypsis ambositrae*) that are predicted to experience range contraction despite connectivity, the probability of future extinction is significantly higher. Nonetheless, using predictions that do not include connectivity is unrealistic and may predict future suitable habitats (i.e., range expansions) to regions without considering whether plants can disperse there (Urban 2015). It should be pointed out that the measure of corridor connectivity included in the prediction of range shift

for 84 endangered and critically endangered plant species do not explicitly measure dispersal capacity. Importantly though, it serves as a robust proxy for dispersal pathways under environmental change.

7.4.1 Potential of extinction and range contraction

Most endangered and critically endangered species were predicted to experience range contraction as a consequence of climate and LULCC, suggesting they are sensitive to these two drivers of environmental change. It is worth noting that there is no evidence that current range size will support or mitigate against future risk of extinctions, since species that were predicted to become highly sensitive to climate and LULCC do not currently have the smallest or biggest range sizes. Nevertheless, spatial vulnerabilities (measured from disruption and exposure indices) and the influence of corridor connectivity between habitats under climate and LULCC were determined for endangered and critically endangered species in Madagascar (Mantyka-Pringle et al. 2015, Choe et al. 2017). The results suggest that whether low or high emissions is achieved in the future the most endangered plant species in Madagascar are likely to be impacted; while some species may thrive (range expansion) under environmental change others will be at serious risk of extinctions (range contraction). Furthermore, these results highlight a growing concern for the most 'at risk' species in this region (i.e., IUCN red listed endangered and critically endangered plant), providing additional evidence that the coupled effects of climate change and deforestation/forest degradation are likely to have severe consequences for species habitats in the future (Feeley et al. 2012). It is possible that examining plant assemblages rather than species-specific cases may reveal different outcomes (i.e., significantly higher species range contraction) in the vulnerabilities of entire species communities. Boakes et al. (2018) reveal similar risks to multispecies facing identical environmental pressures in a tropical region. Moreover, climate and LULCC may not be the only factors influencing species survival. For instance, future novel assemblages caused by differential dispersal rates may demonstrate currently unknown biotic relationships and as a result the extinction for some species despite

predicted suitable habitat (Midgley et al. 2006, Methorst et al. 2017). Thus, it may appear that whether from examining species-specific responses or looking at entire assemblages, the species in tropical habitats are under similar threats of extinction.

7.4.2 Assessing range shifts and upslope displacements

Regardless of the scenario, all plant species will experience range-shift in the future in response to both climate and LULCC. Additionally, species' potential to track suitable habitats is likely to be determined by habitat connectivity. Whether low or high emission scenario is considered, it appears that the average predictions of species' range-shift in Madagascar ($\geq$ 350 km on average) will be within the range of predictions made for Amazon forests (Feeley and Rehm 2012) and are consistent with meta-analysis of global plants range shift under climate change (Chen et al. 2011). Collectively, these results suggest that in the future species range in Madagascar will be farther from current range, these expected shifts in suitable climate and land use land cover conditions may erode biodiversity in the region (Pressey et al. 2007, Brown et al. 2015). Perhaps to better predict adverse changes to biodiversity, future modelling approaches should include corridor connectivity when extrapolating to future dates. In the absence of physiological data, including species dispersal rates, corridor connectivity affords conservation planners a means of gauging the ecological integrity of the landscape.

Species' range displacements will differ with corridor connectivity under future low and high scenarios (i.e., more species will displace downwards under combined high emission scenario with connectivity). Range disjunction is now a likely expected outcome for some of the most endangered and critically endangered species in Madagascar (Kuhn et al. 2016). There is also evidence that the severity of lowland attrition will be most evident under low emission scenario, although with corridor connectivity playing a major role. Confirming the initial expectation for Madagascar that without corridor connectivity plant species will be unable to reach elevated areas with favourable climatic conditions. Also,

downslope displacement is expected under combined high emission scenario. There is also supporting evidence that under future emission scenarios most species range will be confined to mid-elevation and thus intermediate elevation specialist may be the dominant suite of species to emerge from environmental change (Laurance et al. 2011b). Plants are relatively slow dispersers and would likely respond to climate change at a much slower rate compared to other species (Auffret et al. 2017). For instance, upslope displacements were considerable smaller than those assessed for herpetological assemblages in montane regions of Madagascar by Raxworthy et al. (2008). Similar constrains in species dispersals were determined as limiting factors for range expansions in the eastern arc mountains of Tanzania and Kenya (Platts et al. 2013). It is highly likely that for some species, range displacements may contradict initial expectations and appear out of sync with common expectations (Kuhn et al. 2016).

Nonetheless, range shift hotspots will dominate the eastern humid forest. Indicating that the eastern forest corridor will remain a priority area for conservation in the future (Hannah et al. 2008, Zelazowski et al. 2011). This is evident from the multiple number of species range contractions predicted for the same geographical locations under combined low and high emission scenarios. The implications are that entire communities of plants may be at risk of extinction and that the coupled effect of climate change, deforestation and forest degradation may be most severe in humid forests (Bertrand et al. 2011, Urban et al. 2012). It is also possible that species range contractions in humid forest will be countered by their expansion elsewhere – suggesting that humid forest may be a hot-bed for range displacements (i.e., more upward or downward range movement) compared to other eco-regions (e.g., dry forest). However, the latter was not explicitly determined in this project. Moreover, species range expansions are dependent on spatial coincidence with other favourable environmental factors (e.g., soil) that are vital for plant survival (Figueiredo et al. 2018).

The fact that multiple species range contraction per location increased with corridor connectivity only reaffirms the importance of including other abiotic variables. This suggests that corridors will not necessarily translate to range expansions in all areas of Madagascar under low and high emission scenarios. Irrespective of the emission scenario, one outcome is almost certain: sizeable numbers of endangered and critically endangered species will experience range contraction and lowland attrition.

7.4 Conclusion

Substantial species range contractions, range-shifts and lowland attrition due to upward range displacement are predicted as responses to climate and LULCC in Madagascar. Using a spatially-explicit approach that incorporates corridor connectivity (as a proxy for dispersal pathways) suggests that potential range-shift hotspots will be predominantly in the eastern part of Madagascar. This may justify the need for the already concentrated conservation efforts and resources towards that region, but it is worth noting that species in other regions including the dry forests are similarly vulnerable. In terms of absolute number of species range contractions this may compare very little to humid forests, nevertheless, the potential of species extinction exists in other regions with similar consequences for ecosystem functioning and services. Therefore, conservation efforts should focus on a more species-specific approach when designing future intervention programmes, as this is likely to mitigate against biome/regional bias. It is highly likely that similar threats to species range will manifest under environmental change in other tropical biomes, as such conservationists may gain from adapting current management strategies to range shift in those regions. Though this is assuming current corridor connectivity exists in those places and are sufficiently viable to support range expansions. The preservation of tropical biodiversity may rely on plant species dispersals under environmental change and to facilitate their responses robust assessments that include the available means by which the landscapes can facilitate range-shift for the most vulnerable species needs to be considered.

Chapter Eight

8.1 Conclusion

The preceding chapters provide convincing evidence that the coupled effects of climate change and land use land cover change (LULCC) will impact the distribution of endangered and critically endangered plant species in Madagascar. Regardless of which emission scenario is considered, range-shift gap is a certain outcome for the 84 selected species in Madagascar. While some species' range will contract, others are expected to expand by 2050. The potential synergistic effects of climate-driven changes along with deforestation and forest degradation will displace many endangered and critically endangered plants from their current habitats in the near future. Nonetheless, deforestation and forest degradation are driving rapid rates of habitat loss and for international conservation initiatives, such as Reduced Emissions from Deforestation and Degradation (REDD+) their approach to the prevention of biodiversity loss must be balanced and include regions outside protected areas. However, robust assessment of LULCC maps will require continual monitoring and the availability of cloud-free satellite imagery. The latter challenge was encountered during the selection of imagery for this project. There is the risk that without high-quality and cloud-free imagery the causes of LULCC in the tropics are likely to be underestimated.

Despite the data limitations conservation of biodiversity in the region requires assessments that are realistic and that adequately characterise aspects of the landscapes with direct consequences on range-shifts (e.g., dispersal corridors) – like the spatially-explicit approaches used in this project. To better quantify range-shift, studies that assess landscape changes with very high resolution remotely sensed data (i.e., < 5 m) should be encouraged. Though this will depend on whether such images are available for significant portions of the region. Doing so may confirm the results of this project and enable further characterisation of forest losses at eco-regional scales, such as those that pertain to leakages between biomes.

On the other hand, incorporating very high-resolution imagery using similar techniques could determine the impact of dominant land cover change transitions at micro-ecological scales and better calibrate upscaling techniques especially as it relates to plant functional traits in natural habitats. At the very least higher resolution data-sets will guarantee continual monitoring (i.e., increase temporal resolution) of the states of natural habitats in this biodiversity hotspot. Moreover, measurement of habitat fragmentation and the impact of landscape connectivity at various threshold distances is required at all landscape scales, including protected areas. In the meantime, this project has accounted for differences in rates of deforestation and forest degradation, determined baseline LULCC at relatively fine-scales (i.e., eco-regional), modelled future LULCC, estimated corridor connectivity, constructed hierarchical species distributions and predicted plant range-shift gaps with several spatial indices. The combination of these aspects of environmental change enabled the quantification of range-shift gaps for some of the most endangered plant species in Madagascar. It is worth stating that these results are by no means conclusive, for instance, Poisson processes accounts for presence intensity and could potentially quantify range-shift gaps better than Binomial species distribution models. However, this modelling approach was computationally expensive and thus not feasible for the geographical scale at which I intended to predict range-shift gaps. As a result, I recommend that future assessments of tropical species distribution seek ways to develop efficient modelling approaches of range-shift gaps in the region.

Nonetheless, there is now empirical evidence that range-shift hotspots will be predominantly in the eastern corridor of a biodiversity hotspot irrespective of which emission scenario is reached in the future. Therefore, conservationist and other relevant stakeholders should sustain current interventions in the humid forests and incorporate products from spatially-explicit analysis to decision making in anticipation of the inevitable impact of environmental change on species distribution.

References

Aavik, T., R. Holderegger, and J. Bolliger. 2013. The structural and functional connectivity of the grassland plant Lychnis flos-cuculi. Heredity **112**:471.

Achard, F., R. Beuchle, P. Mayaux, H. J. Stibig, C. Bodart, A. Brink, S. Carboni, B. Desclée, F. Donnay, and H. D. Eva. 2014. Determination of tropical deforestation rates and related carbon losses from 1990 to 2010. Glob Chang Biol **20**:2540-2554.

Achard, F., R. DeFries, H. Eva, M. Hansen, P. Mayaux, and H. J. Stibig. 2007. Pan-tropical monitoring of deforestation. Environmental Research Letters **2**:045022.

Achard, F., H.-J. Stibig, H. D. Eva, E. J. Lindquist, A. Bouvet, O. Arino, and P. Mayaux. 2010. Estimating tropical deforestation from Earth observation data. Carbon **1**:271-287.

Addo-Bediako, A., L. S. Chown, and J. K. Gaston. 2000. Thermal tolerance, climatic variability and latitude. Proc. R. Soc. London **267**:739 - 745.

Aguiar, A. P. D., I. C. G. Vieira, T. O. Assis, E. L. Dalla-Nora, P. M. Toledo, R. A. O. Santos-Junior, M. Batistella, A. S. Coelho, E. K. Savaget, L. E. O. C. Aragão, C. A. Nobre, and J. P. H. Ometto. 2016. Land use change emission scenarios: anticipating a forest transition process in the Brazilian Amazon. Glob Chang Biol **22**:1821-1840.

Aldwaik, S. Z., and R. G. Pontius. 2012. Intensity analysis to unify measurements of size and stationarity of land changes by interval, category, and transition. Landscape and Urban Planning **106**:103-114.

Aleman, J. C., M. A. Jarzyna, and A. C. Staver. 2017. Forest extent and deforestation in tropical Africa since 1900. Nature Ecology & Evolution.

Allnutt, T. F., G. P. Asner, C. D. Golden, and G. V. Powell. 2013. Mapping recent deforestation and forest disturbance in northeastern Madagascar. Tropical Conservation Science **6**:1-15.

Anderson-Teixeira, K. J., A. D. Miller, J. E. Mohan, T. W. Hudiburg, B. D. Duval, and E. H. Delucia. 2013. Altered dynamics of forest recovery under a changing climate. Glob Chang Biol **19**:2001-2021.

Anderson, R. P., Peterson, A. T and Gomez-Laverde, M. 2002. Using niche-based GIS modeling to test geographic predictions of competitive exclusion and competitive release in South American pocket mice. Oikos **98**:3-16.

Asner, G. P., C. B. Anderson, R. E. Martin, D. E. Knapp, R. Tupayachi, F. Sinca, and Y. Malhi. 2014. Landscape-scale changes in forest structure and functional traits along an Andes-to-Amazon elevation gradient. Biogeosciences **11**:843-856.

Asner, G. P., E. N. Broadbent, P. J. Oliveira, M. Keller, D. E. Knapp, and J. N. Silva. 2006. Condition and fate of logged forests in the Brazilian Amazon. Proceedings of the National Academy of Sciences **103**:12947-12950.

Asner, G. P., M. Keller, and J. N. Silva. 2004. Spatial and temporal dynamics of forest canopy gaps following selective logging in the eastern Amazon. Glob Chang Biol **10**:765-783.

Asner, G. P., D. E. Knapp, A. Balaji, and G. Páez-Acosta. 2009. Automated mapping of tropical deforestation and forest degradation: CLASlite. Journal of Applied Remote Sensing **3**:033543-033543-033524.

Asner, G. P., D. E. Knapp, E. N. Broadbent, P. J. C. Oliveira, M. Keller, and J. N. Silva. 2005. Selective Logging in the Brazilian Amazon. Science **310**:480-482.

Asner, G. P., S. R. Loarie, and U. Heyder. 2010. Combined effects of climate and land-use change on the future of humid tropical forests. Conservation Letters **3**:395-403.

Atkinson, P. M., and A. R. L. Tatnall. 1997. Introduction Neural networks in remote sensing. International Journal of Remote Sensing **18**:699-709.

Auffret, A. G., Y. Rico, J. M. Bullock, D. A. P. Hooftman, R. J. Pakeman, M. B. Soons, A. Suárez-Esteban, A. Traveset, H. H. Wagner, and S. A. O. Cousins. 2017. Plant functional connectivity – integrating landscape structure and effective dispersal. Journal of Ecology **105**:1648-1656.

Austin, M. 2002. Spatial prediction of species distribution: an interface between ecological theory and statistical modelling. Ecological Modelling **157**:101-118.

Baker, T. R., D. M. Vela Díaz, V. Chama Moscoso, G. Navarro, A. Monteagudo, R. Pinto, K. Cangani, N. M. Fyllas, G. Lopez Gonzalez, W. F. Laurance, S. L. Lewis, J. Lloyd, H. ter Steege, J. W. Terborgh, and O. L. Phillips. 2016. Consistent, small effects of treefall disturbances on the composition and diversity of four Amazonian forests. Journal of Ecology **104**:497-506.

Barlow, J., T. A. Gardner, I. S. Araujo, T. C. Ávila-Pires, A. B. Bonaldo, J. E. Costa, M. C. Esposito, L. V. Ferreira, J. Hawes, M. I. M. Hernandez, M. S. Hoogmoed, R. N. Leite, N. F. Lo-Man-Hung, J. R. Malcolm, M. B. Martins, L. A. M. Mestre, R. Miranda-Santos, A. L. Nunes-Gutjahr, W. L. Overal, L. Parry, S. L. Peters, M. A. Ribeiro-Junior, M. N. F. da Silva, C. da Silva Motta, and C. A. Peres. 2007. Quantifying the biodiversity value of tropical primary, secondary, and plantation forests. Proceedings of the National Academy of Sciences **104**:18555-18560.

Barlow, J., G. D. Lennox, J. Ferreira, E. Berenguer, A. C. Lees, R. M. Nally, J. R. Thomson, S. F. d. B. Ferraz, J. Louzada, V. H. F. Oliveira, L. Parry, R. Ribeiro de Castro Solar, I. C. G. Vieira, L. E. O. C. Aragão, R. A. Begotti, R. F. Braga, T. M. Cardoso, R. C. d. O. Jr, C. M. Souza Jr, N. G. Moura, S. S. Nunes, J. V. Siqueira, R. Pardini, J. M. Silveira, F. Z. Vaz-de-Mello, R. C. S. Veiga, A. Venturieri, and T. A. Gardner. 2016. Anthropogenic disturbance in tropical forests can double biodiversity loss from deforestation. Nature **535**:144-147.

Beale, C. M., M. J. Brewer, and J. J. Lennon. 2014. A new statistical framework for the quantification of covariate associations with species distributions. Methods in Ecology and Evolution **5**:421-432.

Beaumont, L. J., L. Hughes, and A. J. Pitman. 2008. Why is the choice of future climate scenarios for species distribution modelling important? Ecol Lett **11**:1135-1146.

Beaumont, L. J., A. J. Pitman, M. Poulsen, and L. Hughes. 2007. Where will species go? Incorporating new advances in climate modelling into projections of species distributions. Glob Chang Biol **13**:1368-1385.

Beier, P., W. Spencer, R. F. Baldwin, and B. H. McRae. 2011. Toward Best Practices for Developing Regional Connectivity Maps. Conservation Biology **25**:879-892.

Berenguer, E., J. Ferreira, T. A. Gardner, L. E. O. C. Aragão, P. B. De Camargo, C. E. Cerri, M. Durigan, R. C. D. Oliveira, I. C. G. Vieira, and J. Barlow. 2014. A large-scale field assessment of carbon stocks in human-modified tropical forests. Glob Chang Biol **20**:3713-3726.

Bertrand, R., J. Lenoir, C. Piedallu, G. Riofrio-Dillon, P. de Ruffray, C. Vidal, J. C. Pierrat, and J. C. Gegout. 2011. Changes in plant community composition lag behind climate warming in lowland forests. Nature **479**:517-520.

Besag, J. 1974. Spatial interaction and the statistical analysis of lattice systems. Journal of the Royal Statistical Society. Series B (Methodological) **36**:192-236.

Betts, R. A., L. Alfieri, C. Bradshaw, J. Caesar, L. Feyen, P. Friedlingstein, L. Gohar, A. Koutroulis, K. Lewis, C. Morfopoulos, L. Papadimitriou, K. J. Richardson, I. Tsanis, and K. Wyser. 2018. Changes in climate extremes, fresh water availability and vulnerability to food insecurity projected at 1.5°C and 2°C global warming with a higher-resolution global climate model. Philosophical Transactions of the Royal Society A: Mathematical, Physical and Engineering Sciences **376**.

Bhaskar, R., F. Arreola, F. Mora, A. Martinez-Yrizar, M. Martinez-Ramos, and P. Balvanera. 2017. Response diversity and resilience to extreme events in tropical dry secondary forests. Forest Ecology and Management.

Blaise, P., B. Olivier, K. Christoph, D. Curtis, and G. Antoine. 2017. Selecting predictors to maximize the transferability of species distribution models: lessons from cross-continental plant invasions. Global Ecology and Biogeography **26**:275-287.

Boakes, E. H., N. J. B. Isaac, R. A. Fuller, G. M. Mace, and P. J. K. McGowan. 2018. Examining the relationship between local extinction risk and position in range. Conservation Biology **32**:229-239.

Bodin, Ö., M. Tengö, A. Norman, J. Lundberg, and T. Elmqvist. 2006. The value of small size: loss of forest patches and ecological thresholds in southern Madagascar. Ecological Applications **16**:440-451.

Boucher, D., P. Elias, J. Faires, and S. Smith. 2014. Deforestation success stories: Tropical nations where forest protection and reforestation policies have worked. Union of Concerned Scientists.

Bowker, J. N., A. De Vos, J. M. Ament, and G. S. Cumming. 2017. Effectiveness of Africa's tropical protected areas for maintaining forest cover. Conservation Biology **31**:440-451.

Brown, J. H. 2014. Why are there so many species in the tropics? Journal of Biogeography **41**:8-22.

Brown, K. A., J. Carter Ingram, D. F. B. Flynn, R. Razafindrazaka, and V. Jeannoda. 2009. Protected Area Safeguard Tree and Shrub Communities from Degradation and Invasion: A Case Study in Eastern Madagascar. Environmental Management **44**:136-148.

Brown, K. A., Z. J. Farris, G. Yesuf, B. D. Gerber, F. Rasambainarivo, S. Karpanty, M. J. Kelly, J. C. Razafimahaimodison, E. Larney, P. C. Wright, and S. E. Johnson. 2016. Modeling co-occurrence between toxic prey and naïve predators in an incipient invasion. Biodiversity and Conservation **25**:2723-2741.

Brown, K. A., and J. Gurevitch. 2004. Long-term impacts of logging on forest diversity in Madagascar. Proc Natl Acad Sci U S A **101**:6045-6049.

Brown, K. A., S. E. Johnson, K. E. Parks, S. M. Holmes, T. Ivoandry, N. K. Abram, K. E. Delmore, R. Ludovic, H. E. Andriamaharoa, T. M. Wyman, and P. C. Wright. 2013. Use of provisioning ecosystem services drives loss of functional traits across land use intensification gradients in tropical forests in Madagascar. Biological Conservation **161**:118-127.

Brown, K. A., K. E. Parks, C. A. Bethell, S. E. Johnson, and M. Mulligan. 2015. Predicting Plant Diversity Patterns in Madagascar: Understanding the Effects of Climate and Land Cover Change in a Biodiversity Hotspot. PloS one, **10**: p.e0122721.

Burivalova, Z., M. R. Bauert, S. Hassold, N. T. Fatroandrianjafinonjasolomiovazo, and L. P. Koh. 2015. Relevance of Global Forest Change Data Set to Local Conservation: Case Study of Forest Degradation in Masoala National Park, Madagascar. Biotropica **47**:267-274.

Busch, J., R. Dave, L. Hannah, A. Cameron, A. Rasolohery, P. Roehrdanz, and G. Schatz. 2012. Climate change and the cost of conserving species in Madagascar. Conservation Biology **26**:408-419.

Bush, A., D. Nipperess, D. Duursma, G. Theischinger, E. Turak, and L. Hughes. 2014. Continental-Scale Assessment of Risk to the Australian Odonata from Climate Change. PLoS One **9**:e88958.

Calabrese, J. M., G. Certain, C. Kraan, and C. F. Dormann. 2014. Stacking species distribution models and adjusting bias by linking them to macroecological models. Global Ecology and Biogeography **23**:99-112.

Castella, J.-C., G. Lestrelin, C. Hett, J. Bourgoin, Y. R. Fitriana, A. Heinimann, and J.-L. Pfund. 2013. Effects of Landscape Segregation on Livelihood Vulnerability: Moving From Extensive Shifting Cultivation to Rotational Agriculture and Natural Forests in Northern Laos. Human Ecology **41**:63-76.

Castello, L., and M. N. Macedo. 2016. Large-scale degradation of Amazonian freshwater ecosystems. Glob Chang Biol **22**:990-1007.

Cazzolla Gatti, R., S. Castaldi, J. A. Lindsell, D. A. Coomes, M. Marchetti, M. Maesano, A. Di Paola, F. Paparella, and R. Valentini. 2015. The impact of selective logging and clearcutting on forest structure, tree diversity and above-ground biomass of African tropical forests. Ecological Research **30**:119-132.

CEPF. 2005. Madagascar and Indian ocean and islands hotspot: Madagascar briefing book.

Chakraborty, A., A. E. Gelfand, A. M. Wilson, A. M. Latimer, and J. A. Silander. 2011. Point pattern modelling for degraded presence-only data over large regions. Journal of the Royal Statistical Society: Series C (Applied Statistics) **60**:757-776.

Chazdon, R. L. 2014. Second growth: The promise of tropical forest regeneration in an age of deforestation. University of Chicago Press.

Chazdon, R. L., E. N. Broadbent, D. M. A. Rozendaal, F. Bongers, A. M. A. Zambrano, T. M. Aide, P. Balvanera, J. M. Becknell, V. Boukili, P. H. S. Brancalion, D. Craven, J. S. Almeida-Cortez, G. A. L. Cabral, B. de Jong, J. S. Denslow, D. H. Dent, S. J. DeWalt, J. M. Dupuy, S. M. Durán, M. M. Espírito-Santo, M. C. Fandino, R. G. César, J. S. Hall, J. L. Hernández-Stefanoni, C. C. Jakovac, A. B. Junqueira, D. Kennard, S. G. Letcher, M. Lohbeck, M. Martínez-Ramos, P. Massoca, J. A. Meave, R. Mesquita, F. Mora, R. Muñoz, R. Muscarella, Y. R. F. Nunes, S. Ochoa-Gaona, E. Orihuela-Belmonte, M. Peña-Claros, E. A. Pérez-García, D. Piotto, J. S. Powers, J. Rodríguez-Velazquez, I. E. Romero-Pérez, J. Ruíz, J. G. Saldarriaga, A. Sanchez-Azofeifa, N. B. Schwartz, M. K. Steininger, N. G. Swenson, M. Uriarte, M. van Breugel, H. van der Wal, M. D. M. Veloso, H. Vester, I. C. G. Vieira, T. V. Bentos, G. B. Williamson, and L. Poorter. 2016. Carbon sequestration potential of second-growth forest regeneration in the Latin American tropics. Science Advances **2**: p.e1501639.

Chazdon, R. L., C. A. Peres, D. Dent, D. Sheil, A. E. Lugo, D. Lamb, N. E. Stork, and S. E. Miller. 2009. The Potential for Species Conservation in Tropical Secondary Forests. Conservation Biology **23**:1406-1417.

Chen, I. C., J. K. Hill, R. Ohlemuller, D. Roy, and C. D. Thomas. 2011. Rapid Range Shifts of Species Associated with High Levels of Climate Warming. Science **333**:1024 - 1026.

Choe, H., J. H. Thorne, R. Hijmans, J. Kim, H. Kwon, and C. Seo. 2017. Meta-corridor solutions for climate-vulnerable plant species groups in South Korea. Journal of Applied Ecology **54**:1742-1754.

Coe, M. T., T. R. Marthews, M. H. Costa, D. R. Galbraith, N. L. Greenglass, H. M. Imbuzeiro, N. M. Levine, Y. Malhi, P. R. Moorcroft, M. N. Muza, T. L. Powell, S. R. Saleska, L. A. Solorzano, and J. Wang. 2013. Deforestation and climate feedbacks threaten the ecological integrity of south-southeastern Amazonia. Philos Trans R Soc Lond B Biol Sci **368**:20120155.

Colwell, R. K. 2011. Biogeographical gradient theory. Pages 309-330 *in* M. S. Samuel and R. W. Michael, editors. The theory of ecology. University of Chicago Press.

Colwell, R. K., G. Brehm, C. L. Cardelus, A. C. Gilman, and J. T. Longino. 2008. Global warming, elevational range shifts, and lowland biotic attrition in the wet tropics. Science **322**:258-261.

Consiglio, T., G. E. Schatz, G. Mcpherson, P. P. Lowry, J. Rabenantoandro, Z. S. Rogers, R. Rabevohitra, and D. Rabehevitra. 2006. Deforestation and plant diversity of Madagascar's littoral forests. Conservation Biology **20**:1799-1803.

Corlett, R. T. 2011. Impacts of warming on tropical lowland rainforests. Trends in ecology & evolution **26**:606-613.

Corson, C. 2012. From Rhetoric to Practice: How High-Profile Politics Impeded Community Consultation in Madagascar's New Protected Areas. Society & Natural Resources **25**:336-351.

Crimmins, S. M., S. Z. Dobrowski, J. A. Greenberg, J. T. Abatzoglou, and A. R. Mynsberge. 2011. Changes in climatic water balance drive downhill shifts in plant species' optimum elevations. Science **331**:324-327.

Crowley, B. E. 2010. A refined chronology of prehistoric Madagascar and the demise of the megafauna. Quaternary Science Reviews **29**:2591-2603.

DeFries, R. S., T. Rudel, M. Uriarte, and M. Hansen. 2010. Deforestation driven by urban population growth and agricultural trade in the twenty-first century. Nature Geoscience **3**:178.

DeVries, B., J. Verbesselt, L. Kooistra, and M. Herold. 2015. Robust monitoring of small-scale forest disturbances in a tropical montane forest using Landsat time series. Remote Sensing of Environment **161**:107-121.

Dewar, R. E., and A. F. Richard. 2007. Evolution in the hypervariable environment of Madagascar. Proceedings of the National Academy of Sciences **104**:13723-13727.

Diego P. Vázquez, and Richard D. Stevens. 2004. The Latitudinal Gradient in Niche Breadth: Concepts and Evidence. The American Naturalist **164**:E1-E19.

Diez, J. M., and H. R. Pulliam. 2007. Hierarchical analysis of species distributions and abundance across environmental gradients. Ecology **88**:3144-3152.

Dillon, M. E., G. Wang, and R. B. Huey. 2010. Global metabolic impacts of recent climate warming. Nature **467**:704.

Dimobe, K., A. Ouédraogo, S. Soma, D. Goetze, S. Porembski, and A. Thiombiano. 2015. Identification of driving factors of land degradation and deforestation in the Wildlife Reserve of Bontioli (Burkina Faso, West Africa). Global Ecology and Conservation **4**:559-571.

Domisch, S., A. M. Wilson, and W. Jetz. 2016. Model-based integration of observed and expert-based information for assessing the geographic and environmental distribution of freshwater species. Ecography **39**:1078-1088.

Dormann, C. F. 2007. Promising the future? Global change projections of species distributions. Basic and Applied Ecology **8**:387-397.

Du Puy, D., and J. Moat. 1996. A refined classification of the primary vegetation of Madagascar based on the underlying geology: using GIS to map its distribution and to assess its conservation status. Biogéographie de Madagascar **1996**:205-218.

Dullinger, S., A. Gattringer, W. Thuiller, D. Moser, N. E. Zimmermann, A. Guisan, W. Willner, C. Plutzar, M. Leitner, T. Mang, M. Caccianiga, T. Dirnböck, S. Ertl, A. Fischer, J. Lenoir, J.-C. Svenning, A. Psomas, D. R. Schmatz, U. Silc, P. Vittoz, and K. Hülber. 2012. Extinction debt of high-mountain plants under twenty-first-century climate change. Nature Climate Change **2**:619.

Eklund, J., F. G. Blanchet, J. Nyman, R. Rocha, T. Virtanen, and M. Cabeza. 2016. Contrasting spatial and temporal trends of protected area effectiveness in mitigating deforestation in Madagascar. Biological Conservation **203**:290-297.

Elderd, B. D., and T. E. X. Miller. 2016. Quantifying demographic uncertainty: Bayesian methods for integral projection models. Ecological Monographs **86**:125-144.

Elith, J., C. H. Graham, R. P. Anderson, M. Dudík, S. Ferrier, A. Guisan, R. J. Hijmans, F. Huettmann, J. R. Leathwick, A. Lehmann, J. Li, L. G. Lohmann, B. A. Loiselle, G. Manion, C. Moritz, M. Nakamura, Y. Nakazawa, J. McC. M. Overton, A. Townsend Peterson, S. J. Phillips, K. Richardson, R. Scachetti-Pereira, R. E. Schapire, J. Soberón, S. Williams, M. S. Wisz, and N. E. Zimmermann. 2006. Novel methods improve prediction of species' distributions from occurrence data. Ecography **29**:129-151.

Elith, J., M. Kearney, and S. Phillips. 2010. The art of modelling range-shifting species. Methods in Ecology and Evolution **1**:330-342.

Elith, J., and J. R. Leathwick. 2009. Species Distribution Models: Ecological Explanation and Prediction Across Space and Time. Annual Review of Ecology, Evolution, and Systematics **40**:677-697.

Elith, J., S. J. Phillips, T. Hastie, M. Dudík, Y. E. Chee, and C. J. Yates. 2011. A statistical explanation of MaxEnt for ecologists. Diversity and Distributions **17**:43-57.

Elliott, J., D. Deryng, C. Müller, K. Frieler, M. Konzmann, D. Gerten, M. Glotter, M. Flörke, Y. Wada, N. Best, S. Eisner, B. M. Fekete, C. Folberth, I. Foster, S. N. Gosling, I. Haddeland, N. Khabarov, F. Ludwig, Y. Masaki, S. Olin, C. Rosenzweig, A. C. Ruane, Y. Satoh, E. Schmid, T. Stacke, Q. Tang, and D. Wisser. 2014. Constraints and potentials of future irrigation water availability on agricultural production under climate change. Proceedings of the National Academy of Sciences **111**:3239-3244.

Elmqvist, T., M. Somers, M. Pyykönen, M. Tengö, F. Rakotondrasoa, E. Rabakonandrianina, and C. Radimilahy. 2007. Patterns of Loss and Regeneration of Tropical Dry Forest in Madagascar: The Social Institutional Context. PLoS One **2**:e402.

Elsa, M. O., P. A. Gregory, and F. L. Eric. 2017. Deforestation risk due to commodity crop expansion in sub-Saharan Africa. Environmental Research Letters **12**:044015.

ESRI, R. 2015. ArcGIS desktop: release 10. Environmental Systems Research Institute, CA.

Estrada, E., Bodin, xd, and rjan. 2008. Using Network Centrality Measures to Manage Landscape Connectivity. Ecological Applications **18**:1810-1825.

FAO. 2015. Global forest resources assessment 2015. UN Food and Agriculture Organisation, Rome.

Feeley, K., J.,. 2012. Distributional migrations, expansions, and contractions of tropical plant species as revealed in dated herbarium records. Glob Chang Biol **18**:1335-1341.

Feeley, K., J.,, Y. Malhi, P. Zelazowski, and M. Silman, R.,. 2012. The relative importance of deforestation, precipitation change, and temperature sensitivity in determining the future distributions and diversity of Amazonian plant species. Glob Chang Biol **18**:2636-2647.

Feeley, K., J.,, and M. Silman, R.,. 2010a. Land-use and climate change effects on population size and extinction risk of Andean plants. Glob Chang Biol **16**:3215-3222.

Feeley, K. J., and E. M. Rehm. 2012. Amazon's vulnerability to climate change heightened by deforestation and man-made dispersal barriers. Glob Chang Biol **18**:3606-3614.

Feeley, K. J., and M. R. Silman. 2010b. Biotic attrition from tropical forests correcting for truncated temperature niches. Glob Chang Biol **16**:1830-1836.

Feldt, T., and E. Schlecht. 2016. Analysis of GPS trajectories to assess spatio-temporal differences in grazing patterns and land use preferences of domestic livestock in southwestern Madagascar. Pastoralism **6**:5.

Feng, X., M. Uriarte, G. González, S. Reed, J. Thompson, J. K. Zimmerman, and L. Murphy. 2018. Improving predictions of tropical forest response to climate change through integration of field studies and ecosystem modeling. Glob Chang Biol **24**:e213-e232.

Ferguson, B. 2009. REDD comes into fashion in Madagascar. Madagascar Conservation & Development **4**.

Ferrer-Paris, J. R., J. P. Rodríguez, T. C. Good, A. Y. Sánchez-Mercado, K. M. Rodríguez-Clark, G. A. Rodríguez, and A. Solís. 2013. Systematic, large-scale national biodiversity surveys: NeoMaps as a model for tropical regions. Diversity and Distributions **19**:215-231.

Fick, S. E., and R. J. Hijmans. 2017. WorldClim 2: new 1-km spatial resolution climate surfaces for global land areas. International Journal of Climatology **37**:4302-4315.

Figueiredo, F. O. G., G. Zuquim, H. Tuomisto, G. M. Moulatlet, H. Balslev, and F. R. C. Costa. 2018. Beyond climate control on species range: The importance of soil data to predict distribution of Amazonian plant species. Journal of Biogeography **45**:190-200.

Fine, P. V., R. H. Ree, and R. J. Burnham. 2009. The disparity in tree species richness among tropical, temperate and boreal biomes: the geographic area and age hypothesis. Tropical Forest Community Ecology:31-45.

Fletcher, R. J., C. W. Maxwell, J. E. Andrews, and W. L. Helmey-Hartman. 2013. Signal detection theory clarifies the concept of perceptual range and its relevance to landscape connectivity. Landscape Ecology **28**:57-67.

Foltête, J.-C., C. Clauzel, G. Vuidel, and P. Tournant. 2012. Integrating graph-based connectivity metrics into species distribution models. Landscape Ecology **27**:557-569.

Fuller, T., M. Munguía, M. Mayfield, V. Sánchez-Cordero, and S. Sarkar. 2006. Incorporating connectivity into conservation planning: A multi-criteria case study from central Mexico. Biological Conservation **133**:131-142.

Ganzhorn, J. U., P. P. Lowry, G. E. Schatz, and S. Sommer. 2001. The biodiversity of Madagascar: one of the world's hottest hotspots on its way out. Oryx **35**:346-348.

Gasparri, N. I., T. Kuemmerle, P. Meyfroidt, Y. le Polain de Waroux, and H. Kreft. 2016. The Emerging Soybean Production Frontier in Southern Africa: Conservation Challenges and the Role of South-South Telecouplings. Conservation Letters **9**:21-31.

Gautier, L., Tahinarivony, A. J., Ranirison, P. and Wohlhauser, S. 2018. Vegetation. Goodman, S. M., Raherilalao, M. J. & Wohlhauser, S. (eds.).The terrestrial protected areas of Madagascar: their history, description, and biota. Antananarivo Association Vahatra

Gelfand, A. E., J. A. Silander, S. Wu, A. Latimer, P. O. Lewis, A. G. Rebelo, and M. Holder. 2006. Explaining species distribution patterns through hierarchical modeling.41-92.

Gelfand, A. E., and A. F. M. Smith. 1990. Sampling-Based Approaches to Calculating Marginal Densities. Journal of the American Statistical Association **85**:398-409.

Ghazoul, J., Z. Burivalova, J. Garcia-Ulloa, and L. A. King. 2015. Conceptualizing Forest Degradation. Trends in Ecology & Evolution **30**:622-632.

Gibson, L., T. M. Lee, L. P. Koh, B. W. Brook, T. A. Gardner, J. Barlow, C. A. Peres, C. J. Bradshaw, W. F. Laurance, and T. E. Lovejoy. 2011. Primary forests are irreplaceable for sustaining tropical biodiversity. Nature **478**:378-381.

Golding, N., and B. V. Purse. 2016. Fast and flexible Bayesian species distribution modelling using Gaussian processes. Methods in Ecology and Evolution **7**:598-608.

Gonçalves, J., P. Alves, I. Pôças, B. Marcos, R. Sousa-Silva, Â. Lomba, and J. P. Honrado. 2016. Exploring the spatiotemporal dynamics of habitat suitability to improve conservation management of a vulnerable plant species. Biodiversity and Conservation **25**:2867-2888.

Good, T. C., M. L. Zjhra, and C. Kremen. 2006. Addressing data deficiency in classifying extinction risk: a case study of a radiation of Bignoniaceae from Madagascar. Conservation Biology **20**:1099-1110.

Goodman, R. C., and M. Herold. 2014. Why maintaining tropical forests is essential and urgent for a stable climate-working Paper 385.

Goodman, S. M., and J. P. Benstead. 2003. Natural history of Madagascar. University of Chicago Press.

Gray, C. L., S. L. Hill, T. Newbold, L. N. Hudson, L. Börger, S. Contu, A. J. Hoskins, S. Ferrier, A. Purvis, and J. P. Scharlemann. 2016. Local biodiversity is higher inside than outside terrestrial protected areas worldwide. Nature Communications **7**.

Grinand, C., F. Rakotomalala, V. Gond, R. Vaudry, M. Bernoux, and G. Vieilledent. 2013. Estimating deforestation in tropical humid and dry forests in Madagascar from 2000 to 2010 using multi-date Landsat satellite images and the random forests classifier. Remote Sensing of Environment **139**:68-80.

Guisan, A., and W. Thuiller. 2005. Predicting species distribution: offering more than simple habitat models. Ecol Lett **8**:993-1009.

Gurrutxaga, M., L. Rubio, and S. Saura. 2011. Key connectors in protected forest area networks and the impact of highways: A transnational case study from the Cantabrian Range to the Western Alps (SW Europe). Landscape and Urban Planning **101**:310-320.

Guth, P. 2010. Geomorphometric comparison of ASTER GDEM and SRTM.*in* A special joint symposium of ISPRS Technical Commission IV & AutoCarto in conjunction with ASPRS/CaGIS.

Hall, J., N. D. Burgess, J. Lovett, B. Mbilinyi, and R. E. Gereau. 2009. Conservation implications of deforestation across an elevational gradient in the Eastern Arc Mountains, Tanzania. Biological Conservation **142**:2510-2521.

Hampe, A. 2011. Plants on the move: The role of seed dispersal and initial population establishment for climate-driven range expansions. Acta Oecologica **37**:666-673.

Hannah, L., R. Dave, P. P. Lowry, S. Andelman, M. Andrianarisata, L. Andriamaro, A. Cameron, R. Hijmans, C. Kremen, J. Mackinnon, H. H. Randrianasolo, S. Andriambololonera, A. Razafimpahanana, H. Randriamahazo, J. Randrianarisoa, P. Razafinjatovo, C. Raxworthy, G. E. Schatz, M. Tadross, and L. Wilme. 2008. Climate change adaptation for conservation in Madagascar. Biol Lett **4**:590-594.

Hansen, M. C., P. V. Potapov, R. Moore, M. Hancher, S. A. Turubanova, A. Tyukavina, D. Thau, S. V. Stehman, S. J. Goetz, T. R. Loveland, A. Kommareddy, A. Egorov, L. Chini, C. O. Justice, and J. R. Townshend. 2013. High-resolution global maps of 21st-century forest cover change. Science **342**:850-853.

Hansen, M. C., S. V. Stehman, and P. V. Potapov. 2010. Quantification of global gross forest cover loss. Proceedings of the National Academy of Sciences **107**:8650-8655.

Hansen, M. C., S. V. Stehman, P. V. Potapov, T. R. Loveland, J. R. Townshend, R. S. DeFries, K. W. Pittman, B. Arunarwati, F. Stolle, and M. K. Steininger. 2008. Humid tropical forest clearing from 2000 to 2005 quantified by using multitemporal and multiresolution remotely sensed data. Proceedings of the National Academy of Sciences **105**:9439-9444.

Harper, G. J., M. K. Steininger, C. J. Tucker, D. Juhn, and F. Hawkins. 2008. Fifty years of deforestation and forest fragmentation in Madagascar. Environmental Conservation **34**.

Harris, N. L., S. Brown, S. C. Hagen, S. S. Saatchi, S. Petrova, W. Salas, M. C. Hansen, P. V. Potapov, and A. Lotsch. 2012. Baseline Map of Carbon Emissions from Deforestation in Tropical Regions. Science **336**:1573-1576.

He, K., S.,, B. Bradley, A.,, A. Cord, F.,, D. Rocchini, M. N. Tuanmu, S. Schmidtlein, W. Turner, M. Wegmann, and N. Pettorelli. 2015. Will remote sensing shape the next generation of species distribution models? Remote Sensing in Ecology and Conservation **1**:4-18.

Heller, N. E., and E. S. Zavaleta. 2009. Biodiversity management in the face of climate change: A review of 22 years of recommendations. Biological Conservation **142**:14-32.

Henderson, E. B., J. L. Ohmann, M. J. Gregory, H. M. Roberts, and H. Zald. 2014. Species distribution modelling for plant communities: stacked single species or multivariate modelling approaches? Applied vegetation science **17**:516-527.

Herold, M., R. M. Román-Cuesta, D. Mollicone, Y. Hirata, P. Van Laake, G. P. Asner, C. Souza, M. Skutsch, V. Avitabile, and K. MacDicken. 2011. Options for monitoring and estimating historical carbon emissions from forest degradation in the context of REDD+. Carbon Balance Manag **6**:13.

Herrera, J. P. 2017. Prioritizing protected areas in Madagascar for lemur diversity using a multidimensional perspective. Biological Conservation **207**:1-8.

Higgins, S., I.,, R. O'Hara, B.,, and C. Römermann. 2012. A niche for biology in species distribution models. Journal of Biogeography **39**:2091-2095.

Hoffmann, A. A., and C. M. Sgrò. 2011. Climate change and evolutionary adaptation. Nature **470**:479.

Hong-Wa, C., and T. P. F. Arroyo. 2012. Climate-induced range contraction in the Malagasy endemic plant genera Mediusella and Xerochlamys (Sarcolaenaceae). Plant Ecology and Evolution **145**:302-312.

Houghton, R. A. 2013. The emissions of carbon from deforestation and degradation in the tropics: past trends and future potential. Carbon Management **4**:539-546.

Houghton, R. A., B. Byers, and A. A. Nassikas. 2015. A role for tropical forests in stabilizing atmospheric CO2. Nature Climate Change **5**:1022.

Huang, M., and G. P. Asner. 2010. Long-term carbon loss and recovery following selective logging in Amazon forests. Global Biogeochemical Cycles **24**.

Ibáñez, I., D. S. W. Katz, D. Peltier, S. M. Wolf, and B. T. Connor Barrie. 2014. Assessing the integrated effects of landscape fragmentation on plants and plant communities: the challenge of multiprocess–multiresponse dynamics. Journal of Ecology **102**:882-895.

Ingram, J. C., T. P. Dawson, and R. J. Whittaker. 2005. Mapping tropical forest structure in southeastern Madagascar using remote sensing and artificial neural networks. Remote Sensing of Environment **94**:491-507.

Irwin, M. T., P. C. Wright, C. Birkinshaw, B. L. Fisher, C. J. Gardner, J. Glos, S. M. Goodman, P. Loiselle, P. Rabeson, and J.-L. Raharison. 2010. Patterns of species change in anthropogenically disturbed forests of Madagascar. Biological Conservation **143**:2351-2362.

IUCN. 2017. The IUCN Red List of Threatened Species. Version 2017-1.

Jantz, S. M., B. Barker, T. M. Brooks, L. P. Chini, Q. Huang, R. M. Moore, J. Noel, and G. C. Hurtt. 2015. Future habitat loss and extinctions driven by land-use change in biodiversity hotspots under four scenarios of climate-change mitigation. Conservation Biology **29**:1122-1131.

Jiménez-Valverde, A. 2012. Insights into the area under the receiver operating characteristic curve (AUC) as a discrimination measure in species distribution modelling. Global Ecology and Biogeography **21**:498-507.

Jiménez-Valverde, A., P. Acevedo, A. M. Barbosa, J. M. Lobo, and R. Real. 2013. Discrimination capacity in species distribution models depends on the representativeness of the environmental domain. Global Ecology and Biogeography **22**:508-516.

Jones, K. R., O. Venter, R. A. Fuller, J. R. Allan, S. L. Maxwell, P. J. Negret, and J. E. M. Watson. 2018. One-third of global protected land is under intense human pressure. Science **360**:788-791.

Kearney, M., and W. Porter. 2009. Mechanistic niche modelling: combining physiological and spatial data to predict species' ranges. Ecol Lett **12**:334-350.

Kearney, M. R., B. A. Wintle, and W. P. Porter. 2010. Correlative and mechanistic models of species distribution provide congruent forecasts under climate change. Conservation Letters **3**:203-213

Keenan, R. J., G. A. Reams, F. Achard, J. V. de Freitas, A. Grainger, and E. Lindquist. 2015. Dynamics of global forest area: Results from the FAO Global Forest Resources Assessment 2015. Forest Ecology and Management **352**:9-20.

Kennedy, R. E., Z. Yang, and W. B. Cohen. 2010. Detecting trends in forest disturbance and recovery using yearly Landsat time series: 1. LandTrendr — Temporal segmentation algorithms. Remote Sensing of Environment **114**:2897-2910.

Kreyling, J., D. Wana, and C. Beierkuhnlein. 2010. Potential consequences of climate warming for tropical plant species in high mountains of southern Ethiopia. Diversity and Distributions **16**:593-605.

Kuhn, E., J. Lenoir, C. Piedallu, and J.-C. Gégout. 2016. Early signs of range disjunction of submountainous plant species: an unexplored consequence of future and contemporary climate changes. Glob Chang Biol **22**:2094-2105.

Kull, C. A. 2002a. The "Degraded" Tapia Woodlands of Highland Madagascar: Rural Economy, Fire Ecology, and Forest Conservation. Journal of Cultural Geography **19**:95-128.

Kull, C. A. 2002b. Madagascar's Burning Issue: The Persistent Conflict over Fire. Environment: Science and Policy for Sustainable Development **44**:8-19.

Kull, C. A. 2012. Air photo evidence of historical land cover change in the highlands: Wetlands and grasslands give way to crops and woodlots.

Lahoz-Monfort, J. J., G. Guillera-Arroita, and B. A. Wintle. 2014. Imperfect detection impacts the performance of species distribution models. Global Ecology and Biogeography **23**:504-515.

Laita, A., J. S. Kotiaho, and M. Mönkkönen. 2011. Graph-theoretic connectivity measures: what do they tell us about connectivity? Landscape ecology **26**:951-967.

Lambin, E. F. 1999. Monitoring forest degradation in tropical regions by remote sensing: some methodological issues. Global Ecology and Biogeography **8**:191-198.

Lambin, E. F., H. J. Geist, and E. Lepers. 2003. Dynamics of Land-Use and Land-Cover Change in Tropical Regions. Annual Review of Environment and Resources **28**:205-241.

Lambin, E. F., B. L. Turner, H. J. Geist, S. B. Agbola, A. Angelsen, J. W. Bruce, O. T. Coomes, R. Dirzo, G. Fischer, C. Folke, P. S. George, K. Homewood, J. Imbernon, R. Leemans, X. Li, E. F. Moran, M. Mortimore, P. S. Ramakrishnan, J. F. Richards, H. Skånes, W. Steffen, G. D. Stone, U. Svedin, T. A. Veldkamp, C. Vogel, and J. Xu. 2001. The causes of land-use and land-cover change: moving beyond the myths. Global Environmental Change **11**:261-269.

Lathuillière, J. M., S. M. Johnson, and D. S. Donner. 2012. Water use by terrestrial ecosystems: temporal variability in rainforest and agricultural contributions to evapotranspiration in Mato Grosso, Brazil. Environmental Research Letters **7**:024024.

Latimer, A. M., S. Wu, A. E. Gelfand, and J. A. Silander. 2006. Building statistical models to analyze species distributions. Ecological Applications **16**:33 - 50.

Laurance, W. F., D. Carolina Useche, J. Rendeiro, M. Kalka, C. J. A. Bradshaw, S. P. Sloan, S. G. Laurance, M. Campbell, K. Abernethy, P. Alvarez, V. Arroyo-Rodriguez, P. Ashton, J. Benítez-Malvido, A. Blom, K. S. Bobo, C. H. Cannon, M. Cao, R. Carroll, C. Chapman, R. Coates, M. Cords, F. Danielsen, B. De Dijn, E. Dinerstein, M. A. Donnelly, D. Edwards, F. Edwards, N. Farwig, P. Fashing, P.-M. Forget, M. Foster, G. Gale, D. Harris, R. Harrison, J. Hart, S. Karpanty, W. John Kress, J. Krishnaswamy, W. Logsdon, J. Lovett, W. Magnusson, F. Maisels, A. R. Marshall, D. McClearn, D. Mudappa, M. R. Nielsen, R. Pearson, N. Pitman, J. van der Ploeg, A. Plumptre, J. Poulsen, M. Quesada, H. Rainey, D. Robinson, C. Roetgers, F. Rovero, F. Scatena, C. Schulze, D. Sheil, T. Struhsaker, J. Terborgh, D. Thomas, R. Timm, J. Nicolas Urbina-Cardona, K. Vasudevan, S. Joseph Wright, J. Carlos Arias-G, L. Arroyo, M. Ashton, P. Auzel, D. Babaasa, F. Babweteera, P. Baker, O. Banki, M. Bass, I. Bila-Isia, S. Blake, W. Brockelman, N. Brokaw, C. A. Brühl, S. Bunyavejchewin, J.-T. Chao, J. Chave, R. Chellam, C. J. Clark, J. Clavijo, R. Congdon, R. Corlett, H. S. Dattaraja, C. Dave, G. Davies, B. de Mello Beisiegel, R. de Nazaré Paes da Silva, A. Di Fiore, A. Diesmos, R. Dirzo, D. Doran-Sheehy, M. Eaton, L. Emmons, A. Estrada, C. Ewango, L. Fedigan, F. Feer, B. Fruth, J. Giacalone Willis, U. Goodale, S. Goodman, J. C. Guix, P. Guthiga, W. Haber, K. Hamer, I. Herbinger, J. Hill, Z. Huang, I. Fang Sun, K. Ickes, A. Itoh, N. Ivanauskas, B. Jackes, J. Janovec, D. Janzen, M. Jiangming, C. Jin, T. Jones, H. Justiniano, E. Kalko, A. Kasangaki, T. Killeen, H.-b. King, E. Klop, C. Knott, I. Koné, E.

Kudavidanage, J. Lahoz da Silva Ribeiro, J. Lattke, R. Laval, R. Lawton, M. Leal, M. Leighton, M. Lentino, C. Leonel, J. Lindsell, L. Ling-Ling, K. Eduard Linsenmair, E. Losos, A. Lugo, J. Lwanga, A. L. Mack, M. Martins, W. Scott McGraw, R. McNab, L. Montag, J. Myers Thompson, J. Nabe-Nielsen, M. Nakagawa, S. Nepal, M. Norconk, V. Novotny, S. O'Donnell, M. Opiang, P. Ouboter, K. Parker, N. Parthasarathy, K. Pisciotta, D. Prawiradilaga, C. Pringle, S. Rajathurai, U. Reichard, G. Reinartz, K. Renton, G. Reynolds, V. Reynolds, E. Riley, M.-O. Rödel, J. Rothman, P. Round, S. Sakai, T. Sanaiotti, T. Savini, G. Schaab, J. Seidensticker, A. Siaka, M. R. Silman, T. B. Smith, S. S. de Almeida, N. Sodhi, C. Stanford, K. Stewart, E. Stokes, K. E. Stoner, R. Sukumar, M. Surbeck, M. Tobler, T. Tscharntke, A. Turkalo, G. Umapathy, M. van Weerd, J. Vega Rivera, M. Venkataraman, L. Venn, C. Verea, C. Volkmer de Castilho, M. Waltert, B. Wang, D. Watts, W. Weber, P. West, D. Whitacre, K. Whitney, D. Wilkie, S. Williams, D. D. Wright, P. Wright, L. Xiankai, P. Yonzon, and F. Zamzani. 2012. Averting biodiversity collapse in tropical forest protected areas. Nature **489**:290.

Laurance, W. F., D. Carolina Useche, L. P. Shoo, S. K. Herzog, M. Kessler, F. Escobar, G. Brehm, J. C. Axmacher, I. C. Chen, and L. A. Gámez. 2011. Global warming, elevational ranges and the vulnerability of tropical biota. Biological Conservation **144**:548-557.

Lawson, C. R., J. A. Hodgson, R. J. Wilson, S. A. Richards, and R. Freckleton. 2014. Prevalence, thresholds and the performance of presence–absence models. Methods in Ecology and Evolution **5**:54-64.

Lee, D. S., J. C. Storey, M. J. Choate, and D. Hayes. 2004. Four years of Landsat-7 on-orbit geometric calibration and performance. IEEE Transactions on Geoscience and Remote Sensing **42**:2786-2795.

Leimu, R., P. I. A. Mutikainen, J. Koricheva, and M. Fischer. 2006. How general are positive relationships between plant population size, fitness and genetic variation? Journal of Ecology **94**:942-952.

Levins, R. 1968. Evolution in changing environments: some theoretical explorations. Princeton University Press.

Li, J. Y., and Y. H. Wang. 2012. An Improved Slope Classification Mapping Method. Pages 2069-2072 *in* Applied Mechanics and Materials. Trans Tech Publ.

Li, W., P. Ciais, N. MacBean, S. Peng, P. Defourny, and S. Bontemps. 2016. Major forest changes and land cover transitions based on plant functional types derived from the ESA CCI Land Cover product. International Journal of Applied Earth Observation and Geoinformation **47**:30-39.

Lichstein, J. W., T. R. Simons, S. A. Shriner, and K. E. Franzreb. 2002. Spatial autocorrelation and autoregressive models in ecology. Ecological Monographs **72**:445-463.

Lindborg, R., and O. Eriksson. 2004. Historical landscape connectivity affects pressent plant species diversity. Ecology **85**:1840-1845.

Liu, C., P. M. Berry, T. P. Dawson, and R. G. Pearson. 2005. Selecting thresholds of occurrence in the prediction of species distributions. Ecography **28**:385-393.

Liu, C., G. Newell, and M. White. 2016. On the selection of thresholds for predicting species occurrence with presence-only data. Ecology and evolution **6**:337-348.

Llopis, J. C., C. J. Gardner, and X. Vincke. 2015. Land-use and land-cover change in a global biodiversity conservation priority. The case of the spiny forest of Madagascar Pages pp. 15 - 17 GLP News. IGBP & Future Earth.

Lobo, J. M. 2008. More complex distribution models or more representative data? Biodiversity informatics **5**.

Maggiori, E., Y. Tarabalka, G. Charpiat, and P. Alliez. 2017. Convolutional neural networks for large-scale remote-sensing image classification. IEEE Transactions on Geoscience and Remote Sensing **55**:645-657.

Malcolm, J. R., C. Liu, R. P. Neilson, L. Hansen, and L. E. E. Hannah. 2006. Global Warming and Extinctions of Endemic Species from Biodiversity Hotspots. Conservation Biology **20**:538-548.

Males, J. 2018. Geography, environment and organismal traits in the diversification of a major tropical herbaceous angiosperm radiation. AoB PLANTS **10**:ply008-ply008.

Mantyka-Pringle, C. S., P. Visconti, M. Di Marco, T. G. Martin, C. Rondinini, and J. R. Rhodes. 2015. Climate change modifies risk of global biodiversity loss due to land-cover change. Biological Conservation **187**:103-111.

Marco, A., J. M. Nilsson, M. Stéphanie, T. Wilfried, and M. David. 2015. Extending networks of protected areas to optimize connectivity and population growth rate. Ecography **38**:273-282.

Marshall, A. R., S. Willcock, P. J. Platts, J. C. Lovett, A. Balmford, N. D. Burgess, J. E. Latham, P. K. T. Munishi, R. Salter, D. D. Shirima, and S. L. Lewis. 2012. Measuring and modelling above-ground carbon and tree allometry along a tropical elevation gradient. Biological Conservation **154**:20-33.

Marta, C., Z. David, and A. A. T.R. 2016. Measuring ecological specialization along a natural stress gradient using a set of complementary niche breadth indices. Journal of Vegetation Science **27**:892-903.

Martin, G. M., N. Bellouin, W. J. Collins, I. D. Culverwell, P. R. Halloran, S. C. Hardiman, T. J. Hinton, C. D. Jones, R. E. McDonald, A. J. McLaren, F. M. O'Connor, M. J. Roberts, J. M. Rodriguez, S. Woodward, M. J. Best, M. E. Brooks, A. R. Brown, N. Butchart, C. Dearden, S. H. Derbyshire, I. Dharssi, M. Doutriaux-Boucher, J. M. Edwards, P. D. Falloon, N. Gedney, L. J. Gray, H. T. Hewitt, M. Hobson, M. R. Huddleston, J. Hughes, S. Ineson, W. J. Ingram, P. M. James, T. C. Johns, C. E. Johnson, A. Jones, C. P. Jones, M. M. Joshi, A. B. Keen, S. Liddicoat, A. P. Lock, A. V. Maidens, J. C. Manners, S. F. Milton, J. G. L. Rae, J. K. Ridley, A. Sellar, C. A. Senior, I. J. Totterdell, A. Verhoef, P. L. Vidale, and A. Wiltshire. 2011. The HadGEM2 family of Met Office Unified Model climate configurations. Geosci. Model Dev. **4**:723-757.

Martínez, P., R. Pérez, A. Plaza, P. Aguilar, M. Cantero, and J. Plaza. 2006. Endmember extraction algorithms from hyperspectral images. Annals of Geophysics **49**.

McCain, C. M., and R. K. Colwell. 2011. Assessing the threat to montane biodiversity from discordant shifts in temperature and precipitation in a changing climate. Ecol Lett **14**:1236-1245.

McConnell, W. J., and C. A. Kull. 2014. Deforestation in Madagascar: Debates over the island's forest cover and challenges of measuring forest change.*in* I. R. Scales, editor. Conservation and environmental Management in Madagascar. Routledge Taylor & Francis Group.

McRae, B. H., B. G. Dickson, T. H. Keitt, and V. B. Shah. 2008. Using circuit theory to model connectivity in ecology, evolution and conservation. Ecology **89**:2712-2724.

McRae, B. H., S. A. Hall, P. Beier, and D. M. Theobald. 2012. Where to Restore Ecological Connectivity? Detecting Barriers and Quantifying Restoration Benefits. PLoS One **7**:e52604.

McRae, B. H., and D. M. Kavanagh. 2014. Linkage Mapper Connectivity Analysis Software. The Nature Conservancy, Seattle WA.

Menke, S., D. Holway, R. Fisher, and W. Jetz. 2009. Characterizing and predicting species distributions across environments and scales: Argentine ant occurrences in the eye of the beholder. Global Ecology and Biogeography **18**:50-63.

Merow, C., A. M. Latimer, A. M. Wilson, S. M. McMahon, A. G. Rebelo, and J. A. Silander. 2014. On using integral projection models to generate demographically driven predictions of species' distributions: development and validation using sparse data. Ecography **37**:1167-1183.

Methorst, J., K. Böhning-Gaese, I. Khaliq, and C. Hof. 2017. A framework integrating physiology, dispersal and land-use to project species ranges under climate change. Journal of Avian Biology **48**:1532-1548.

Midgley, G., G. Hughes, W. Thuiller, and A. Rebelo. 2006. Migration rate limitations on climate change-induced range shifts in Cape Proteaceae. Diversity and Distributions **12**:555-562.

Mitchell, A. 1999. The ESRI guide to GIS analysis: geographic patterns & relationships. ESRI, Inc.

Moat, J., and P. Smith. 2007. Atlas of the Vegetation of Madagascar Vegetation/Atlas de la Vegetation de Madagascar (text in English and French). Royal Botanical Gardens, Kew.

Montesino Pouzols, F., T. Toivonen, E. Di Minin, A. S. Kukkala, P. Kullberg, J. Kuusterä, J. Lehtomäki, H. Tenkanen, P. H. Verburg, and A. Moilanen. 2014. Global protected area expansion is compromised by projected land-use and parochialism. Nature **516**:383.

Mora, F., V. J. Jaramillo, R. Bhaskar, M. Gavito, I. Siddique, J. E. K. Byrnes, and P. Balvanera. 2018. Carbon Accumulation in Neotropical Dry Secondary Forests: The Roles of Forest Age and Tree Dominance and Diversity. Ecosystems **21**:536-550.

Morin, X., and W. Thuiller. 2009. Comparing niche- and process-based models to reduce prediction uncertainty in species range shifts under climate change. Ecology **90**:1301-1313.

Mukul, S. A., and J. Herbohn. 2016. The impacts of shifting cultivation on secondary forests dynamics in tropics: A synthesis of the key findings and spatio temporal distribution of research. Environmental Science & Policy **55**:167-177.

Myers, N., R. A. Mittermeier, C. G. Mittermeier, G. A. Da Fonseca, and J. Kent. 2000. Biodiversity hotspots for conservation priorities. Nature **403**:853.

Nakazato, T., D. L. Warren, and L. C. Moyle. 2010. Ecological and geographic modes of species divergence in wild tomatoes. American Journal of Botany **97**:680-693.

Neeff, T., R. M. Lucas, J. dos Santos, xe, R. o, E. S. Brondizio, and C. C. Freitas. 2006. Area and Age of Secondary Forests in Brazilian Amazonia 1978-2002: An Empirical Estimate. Ecosystems **9**:609-623.

Nobre, P., M. Malagutti, D. F. Urbano, R. A. de Almeida, and E. Giarolla. 2009. Amazon deforestation and climate change in a coupled model simulation. Journal of Climate **22**:5686-5697.

Nunes, L., A.,, and R. Pearson, G.,. 2017. A null biogeographical test for assessing ecological niche evolution. Journal of Biogeography **44**:1331-1343.

Okin, G. S., M. M.-d. l. Heras, P. M. Saco, H. L. Throop, E. R. Vivoni, A. J. Parsons, J. Wainwright, and D. P. C. Peters. 2015. Connectivity in dryland landscapes: shifting concepts of spatial interactions. Frontiers in Ecology and the Environment **13**:20-27.

Olofsson, P., G. M. Foody, M. Herold, S. V. Stehman, C. E. Woodcock, and M. A. Wulder. 2014. Good practices for estimating area and assessing accuracy of land change. Remote Sensing of Environment **148**:42-57.

Panfil, S. N., and C. A. Harvey. 2015. REDD+ and Biodiversity Conservation: A Review of the Biodiversity Goals, Monitoring Methods, and Impacts of 80 REDD+ Projects. Conservation Letters **9**:143-150.

Parmesan, C., and G. Yohe. 2003. A globally coherent fingerprint of climate change impacts across natural systems. Nature **421**:37.

Pérez-Vega, A., J.-F. Mas, and A. Ligmann-Zielinska. 2012. Comparing two approaches to land use/cover change modeling and their implications for the assessment of biodiversity loss in a deciduous tropical forest. Environmental Modelling & Software **29**:11-23.

Pete, S., H. J. I., B. Mercedes, S. Jaroslava, H. Richard, P. Genxing, W. P. C., C. J. M., A. Tapan, R. Cornelia, P. Keith, K. Peter, C. M. Francesca, E. J. A., M. Richard, G. R. I., A. Susumu, B. Alberte, J. A. K., M. Jeroen, and P. T. A. M. 2016. Global change pressures on soils from land use and management. Glob Chang Biol **22**:1008-1028.

Petitpierre, B., C. Kueffer, O. Broennimann, C. Randin, C. Daehler, and A. Guisan. 2012. Climatic niche shifts are rare among terrestrial plant invaders. Science **335**:1344-1348.

Phillips, J. S., M. Dudík, J. Elith, H. C. Graham, A. Lehmann, J. Leathwick, and S. Ferrier. 2009. Sample selection bias and presence-only distribution models: implications for background and pseudo-absence data. Ecological Applications **19**:181-197.

Phillips, O. L., and R. J. W. Brienen. 2017. Carbon uptake by mature Amazon forests has mitigated Amazon nations' carbon emissions. Carbon Balance Manag **12**:1.

Phillips, S. J., and J. Elith. 2013. On estimating probability of presence from use–availability or presence–background data. Ecology **94**:1409-1419.

Pickard, B., J. Gray, and R. Meentemeyer. 2017. Comparing Quantity, Allocation and Configuration Accuracy of Multiple Land Change Models. Land **6**:52.

Pienaar, B., D. I. Thompson, B. F. N. Erasmus, T. R. Hill, and E. T. F. Witkowski. 2015. Evidence for climate-induced range shift in Brachystegia (miombo) woodland. South African Journal of Science **111**:1-9.

Platts, P. J., R. E. Gereau, N. D. Burgess, and R. Marchant. 2013. Spatial heterogeneity of climate change in an Afromontane centre of endemism. Ecography **36**:518-530.

Pontius, R. G., and M. Millones. 2011. Death to Kappa: birth of quantity disagreement and allocation disagreement for accuracy assessment. International Journal of Remote Sensing **32**:4407-4429.

Poorter, L., F. Bongers, T. M. Aide, A. M. A. Zambrano, P. Balvanera, J. M. Becknell, V. Boukili, P. H. Brancalion, E. N. Broadbent, and R. L. Chazdon. 2016. Biomass resilience of Neotropical secondary forests. Nature **530**:211-214.

Porfirio, L. L., R. M. B. Harris, E. C. Lefroy, S. Hugh, S. F. Gould, G. Lee, N. L. Bindoff, and B. Mackey. 2014. Improving the Use of Species Distribution Models in Conservation Planning and Management under Climate Change. PLoS One **9**:e113749.

Pressey, R. L., M. Cabeza, M. E. Watts, R. M. Cowling, and K. A. Wilson. 2007. Conservation planning in a changing world. Trends in ecology & evolution **22**:583-592.

Prestele, R., P. Alexander, M. D. A. Rounsevell, A. Arneth, K. Calvin, J. Doelman, D. A. Eitelberg, K. Engström, S. Fujimori, T. Hasegawa, P. Havlik, F. Humpenöder, A. K. Jain, T. Krisztin, P. Kyle, P. Meiyappan, A. Popp, R. D. Sands, R. Schaldach, J. Schüngel, E. Stehfest, A. Tabeau, H. Van Meijl, J. Van Vliet, and P. H. Verburg. 2016. Hotspots of uncertainty in land-use and land-cover change projections: a global-scale model comparison. Glob Chang Biol **22**:3967-3983.

Quintano, C., A. Fernández-Manso, Y. E. Shimabukuro, and G. Pereira. 2012. Spectral unmixing. International Journal of Remote Sensing **33**:5307-5340.

R Core Team. 2016. R: A language and environment for statistical computing. R Foundation for Statistical Computing, Vienna, Austria. 2014.

Radinger, J., F. Essl, F. Hölker, P. Horký, O. Slavík, and C. Wolter. 2017. The future distribution of river fish: The complex interplay of climate and land use changes, species dispersal and movement barriers. Glob Chang Biol **23**:4970-4986.

Rakotondrasoa, O. L., F. Malaisse, G. L. Rajoelison, T. M. Razafimanantsoa, M. R. Rabearisoa, B. S. Ramamonjisoa, N. Raminosoa, F. J. Verheggen, M. Poncelet, and É. Haubruge. 2012. Tapia forest, endemic ecosystem to Madagascar: ecology, functions, causes of degradation and transformation: a review. Biotechnologie, Agronomie, Société et Environnement **16**:541-552.

Rasmussen, C. E., and C. K. I. Williams. 2006. Gaussian Processes For Machine Learning. MIT Press.

Raúl, G. V., S. Jens-Christian, Z. M. A., P. D. W., and A. M. B. 2015. Evaluating the combined effects of climate and land-use change on tree species distributions. Journal of Applied Ecology **52**:902-912.

Raxworthy, C. J., R. G. Pearson, N. Rabibisoa, A. M. Rakotondrazafy, J.-B. Ramanamanjato, A. P. Raselimanana, S. Wu, R. A. Nussbaum, and D. A. Stone. 2008. Extinction vulnerability of tropical montane endemism from warming and upslope displacement: a preliminary appraisal for the highest massif in Madagascar. Glob Chang Biol **14**:1703-1720.

Razafindratsima, O. H., K. A. Brown, F. Carvalho, S. E. Johnson, P. C. Wright, and A. E. Dunham. 2018. Edge effects on components of diversity and above-ground biomass in a tropical rainforest. Journal of Applied Ecology **55**:977-985.

Redding, D. W., T. C. D. Lucas, T. M. Blackburn, and K. E. Jones. 2017. Evaluating Bayesian spatial methods for modelling species distributions with clumped and restricted occurrence data. PLoS One **12**:e0187602.

Rocchini, D. 2014. Remote sensing of biodiversity: measuring ecological complexity from space. In SAGEO'14 (Spatial Analysis and GEOmatics).

Rodríguez-Castañeda, G., and M. Sykes. 2013. The world and its shades of green: a meta-analysis on trophic cascades across temperature and precipitation gradients. Global Ecology and Biogeography **22**:118-130.

Rudel, T. K., O. T. Coomes, E. Moran, F. Achard, A. Angelsen, J. Xu, and E. Lambin. 2005. Forest transitions: towards a global understanding of land use change. Global Environmental Change **15**:23-31.

Ruth, D., H. Andrew, N. A. C., and H. M. C. 2005. Increasing isolation of protected areas in tropical forests over the past twenty years. Ecological Applications **15**:19-26.

Ryan, C. M., R. Pritchard, I. McNicol, M. Owen, J. A. Fisher, and C. Lehmann. 2016. Ecosystem services from southern African woodlands and their future under global change. Philosophical Transactions of the Royal Society B: Biological Sciences **371**.

Saura, S., and L. Pascual-Hortal. 2007. A new habitat availability index to integrate connectivity in landscape conservation planning: Comparison with existing indices and application to a case study. Landscape and Urban Planning **83**:91-103.

Saura, S., and L. Rubio. 2010. A common currency for the different ways in which patches and links can contribute to habitat availability and connectivity in the landscape. Ecography **33**:523-537.

Saura, S., P. Vogt, J. Velázquez, A. Hernando, and R. Tejera. 2011. Key structural forest connectors can be identified by combining landscape spatial pattern and network analyses. Forest Ecology and Management **262**:150-160.

Scales, I. R. 2012. Lost in translation: conflicting views of deforestation, land use and identity in western Madagascar. The Geographical Journal **178**:67-79.

Schatz, G. E. 2002. Taxonomy and herbaria in service of plant conservation: lessons from Madagascar's endemic families. Annals of the Missouri Botanical Garden:145-152.

Schliep, E. M., N. K. Lany, P. L. Zarnetske, R. N. Schaeffer, C. M. Orians, D. A. Orwig, and E. L. Preisser. 2018. Joint species distribution modelling for spatio-temporal occurrence and ordinal abundance data. Global Ecology and Biogeography 27:142-155.

Schwarz, G. 1978. Estimating the Dimension of a Model. The Annals of Statistics **6**:461-464.

Segan, D. B., D. G. Hole, C. I. Donatti, C. Zganjar, S. Martin, S. H. M. Butchart, and J. E. M. Watson. 2015. Considering the impact of climate change on human communities significantly alters the outcome of species and site-based vulnerability assessments. Diversity and Distributions **21**:1101-1111.

Skelly, D. K., L. N. Joseph, H. P. Possingham, L. K. Freidenburg, T. J. Farrugia, M. T. Kinnison, and A. P. Hendry. 2007. Evolutionary responses to climate change. Conserv Biol **21**:1353-1355.

Slatyer, R., A.,, M. Hirst, and J. Sexton, P.,. 2013. Niche breadth predicts geographical range size: a general ecological pattern. Ecol Lett **16**:1104-1114.

Sloan, S., and J. A. Sayer. 2015. Forest Resources Assessment of 2015 shows positive global trends but forest loss and degradation persist in poor tropical countries. Forest Ecology and Management **352**:134-145.

Soares-Filho, B. S., D. C. Nepstad, L. M. Curran, G. C. Cerqueira, R. A. Garcia, C. A. Ramos, E. Voll, A. McDonald, P. Lefebvre, and P. Schlesinger. 2006. Modelling conservation in the Amazon basin. Nature **440**:520-523.

Soberón, J., and M. Nakamura. 2009. Niches and distributional areas: concepts, methods, and assumptions. Proceedings of the National Academy of Sciences **106**:19644-19650.

Staniczenko, P. P. A., P. Sivasubramaniam, K. B. Suttle, and R. G. Pearson. 2017. Linking macroecology and community ecology: refining predictions of species distributions using biotic interaction networks. Ecol Lett **20**:693-707.

Steininger, M. K. 2000. Satellite estimation of tropical secondary forest above-ground biomass: Data from Brazil and Bolivia. International Journal of Remote Sensing **21**:1139-1157.

Stibig, H.-J., F. Achard, S. Carboni, R. Raši, and J. Miettinen. 2014. Change in tropical forest cover of Southeast Asia from 1990 to 2010. Biogeosciences **11**:247-258.

Struebig, M. J., M. Fischer, D. L. A. Gaveau, E. Meijaard, S. A. Wich, C. Gonner, R. Sykes, A. Wilting, and S. Kramer-Schadt. 2015a. Anticipated climate and land-cover changes reveal refuge areas for Borneo's orang-utans. Glob Chang Biol **21**:2891-2904.

Struebig, M. J., A. Wilting, D. L. Gaveau, E. Meijaard, R. J. Smith, M. Fischer, K. Metcalfe, S. Kramer-Schadt, and B. M. D. Consortium. 2015b. Targeted conservation to safeguard a biodiversity hotspot from climate and land-cover change. Current Biology **25**:372-378.

Synes, N. W., and P. E. Osborne. 2011. Choice of predictor variables as a source of uncertainty in continental-scale species distribution modelling under climate change. Global Ecology and Biogeography **20**:904-914.

Tadross, M., L. Randriamarolaza, Z. Rabefitia, and K. Zheng. 2008. Climate change in Madagascar; recent past and future. Washington DC (World Bank).

Taylor, P. D. 2006. Landscape connectivity: a return to the basics. Connectivity conservation:29-43.

Taylor, P. D., L. Fahrig, K. Henein, and G. Merriam. 1993. Connectivity Is a Vital Element of Landscape Structure. Oikos **68**:571-573.

Thomas, C. D., P. K. Gillingham, R. B. Bradbury, D. B. Roy, B. J. Anderson, J. M. Baxter, N. A. Bourn, H. Q. Crick, R. A. Findon, and R. Fox. 2012. Protected areas facilitate species' range expansions. Proc Natl Acad Sci USA:14063-14068.

Thuiller, W. 2004. Patterns and uncertainties of species' range shifts under climate change. Glob Chang Biol **10**:2020-2027.

Thuiller, W., C. Albert, M. B. Araujo, P. M. Berry, M. Cabeza, A. Guisan, T. Hickler, G. F. Midgely, J. Paterson, F. M. Schurr, M. T. Sykes, and N. E. Zimmermann. 2008. Predicting global change impacts on plant species' distributions: Future challenges. Perspectives in Plant Ecology Evolution and Systematics **9**:137-152.

Tischendorf, L., and L. Fahrig. 2000. On the Usage and Measurement of Landscape Connectivity. Oikos **90**:7-19.

UN. 2016. Report of the Conference Parties on its twenty-first session, held in Paris, 30 November to 13 December 2015. Addendum Part two: Action taken by the Conference of the Parties at its twenty-first session. United Nations Framework Convention on Climate Change, Paris.

Urban, M. C. 2015. Accelerating extinction risk from climate change. Science **348**:571-573.

Urban, M. C., J. J. Tewksbury, and K. S. Sheldon. 2012. On a collision course: competition and dispersal differences create no-analogue communities and cause extinctions during climate change. Proceedings of the Royal Society B: Biological Sciences **279**:2072-2080.

Vågen, T.-G. 2006. Remote sensing of complex land use change trajectories—a case study from the highlands of Madagascar. Agriculture, Ecosystems & Environment **115**:219-228.

van Vuuren, D. P., J. Edmonds, M. Kainuma, K. Riahi, A. Thomson, K. Hibbard, G. C. Hurtt, T. Kram, V. Krey, J.-F. Lamarque, T. Masui, M. Meinshausen, N. Nakicenovic, S. J. Smith, and S. K. Rose. 2011. The representative concentration pathways: an overview. Climatic Change **109**:5.

Vasudev, D., R. J. Fletcher, V. R. Goswami, and M. Krishnadas. 2015. From dispersal constraints to landscape connectivity: lessons from species distribution modeling. Ecography **38**:967-978.

Velázquez, J., J. Gutiérrez, A. Hernando, and A. García-Abril. 2017. Evaluating landscape connectivity in fragmented habitats: Cantabrian capercaillie (Tetrao urogallus cantabricus) in northern Spain. Forest Ecology and Management **389**:59-67.

Verburg, P. H., J. van de Steeg, A. Veldkamp, and L. Willemen. 2009. From land cover change to land function dynamics: A major challenge to improve land characterization. Journal of Environmental Management **90**:1327-1335.

Vermote, E. F., D. Tanre, J. L. Deuze, M. Herman, and J. J. Morcette. 1997. Second Simulation of the Satellite Signal in the Solar Spectrum, 6S: an overview. IEEE Transactions on Geoscience and Remote Sensing **35**:675-686.

Vieilledent, G., O. Gardi, C. Grinand, C. Burren, M. Andriamanjato, C. Camara, C. Gardner, J.,, L. Glass, A. Rasolohery, R. Rakoto, Harifidy,, V. Gond, and J. R. Rakotoarijaona. 2016. Bioclimatic envelope models predict a decrease in tropical forest carbon stocks with climate change in Madagascar. Journal of Ecology **104**:703-715.

Vieilledent, G., C. Grinand, and R. Vaudry. 2013. Forecasting deforestation and carbon emissions in tropical developing countries facing demographic expansion: a case study in Madagascar. Ecology and evolution **3**:1702-1716.

Vieilledent, G., A. Latimer, A. Gelfand, C. Merow, A. Wilson, F. Mortier, and J. Silander Jr. 2014. hSDM: hierarchical Bayesian species distribution models. R package version **1**.

Vogt, P. 2016. Guidos Toolbox (Graphical User Interface for the Description of image Objects and their Shapes): Digital image analysis software.

Vogt, P., J. R. Ferrari, T. R. Lookingbill, R. H. Gardner, K. H. Riitters, and K. Ostapowicz. 2009. Mapping functional connectivity. Ecological Indicators **9**:64-71.

Vogt, P., K. H. Riitters, C. Estreguil, J. Kozak, T. G. Wade, and J. D. Wickham. 2007. Mapping Spatial Patterns with Morphological Image Processing. Landscape ecology **22**:171-177.

Vranckx, G. U. Y., H. Jacquemyn, B. Muys, and O. Honnay. 2012. Meta-analysis of susceptibility of woody plants to loss of genetic diversity through habitat fragmentation. Conservation Biology **26**:228-237.

Waeber, P., L. Wilmé, B. Ramamonjisoa, C. Garcia, D. Rakotomalala, Z. Rabemananjara, C. Kull, J. Ganzhorn, and J.-P. Sorg. 2015. Dry forests in Madagascar: neglected and under pressure. International Forestry Review **17**:127-148.

Walther, G.-R., S. Berger, and M. T. Sykes. 2005. An ecological 'footprint' of climate change. Proceedings of the Royal Society B: Biological Sciences **272**:1427-1432.

Ward, G., T. Hastie, S. Barry, J. Elith, and J. R. Leathwick. 2009. Presence-Only Data and the EM Algorithm. Biometrics **65**:554-563.

Warren, D. L., R. E. Glor, and M. Turelli. 2010. ENMTools: a toolbox for comparative studies of environmental niche models. Ecography **33**:607-611.

Warren, D. L., and S. N. Seifert. 2011. Ecological niche modeling in Maxent: the importance of model complexity and the performance of model selection criteria. Ecological Applications **21**:335-342.

Warren, R., J. Price, E. Graham, N. Forstenhaeusler, and J. VanDerWal. 2018. The projected effect on insects, vertebrates, and plants of limiting global warming to 1.5°C rather than 2°C. Science **360**:791-795.

Watson, J. E. 2014. Human Responses to Climate Change will Seriously Impact Biodiversity Conservation: It's Time We Start Planning for Them. Conservation Letters **7**:1-2.

Whitfield, A. K., N. C. James, S. J. Lamberth, J. B. Adams, R. Perissinotto, A. Rajkaran, and T. G. Bornman. 2016. The role of pioneers as indicators of biogeographic range expansion caused by global change in southern African coastal waters. Estuarine, Coastal and Shelf Science **172**:138-153.

Whitmore, T. C. 1998. An Introduction to Tropical Rainforests. Oxford University Press, Oxford.

Wiegand, T., E. Revilla, and K. A. Moloney. 2005. Effects of Habitat Loss and Fragmentation on Population Dynamics. Conservation Biology **19**:108-121.

William, F., E. Jane, H. Trevor, and K. D. A. 2015. Bias correction in species distribution models: pooling survey and collection data for multiple species. Methods in Ecology and Evolution **6**:424-438.

Zaehringer, J. G., S. Eckert, and P. Messerli. 2015. Revealing Regional Deforestation Dynamics in North-Eastern Madagascar—Insights from Multi-Temporal Land Cover Change Analysis. Land **4**:454-474.

Zahawi, R. A., J. P. Dandois, K. D. Holl, D. Nadwodny, J. L. Reid, and E. C. Ellis. 2015. Using lightweight unmanned aerial vehicles to monitor tropical forest recovery. Biological Conservation **186**:287-295.

Zelazowski, P., Y. Malhi, C. Huntingford, S. Sitch, and J. B. Fisher. 2011. Changes in the potential distribution of humid tropical forests on a warmer planet. Philos Trans A Math Phys Eng Sci **369**:137-160.

Zeller, K. A., K. McGarigal, and A. R. Whiteley. 2012. Estimating landscape resistance to movement: a review. Landscape ecology **27**:777-797.

Zinner, D., C. Wygoda, L. Razafimanantsoa, R. Rasoloarison, H. T. Andrianandrasana, J. U. Ganzhorn, and F. Torkler. 2014. Analysis of deforestation patterns in the central Menabe, Madagascar, between 1973 and 2010. Regional Environmental Change **14**:157-166.

Zollner, P. A., and S. L. Lima. 2005. Behavioral tradeoffs when dispersing across a patchy landscape. Oikos **108**:219-230.

Zurell, D., W. Thuiller, J. Pagel, J. S. Cabral, T. Münkemüller, D. Gravel, S. Dullinger, S. Normand, K. H. Schiffers, K. A. Moore, and N. E. Zimmermann. 2016. Benchmarking novel approaches for modelling species range dynamics. Glob Chang Biol **22**:2651-2664.